# Lime based nanomaterials for the conservation of calcareous substrates in heritage structures

OTERO HERMO, Jorge

Available from Sheffield Hallam University Research Archive (SHURA) at:

http://shura.shu.ac.uk/22428/

# Lime based nanomaterials for the conservation of calcareous substrates in heritage structures

Jorge Otero Hermo

May 2018

A thesis submitted in partial fulfilment of the requirements of
Sheffield Hallam University
for the degree of Doctor of Philosophy

**Lime based nanomaterials for the conservation of calcareous substrates in heritage structures**

Jorge Otero Hermo

May, 2018

A thesis submitted in partial fulfilment of the requirements of Sheffield Hallam University for the degree of Doctor of Philosophy

# Abstract

Nanolime is one of the most promising consolidation materials used in the conservation of historic calcareous substrates. Whilst the popularity of nanolime has grown significantly in the last two decades, its consolidation mechanism when applied to highly porous substrates still needs to be fully understood. The aim of this Ph.D. is to understand the consolidation mechanism of a number of nanolime products in highly porous substrates and to investigate new ways to improve nanolime consolidation effectiveness. The research consisted of six experimental programmes: 1) comparing the consolidation effectiveness of three available nanolime products (Nanorestore Plus®, Calosil® and nanolime synthesized following a method developed by researchers of the University of L'Aquila, Italy); 2) investigating the influence of different types of solvent on the consolidation effectiveness of nanolime; 3) investigating the influence of substrate pore structure and nanolime particle size on the consolidation effectiveness of nanolime; 4) investigating the consolidation effectiveness of nanolime on Biocalcarenite from Agrigento, Italy; 5) investigating the consolidation effectiveness of nanolime on Indiana limestone and weathered marble from the Smithsonian National Museum buildings, USA; and 6) investigating the use of additives to improve nanolime consolidation effectiveness. Nanorestore Plus® yielded the highest short-term consolidation effect, measured by means of a Drilling Resistance Measurement System, in both limestones and lime-mortars. However, L'Aquila nanolime showed a higher durability which was attributed to a better developed crystalline structure. A 50%-50% water-isopropanol solvent appeared to be the best option for dispersing nanoparticles synthetized through the L'Aquila's method as it yielded a higher consolidating effectiveness compared to other types of solvents. Results also suggest that due to the different size of their nanoparticles, Nanorestore Plus® could be more suitable to consolidate coarser substrates, while L'Aquila nanolime seems to be more suitable to consolidate substrates with a finer pore structure. Results also demonstrated that L'Aquila nanolime can be used effectively for the consolidation of the biocalcarenite from Agrigento and the weathered marble from the Smithsonian Museum. Furthermore, it was shown that the use of sticky rice in a combined treatment with L'Aquila nanolime improves the consolidation effectiveness although prolonged exposure to moisture can compromise treatment durability. Finally, results also showed that nanolimes yield a higher consolidation degree in substrates composed mainly of calcite (limestones) than in lime-mortars containing silica sand.

# LIST OF OUTPUTS

## Peer Reviewed Journal Articles

**Otero J**., Starinieri V., Charola A. E., A comparison between nanolime treatments on lime-mortar, Construction and Building Materials (paper submitted).

Taglieri G., **Otero J.**, Daniele V., Gioia G., Macera L., Starinieri V., Charola A. E., The biocalcarenite stone of Agrigento (Italy): preliminary investigations of compatible nanolime treatments, Journal of cultural Heritage. https://doi.org/10.1016/j.culher.2017.11.003.

**Otero, J**., Charola A. E., Grissom C., Starinieri V., An overview of nanolime as a consolidation method for calcareous substrates. Ge-conservación, vol.1, n.11, p.71-78, 2017. ISSN 1989-8568. http://ge-iic.com/ojs/index.php/revista/article/view/455.

## Talks

Taglieri G., **Otero J**., Daniele V., et al., The biocalcarenite stone of Agrigento (Italy): preliminary investigations of compatible nanolime treatments IMEKO International Conference on Metrology for Archaeology and Cultural Heritage Lecce, Italy, October 23rd - 25th, 2017.

**Otero J.**, Taglieri G., Starinieri V., Charola A. E., Nanolime for the conservation of the UNESCO's Archaeological site of the Valle Dei Templi: preliminary results, 7th Symposium of Materials and Engineering Research Institute, Sheffield Hallam University, UK, May 16th, 2017.

**Otero, J**., Charola A. E., Grissom C., Starinieri V., An overview of nanolime as a consolidation method for calcareous substrates. 5th International Conference Youth in Conservation of Cultural Heritage, Yococu2016, Madrid, Spain, Sep 21st - 23rd, 2016.

**Otero, J.,** Charola A. E., Grissom C., What's nanolime?, Smithsonian Museum Conservation Institute, Analytical Studies Group Internship Program 2016 Events, MCI theatre, Washington DC, USA, June 23rd, 2016.

## Posters

**Otero J.**, Zwagerman A., Conservation of the plaster ceiling in the nursery at Craigievar Castle, damaged by salt efflorescence, 18th Triennial Conference ICOM-CC, Copenhagen, Sep 4th - 8th, 2017.

**Otero, J**., Charola A. E., Grissom C., Starinieri V., An overview of nanolime as a consolidation method for calcareous substrates. Chemistry: The science around us Symposium, University of Sheffield, Sheffield, UK, Sep 9th, 2016.

**Otero, J**., Starinieri, V., Mangat P., O'Flaherty, F., Nanolime as a consolidation method for weathered lime-mortars. Materials and Engineering Research Institute symposium, Sheffield Hallam University, Sheffield, UK, Dec 17th, 2015.


## Proceedings


**Otero, J**; Charola A.E; Grissom C, Starinieri V. An overview of nanolime as a consolidation method for calcareous substrates. Proceeding Published by Museo Nacional Centro de Arte Reina Sofia, 5th Internaltional Conference Youth in Conservation of Cultural Heritage, Yococu2016 (21st - 23rd Sep, Madrid-Spain, 2016).

# Acknowledgment

Firstly, I wish to thank my supervisor Dr. Vincenzo Starinieri, who gave me the opportunity to carry out my work at the Sheffield Hallam University. He helped me out and supported me whenever possible. I also wish to thank Prof. Wayne M. Cranton and Dr. Kathy Doherty for selecting me to carry out this research through the Vice-Chancellor Scholarship.

My most sincere gratitude goes to my Ph.D. advisor Dr. Elena A. Charola, who strongly advocated transferring all her knowledge to me and I can't be more grateful. She provided constant help over millions of Skype sessions. She helped me out to understand numerous stone deterioration mechanisms, consolidation processes, theory of conservation, interpretation of results, etc. She also helped me develop my critical thinking skills, judging standards tests, my results and someone else research papers. Her passion for the conservation of historic buildings and her dedication towards sharing her knowledge with future generations has been a real inspiration for me and she is definitely a role-model for my career.

My acknowledgement also goes to the staff of the Materials and Engineering Research Institute at Sheffield Hallam University: to all administrative staff (Corrie, Clare, Jane, Rachel and Gail) for their constant help, especially with the process of the two placements; to Dr. Anthony Bell for his help and good training with XRD-Rietveld refinements; to Paul Allender for his help with both TEM and SEM techniques; to the construction lab technicians (Steve, Ian and Charlie) for their good humour and their support in the lab; and finally to Dr. Francis Clegg and Prof. Chris Sammon for their help with the day to day work in the laboratories.

I would like to thank all the staff that also helped me out during both placements at the Smithsonian's Institution and the University of L'Aquila. Firstly, I want to thank Prof. Giuliana Taglieri for having accepted me for the placement. I am very grateful for all the knowledge I learnt from her and for those long dinners at her house talking

# List of symbols and abbreviations

| a | cm$^2$ | Scotch tape area |
|---|---|---|
| ASTM | | American Standard Testing Method |
| AWT | | Accelerated Weathering Tester |
| A0 | | Starting absorbance |
| At | | Absorbance at time t |
| W/A | | Water and Alcohol solvent |
| B | | Samples treated with LAQ dispersed in butanol |
| BRE | | Building Research Establishment |
| BS-EN | | British Standard - European harmonised Standard |
| CA | g / m$^2$ sec$^{0.5}$ | Water Absorption coefficient by LNEC standard |
| CAL | | Samples treated with Calosil |
| CEN | | European Committee for Standardization |
| Conc | g/L | Concentration |
| CP | | Weathered limestone: capital |
| CSGI | | Centre for Colloids and Surface Science |
| CVC | | Chemical Vapour Condensation |
| DRMS | | Drilling Resistance Measurement System |
| E$_p$ | % | Effective protective efficacy by LNEC standard |
| ET | | Samples treated with LAQ dispersed in ethanol |
| FTIR | | Fourier-transform infrared spectroscopy |
| F | Newton [N] | Force |
| Fo | Newton [N] | Initial force |
| Ff | Newton [N] | Final force |

| | | |
|---|---|---|
| HPMR | | Hydrogen plasma-metal reaction |
| ICOMOS | | International Council on Monuments and Sites |
| ICSD | | Inorganic Crystal Structure Database |
| IP | | Samples treated with LAQ dispersed in isopropanol |
| IR | | Indiana samples treated stored in room condition |
| IRS | | Indiana samples treated stored in room condition and sprayed regularly with carbonated water |
| ISPRA | | Istituto Superiore per la Protezione e la Ricerca Ambientale |
| KS | % | Kinetic Stability |
| LAQ | | Samples treated with nanolime from L'Aquila |
| LS | | Weathered limestone 1 |
| MIP | | Mercury Intrusion Porosimetry |
| MR | | Marble samples treated stored in room condition |
| MRS | | Marble samples treated stored in room condition and sprayed regularly with carbonated water |
| MTMOS | | Methyltrimethoxysilane - Consolidant product |
| M55 | | Marble samples treated and stored in 55%RH |
| M75 | | Marble samples treated and stored in 75%RH |
| NAN | | Samples treated with Nanorestore Plus |
| NHLE | | National Heritage List for England |
| P | Pascal [P] | Pressure |
| Qf | g | Weight at asymptotical value (total absorption) by LNEC standard |

| | | |
|---|---|---|
| r | | Radius |
| RH | | Relative Humidity |
| S | $cm^2$ | Base area of the specimen |
| SEM | | Scanning Electron Microscopy |
| SR-LAQ | | Samples treated with sticky rice and nanolime |
| STT | | Scotch Tape Test |
| $S_o$ | [N] Newton | Strength before the treatment |
| $S_f$ | [N] Newton | Strength after the treatment |
| S1 | | Biocalcarenite stone treated with WIP |
| S2 | | Biocalcarenite stone treated with WIP* |
| S3 | | Biocalcarenite stone treated with B |
| S4 | | Biocalcarenite stone treated with WIP |
| S5 | | Biocalcarenite stone treated with WIP |
| S6 | | Biocalcarenite treated with WIP |
| SR | | Samples treated with Sticky rice |
| TEM | | Transmission Electron Microscopy |
| TEOS | | Tetraethyl orthosilicates - Consolidant product |
| Ut | g | Absorbed water at different time, calculated by Ut = Wt - Wo |
| UV-VIS | | Ultraviolet-Visible Spectrophotometry |
| Vs | $cm^3$ | Volume of the sample |
| W | | Samples treated with LAQ dispersed in water |
| Wa | g | Weight at asymptotical value (total absorption) by EN 13755 standard |
| WAC | $g / m^2 \ sec^{0.5}$ | Water Absorption capillarity by EN 13755 standard |
| Wc | g | Final weight of the sample after 28 days after several treatments |
| WET | | Samples treated with LAQ dispersed in 50-50% Water-ethanol |
| Wf | g | Final weight. In the case of treatment, |

| | | weight of the sample after the treatment |
|---|---|---|
| WIP | | Samples treated with LAQ dispersed in 50-50% water-isopropanol |
| Wt | g | Weight of the sample at different times |
| Ws | g | Weight of the sample after 24 hours immersed in water |
| Wo | g | Initial weight. In the case of treatments, the weight of the sample before the treatment |
| wt% | % | weight percent (%) |
| w/w% | % | Mass fraction for percent mass (%) |
| w/v% | % | Weight of solution in the total volume |
| XRD | | X-Ray Diffraction |
| XRF | | X-Ray Fluoresce |
| $\psi$ | g / cm$^3$ | Solvent content |
| $\gamma$ | N·m$^{-1}$ | Surface tension |
| $\theta$ | | Contact angle |
| $\Delta E$ | | Total Color variation |
| $\Delta L$ | | Colour variations, change in white-black |
| $\Delta a$ | | Colour variations, change in red-green |
| $\Delta b$ | | Colour variations, change in blue-yellow |
| $\Delta F$ (%) | % | Percentage of the difference of strength |
| $\Delta P$ | Pascal [P] | Difference of pressure |
| $\Delta W$ | (g/cm$^2$) | Difference of weight |
| $\Delta W$ (%) | % | Percentage of the difference of weight |
| $\rho$ | g/ml | Density |

# List of Figures

# List of Tables

# List of equations

# Table of contents

# Chapter 1:

# Introduction

Cultural heritage refers to the legacy of tangible artefacts and their intangible attributes that are inherited from the past by a group or society and conserved for future generations due to their artistic, cultural or historic value [ICOMOS, 1964]. The conservation of built cultural heritage is regulated by the Government of the United Kingdom by the *Ancient Monuments and Archaeological Areas Law*. This law was promulgated in 1979 to establish a legal framework to ensure the protection, conservation and dissemination of the Cultural Heritage of the United Kingdom. This law states that any conservation and restoration works undertaken in a Cultural Heritage property inscribed on the National Heritage List for England (NHLE) must be carried out taking into consideration the newest developments of science and technology in heritage science.

This doctoral thesis aims to be a scientific contribution to the safeguarding of heritage structures by the study of new lime-based nanomaterials for the conservation of calcareous substrates.

## 1.1 Definition and relevance of the topic

One of the most relevant conservation principles, promulgated by the *Athens Charter for the Restoration of Historic Monuments in 1931* [ICOMOS, 1931], states that historic objects or structures with significant value (artistic, cultural or historical) must be, whenever possible, restored and preserved. Calcareous materials (e.g. limestone, lime-based mortars or plasters) are important construction materials used in Cultural Heritage throughout the history around the world. These substrates are susceptible to several weathering processes (e.g. freeze-thaw, salt damage, dissolution or acid attack) which lead structures to lose some of their original properties [Doehne and Price, 2009].

Consolidation products are used to restore material's original properties. These consolidants must be physico-chemically compatible with the matrix and they must mainly restore the mechanical properties [ICOMOS, 1964]. In recent years the most

used consolidating products are silica-precursor consolidants (e.g. TEOS or MTMOS). These products are used in restoration treatments thanks to their ease of application, good penetration and immediate strength enhancement [Wheeler, 2005]. However, in the case of calcareous substrates, the low physical and mechanical compatibility with the mineral substrate can cause cracks and significant damage in the long-term [Wheeler, 2005; Wheeler, 2008; Ferreira-Pinto and Delgado-Rodrigues, 2008b]. For that reason, a lime-based consolidant (i.e. lime-water) has been traditionally preferred due to its high compatibility and durability [Baglioni et. al., 2014]. However, this technique presents some important limitations such as the reduced impregnation depth and the very slow carbonation process, which in many cases leads to unsatisfactory treatments [Price et. al., 1988].

Nanolime dispersions were created to overcome the limitations of the lime-water technique. The smaller size of the lime particles improves the consolidation effectiveness as the nanoparticles are more reactive and reach higher penetration depths. The popularity of nanolime has been growing since its first synthesis in 2001. Both of the commercial nanolime products (Calosil® and Nanorestore®) have been proven to be effective products for superficial consolidations (e.g. wall-paintings, stuccoes or plasters). In contrast, the results for deeper consolidations of high porous substrates are fewer and often controversial with some unsatisfactory results [Costa and Delgado-Rodrigues, 2012].

Nanolimes are applied in a wide range of concentrations (i.e. 5, 15, 25 or 50 g/L), solvents (i.e. ethanol, propanol, water or a mixture of solvents), application methods (i.e. spray, immersion, absorption by capillarity or brush) and are applied on substrates with different pore structures and mineralogical composition (i.e. lime mortar, limestones, etc). Moreover, nanolimes can be synthesised according to several routes (solvothermal, hydro-plasma, drop to drop method, anion exchange resins, etc.) which lead to nanoparticles with different features (e.g. size, colloidal stability or reactivity). This wide range of variables makes it very difficult to draw accurate conclusions and to establish reliable comparisons among the research data of the literature of each nanolime product. Additionally, there is a lack of documented in-situ consolidation treatments and a lack of research about the nanolime long term performance.

**1.2 Objectives of the research**

This project aims to understand the consolidation mechanism of nanolime in high porous substrates and investigates how to improve nanolime consolidation effectiveness.

This PhD research proposes the following objectives:

- To review existing knowledge of nanolime to produce an overview-paper for publication about the synthesis, applications and factors influencing the performance of nanolime.
- To characterise the two available commercial products (Calosil® and Nanorestore®) and a newly patented nanolime by the University of L'Aquila.
- To provide the first comparison of the consolidation effectiveness of these three nanolimes in highly porous substrates.
- To determine the durability of these three nanolime treatments.
- To determine the influence of different types of solvent on the consolidation effectiveness of L'Aquila nanolime.
- To determine the influence of pore size distribution and nanolime particle size in consolidation treatments.
- To assess the suitability of nanolime for the consolidation of limestone from selected historic structures (Agrigento's biocalcarenite (Agrigento, Italy), Doulting stone (Cathedral of Wells, UK), and Indiana limestone and marble (Smithsonian's National Portrait Gallery in Washington DC, USA) providing the scientific support for a potential in-situ consolidation treatment of these structures.
- To identify additives that can improve nanolime performance.
- To determine the consolidation effectiveness of sticky rice.
- To determine the consolidation effectiveness of a combined sticky-rice-nanolime treatment.
- To assess the durability of sticky rice treatments.
- To develop an optimal nanolime application method.

To achieve these research objectives an experimental research has been carried out at Sheffield Hallam University (UK), the Smithsonian's Museum and Conservation Institute (MCI, USA) and the University of L'Aquila (Italy).

**1.3 Outline of the thesis**

This thesis is composed of five chapters (introduction, literature review, materials and methods, results and conclusions). The appendices comprise a report carried out at the Smithsonian's Museum Conservation Institute (MCI, Appendix A) and the published papers (Appendix B).

**Chapter 2** considers the state of the art and reviews the most relevant literature concerning the consolidation of calcareous substrates and nanolime. This chapter is divided into five sub-chapters:

- *2.1 Historic structures* describes the most common calcareous substrates found in heritage structures.
- *2.2 Decay processes* describes the most common weathering processes of calcareous substrates and describes the most common decay patterns.
- *2.3 Criteria for consolidation* describes the most relevant requirements that a consolidant must meet to achieve an effective consolidation.
- *2.4 Consolidation products* describes the most used consolidation products used in the conservation of heritage structures.
- *2.5 Nanolime as a consolidation method for calcareous substrates* reviews the most relevant literature on nanolime and describes different synthesis routes, applications and factors that influence nanolime performance. The content of this last sub-chapter has been published in the peer-review Journal *GE-Conservation* (DOI: 10.17265/2162-5298).

**Chapter 3** describes the materials and methods used in this research. It details the type of substrates, synthesis of nanolime, nanolime commercial products and lime mortar manufacturing process used in this research. It also details the methodology used to: i) characterize the nanolime products; ii) characterize the substrates; iii) characterize the sticky rice; and iv) evaluate the consolidation effectiveness. Finally it also describes the six research programmes:

1) The literature review points out the need of a robust comparison of the two commercial products (Calosil® and Nanorestore®) and a new nanolime product in process of being commercialized (University of L'Aquila). Thus, the first research programme is a comparison between these three nanolime products. This research is focused on the study of the properties of the nanolime products (reactivity and morphology before and after carbonation) and the consolidation effectiveness in high porous substrates. Finally, this research is also focused on the durability of the consolidation treatments.

2) The review of the most relevant literature also pointed out that the effectiveness of nanolime can be influenced by several factors such as relative humidity, $CO_2$ conditions, type of solvent and nanolime concentration [López-Arce et al. 2010, Taglieri et al, 2017b]. Recent studies [Borsoi et al, 2015a, 2016], concluded that nanolime deposition in the pores is highly influenced by the type of solvent. These researches concluded that nanoparticles tend to migrate back to the surface during the evaporation of the solvent and therefore solvents with slower evaporation rate can enhance the deposition of nanoparticles in the pores in highly porous substrates. Based on this research, research programme 2 aims to study the influence of different types of solvent solvents on the consolidation effectiveness of L'Aquila nanolime in high porous lime-mortars.

3) Nanolime products present a large difference in particle size between products. The aim of this research is to study the influence of substrate pore structure and nanolime particle size on the effectiveness of nanolime treatments. The research is carried out by using two limestones with different pore structures and two nanolimes with different particle size, Nanorestore® (150 to 300 nm) and L'Aquila (20 to 80 nm).

4) The results of this research were published in the Journal of Cultural Heritage (https://doi.org/10.1016/j.culher.2017.11.003). This research carries out preliminary investigations to test the compatibility of a nanolime treatment (LAQ) in biocalcarenite stones from Agrigento, Italy. These stones constitute the building material used for most of the buildings of the UNESCO "Valley

of the Temples" in Agrigento-Sicily, Italy, which is characterised by documented decay [Rossi-Manaresi 1982, Rossi-Manaresi 1991].

5) This research carries out preliminary investigations to test the compatibility of a nanolime treatment in two stones: Indiana limestone (one the most used limestones as building material in USA), and a weathered marble extracted by the Smithsonian's National Portrait Gallery in Washington DC (USA). This research also tested the effectiveness of the nanolime treatment in different environmental conditions in order to study their influence on carbonation.

6) This research carries out investigations to study the use of additives to improve nanolime consolidation effectiveness. Preliminary research was carried out at the Smithsonian's Museum Conservation Institute (MCI) testing several additives: carbonated water, sticky rice and urea ($NH_2CONH_2$). The promising results about the use of one of the additives, i.e. sticky rice, were extended at the Sheffield Hallam University labs testing the effectiveness of a solution of sticky rice as a consolidation treatment alone and in a combined treatment with nanolime. This research also studied the durability of both treatments involving sticky rice.

**Chapter 4** describes the results of the research programmes. The chapter is divided according to the results of the research programmes.

– **4.1**. *A comparison of three nanolime available products* describes the results of the characterisation of the three products in terms of morphology, reactivity, mineralogical composition and colloidal stability. This sub-chapter also describes the results of the consolidation effectiveness and the results of the durability test of the three treatments in highly porous lime-mortars.

– *4.2 Influence of different types of solvent on the effectiveness of nanolime treatments* describes the results of the characterisation of five nanolime dispersions in terms of reactivity, mineralogical composition, colloidal stability and evaporation rate of solvent. This sub-chapter also describes the

results of the consolidation effectiveness of each treatment in highly porous lime-mortars.

- – *4.3 Influence of substrate pore structure and nanolime particle size on the effectiveness of nanolime treatments* describes the results of the consolidation effectiveness of two nanolime products with different nanoparticle sizes (Nanorestore and L'Aquila) on two limestones with different pore size distribution to assess the influence of substrate pore structure and nanolime particle size on nanolime treatments.

- – *4.4 Preliminary investigation of compatible nanolime treatments on Biocalcarenite from Agrigento (Italy)* describes the results of the characterisation of three nanolime dispersions in terms of morphology, reactivity, mineralogical composition and colloidal stability. This sub-chapter also describes the results of the consolidation effectiveness of nanolime treatment on a biocalcarenite stone.

- – **4.5** *Preliminary investigations of compatible nanolime treatments on Indiana limestone and weathered marble from the Smithsonian building* describes the results of the consolidation effectiveness of nanolime on two calcite-based stones (i.e. Indiana limestone and weathered marble) in different environmental conditions.

- – *4.6 The use of additives to improve nanolime effectiveness* describes the results of the experimental research carried out to study the influence of different additives on the carbonation of nanolime. This sub-chapter also included the results of the consolidation effectiveness of sticky rice and a combined treatment of sticky rice-nanolime, and the results of the durability tests of both consolidation treatments.

Finally, conclusions and future work of the Ph.D. are summarized and discussed in Chapter 5.

# Chapter 2
# Literature Review

## 2.1 Historic structures

### 2.1.1 Natural calcareous substrates

Cultural heritage refers to the legacy of tangible artefacts and their intangible attributes that are inherited from the past by a group or society and conserved for future generations due to their artistic, cultural or historic value [ICOMOS, 1964]. One important part of the tangible heritage is represented by architectural and archaeological structures. A large number of historic structures in the UK are made of calcareous building materials (e.g. limestone and lime mortar) due to the abundance of calcareous rocks in the country's geological context. These materials have been used since ancient times as their strength and durability make them well-suited for the construction of columns, beams, capitals, arches, catenaries, retaining walls, abutments, dams, barrages, roads, etc. [English Heritage, 2012a].

Calcareous rocks can be of either sedimentary or metamorphic origin. Sedimentary rocks are the result of the compaction and cementation of loose sediment through geological times. Metamorphic rocks are formed when rock material is subjected to intense heat and pressure in the crust of the earth, causing its properties to change. The main types of sedimentary and metamorphic calcareous rocks are listed below:

- **Limestone** – Limestones are sedimentary rocks composed mostly of calcium carbonate ($CaCO_3$, in the form of calcite, aragonite or vaterite). They often contain small amounts of other minerals such as quartz, clay minerals, feldspars or mica. Limestone is an important construction material in many historic buildings around the world. In the UK, examples of important historic buildings built using limestones of various types are St. Paul's Cathedral (Portland stone), the Llandaff Cathedral (Dundry and Lias stone), and the Wells Cathedral (Doulting stone, Fig. 1a).

- **Dolomite** – Dolomite is a sedimentary carbonate rock composed of calcium and magnesium carbonate ($CaMg(CO_3)_2$. It is also called "magnesium

limestone" as it contains between 5 to 40% of magnesium carbonate [Tucker, 2003]. Dolomite was used as a construction material in important buildings such as the House of Parliament at Westminster and the York Minster (Fig. 1b).

- **Travertine** – Travertine is a sedimentary rock formed by the precipitation of carbonate minerals deposited from fresh waters in various environments such as spring (including hot springs), waterfalls, fluvial and lacustrine. It can be extremely porous and usually appears light in colour [Tucker, 2003]. Travertine was extensively used during the Roman Empire as a building material for aqueducts, monuments and amphitheatres. Travertine is the main construction material of the UNESCO World Heritage Site of the Colosseum (Rome, Italy, Fig. 1c), as well as the 20th century Getty Center (Los Angeles, USA).

- **Marble** – Marble is a metamorphic rock originating from the recrystallization of limestone or dolomite. Marble has been extensively used since classical times for sculptures and as a building material due to its homogeneity, ease of carving and relatively good resistance to shattering [Tucker, 2003]. Marble is the main construction material in UNESCO World Heritage Sites such as the Taj Mahal (Agra, India) and the Parthenon (Athens, Greece, Fig 1d).



a)                                          b

Figure 1. Calcareous stones used in Cultural Heritage: a) Wells Cathedral (Somerset, UK); b) York Minster (North Yorkshire, UK); c) UNESCO World Heritage Site of the Colosseum (Roma, Italy); d) UNESCO World Heritage Site of the Parthenon (Athens, Greece).

Limestones are classified according to two classification schemes:

– **Folk classification** – This classification, devised by Robert L. Folk [Folk, 1959], divides limestones into two groups: allochemical and orthochemical (Fig. 2). Allochemical rocks contain grains (allochems) that may consist of fossils, ooids, peloids or intraclasts, which are embedded in a matrix. Allochems can be contained in a microcrystalline calcite matrix (also called micrite) or in a sparry calcite cement (also called sparite). Orthochemical rocks are rocks in which the carbonate has crystallised in place.
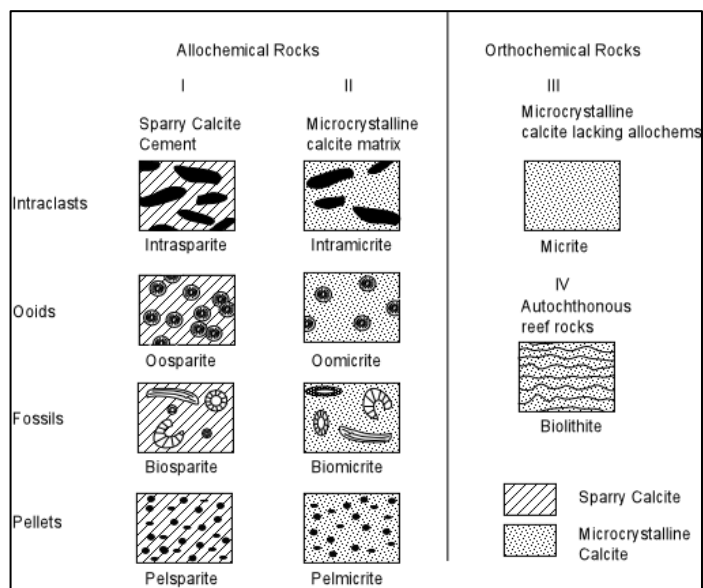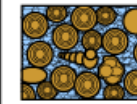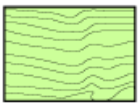


Figure 2. Folk Classification (image: Folk, 1959)

- **Dunham classification** – This classification, which was modified by Embry and Klovan in 1971 [Dunham, 1962; Embry and Klovan 1971], is based on the depositional texture of the rock (Fig.3). The classification divides limestones into two groups; those whose original components were not bound together during deposition and those whose original components formed in place and consist of intergrowths of skeletal material. The first group is further subdivided into mud-supported and grain-supported textures.



C. G. St. C. Kendall, 2005 (after Dunham, 1962, AAPG Memoir 1)

**Figure 3**. Dunham Classification (image: www.sepmstrata.org/page.aspx?pageid=89)

*2.1.2 Artificial calcareous substrates*

Lime mortar can be defined as a mixture of aggregates, water and lime (and in some cases other additives) in the proportions necessary to give the mixture proper workability in its fresh state and adequate physical (porosity, permeability to water, etc.) and mechanical (resistance, deformability, adhesion, outward aspect, durability, etc.) properties in its hardened state [BS EN 459-1-2015]. The construction of the majority of buildings from ancient Rome to the 19th century involved the use of lime mortars in floors, masonry work, wall paintings, renders and architectural sculptures. The earliest documented use of lime as a construction material dates back to approximately 4,000 B.C. when the ancient Egyptians used lime mortars for plastering the pyramids [Mtani, 2015]. In addition, it is well documented that the

Roman Empire used lime-based mortars extensively throughout its history and Vitruvius, in his book *De Architectura* [Vitruvius, 1962], provides guidelines for lime mortar's uses and mixes. For centuries, this book has been used as a guideline by manufacturers around the world in relation to the extraction of binders, processing, mixing proportions, aggregates and application methods.

According to the BS EN 459 standard, the components of lime mortar are:

- **Binder** – Binders are materials that, when mixed with water, generate plastic masses that harden - resulting in a compact mass that is resistant to mechanical stresses and atmospheric agents [Gottardi, 1978]. Two main types of binder are used in lime mortars:

  - **Non-hydraulic lime** – Also known as hydrated lime or air lime. Air lime is used for the preparation or the production of materials used in building construction as well as in civil engineering when appropriately batched and mixed with water, forms a paste that improves the workability (values of flow and penetration) and water retention of mortars. The carbonation of hydrates in contact with atmospheric carbon dioxide forms calcium carbonate which develops strength and contributes to the durability of mortars containing building lime (hence the name of air lime) [BS EN 459-1:2015]. Non-hydraulic lime is produced by burning chalk or limestone (>95 % $CaCO_3$) at 850-900 °C to form quicklime (calcium oxide). The following endothermic reaction takes place during the burning process:

  $$CaCO_3 \rightarrow CaO + CO_2 \qquad (1)$$
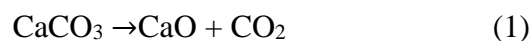
  Once this process is completed, the quicklime is mixed with water in a process called slaking. During the slaking the calcium oxide reacts with water to produce calcium hydroxide in an exothermic reaction, according to this formula:

$$CaO + H_2O \rightarrow Ca(OH)_2 \qquad\qquad (2)$$
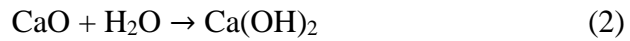
If the amount of water used in the slaking process is calculated stoichiometrically, lime in powder form (also called hydrated lime) is produced. If the quicklime is slaked with an excess of water, the final product is called lime putty. Lime putty is a traditional material described by Plinius and Vitruvius in ancient times [Pliny, 1971; Vitruvius 1962]. Both hydrated lime and lime putty have the same chemical composition, but while hydrated lime is powder form, lime putty consists of a paste with plastic consistency. Both hydrated lime and lime putty set and cure in air, by reacting with $CO_2$ in a process called carbonation:

$$Ca(OH)_2 + CO_2 \rightarrow CaCO_3 + H_2O \qquad\qquad (3)$$

Sub-families and forms of air lime are given [BS EN 459-1:2015]:

- Sub-families of air lime
    - Calcium lime (CL) – Calcium lime is an air lime consisting mainly of calcium oxide and/or calcium hydroxide without any hydraulic or pozzolanic addition.
    - Dolomitic lime (DL) – Dolomitic lime is an air lime consisting mainly of calcium magnesium oxide and/or calcium magnesium hydroxide without any hydraulic or pozzolanic addition
- Forms of air lime
    - Quick-lime (Q) – Quicklime is an air lime mainly in the oxide form which reacts exothermically on contact with water. Quicklime is available in a range of sizes from lump to powder
    - Hydrated lime (S, S PL or S ML) – Hydrated lime is an air lime mainly in the hydroxide

form produced by the controlled slaking of quicklime. Hydrated lime is available as powder (S), putty (S PL) or slurry (S ML).

Conformity of air lime concerning strength, physical and chemical properties are included in the European Standard [BS EN 459-1:2015].

**Hydraulic lime** – Hydraulic lime is a binder that sets and hardens through reaction with both air (carbonation) and water (hydration). It is produced in the same way as non-hydraulic lime, but using limestones containing clay (6 to 20%) [Pecchioni et. al., 2008; English Heritage, 2012b] and higher burning temperatures (900 - 1050 °C). During its calcination the clay minerals (hydrous aluminium silicates) dehydrate forming free silica ($SiO_2$), alumina ($Al_2O_3$) and iron oxides (FeO) that combine which calcium oxide (CaO) forming calcium silicates ($Ca_2SiO_4$), aluminates ($CaOAl_2O_3$) and ferrites ($CaFe_2O_3$). The hardening occurs by both carbonation and the reaction of calcium silicates and aluminates with water in a reaction called hydration. The resulting material is composed of calcium carbonate and calcium silicates and aluminate hydrates, which contribute to the setting and hardening of the mortar [Mariani, 2006]. Hydraulic lime sets faster than non-hydraulic lime due to the hydration process occurring, and it has higher final strength than non-hydraulic lime and is also less breathable and flexible [English Heritage, 2012b].

- **Aggregates** – According to the BS EN 13139, aggregates are granular material used in construction to deliver mechanical properties. Aggregates are a broad category of coarse to medium grained particulate material that are used in construction and can be composed of sand (fluvial, quarry or marine), artificial crushed rocks, natural pozzolanic materials, artificial pozzolanic materials or hardened mortar fragments [BS EN 13139]. Coarse aggregates are granular materials with aggregate sizes of 4 mm or higher, fine

aggregates are granular material with smaller aggregate size less than 4mm, and fines are particle size faction of an aggregate which passes the 0.063mm sieve [BS EN 13139]. Aggregates are used to strengthen the overall composite material. All aggregates should be washed to eliminate impurities which can negatively affect the setting process and durability of the mortar [Pecchioni et. al., 2008]. The size and mineralogical composition of the aggregates have a significant effect on the performance, mechanical strength, porosity and appearance of lime mortar [Pecchioni et. al., 2008]. The use of aggregates with a wide range of sizes allows smaller grains to fill the space among bigger grains, reducing both porosity and shrinkage of the mortar [Pecchioni et. al., 2008]. The morphology of aggregates also influences the workability of mortar in the fresh state [Geoffrey, 2003]. The specific surface of the aggregate grains affects their adhesion to the binder and the amount of water that needs to be added to the mixture [Pecchioni et. al., 2008].

– **Water** – The quality of water can affect the setting and strength of the mortar. Water should not contain organic impurities or dissolved salts as these can be detrimental to the durability and hardening of the mortar [Pecchioni et. al., 2008]. Water should be used in appropriate amounts as it affects mortar porosity; mortars made with too little water will have too low workability, while too much water will decrease mortar strength by holding the grains apart, thus leaving an open structure when dry [Pecchioni et. al, 2008].

– **Additives** – Additives are substances which are added to the mortar mixture to improve certain properties (e.g. mechanical properties or hydrophobicity) and/or increase workability. The main types of additives that have been used in lime mortars throughout history are of proteinic nature, polysaccharides (i.e. sugars), oils, and fats [Pecchioni et. al., 2008]. Such as wax, egg white, gypsum, keratin, rice flour, cactus, blood and casein [Biçer-Simsir et. al., 2009].

The main applications of mortars for traditional buildings have historically been [English Heritage, 2012b]:

- **Bedding** (Fig. 4a) – Bedding mortars are used to lay down masonry units (brick or stone) in wall construction or as preparatory layers for pavements. They are usually mixed at a 1:2.5 (lime:sand) ratio [English Heritage, 2012b].

- **Pointing** (Fig. 4b) – Pointing is a technique for filling joint faces, whereby bedding mortar is deliberately raked out to receive additional mortar during the construction work. It is typically mixed at a similar lime:sand ratio (1:2.5) as bedding mortars [English Heritage, 2012b].

- **Rendering** (Fig. 4c) – Internal and external lime renders were traditionally applied to both disguise and protect walls. Materials and techniques for application and finishing have varied enormously over time, geographically, and depending on the status of the building [English Heritage, 2012b]. Renders were traditionally applied in three layers to allow for a smooth finish and sufficient breathability [Vitruvius, 1962]: The first and second layer from the substrate generally consisted of a lime putty at a ratio of 2:5 proportions (lime:sand), and the third external layer at a ratio of 2:3 (lime:sand) and finer sand [Vitruvius, 1962].

- **Stuccoes** (Fig. 4d) – Stucco, an Italian word meaning *plaster,* nowadays refers to both decorative plasterwork coating for walls and ceilings and sculptural and artistic materials in architecture. Traditional stucco is made of lime, fine sand aggregates and water, with gypsum often being added to accelerate the setting process [English Heritage, 2012b].



a)
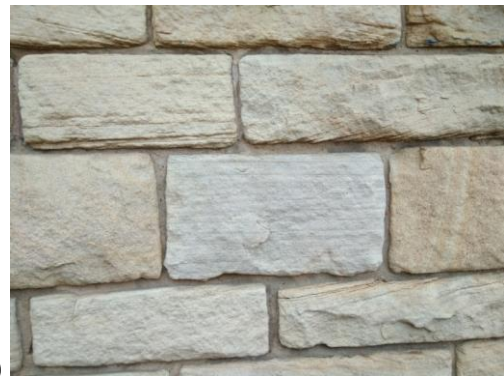


b)

**Figure 4.** Applications of mortar: a) bedding a stone floor (image: buildingconservationdirectory.com); b) pointing of St William of York Church, Sheffield; c) lime rendered buildings in Plaza de Mazarelos, UNESCO World Heritage Centre of Santiago de Compostela (Galicia, Spain); d) decorative stucco at Craigievar Castle in Abeerdeenshire, Scotland, UK.

## 2.2 Decay processes in calcareous substrates

The main processes of deterioration affecting calcareous substrates are described in this sub-chapter. The vulnerability of calcareous materials depends on their inherent composition as well as on various environmental factors [Doehne and Price, 2009].

*2.2.1 Properties of calcareous substrates that control their deterioration processes*

The main interacting factors in the deterioration processes affecting calcareous substrates are:

- **Mineralogical and chemical composition** – The chemical and mineralogical composition of the substrate affect its behaviour when it is exposed to the environment. Some minerals present vulnerability to different environmental conditions and can undergo several decay processes such as dissolution in water, swelling, thermal expansion, etc. [Doehne and Price, 2009], which is explained in section 2.2.2. Calcium carbonate is vulnerable to water, acidic conditions (pH < 7) and certain atmospheric pollutants (see section 2.2.2). Additionally, the presence within the substrate of other minerals can lead to other decay processes. For example, clay minerals absorb water causing the mineral to swell, leading to a loss of mechanical resistance in the material [Doehne and Price, 2009]. If present, silicate-based minerals

can also suffer deterioration by hydrolysis (e.g. Na, K feldspar undergo hydrolysis to form kaolinite,etc) [Hansen et al, 2003].

–  **Porosity and pore structure** –Porosity, pore size distribution and pore connectivity represent important factors in substrate conservation [Doehne and Price, 2009]. Pore structure affects water transport within the substrate [Charola and Wendler, 2015] and processes such as the crystallisation of soluble salts [Charola, 2000]. Major decay by soluble salt crystallisation occurs when stones have larger pores connected to smaller pores, which generate a higher crystallisation pressure [Scherer, 1999]. The porosity of calcareous substrates (e.g. limestones) generally tends to be high (10-20%). This means that they can absorb large amounts of water, increasing the risk of decay associated with the presence of soluble salts [Scherer, 1999]. According to the literature, pores are classified as coarse pores (>1mm), micropores or capillary pores (1mm and 0.1 µm) and nanopores (0.1 µm to <10nm) [Charola and Wendler, 2015]. However, there is a vast literature addressing this topic and other authors have classified the pores as macropores (1mm to 1µm), mesopores (1 µm to 0.5µm) and micropores (0.5 µm to 1nm) [Thomson et al, 2007].

–  **Mechanical properties** – The mechanical resistance of stone refers to its ability to resist structural pressures. Mechanical properties are related to mineral isotropy and anisotropy, porosity, type of mineral, orientation of the layers, and the density of the stone [Doehne and Price, 2009].

–  **Thermal properties** – The thermal expansion coefficient and thermal conductivity of minerals influence substrate durability. Building materials expand with temperature and contract when cooled. In the case of calcareous stones, calcite expands and contracts in different directions than other minerals, as calcite crystals are strongly anisotropic if compared with other minerals [Charola et al, 2010].

Thus calcareous stones containing different types of minerals with different thermal expansion coefficients present higher vulnerability. The different minerals can each expand and contract uniquely, causing mechanical stresses between individual minerals and the stone [Doehne and Price, 2009].

*2.2.2 Environmental causes of deterioration*

The main environmental causes of deterioration are:
- **Water** – Water (in any state) can be considered the most important environmental factor as it is involved in most of the decay processes affecting calcareous substrates, which involve physical, chemical and biological deterioration processes. Water can directly generate physical damage through pressure upon freezing (after several freeze-thaw cycles) as water volume increases by 10% when transformed from liquid to solid, causing pore system damage that may result in the formation of micro-fissures and cracks in the structure (see section 2.2.3.). Water can dissolve and transport soluble salts and pollutants which may carry out further decay processes. Water can also generate chemical processes such as the dissolution of minerals (e.g. calcium carbonate) and leaching of the binder in lime mortars which is aggravated in cold conditions and saturated conditions [Forster et al, 2014; Banfill et al, 2016] and physico-chemical processes, such as swelling of clays (expansion and contraction depending on the amount of water present). Water is also essential for the growth of microorganisms and plants [Charola, 2000].

Water can penetrate a building in a liquid or vapour state. As a liquid, water ingress is achieved by capillarity rise from the ground (Fig. 5), or by infiltration of rain waters. Water capillary rise is related to the superficial tension of water and pore diameter [BS EN 459-1-2015]. Materials with large pore diameters (> 0.1 mm) tend to absorb water by capillarity more quickly and also tend to dry more quickly. Contrastingly, a material with many small diameter (< 0.1 mm) pores

will absorb water more slowly, but the water absorbed by capillarity rise reaches higher height in a building structure. The structure will also dry more slowly because pore systems of smaller diameter tend to retain water [Charola and Wendler, 2015]. The water circulation on the structure is also influenced to seasonal variations of relative humidity, temperature and presence of soluble salts [Hall et al, 2010]. In the form of vapour, water penetrates by diffusion into the material pores. The amount of water that will be retained (absorbed) by the material will depend on its characteristics and the environmental relative humidity [Charola et. al., 2009]. Generally, a higher amount of finer pores and a denser structure is associated with greater retention of moisture in the structure, which increases the risk of decay processes such as freeze-thaw or bio-colonization [Charola and Wendler, 2015].
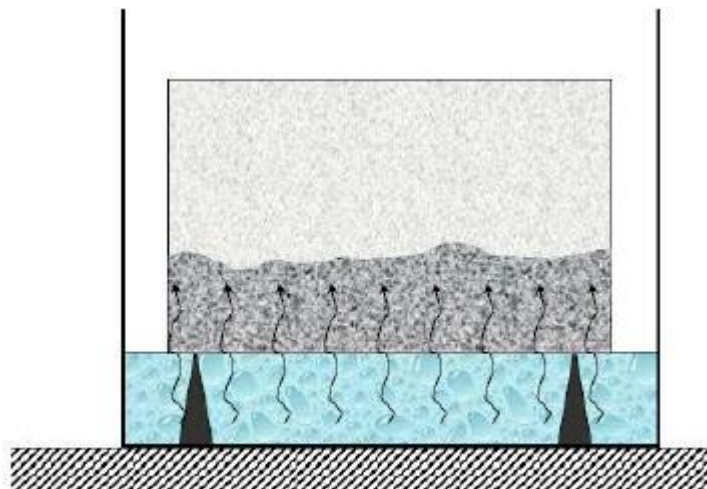


**Figure 5.** Capillary rise in a building (image: Şengün et al, 2014)

The most important decay process caused directly by the action of water in calcareous substrates is the dissolution of the calcium carbonate mineral [Doehne and Price, 2009]. Many minerals present in mortars and building stones, such as calcium carbonate, are thermodynamically unstable. Therefore, these minerals are under-saturated if they come into contact with natural waters, e.g. rainwater [Charola et. al., 2009]. Lime-based materials are highly susceptible to

chemical dissolution by water, which causes the original material to disintegrate. Calcium carbonate, the main component of lime-materials, is a compound which can be considered insoluble in water. However, rainwater always dissolves the carbon dioxide ($CO_2$) present in the air to form carbonic acid ($H_2CO_3$). Carbonic acid is partially dissociated in the bicarbonate ion ($HCO_3^-$), and the hydrogen ion ($H^+$), which is a corrosive agent [Charola et. al., 2009] in the following reaction:

$$H_2O + CO_2 \leftrightarrows H_2CO_3 \leftrightarrows HCO_3^- + H^+ \qquad (4)$$
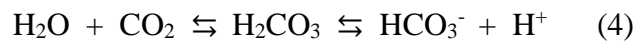
Therefore, "pure" rainwater, even without any pollutants such as sulphur or nitrogen oxides, is acidic with a pH of approximately 5.6 and so dissolves the $CaCO_3$ following this reaction [Charola et. al., 2009]:

$$CaCO_3 + H^+ \rightarrow HCO_3^- + Ca^{++} \qquad (5)$$
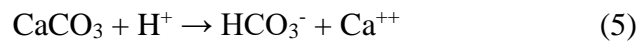
The dissolution of calcium carbonate is a slow phenomenon and its effect is only perceptible in the long term, since it can take several centuries to cause visible effects. This process is accelerated in high porous substrates (porosity >10 %) and in the presence of air pollutants (e.g. sulfuric and nitric acids) [Charola et. al., 2009]. In this case, the pH of the rain decreases to values as low as 3 or 4. Therefore, as pH is a logarithmic function, the concentration of hydrogen ion ($H^+$) is increased between 100 to 1000 times, which accelerates the dissolution process [Charola et. al., 2009]. The dissolution of calcium carbonate in limestones leads to decay patterns such as alveolization or powdering, described in section 2.2.3.

– **Soluble salts** – soluble salts are considered one of the main causes of the decay of porous substrates [Doehne and Price, 2009]. The most common salts affecting structures are sodium chloride (NaCl), gypsum (calcium sulfate dihydrate, $CaSO_4 \cdot 2H_2O$), sodium sulfate ($Na_2SO_4$), magnesium sulfate ($MgSO_4$), potassium chloride (KCl),

and sodium, potassium or ammonium nitrates ($NaNO_3$, $KNO_3$, $NH_4NO_3$) [Charola, 2000]. The origins of these salts are diverse. Some are found in the soil (e.g. $CaSO_4$ or $NaCl$) and the sea (e.g. $NaCl$), while others are generated by biological colonization (e.g. nitrates, sulphates and ammonium), pollution (e.g. nitrates and sulphates) or are present in the material (e.g. mortars with gypsum in its composition) [Charola, 2000]. Soluble salts can cause physico-mechanical damage due to pressure in the pores caused by crystallisation cycles. Soluble salts can enter structures when they are dissolved in liquid or vaporous water. In the liquid state, two mechanisms can be operative [Charola, 2000]:

- **Capillarity rise** of groundwater – This is the result of the absorption of water and capillary pore structure.
- **Infiltration** of rain water – This requires hydrostatic pressure and depends on the permeability of the material.

In a vaporous state, water can enter through two main mechanisms [Charola 2000]:

- **Condensation**:
    - Surface condensation
    - Capillary condensation in pores

- **Hygroscopicity** – The ability of some salts to absorb moisture in the vapour state

Soluble salts contained in a structure (e.g. a wall) do not cause physical damage unless repeated cycles of dissolution, hydration and crystallisation (evaporation and wetting) occur [Charola 2000]. Therefore, it is important to understand the factors that influence salts' dissolution, hydration and crystallisation.

- **Dissolution and hydration** – The dissolution process occurs when crystallised salts come into contact with water, break their bonds, and form new bonds between the crystal ions and water molecules [Charola, 2000, Charola and Blauer, 2015]. The solubility of salts is related to the ambient temperature, relative humidity and maximum concentration of salts in the structure [Goudie and Viles 1997]. Solubility can also vary if other salts are involved [Charola, 2000]. Due to hygroscopicity of soluble salts, they absorb or release water depending on the ambient relative humidity and temperature causing the crystals to dissolve or re-crystallize [Lubelli et. al., 2006]. The transition point of crystallization/dissolution corresponds to the equilibrium relative humidity of the salt (also called *deliquescence point*), which occurs at a specific ambient relative humidity and temperature depending on the type of salt [Charola, 2000]. Each soluble salt has a specific transition point [Charola, 2000]. Thus, when the ambient relative humidity exceeds the salt's equilibrium relative humidity, the salt tends to dissolve. Conversely, if the relative humidity of the environment is lower, the water evaporates, and the salt tends to crystallise [Arnold and Zehnder, 1987]. The damage occurs as this re-crystallization leads to an increase in molecule volume which applies pressure against the pore walls.

- **Crystallisation** – This process occurs when dissolved salt reaches a supersaturation concentration. Supersaturation conditions can be reached in several ways; i) if the temperature decreases and there is no change in the concentration of the saline solution, ii) if the water evaporates, causing an increase in concentration, iii) by a combination of both situations described above [Charola, 2000].

Soluble salts tend to penetrate the structure while dissolved in water and are transported by water through the pore network. When the water evaporates, the salts crystallise in the place where evaporation has occurred [Charola et. al., 2009]. When the material is completely saturated with water, evaporation occurs on the surface of the material causing the salts to precipitate forming efflorescence (described in section 2.2.3) on the surface [Charola, 2000]. Efflorescence on the surface of a material does not cause physical damage. However, when the substrate is not completely saturated, evaporation occurs below the surface and salt crystallisation also takes place beneath the surface (Fig. 6), forming sub-fluorescence or crypto-florescence [Charola, 2000]. These efflorescences are very harmful as they can cause serious damage to the material in the form of detachment or powdering, depending on the texture of the material (described in section 2.2.3).
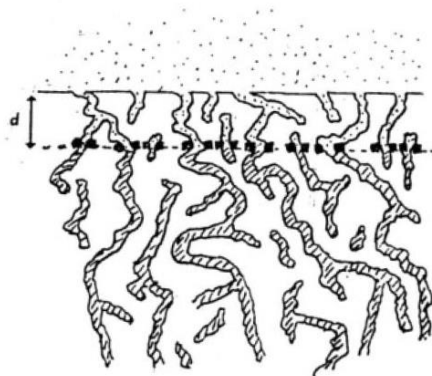


**Figure 6**. Crystallisation of soluble salts in porous material by the evaporation of water. As the material dries, evaporation occurs below the surface, usually in an area parallel to the surface. (Image: Charola, 2009)

- **Pollution** – The main atmospheric pollutants are: $CO_2$, $CO$, $SO_x$, $NH_3$, $O_3$ and $NO_2$ [Watt, 2009]. These pollutants, which are present in the atmosphere (in solid, liquid or gas forms) can cause physico-chemical and aesthetic alterations in calcareous substrates. Air pollutants can originate from both natural (volcanic eruptions, decomposition of organic matter) and anthropogenic sources (industrialization, fossil fuel combustion, vehicle exhausts, etc.). After the industrial revolution in the 18th century and the growth in

the use of motorised transportation (e.g. cars, trucks, etc.), the concentration of pollutants has risen enormously [Doehne and Price, 2009]. There are two processes that can result in the deposition of these pollutants on the substrate [Charola and Ware, 2002]:

- **Dry deposition** – Atmospheric pollutants dispersed in the air deposit on the surface of the substrate.
- **Wet deposition** – Atmospheric pollutants, mainly sulphur oxides and nitrogen oxides, are dissolved in the water present in the air (e.g. rainwater or condensation), following the reactions;

$$SO_2 + H_2O \rightarrow H_2SO_3 \qquad (6)$$
$$H_2SO_3 + \frac{1}{2} O_2 \rightarrow H_2SO_4 \qquad (7)$$
$$NO_x + O_2 + H_2O \rightarrow HNO_3 \qquad (8)$$
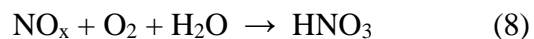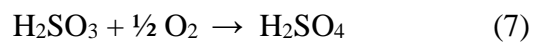
This contaminated water (pH <5) is then deposited on the surface of the substrate.

Both deposition mechanisms are very common in urban or industrialised areas and have received significant attention in recent decades due to the fast deterioration of calcareous substrates in these areas [Charola and Ware 2002, Mitchell and Searle, 2004]. The effect of acidic pollutants on calcareous substrates is the prime cause of decay for calcareous materials in urban areas. This can be seen in the case of structures affected by the so-called acidic rain, which is described below.

*Acidic rain*

Acids have a corrosive effect on calcareous materials. It is well established that either wet or dry deposition of sulphur dioxide significantly dissolves calcium carbonate materials. Sulphuric acid ($H_2SO_4$) further reacts with calcium carbonate materials in a neutralisation reaction [Charola and Ware, 2002]:

$$CaCO_3 + H_2SO_4 \rightarrow CaSO_4 + H_2CO_3 \qquad (9)$$

$$H_2CO_3 \rightarrow CO_2 + H_2O \qquad (10)$$

The precipitation of calcium sulphate ($CaSO_4.2H_2O$, gypsum) entrapping black pollution particles (e.g. soot or dust) forms a black crust on the surface (described in section 2.2.3) that is more soluble in water than calcium carbonate, causing the calcareous material to dissolve and crumble faster. This effect can be exacerbated when other types of pollutants (e.g. NOx), salts (e.g. NaCl) and micro-organisms are present [Grossi et al 2008, Charola and Ware 2002].

–  **Bio-degradation**: Bio-colonization of porous inorganic materials involves a sequence of stages:

▪  **Formation of biofilm** – Water is necessary for all living organisms. Therefore a material which is frequently wet is very likely to be colonized by micro-organisms. A biofilm comprises any group of microorganisms in which cells stick to each other and also often to a surface [Hall et. al., 2004]. The formation of a biofilm begins with the attachment of free-floating microorganisms to a surface [Watnich and Kolter, 2000]. Dust particles, atmospheric pollution gases, pollen, spores and bacteria present in the air become attached to the wet surface and form a rich layer that facilitates the development of microorganisms, commonly called *biofilm* [Charola et. al., 2009]. The consequence of the formation of *biofilm* is that the surface tends to retain more moisture for a longer time, facilitating greater deposition of dust and other substances, as well as the development of microorganisms such as bacteria, algae and fungi (see section 2.2.3, Figure 14a).

- **Formation of lichen** – Once this *biofilm* is formed, lichens can develop, which are associations of algae and fungi [Charola et. al., 2009] (see section 2.2.3, Figure 14b).

- **Formation of mosses and small ferns** – The formation of algae and fungi provides a fertile field for the development of mosses, hepatics and small ferns (see section 2.2.3, Figures 14c).

- **Formation of plants and trees** – The formation of mosses, algae and fungi facilitates the deposition of seeds. Consequently, vegetation begins to grow – first small plants, such as grass or ivy, and later larger plants such as shrubs and trees [Charola et. al., 2009] (see section 2.2.3, Figure 14d).

Deterioration occurs through two fundamental mechanisms:

- **Mechanical or physical action** – Deterioration is caused by the growth of hyphae of fungi, lichens and, fundamentally, plant with roots. The decay mechanism (usually cracks) is due to the growth of roots, rhizoids or hyphae into the substrate, which expand generating stresses that weaken the structure. Some organisms (e.g. fungi) produce less noticeable damage, but can nevertheless contribute to mechanical erosion on the surface and increase its vulnerability to the growth of new colonies of bacteria or fungi [Charola et. al., 2009]. (Section 2.2.3)

- **Chemical action** – Deterioration can be the result of a chemical reaction between acids released by microorganisms and substrate minerals. Such deterioration can be classified according to the type of reaction [Charola et. al., 2009]. In calcareous substrates, the most common reactions are:

- **Acidosis** – This is produced by the dissolution of the substrate and the action of acids such as carbonic acid ($H_2CO_3$), nitric acid ($HNO_3$), sulphuric acid ($H_2SO_4$), etc. These kinds of acid dissolve the calcareous stone and are a source of new microorganisms.
- **Alkalosis** – This results from the release of alkaline or basic compounds, such as $Na^+$ or $NH_4^+$, to form sodium carbonate ($Na_2CO_3$), ammonium carbonate ($(NH_4)_2CO_3$) and some biogenic amines.
- **Formation of complexes or chelates** – This occurs when microorganisms are capable of producing organic compounds that extract specific ions (such as iron, calcium or magnesium) from minerals in colonized calcareous materials to form oxalic, succinic and citric acids, which affect calcareous substrates.
- **Ionic exchange** – Microorganisms and plants can absorb cations such as sodium ($Na^+$) or potassium ($K^+$) as part of their nutritional needs, thus weakening the substrate.

- **Other factors**
  - **Temperature** – Minerals have different thermal expansion coefficients. Materials composed of different types of minerals may experience physical weathering as a result of repeated temperature fluctuations, which cause cycles of expansion and contraction and lead to the formation of fissures and cracks in the material. Substrates composed of different minerals and low porosity (e.g. igneous stones) or soluble salts are more vulnerable to freeze-thaw [De Rosario and Feijoo, 2016]. Temperature is also involved in the physical damage caused by water freeze-thaw cycles, which occurs when water continually seeps into cracks, freezes and then expands,

eventually breaking the rock apart (described in see section 2.2.3).

- ▪ **Wind** – Wind is responsible for the deposition of dust, soluble salts, gases and water on the substrate, which are fundamental in decay mechanisms such as acid rain, calcium carbonate dissolution, microorganisms, etc. Wind also causes mechanical erosion due to the impact of particles (e.g. sand) which are transported by the wind onto the substrate surface [Watt et. al., 2009]. The impact of these solid particles on the surface's material can lead to the gradual erosion of the monument. This impact can be measured as a relation between the density and diameter of the solid particles and the wind speed [Camuffo, 1998].

- ▪ **Animals** – Animals can also contribute to the deterioration of substrates. Insects, birds and rodents can cause physical-mechanical deterioration as they "eat" some of the substrate in mortars (e.g. mortar additives that contains proteins) [Charola et. al., 2009]. In calcareous structures, bird droppings represent the most significant risk, as these deposits are generally very acidic and corrosive to lime-based materials and can also form soluble salts [Charola et. al., 2009].

*2.2.3 Decay patterns*

The decay of calcareous substrates takes place in many different forms. A standardised glossary and terminology to classify the most common decay patterns has been produced by ICOMOS (International Council on Monuments and Sites) [ICOMOS, 2008]. The most common deterioration patterns of calcareous substrates are described below.

- – **Cracks**

  A crack is an individual fissure that is clearly visible to the naked eye. Cracks can be divided in: fracture (crack that crosses completely the stone unite, Fig.

7a), star crack (crack having the form of a star), hair crack (minor crack with width < 0.1 mm), craquele (network of minor cracks, Fig. 7b), and splitting (fracturing along bedding planes). Cracking can be caused by freeze-thaw, vegetation, flaws in the stone, structural pressures, static problems, rusting dowels, too hard repointing mortar, earthquake, etc. [ICOMOS, 2008].



a)                                          b)
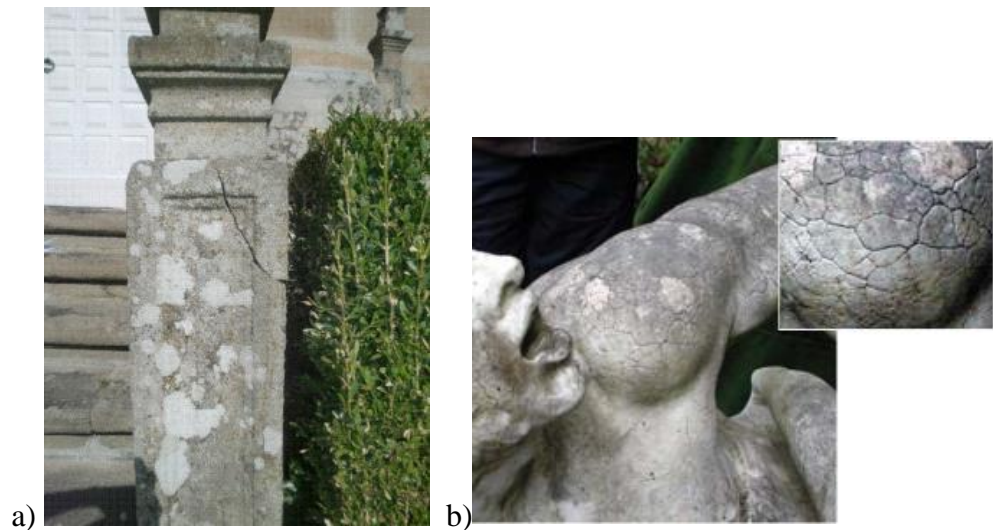
**Figure 7**. Cracks pattern: a) Fissure in a column at the Pazo de A Viña (Galicia, Spain); b) craquele network of a sculpture of Castle Park (Versailles, France) (image, ICOMOS, 2009).

– **Alveolization**

This involves the formation of cavities (alveoles) on the stone surface, which may be interconnected and have variable shapes and sizes (Fig. 8). Alveolization can be associated with other degradation patterns such as disintegration and/or desquamation (described below). Alveolation can be caused by the action of salts or dissolution of calcium carbonate by water or the hydration process of salts [ICOMOS, 2008].



**Figure 8**. Alveolation pattern at the Church of Parroquia de la Mare de Déu dels Dolors, in Manacor (Majorca, Spain).

- **Detachment**

This involves the separation of the most superficial layer of the substrate (parallel to its sound substrate). Detachments can be divided in: Blistering (local swelling of the stone surface, Fig.9a), delamination (affecting laminated stones, detachment in laminae) or exfoliation (detachment in multiple layers sub-parallel to the stone surface, Fig.9b). Most of detachments are caused by crystallising soluble salts (e.g. sub-efflorescences such as $CaSO_4.2H_2O$) and freeze-thaw cycles. [Charola et al, 2007].



a)  b)

**Figure 9**. Detachment pattern: a) Blistering of sandstone (image: ICOMOS Glossary); b) Exfoliation of sandstone ( image: ICOMOS Glossary).

- **Efflorescence**

Efflorescence consists of whitish powdery crystals on the substrate surface (Fig. 10). It is commonly the result of the evaporation of saline water on the surface of porous substrates (described in section 2.2.2). Efflorescence are often constituted of soluble salts such as sodium chloride (halite: NaCl), sulphate (thenardite: $Na_2SO_4$), or magnesium sulphate (epsomite: $MgSO_4.7H_2O$), but they may also be made of less soluble minerals such as calcite ($CaCO_3$), barium sulphate ($BaSO_4$) or amorphous silica ($SiO_2.nH_2O$) [ICOMOS, 2008].
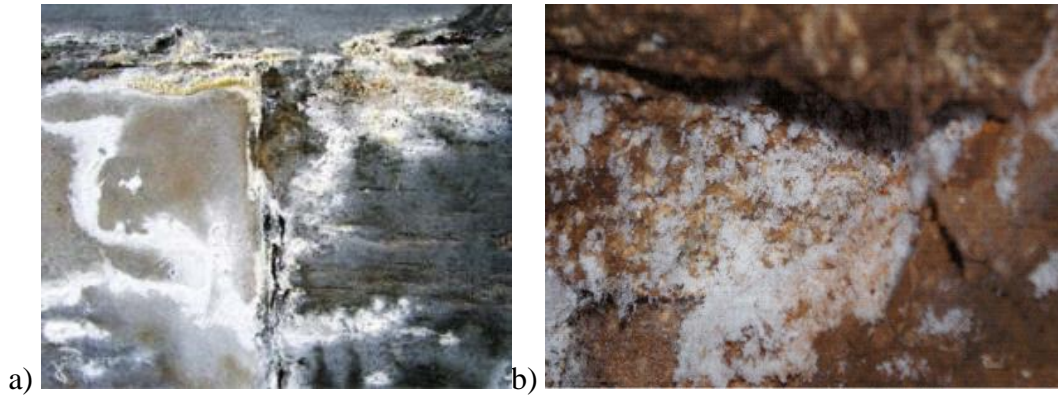
**Figure 10**. Efflorescence pattern: Detail of salt efflorescence at: a) McLennan Arch, Glasgow (Scotland, UK); b) wall at the Pazo de A Viña (Galicia, Spain).

– **Powdering** (or disintegration)

This involves the detachment of single grains of material (Fig. 11). It predominately affects the surface of the substrate, but can also occur at greater depths. Damage generally starts from the surface of the material. It can be divided into subtypes according to the type of affected substrate: powdering (finely grained stones), sugaring (employed mainly for white crystalline marble), sanding (sedimentary e.g. sandstones and igneous e.g. granite stones), etc. Powdering may be caused by the action of water, acidic solutions, pollutants or salts [ICOMOS, 2008].



**Figure 11**. Powdering pattern: a) disintegration due to salt crystallisation of a column at the Pazo de A Viña (Galicia, Spain) b) Sugaring-disintegration of a marble sculpture at the Propyläen, Königsplatz, (Munich, Germany, image: ICOMOS, 2009).

- **Desquamation** (or flaking)

This involves the detachment of a stone scale or stack of scales, not following any stone structure (Fig. 12). The detachment resembles fish-scales, parallel to the stone surface. The thickness of a scale is generally of millimetric to centimetric scale. Desquamation may be the result of salt crystallisation (e.g. NaCl) in the surface and air pollution [ICOMOS, 2008].



a)                              b)
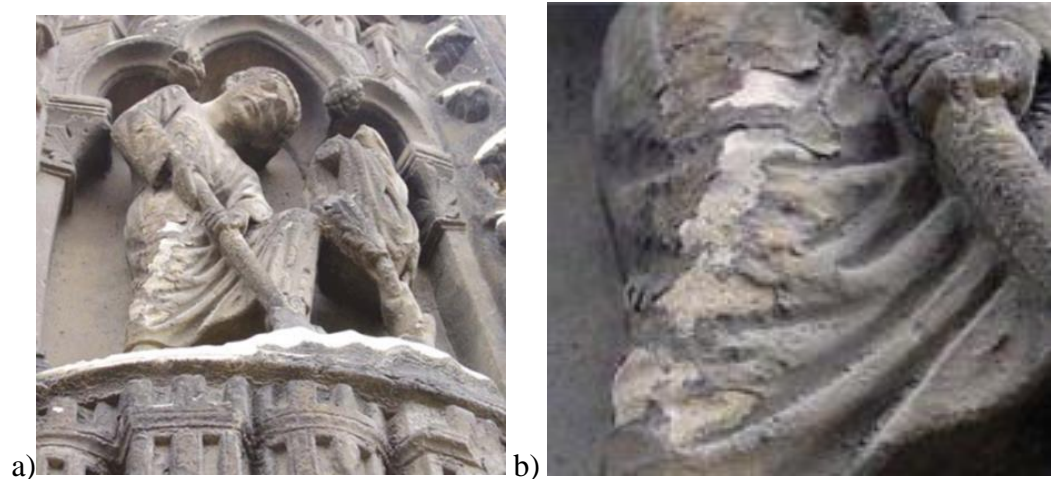
**Figure 12**. Desquamation of a sculpture of the Cathedral of Our Lady of Chartres (Chartres, France, image: ICOMOS, 2009)

- **Crust**

This typically involves the accumulation of materials on the surface of the substrate (e.g. soot and dust). A crust may involve a combination of factors (e.g. pollutants, dust, micro-organism) which react with the stone. A crust is frequently dark coloured (black crust) although light colours can also be found. Crusts may have a uniform thickness and irregular shape (Fig 13a) which can disturb the reading of the stone surface details. One of the most common crusts in calcareous substrates is the black crust formed in urban environments by the formation of gypsum, which absorbs soot, carbon particles, fly ash, etc. as it crystallises (described in section 2.2.2). [ICOMOS, 2008].

**Figure 13**. Crust pattern: a) black crust at the St Giles Cathedral, Edinburgh (Scotland, UK), b) detail of the black crust at the Naumburg Cathedral of St. Peter and St. Paul (Naumburg Cathedral, Germany, Image ICOMOS, 2009).

– **Patina**

This is a chromatic modification of the material, generally resulting from natural or artificial ageing and in most cases not involving visible surface deterioration (Fig. 14). Patinas may be due to the action of bio-colonisation or oxidation of mineral in the stone (e.g. $FeO_3$) [ICOMOS, 2008].
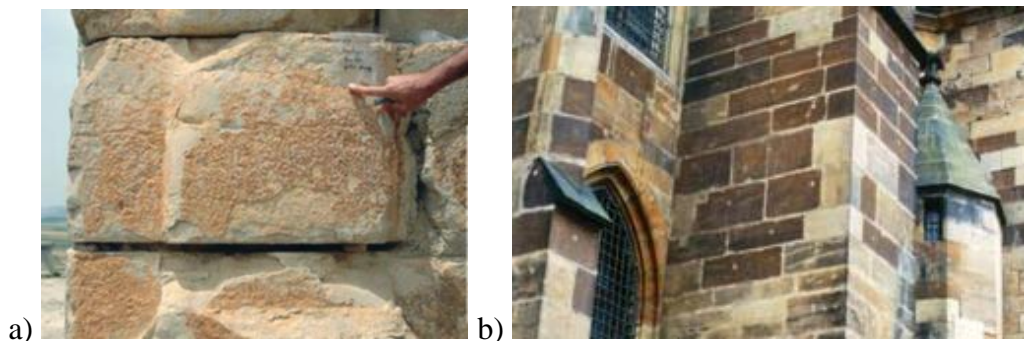


**Figure 14**. Patina pattern: a) oxalate patina developed in limestone at the Volubilis archaeological site (Fes, Morocco, image: ICOMOS, 2009); b) iron rich patina at the Metropolitan Cathedral of Saints Vitus (Prague, Czech Republic, image: ICOMOS, 2009).

– **Biological colonisation**

This refers to the colonisation of a stone by micro-organisms such as bacteria; cyanobacteria; algae, fungi and lichen (symbioses of the latter three); and plants. Biological colonisation can also refer to the influences of other organisms, such

as animals nesting on and in stone (Fig. 15) [ICOMOS, 2008]. Bio-colonisation is described in section 2.2.3.
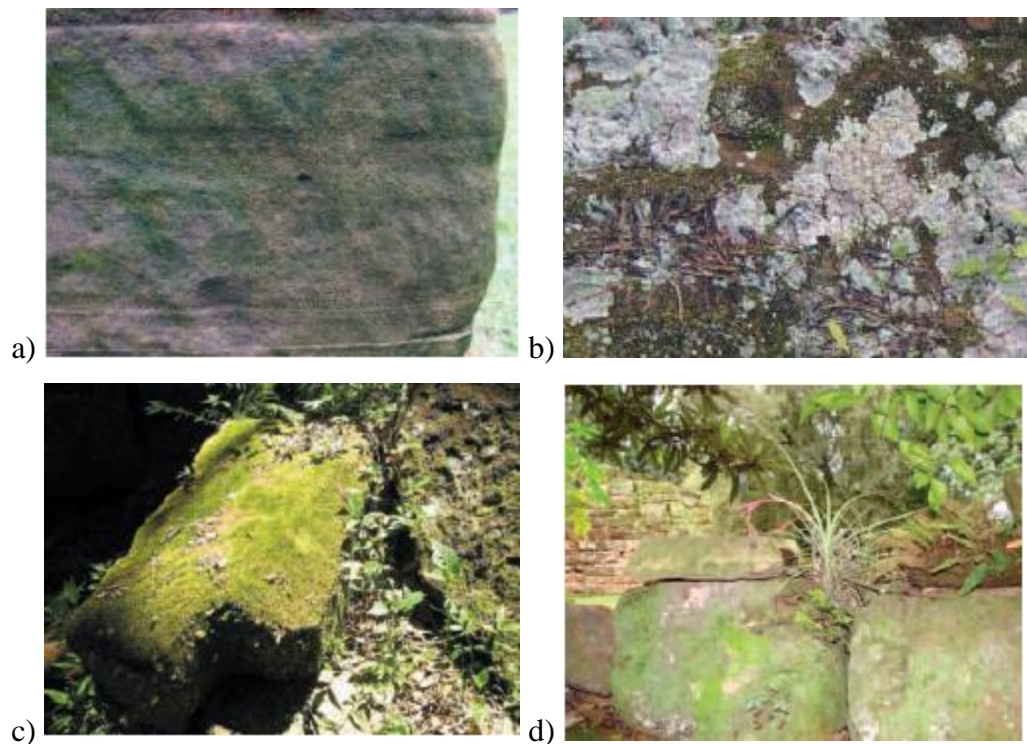


**Figure 15**. Biological colonisation pattern: a) Formation of biofilm; b) formation of lichen; c) formation of moss and plants; d) formation of higher plants. (images: Charola, 2009)

## 2.3 Criteria for consolidation

A consolidation treatment consists of the application of a product onto a weathered substrate (e.g. a substrate affected by disintegration, blistering, desquamation, etc.) to restore its original properties. The application of a consolidating product is necessary to [Young, 1999]:

- recover the cohesion of loose substrate grains.
- recover the cohesion between the weathered layer and the sound substrate.

The criteria that a consolidating product must meet are [Young, 1999; Villegas and Baglioni 2003]:

- **Compatibility with the substrate** – From a chemical point of view, the consolidant should create strong chemical bonds between minerals, and must not affect the crystalline structure of the substrate [Doehne and Price, 2009]. The compatibility can be rated according to its potential inducer of negative effect [Delgado-Rodrigues and Rossi, 2007; Schueremans et al, 2011]. From a physical point of view, the application of the consolidant should yield similar properties for both the treated and untreated substrate, i.e. strength; porosity and thermal expansion must be similar to the original material (inner layer), so that no tensions are created between the treated layer and the inner portion of the substrate [Wheeler et al, 2005]. Compatibility can be analysed by obtaining images of the microstructure being treated using Scanning Electron Microscopy (SEM).

- **Increase mechanical strength** – The treatment must recover the strength of the weathered area to a value similar to that of the sound portion of the treated stone [Wheeler et al, 2005]. Quantitative measurements of substrate strength can be carried out by means of several tests; flexural strength measures (according to European standard BS-EN 12390-5:2009), speed propagation of ultrasound (BS-EN 14579: 2004) or superficial hardness (Scotch Tape Test, ASTM D3359-02). However, none of these tests are suitable to assess the effectiveness of a consolidant product in weathered substrates, as those tests only provide the overall strength of the substrate, and do not provide the strength of the substrate at different depths. For this reason, in 2001, within the framework of the European project EC Hardrock (EC Hardrock SMT4-CT96-2056), a specific tool for this purpose was developed: the "Drilling Resistance Measurement System" (DRMS, section 3.2.5.3.5). The DRMS measures the force required to create a hole at constant rotation (rpm) and lateral feed rate (mm/min). This technique provides information on surface hardness and the depth of penetration of the applied product [Tiano, 2001; Tiano, 2006; Ferreira-Pinto and Delgado-Rodrigues, 2008a].

- **Modify pore structure** – Pore structure is closely related to substrate strength, resistance to salt crystallisation and water freeze-thaw cycles, and water ingress and circulation within the structure [Wheeler et al, 2005]. Generally, weathered

substrates present higher open porosity at the surface. Therefore, the ideal conservation treatment should reduce the porosity on the surface and increase the mechanical strength to values similar to those of the untreated layer [Villegas and Baglioni, 2003]. Porosity must not change abruptly between the treated and untreated area, since this can cause detachments of the treated layer due to salt crystallisation or freeze-thaw decay processes [Young, 1999]. If the treatment significantly increases the number of micropores, the vulnerability of the substrate could even increase, as substrates will take far more time to dry, therefore increasing the risk of biological growth, dissolution and air pollution reactions [Charola et al, 2017]. Treatment must also reduce the amount of capillarity pores (which contribute to capillarity water transfer, and range from approximately 0.1 to 100 micrometres) but not block the coarse pore (bigger than 100 micrometres) to contribute to water permeability. This is commonly called "letting the stone breathe". Porosity measurements can be carried out by means of Mercury Intrusion Porosimetry (MIP), which measures pore size distribution and total pore volume. It can also be accomplished by calculating apparent porosity through immersion in water at atmospheric pressure [ASTM C 97-96].

– **In depth penetration** – Penetration depth is a key factor for the effectiveness of a consolidation treatment [Doehne and Price, 2009]. The consolidation product must adhere both to the untreated and weathered areas. Penetration of the product depends mainly on the microstructural characteristics of the substrate (e.g. open porosity and pore size distribution), properties of the product ( concentration, surface tension, viscosity, etc.), application method and environmental conditions [Daehne and Herm 2013; Baglioni et al. 2014]. The penetrability of the product can be studied using the Drilling Resistance Measurement System (DRMS) or Scanning Electron Microscopy (SEM).

– **Preserve moisture transfer capability** – As water is involved in most decay processes, it is important to study water circulation within the substrate. The behaviour of the substrate in regards to water absorption and loss is a function of its pore system, particularly pore size and distribution [Charola et. al., 2017]. Treatment should reduce the pores with diameter size between approximately

0.1 to 100 micrometres to reduce the structures' absorption of liquid moisture by capillarity and infiltration [Young, 1999]. However, the substrate must remain permeable to water vapour through the substrate in order to prevent the water condensation and the accumulation of harmful agents inside the substrate (e.g. soluble salts and consequent shear stresses) resulting in the dissolution of minerals, growth of bacteria, cracks, blistering, etc. [Doehne and Price, 2009]. Water absorption and loss in a substrate can be calculated by the Standards *Water Absorption Capillary curves and water absorption coefficient* (EN 13755) and *drying curves and drying coefficient* (CEN EN 16322). Water vapour permeability can be measured according to the BS EN 1015-19:1999 standard.

–   **Preserve aesthetic properties** – Consolidation treatments should improve the physical-mechanical properties of the treated material without affecting its aesthetic appearance [ICOMOS, 1931]. However, a side effect of most consolidation treatments (e.g. nanolime) is a chromatic variation of the surface following treatment. Chromatic variations can be assessed using a spectrophotometry test.

–   **Long-term performance** – Demonstrating the long-term effectiveness of a consolidant is essential. There are two approaches to evaluating long-term performance:

  ▪   **Laboratory tests that attempt to accelerate weathering** – These tests expose treated samples to cycles of ultra-violet radiation and moisture condensation to assess their resistance to chemical, photochemical, physical and biological degradation over time. For this purpose, samples can be tested with an Accelerated Weathering Tester (AWT) or through long-term outdoor exposure.

  ▪   **Laboratory tests focused on physico-mechanical behaviour** – These tests measure resistance to salt crystallization (EN 12370), freeze-thaw resistance (BS EN 14617-5:2012), etc.

## 2.4 Consolidation products

During the last century, several consolidation products have been widely used for conservation purposes. These products can be classified in three groups [Villegas and Baglioni, 2003]:

- **Organic consolidants** – e.g. acrylic polymers, epoxy resins, some natural and synthetic waxes, styrene polyester resins, etc. These have a consolidating effect, and in some cases, a hydrophobic effect, due to their composition.

- **Organosilicates consolidants** – e.g. Silicic acid esters and alkoxysilanes. The consolidating action of organosilicates is achieved through the formation of a reticular structure similar to that of silica, making these consolidants well-suited for silica-based materials due to their high compatibility [Wheeler et al, 2005]. The most popular ones are tetraethyl orthosilicates (TEOS) and methyltrimethoxysilane (MTMOS).

- **Inorganic consolidants**: e.g. calcium hydroxide and nano calcium hydroxide (nanolime) in the form of aqueous or alcoholic suspensions, barium hydroxide, alkaline silicates, fluorine derivatives, etc. The main advantages of inorganic consolidants are their long durability, resistance to UV radiation and compatibility with calcareous substrates.

Some of the most widely used consolidating products for calcareous materials are shown in Table 1.

**Table** 1. Consolidating products available on the market

| Commercial name | Company | Type of consolidant |
|---|---|---|
| Tegovakon®V 100 | Evonik | TEOS |
| Paraloid™ B-72 | Rohm & Haas | Acrylic resin |
| ESTEL 1000® | C.T.S | TEOS |
| Mowilith M 30® | Celanese | Acrylic vinyl |
| Primal AC33® | Rohm & Haas | Acrylic polymer |
| UCAD-2o® | University of Cadiz | Nano Siloxane |
| Calosil® | IBZ-Freiberg | Nano $Ca(OH)_2$ |
| Nanorestore Plus® | CSGI | Nano $Ca(OH)_2$ |

In this context, several of those products have been subjected to rigorous testing over several decades. Their effectiveness depends on the characteristics of the substrate on which they are applied, the properties of the product itself, product-substrate compatibility, methods and conditions of application, plus other factors [Doehne and Price, 2009]. Organic and organosilicate products have been widely used in the field of building restoration (involving any type of stone) for the last 50 years. The use of TEOS and MTMOS has obtained very good results for silicate-based stones [Wheeler, 2008]. In the case of calcareous substrates, these consolidants proved to be effective in the short and medium term. However, in the long term, their low compatibility with the carbonate mineral in the substrate and short durability caused substrate degradation. The main drawbacks are:

- **Organosilicates** (e.g. TEOS and MTMOS) – These are able to penetrate into stone to produce mass consolidation. However, these products do not chemically bond with the substrate [Doehne and Price, 2009, Wheeler et al, 2005]. TEOS can fill voids (porosity) but does not promote significant cohesive forces [Doehne and Price, 2009]. The use of alkoxysilanes presents poor compatibility (low chemical compatibility) with calcareous substrates and clay-rich substrates [Doehne and Price, 2009]. This cause cracks on the structure, thus jeopardising it as it is shown in Figure 16 [Wheeler et al, 2005; Wheeler, 2008; Ferreira-Pinto and Delgado-Rodrigues, 2008b].

- **Organics** (e.g. acrylics) – These have; low penetration, usually produce a hard crust, high strength, and high incompatibility between carbonate groups and polymers. In addition, this type of product has poor resistance to high temperatures (60ºC, e.g. Paraloid B-72) and high waterproofing effect of the substrate (such as in the case of waxes) which makes the substrate not permeable to water vapour [Charola and Tucci, 1986].

**Figure 16**. Detachment in limestone due to the incompatibility of TEOS

According to the drawbacks described above, one can conclude that organic based products and organosilicates are not suitable solutions for consolidation treatments in calcareous substrates due to the poor chemical compatibility between the carbonate matrix and organic consolidant [Baglioni et al, 2014].

For this reason, inorganic consolidants, which are highly compatible with the mineralogical nature of the decayed calcareous substrate, have been widely studied [Hansen et. al., 2003]. One of the best known inorganic consolidants from historical times is the calcium hydroxide colloidal solution, the so-called *lime-water* method (Fig. 17). This method is a saturated solution of calcium hydroxide with a maximum concentration of 1.5g/L with lime particles in a colloidal suspension, and has been used for centuries to consolidate deteriorated limestone or plaster [Hansen et. al. 2003]. It has the advantage of being durable and compatible with the substrate as it is based on the precipitation of calcium carbonate into the pores of the treated material by reaction of the calcium hydroxide with the atmospheric carbon dioxide ($CO_2$). The main constraint of the limewater technique is the slow carbonation process and low consolidation depth due to limited penetration of carbon dioxide into the substrate [Henriques and Charola, 1996]. Furthermore, the application of limewater can cause whitening of the treated surface due to poor penetration of particles in the pores [Hansen et. al., 2003] and the use of high amounts of water can considerably

increase the risk of salt mobilization, biological colonization or freeze-thaw effects [Rodriguez-Navarro et. al., 2013].

The effectiveness of limewater has been widely discussed in the literature. Price et. al. in the 1980s [Price et. al., 1988] concluded that, when using limewater, most particles are deposited within 2 mm from the surface, thus yielding an ineffective consolidation. This has led some stone conservators to be sceptical of this treatment. Nonetheless, Brajer [Brajer and Kalsbeek, 1999] demonstrated that a prolonged uninterrupted application can produce a noticeable consolidation effect. Some other authors have also obtained successful treatments and so brought new perspectives to its practical application such as the use of lime poultices and of an increased number of limewater applications [Bracci et. al. 2008; Slizkova et. al., 2015]. Despite this, the consolidation effect of the limewater technique does not meet all the consolidation criteria due to its low penetration (< 2mm from the surface), the tedious application method, which requires a high number of applications (more than 140 consecutive applications) [Brajer and Kalsbeek, 1999], and the low strength increase achieved for the weathered layer [Baglioni et al, 2014].



**Figure 17.** Limewater technique application (image: Austrian Archaeological Institute)

Barium hydroxide, which is commonly called the *Ferroni-Dini method*, or the Florentine method, is another inorganic consolidant which has been used for many years in the conservation of sulphate polluted wall-paintings, especially those

affected by gypsum ($CaSO_4$) [Baglioni et al, 2014]. This method consists of applying an ammonium carbonate and barium hydroxide aqueous solution loaded on poultices in a two-step process [Chelazzi et al, 2013]. The ammonium carbonate turns gypsum into soluble ammonium sulphate, which is absorbed by the poultices and removed from the surface. The barium hydroxide converts the ammonium sulphate into barium sulphate, which is insoluble, thereby preventing damage by salt crystallisation [Chelazzi et al, 2013]. The barium hydroxide also reacts with the calcium carbonate to form more barium carbonate and calcium carbonate. Therefore, this treatment consolidates the calcareous surface and mitigates the damage of sulphate salts. The reaction process follows this equation [Chelazzi et al, 2013]:

$$CaSO_4 \cdot 2\,H_2O + (NH_4)CO_3 \rightarrow (NH_4)_2\,SO_4 + CaCO_3 + 2H_2O \qquad (11)$$

$$(NH_4)_2SO_4 + Ba(OH)_2 \rightarrow BaSO_4 + 2NH_3 + 2H_2O \qquad (12)$$

$$Ba(OH)_2 + CaCO_3 \rightarrow Ca(OH)_2 + BaCO_3 \qquad (13)$$

$$Ca(OH)_2 + CO_2 \rightarrow CaCO_3 + H_2O \qquad (14)$$

$$Ba(OH)_2 + CO_2 \rightarrow BaCO_3 + H_2O \qquad (15)$$
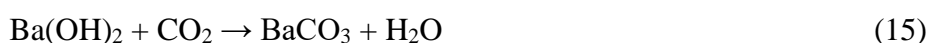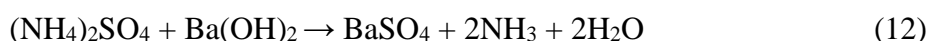
When applied to a calcareous material, barium hydroxide can form a coating of barium carbonate, which is more resistant than calcium carbonate to acid rain [Bracci et al. 2008; Doehne and Price, 2009]. In addition, barium hydroxide is much more soluble in water (56 g/l) compared to calcium hydroxide (1,5 g/l) [Hansen et al. 2003], allowing for a higher amount of binding agent and a fairly in-depth consolidation action [Bracci et al. 2008; Delgado-Rodrigues and Ferreira-Pinto, 2016]. However, barium hydroxide cannot be considered totally compatible with the carbonate substrates because small amounts of barium (as barium carbonate or sulphate) are introduced into the calcium carbonate crystalline matrix [Giorgi. et. al. 2000].

Recent developments in nanoscience and nanotechnology have opened up new possibilities within numerous scientific areas. When applied to the science of cultural heritage conservation, nanotechnology brings new products with properties that can be far superior to traditional treatments. The synthesis of nanoparticles of $Ca(OH)_2$ (nanolimes) reduces some of the problems associated with micro-sized calcium hydroxide (such as the incomplete conversion to calcium carbonate, aesthetic

alterations after treatment and low depth of penetration into the porous substrate) due to the better features of the nanoparticles [Baglioni et. al., 2014]. The crystals of traditional calcium hydroxide particles range between 0.5 μm to 10 microns depending on the age of the lime putties [Lopes-Margalha et al, 2013], which is highly reduced with nanolime presenting higher consolidation effectiveness.

The popularity of nanolime is growing. In recent years, nanolime commercial products have become some of the UK's most commonly used consolidants for the conservation of historic structures involving calcareous stones (Fig. 18) and its use has increased year after year in England [Newman, 2017].



**Figure 18.** Treatment with Calosil (image: ibz-freiberg.de)

## 2.5 Nanolime as a consolidation method for calcareous substrates

The content of this sub-chapter has been published in the GE-IIC Conservation Journal (DOI:10.17265/2162-5298.).

### 2.5.1 Introduction

The recent development of nanoscience and nanotechnology has opened new lines to new applications in many scientific fields, including that of the conservation of

cultural heritage. One example of a nanomaterial developed over the last decades is the so-called "nanolime", nanoscale particles of $Ca(OH)_2$ with potentially superior consolidation properties compared to traditional lime-based treatments. So far, nanolime has been studied mainly within the built cultural heritage conservation field.

Scientific investigations of nanolime began around the year 2000 at the University of Florence CSGI, in Italy, with the first results on its synthesis and application for the conservation of wall-paintings published in 2001 [Ambrosi et al. 2001]. The researchers in Florence modified the synthesis methodology several times by reactions in diols (Salvadori and Dei 2001), aqueous solutions [Ambrosi et al. 2001] or water-in-oil (w/o) micro-emulsions [Nanni and Dei 2003]. In 2003, another research group [Ziegenbalg 2003] prepared nanolime from a heterogeneous-phase reaction, which was patented under the brand name Calosil®. Calosil® (Fig. 19a) and was the first nanolime product introduced to the market in 2006 (IBZ-Salzchemie GmbH & Co. KG) followed by Nanorestore® (CSGI) in 2008 (Fig 19b). With these products made available to the scientific community, European researchers began investigating the properties and consolidation efficacy of nanolime. Three main EU research projects, STONECORE (2008 - 2011), NANOMATCH (2011 - 2014) and NanoforART (2012 - 2015) have made significant contributions to understanding the technologies and preparing the way for a range of applications of nanolime in the conservation field.



**Figure 19**. Nanolime products:  a) Calosil®; b) Nanorestore Plus®

*2.5.2 Synthesis*

Nanoparticles can be produced through either the top-down or bottom-up processes. In the top-down method the nanoparticles are created by "breaking" a bulk micro-scale particle until fragments in the nanometer range are obtained. This normally involves using a source of high energy in processes such as laser ablation, thermal decomposition or mechanical milling. In the bottom-up method, the nanoparticles are built atom by atom through chemical precipitation, using several techniques for the deposition and crystal growth from vapour (Chemical Vapour Condensation (CVC)), hydrogen plasma-metal reaction (HPMR) and liquid phases (micro-emulsions, solvo-thermal, etc.). Most calcium hydroxide nanoparticles are synthesised through the bottom-up reaction by chemical precipitation from a liquid phase.

A survey of different synthesis methods from the scientific literature is summarised in Table 2. In 1997, colloidal dispersions of calcium hydroxide in organic solvents were obtained [Delfort 1997] and, in 2000, the CSGI-group [Giorgi et al. 2000] also obtained stable alcohol dispersions of $Ca(OH)_2$ particles. Both researchers found that dispersions in alcohol are far more stable and able to incorporate larger amounts of lime than limewater. With the aim of preparing stable nanoparticles of $Ca(OH)_2$, the researchers at CSGI carried out a series of studies based on the works of the Matijevic group [Pe et al. 1998] in the field of colloid synthesis. They reported that nucleation of nanoscale particles is affected by reaction time, high temperature (above 100°C) and high degree of super saturation, and it can be achieved with slow synthesis and peptisation processes. In 2001, the CSGI group [Dei and Giorgi 2001] obtained $Ca(OH)_2$ particles (1-2µm) by a hydrolytic method at medium-high temperature (60°C) and super-saturation. In order to reduce the size of particles, they synthesised calcium hydroxide nanoparticles (30-60 nm) from diols, which allowed higher temperatures to be reached during the process [Salvadori and Dei 2001]. However, this synthesis method proved to be time consuming and produced a low quantity of nanoparticles. In the same year, they successfully obtained highly reactive and colloidal sub-micrometer $Ca(OH)_2$ particles (±300 nm) via an homogeneous phase following the aqueous reaction $CaCl_2 + 2NaOH \rightarrow Ca(OH)_2 + 2NaCl$, heated up to 90 °C under supersaturation conditions [Ambrosi et al. 2001]. The second process has drawbacks; i) slow mixing rates; ii) the necessity of

removing the produced NaCl by washing; and, iii) low yield of nanoparticles production.

Ca(OH)$_2$ nanoparticles (2-10 nm) were also obtained using w/o micro-emulsions [Nanni and Dei 2003], but low yield and high production time make this method less practical. The synthesis method developed by CSGI [Dei and Giorgi 2001; Ambrosi et al. 2001; Dei and Salvadori 2006], which was commonly named "drop by drop method", was also adopted by several research groups with the aim of refining the synthesis process and properties [Sequeira et. al. 2006; Daniele et. al. 2008; Daniele et. al., 2010]. In 2013, the Taglieri team [Daniele et al, 2012] managed to reduce the synthesis time while decreasing the particle size (<50 nm) by adding a surfactant (Triton X-100) in the initial aqueous solution. In other synthesis pathways based on CSGI researches, Roy [Roy et al, 2010] obtained nanolime by hydrolysing calcium nitrate tetrahydrate [Ca(NO$_3$)$_2$·4H$_2$O] as a precursor in diols at a high temperature (175°C) and Samanta [Samanta et al. 2016] synthesised nanolime using calcium nitrate dihydrate [(NO$_3$)$_2$·2H$_2$O] as a precursor in an aqueous medium at room temperature without requiring purification, obtaining nanoparticles of about 250 nm.

Other approaches for obtaining nanosized Ca(OH)$_2$ use calcium alkoxides as precursors [Ziegenbalg 2003; Poggi et al. 2016; Rodriguez-Navarro et al. 2013]. Nanolime also has been developed from a hydrogen plasma-metal reaction method (HPMR), obtaining low cost, high purity and crystalline particles (10-100nm) [Liu et al. 2010], and recently the Taglieri team [Taglieri et al. 2015] synthesised nanolime by means of an anion-exchange process using an anion-exchange resin (OH$^-$ group), obtaining nanoparticles with better features in terms of size, morphology and reactivity, and reducing the synthesis time by eliminating purification processes.

**Table 2.** Brief summary of literature on the synthesis of nanolime

| Year | Research group | Synthesis route | Inorganic precursor(s) | Synthesis media | T (°C) | PS (nm) |
|------|----------------|-----------------|------------------------|-----------------|--------|---------|
| 2001 | CSGI group | CP-HS | $CaCl_2$ and NaOH | aqueous | 60 | 1-2 (µm) |
| 2001 | CSGI group | CP-HS | $CaCl2·2H_2O$ and NaOH | diols | 195 | 30-150 |
| 2001 | CSGI group | CP-HS | $CaCl2·2H_2O$ and NaOH | aqueous | 90 | 300 |
| 2003 | CSGI group | CP-HS | $CaCl2·2H_2O$ and NaOH | w/o microemulsions | ≤ 15 | 2-10 |
| 2010 | Bhattacharya et al. | CP-HS | $Ca(NO_3)_2·4H_2O$ and NaOH | diol (1,2-ethanediol) | 115 | 35 |
| 2010 | Liu et al. | CP-HPMR | melted Ca ingot and $H_2O$ | H plasma | room T | 10-100 |
| 2012 | Taglieri et al. | CP-HS | $CaCl_2$ and NaOH | aqueous & Triton-X100 | 90 | <100 |
| 2015 | Taglieri et al. | CP-HS | $CaCl_2$ $2H_2O$ and AER (OH) | Aqueous | room T | <100 |
| 2016 | Samanta et al. | CP-HS | $Ca(NO_3)_2·2H_2O$ and NaOH | aqueous | room T | 350 |
| 2016 | CSGI group | CP-HPS | calcium metal | alcohol and H2O (high P & T) | 65-130 | 200 |

CP (chemical precipitation), HS (homogeneous synthesis), HPS (heterogeneous phase synthesis), HPMR (hydrogen plasma metal reaction)
$Ca(NO_3)_2$ $·4H_2O$ (calcium nitrate tetrahydrate), CaO (calcium oxide), w/o (water in oil), P (pressure), T (temperature), PS (particle size),
Ca (calcium), $CaCl_2$ (calcium chloride), NaOH (sodium hydroxide), w/o (water in oil), H (hydrogen), AER (anion exchange resin),
wash (washing with deionized water), pept (peptization process)

### 2.5.3 Applications

During the last two decades nanolimes have been tested as conservation treatments for various substrates. Most of these studies focused on the pre-consolidation of wall paintings, limestone, lime mortars, renders and plasters; and on the de-acidification of cellulose-based materials such as paper, canvas and wood [Poggi et al. 2016].

The use of lime dispersions in alcohol was first reported by Giorgi et al. [Giorgi et al. 2000], who obtained higher consolidation effect than with aqueous solutions and less superficial white glazing. Later, Ambrosi and co-workers, [Ambrosi et al. 2001, Dei and Giorgi 2001] successfully tested the first synthesized $Ca(OH)_2$ nanoparticles in lime mortar, limestone and wall-paintings, achieving a good re-adhesion of detached pigment flakes without side effects. The nanolime developed by CSGI was further tested on several Italian frescoes [Baglioni and Giorgi 2006b], limestone and a wall-painting in the archaeological site of Calakmul in Mexico [Baglioni and Giorgi, 2006a], achieving a good degree of consolidation. All work undertaken by CSGI between 2001 and 2006 achieved better superficial re-cohesion and quicker carbonation with fewer applications than limewater and without any aesthetic changes; thus demonstrating that nanolime is so far the best treatment for the consolidation of wall paintings.

Calosil® and Nanorestore® were tested by several authors in Europe since 2008. Using Calosil®, Drdácký [Drdácký et al. 2009] documented significant strength increase in lime mortars with far fewer applications than with limewater. Other authors [Daniele et al. 2008; Campbell et al. 2011; Daniele and Taglieri 2011] studied the consolidation and penetration of nanolime on limestone(s) and lime-mortars, finding high superficial strengthening, despite nanolime penetration only occurring within 200 $\mu m^{-1}$ mm from the surface, depending on the porosity and degree of deterioration of the treated limestone [Ruffolo et al. 2014]. These results highlight the importance of the material's pore structure in the effectiveness and penetration of the product. Other authors [Borsoi et al. 2012; Costa and Delgado-Rodrigues, 2012] observed insufficient nanolime penetration, no consolidation and nanolime migration back to the surface of the substrate in highly porous limestone, renders and mortars. Afterwards, it was verified that this phenomenon occurs during evaporation of the solvent [Borsoi et al. 2015a]. The strength and penetrability of Calosil® products in plasters, lime mortars and wall paintings was also studied [Daehne and Herm 2013]. It was found that the strength of lime mortar can be increased up to seven times when Calosil® E-25 is applied with cellulose ether gels (hydroxypropylcellulose gel) and that the addition of a low amount of Calosil®-Micro (contains 1-3 µm calcium hydroxide particles) enhances penetration and reduces back-migration.

Treatments combining nanolime and other products were also studied. The CSGI-team [Baglioni et al. 2003; Baglioni et al. 2006b] used a combined treatment of barium hydroxide and nanolime for the treatment (desulphation and consolidation) of wall paintings. This combined application was improved later in 2010 [Giorgi et al. 2010] with nanoparticles of both barium and calcium hydroxides. The combination of nanolime dispersions (CaLoSiL®) with silicic acid esters (SAE) can be used to enhance the affinity of SAE to a calcareous matrix [Piaszczynski and Wolf 2011]. Photo-catalytic nanolime [Nuño et al. 2015] has been successfully used for self-cleaning coatings and environmental pollution control.

*2.5.4 Factors influencing nanolime performance*

There are several factors influencing the effectiveness of nanolime as a consolidant: nanolime characteristics (concentration and type of solvent, particle size, morphology and specific surface area), physical and mechanical characteristics of the substrate, extrinsic factors (RH, temperature, exposure time, $CO_2$ available) and application method. Some of the scientific literature explains its effectiveness as a consolidant.

It has been shown that nanolimes have superior consolidation properties to limewater, including both higher and faster carbonation with greater penetration [Ambrosi et al. 2001; Dei and Giorgi 2001; Dei and Salvadori 2006]. A short-chain alcohol dispersion provides the following benefits; i) greater colloidal stability [Dei and Giorgi 2001], ii) solvent evaporation so that higher concentrations of $Ca(OH)_2$ are attained [Giorgi et al. 2000], iii) higher amounts of lime (up to 30 times higher), resulting in an increased lime incorporation into the treated substrate and lower number of applications [Dei and Salvadori 2006], iv) enhancement of carbonation kinetics and $CaCO_3$ polymorph nucleation [Rodriguez-Navarro et al. 2013], v) significant reduction of the amount of water introduced into the treated material. Nanoparticles in an alcohol dispersion penetrate better in porous structures and carbonate faster due to their higher specific surface area [Sequeira et al. 2006].

The role of the solvent for in-depth consolidation was studied recently [Borsoi et al. 2016]. It was found that solvents with high boiling points improve the depth of nanolime deposition in stones with large pores (35–40 µm), while solvents with lower boiling points perform better in materials with finer pores (0.5-2 µm), which reduce nanolime migration back to the surface during the solvent drying. Comparison of different concentrations (5 and 25 g/L in isopropanol) of different products (Calosil®, Nanorestore® and Merck®) for the consolidation of lime mortars found that lower concentrations (Calosil® 5 g/L) yield the most significant improvement in the degree of carbonation in the pores [Arizzi et al. 2015]. A percentage of residual water content in the alcohol medium (1:10 w/a ratio) clearly enhanced the carbonation process [Dei and Salvadori 2006; Daniele and Taglieri 2010]. The colloidal behaviour of $Ca(OH)_2$ nanoparticles in alcohol was studied

[Rodriguez-Navarro et al. 2013; Rodriguez-Navarro et al. 2016] and showed that, upon contact with alcohol, $Ca(OH)_2$ nanoparticles partially transform into Ca-alkoxides via the reaction $Ca(OH)_2 + 2ROH \rightleftarrows Ca(OR)_2 + 2H_2O$. The Ca-alkoxide conversion is time-dependent; therefore a long period of storage will produce higher conversion. The rate of carbonation of $Ca(OH)_2$ particles is reduced by this conversion, so that a freshly prepared alcohol dispersion should be preferred. The influence of repeated applications (1 to 6) of Calosil® with different concentrations on high porosity stone showed that the appropriate amount of consolidant has to be chosen in relation to the stone porosity; the optimal treatment for stones with large pores (±48 µm) seems to be 2 applications of Calosil® at 25 g/L concentration [Slizkova et al. 2012].

Relative humidity, temperature, and exposure time strongly influence the carbonation kinetics and the precipitation of $CaCO_3$ polymorphs [López-Arce et al. 2010]. It was shown that the nucleation of polymorphs varies as a function of RH and time, and the optimum carbonation rate is achieved at high RH (75-90% RH). The full carbonation may be achieved in 9-10 days at room temperature, ambient $CO_2$ concentration and high RH values (75%) [Baglioni et al. 2014]. An important factor in the consolidation of porous substrates using nanolime is the availability of sufficient $CO_2$ in the pores of the treated material for the calcium hydroxide to fully carbonate. Some research groups investigated the possibility of increasing the amount of $CO_2$ in the pores of treated substrates. For example, the Taglieri team [Daniele et al. 2008] achieved full and faster carbonation by adding sodium bicarbonate ($NaHCO_3$) to the alcohol solution. However, the addition of $NaHCO_3$ may induce the formation of salt efflorescence. Other researchers [Lopez-Arce and Zornoza-Indart 2015] obtained good results and a full conversion in 21 days by creating a $CO_2$-rich atmosphere in a yeast-sugar environment.

# Chapter 3

# Materials and Methods

## 3.1. Materials

### 3.1.1 Lime and sand for mortar preparation

Singleton Birch Ultralime CL90 ($\geq$ 98% $Ca(OH)_2$, as confirmed by XRD and XRF) and silica sand from Pentney (UK) were used for the mortar mixes. The sand grading is shown in Figure 20. The mineralogical composition of the sand, which was determined by XRD (*PANalytical XPert PRO,* section 3.2.5.2.2) using Rietveld refinements, is 96.3% Quartz ($SiO_2$, ICSD #00-046-1045) and 3.7% Potassium Feldspar ($KAlSi_3O_8$, ICSD #01-076-0831).
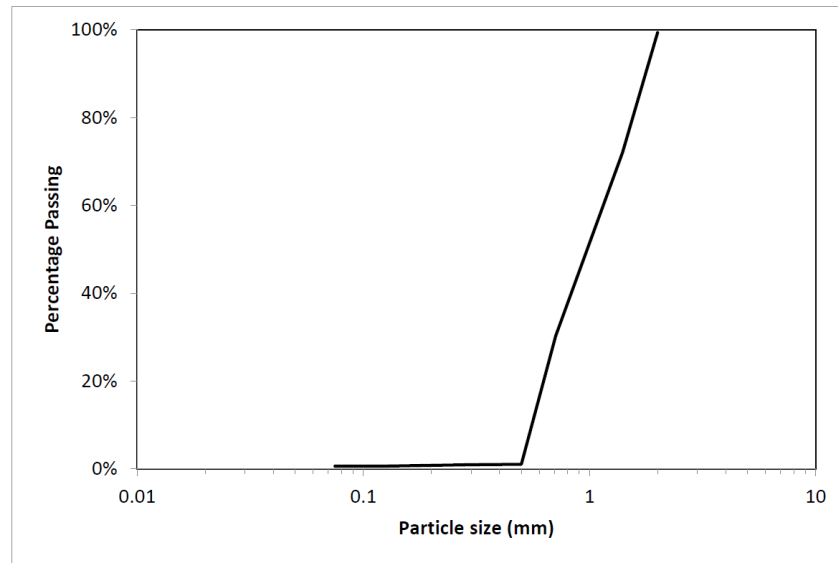
**Figure 20**. Sand grading

### 3.1.2 Lime mortars

The elemental composition of the mortar was determined by X-Ray Fluorescence (*PANalytical MagiX PRO XRF* spectrometer, section 3.2.5.2.3) on pressed powder samples by calculating the elemental weight percentages from total oxide X-Ray analysis. Results are shown in Table 3.

**Table 3.** Elemental composition of the mortar (wt. %) from XRF analysis.

| Ca | Si | Fe | S | Al | K | P |
|---|---|---|---|---|---|---|
| 26.9 (±0.1) | 68.7 (±0.5) | 0.2 (±0.01) | 0.2 (±0.2) | 1.3 (±0.3) | 1.1 (±0.3) | 1.4 (±0.3) |

The mineralogical composition was determined by X-Ray Diffraction (XRD). Quantitative analysis by Rietveld refinement shows the mineralogical composition of the mortar is 82.3 (±2.1) % quartz ($SiO_2$, ICSD #00-046-1045) and 17.7 (±1.8) % Calcite ($CaCO_3$, ICSD #00-005-0586). The pore structure of the mortar was determined by Mercury Intrusion Porosimetry (MIP, section 3.2.5.2.1). The pore size distribution of the mortar is shown in Figure 21. It can be seen that the pore sizes have a tri-modal distribution, coarser pores with diameters between 17 μm and 100 μm, intermediate pores with diameter between 1 μ and 17 μm and finer pores with diameters between 0.06 μm and 1 μm. The porosity of the mortar measured by MIP was 22.63 (±2.8) %.
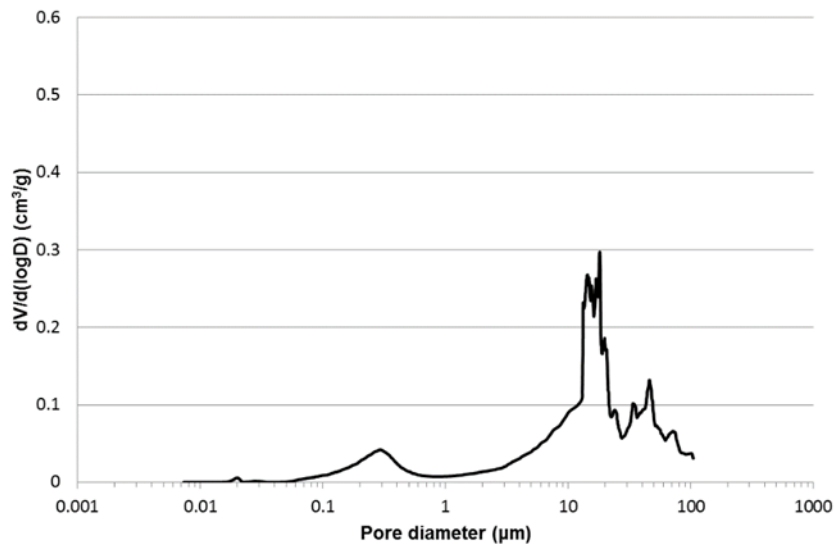


**Figure 21**. Differential volume of intruded mercury versus pore diameter of the mortar

*3.1.3 Stones*

Five stones were used for the tests:

- **Weathered limestone 1**: This sample, which is shown in Figure 22a, is a weathered Doulting stone capital from the Wells Cathedral (Somerset, UK), a building listed as Grade I in the National Heritage List for England (NHLE) [Historic England, 2011]. This capital was used by Price et. al. for a research experiment in the 1980s [Price, 1989; Doehne and Price, 2009]. In Price's experiment, the left-hand side (Fig. 22a) was treated with Brethane (a MTMOS based product) whilst the right-hand side was left untreated [Price, 1989]. After the experiment, the capital was stored in the Building Research Establishment (BRE) outdoor historic stone deposit (Watford, UK). In the present Ph.D. research, only the untreated area which had not been treated with the Brethane was used. Doulting limestone is a clastic sedimentary rock composed of fragments of older Carboniferous limestones which were eroded and later re-deposited and cemented together [Price, 1989]. The rock can be classified as intramicrite [Folk, 1959] or grainstone [Dunham 1962]. This stone is referred to as CP.

a) ⠀⠀⠀⠀⠀⠀⠀⠀⠀⠀⠀⠀⠀⠀⠀⠀⠀⠀⠀⠀⠀⠀⠀⠀⠀⠀⠀ b)
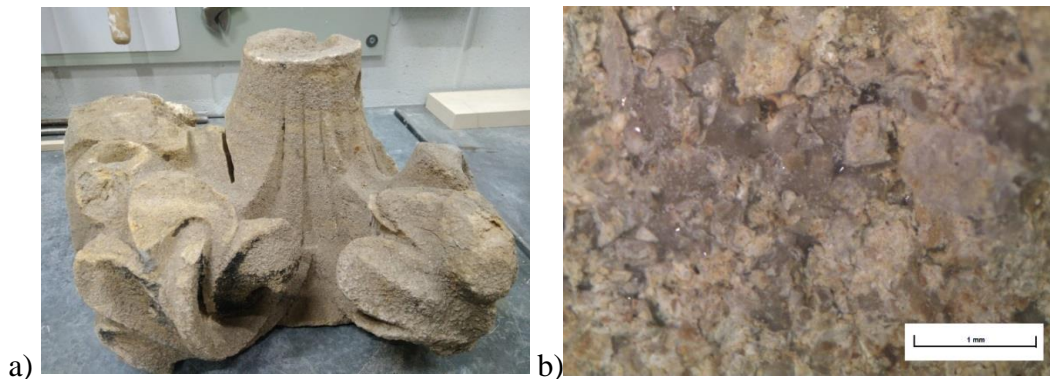
**Figure 22**. Weathered capital of Doulting stone (referred as CP) from the Wells Cathedral (UK). a) capital; b) stereomicroscope image of a fragment of Doulting stone

The elemental composition of this stone was determined by XRF and is reported in the following Table 4.

**Table 4.** XRF analysis of the CP sample (wt %).

| Ca | P | Si | Fe | Al | S | K |
|---|---|---|---|---|---|---|
| 93.4 (±0.2) | 1.3 (±0.04) | 2.00 (±0.09) | 0.7 (±0.004) | - | 1.7 (±0.03) | 0.3 (±0.01) |

XRD-Rietveld refinement shows that Calcite ($CaCO_3$, ICSD #01-086-2334) is the only detected mineral in the stone , suggesting that other mineral phases (e.g. feldspar containing P, Si, Fe, K, Al and S, which were elements detected by XRF) could be present in amorphous or poorly crystallised phases or in amounts below the instrument detection limit (< 1%). The pore structure, which was determined by Mercury Intrusion Porosimetry (MIP), shows that CP has most of the pores in the range 10 to 100 μm and 0.2 to 2 μm (Fig. 23). The porosity of the stone is 14.1 (±0.42) % and the density is 2.0801 (±0.03) $g/cm^3$.
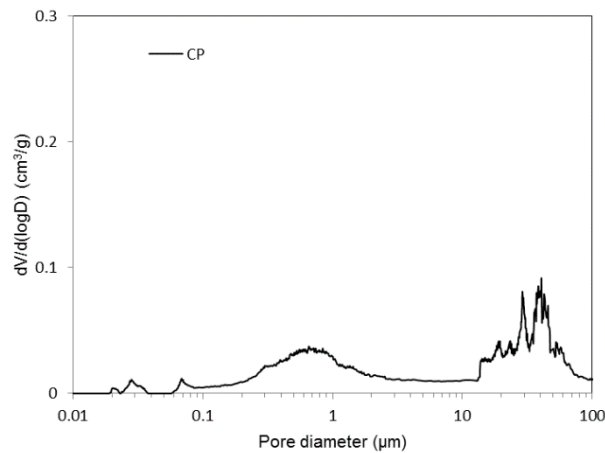


**Figure 23**. Differential volume of intruded mercury versus pore diameter of CP stone

35 x 35 x 35 mm cubes were obtained from the capital for testing.

– **Weathered limestone 2** (Fig. 24): The origin of this piece is unknown. The specimen was stored in the Building Research Establishment (BRE) outdoor historic stone deposit. It is a sedimentary rock composed of ooids cemented by sparry calcite. The rock can be classified as a intrasparite [Folk, 1959] or

Grainstone [Dunham 1962]. The surface of the stone is covered by a black crust (Fig. 24b). This stone is referred to as LS.
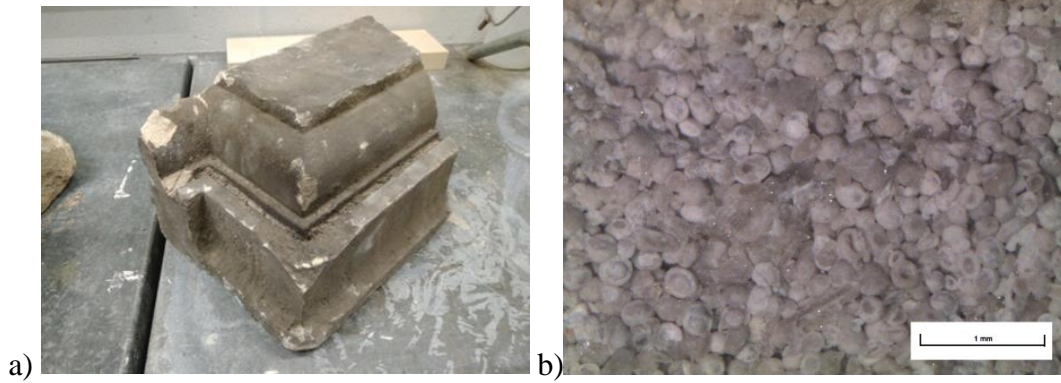


**Figure 24**. Weathered limestone (referred to as LS). a) Studied limestone showing a black patina on the surface; b) stereomicroscope image of the limestone.

The elemental composition of this stone was calculated by XRF and is reported in Table 5.

**Table 5.** XRF analysis of the LS sample (wt %).

| Ca | P | Si | Fe | Al | S | K |
|-----|-----|-----|-----|-----|-----|-----|
| 95.2 | 1.3 | 1.15 | 0.9 | 0.5 | 0.3 | 0.2 |
| ($\pm0.2$) | ($\pm0.03$) | ($\pm0.07$) | ($\pm0.03$) | ($\pm0.2$) | ($\pm0.01$) | ($\pm0.01$) |

XRD-Rietveld refinement shows that Calcite ($CaCO_3$, ICSD #01-086-2334) is the only detected mineral in this stone, suggesting that any other mineral phases (e.g. feldspar containing P, Si, Fe, K, Al and S, which were elements detected by XRF) could be present in amorphous or poorly crystallised phases or in amounts below the instrument detection level ($< 1\%$). The pore structure, as determined by Mercury Intrusion Porosimetry (MIP), shows the majority of pores having diameters between 20 and 50 μm and 0.1 and 03 μm. (Fig. 25). The porosity of this stone is 16.3 ($\pm0.22$) % and the density is 2.0354 ($\pm0.05$) g/cm$^3$.
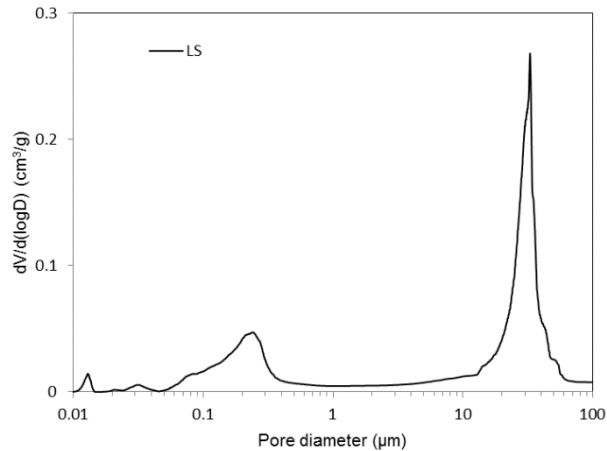
**Figure 25.** Differential volume of intruded mercury versus pore diameter of the LS stone

This stone was also cut into 35 x 35 x 35 mm cubes for testing making sure that their surface was free of the black crust.

– **Biocalcarenite stones from Agrigento-Sicily, Italy** (Fig. 26): These stones were obtained from the local quarry of Villaseta near the Temples (Agrigento, Italy), and they represent the same type of rock used for construction of the UNESCO Archaeological Site of the *Valley of the Temples* in Agrigento [Bernardo et al, 2000]; which is characterised by a documented advanced decay [Rossi-Manaresi 1982, Rossi-Manaresi 1991]. A general examination was performed using a stereomicroscope showing that the stones are rocks of clastic sedimentary origin composed mainly of bioclasts and whole skeletal fossil remains of marine aquatic organisms. The observed bioclasts and whole skeletal fossil remains belonged to marine bivalves, gastropods, rhodoliths, echinoderms and bryozoans. Carbonate lithoclasts were also observed together with few quartz grains. All grains are bound together by a fine-grained calcite (micrite). Based on these results, the stone samples can be classified as calcarenite [Grabau, 1904], biomicrite [Folk, 1959] or grainstone [Dunham 1962] commonly defined as biocalcarenite and belonging to the limestone rock deposits described as 'Formazione di Agrigento' [ISPRA, 1960].
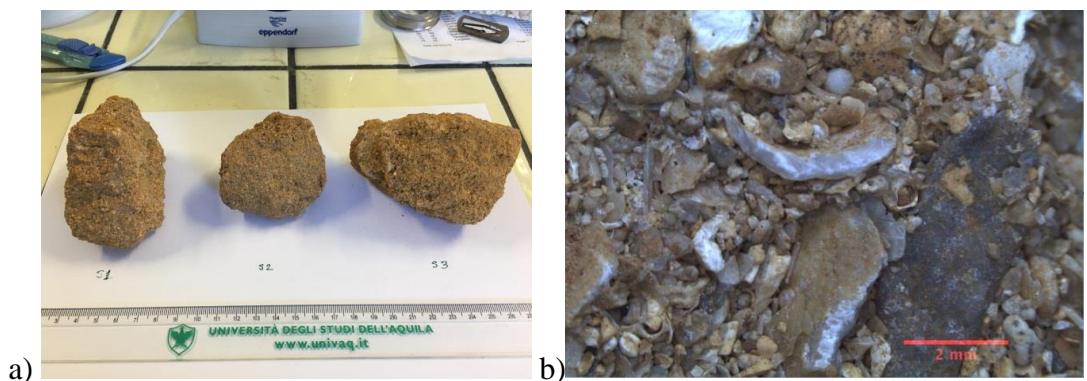
**Figure 26**. Biocalcarenite stone from Agrigento (Italy): a) used stone samples; b) detail of the surface of the stone.

The elemental analysis of this stone is reported in Table 6.

**Table 6.** XRF analysis of the biocalcarenite sample (wt %).

| Ca | Fe | Si | Mg | Al | P | K |
|---|---|---|---|---|---|---|
| 23.3 | 1.67 | 7.20 | 0.40 | 0.34 | 0.11 | 0.14 |
| (±0.3) | (±0.1) | (±0.6) | (±0.1) | (±0.1) | (±0.1) | (±0.2) |

The mineralogical composition was determined by X-Ray Diffraction (XRD). Quantitative analysis by Rietveld refinement shows the mineralogical composition of the biocalcarenite is 88.8% magnesium calcite carbonate, i.e. dolomite ($Mg_{0.03}Ca_{0.97}(CO_3)$, ICSD# 980086161), 9.9% quartz ($SiO_2$, ICSD# 980083849), 1.3% lipscombite ($Fe_{2.95}(PO_4)_2(OH)_2$, ICSD# 980202937) (Fig 27a). XRD results were confirmed by the FTIR investigation (Fig. 27b, described in section 3.2.5.2.4). The absorbance bands at 712, 876, 1429 cm$^{-1}$, assigned to the calcite, were readily detectable. For quartz, the absorbance bands at 798 and 1079 cm$^{-1}$ can be attributed to absorbance of the SiO band. The peaks for goethite at 796, 912 and 1044 cm$^{-1}$ cannot be easily distinguished due to the low concentration and the shifting with Si-O and carbonate groups.
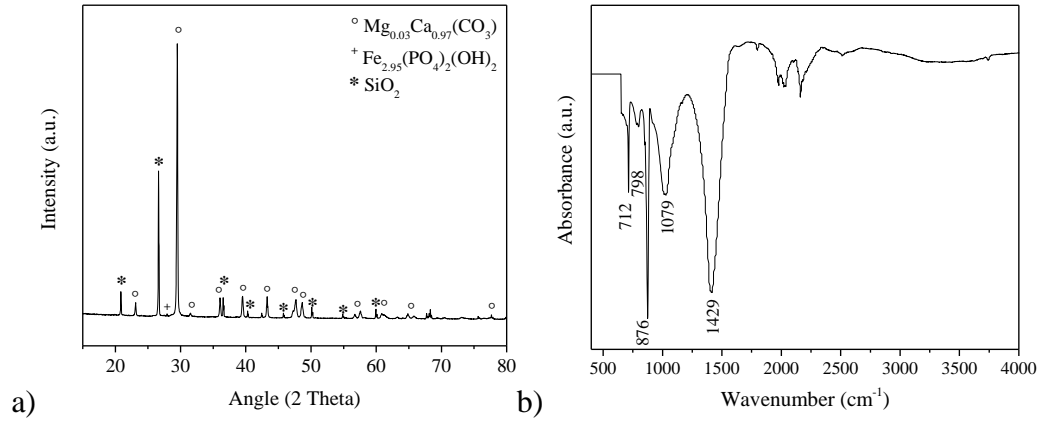
**Figure 27**. a) XRD and b) FTIR spectra of the biocalcarenite sample

The pore structure of the biocalcarenite was determined by Mercury Intrusion Porosimetry (MIP). Due the heterogeneity of the stone, three samples were analysed and the pore size distributions are shown in Figure 28. All three samples have pores with diameters in the 10-100 µm range (which present larger capillary pores range that allows the absorption by capillarity of larger volume of water) [Charola and Wendler, 2015]. The porosity of the biocalcarenite measured by MIP was 26.1 ($\pm$3.2) % and the density is 1.8982 ($\pm$0.12) g/cm$^3$. This is in line with the literature results which assessed porosity in the range 20-30% for the biocalcarenite of Agrigento's Temples [Bernardo et al, 2000].
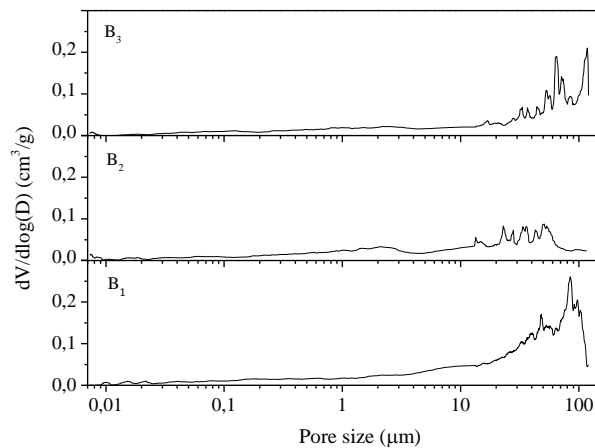


**Figure 28**. Pore size distribution (MIP) obtained from three samples of biocalcarenite.

These stones were tested maintaining their irregular shape as found in the quarry (≈15 x 8 x 5 cm).

−  **Weathered marble**: This marble block was a cornice of one of the Smithsonian's buildings in Washington D.C, USA. It was taken from a pile of architectural marble blocks stored in the stone deposit at the Smithsonian Garber facility (Suitland, Md., USA). The stone is a fine-grained marble with two weathered surfaces (black crust). This cornice was cut into 50 x 50 x 50 mm cubes being one of the faces curved as it is shown in Figure 29.



a)                                                                      b)
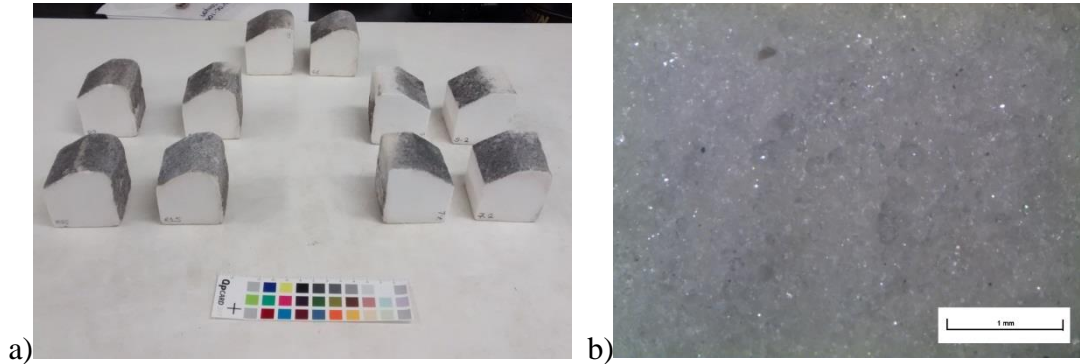
**Figure 29**. Marble samples ; b) steromicroscope image of the marble sample

The elemental analysis of the superficial black crust and the core of this stone is reported in Table 7. XRD-Rietveld refinement shows the only detected mineral in the marble core is Calcite ($CaCO_3$, ICSD #00-005-0586). However, quantitative analysis by Rietveld refinement of the black crust shows the mineralogical composition of the black crust is 84.4% calcite ($CaCO_3$, ICSD #00-005-0586), ICSD# 980086161), and 15.6% gypsum (calcium sulphate, $CaSO_4$, ICSD# 01-076-1746). This result was confirmed by XRF (Table 7), which showed that the black crust consists mainly of gypsum ($CaSO_4$) resulting from the reaction of $CaCO_3$ with acidic rain, as explained in section 2.2.2.

**Table 7.** XRF analysis of the marble sample (wt %).

|  | Ca | P | Si | Al | S | Sr | Ti |
|---|---|---|---|---|---|---|---|
| **Core** | 98.7 (±0.3) | 0.69 (±0.03) | 0.38 (±0.1) | - | - | 0.04 (±0.02) | 0.19 (±0.002) |
| **Black crust** | 96.4 (±0.3) | 0.41 (±0.01) | 0.45 (±0.06) | 0.14 (±0.02) | 2.4 (±0.03) | - | - |

The pore structure of the weathered portion of the stone (1 cm from the surface), was determined by MIP. Results show the majority of pores having diameters between 1 to 30 µm, where the high amount of pores have a diameter between 10 to 20 µm. This sample also presents some fine pores with diameter between 0.01 to and 0.02 µm and between 0.02 to 0.06 µm. (Fig. 30). The porosity of this stone is 6.0 (±0.52) % and the density is 2.144 (±0.08) g/cm$^3$.
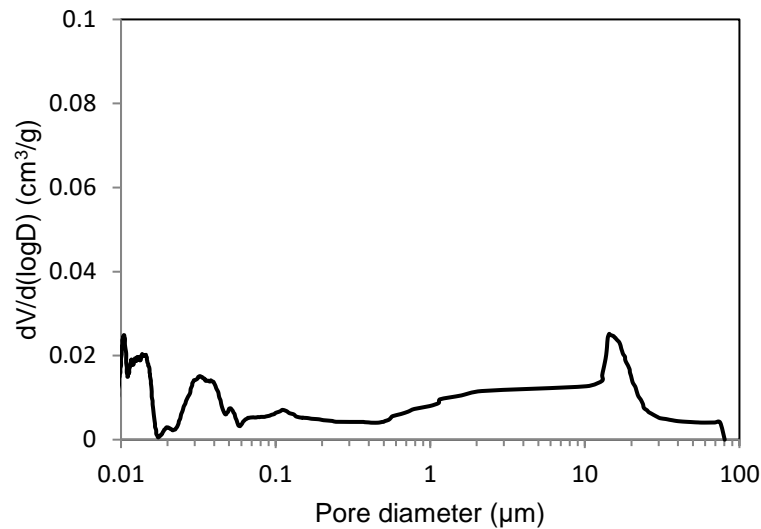


**Figure 30**. Pore size distribution (MIP) of the outer portion of the marble sample.

- **Indiana limestone**: Indiana limestone is a limestone used as building material in the USA (Fig. 31). It is a sedimentary rock composed of bioclasts and intraclasts cemented together by sparry calcite cement. The rock can be classified as a biointrasparite [Folk, 1959] or Grainstone [Dunham 1962]
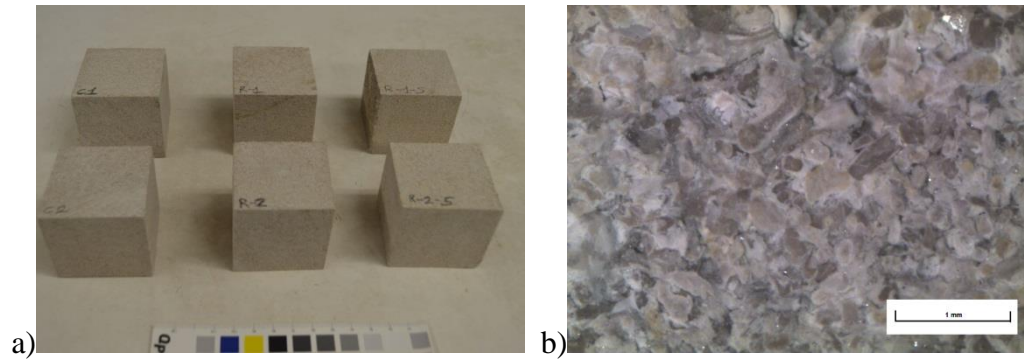
**Figure 31**. Indiana limestone; b) steromicroscope image of the limestone.

The elemental analysis of this stone is reported in Table 8.

**Table 8.** XRF analysis of the Indiana limestone sample (wt %).

| Ca | P | Si | Fe | S | Mg | Sr |
|---|---|---|---|---|---|---|
| 97.7 | 0.45 | 0.81 | 0.18 | 0.19 | 0.61 | 0.03 |
| ($\pm$0.2) | ($\pm$0.02) | ($\pm$0.06) | ($\pm$0.001) | ($\pm$0.01) | ($\pm$0.04) | ($\pm$0.002) |

XRD-Rietveld refinement shows the only mineral detected is calcite ($CaCO_3$, ICSD #00-005-0586), suggesting that any other mineral phases (e.g. feldspar containing P, Si, Fe, Mg, Sr and S, which were elements detected by the XRF) could be present in amorphous or poorly crystallised phases or in amounts below the instrument detection level ($< 1\%$).

The pore structure of Indiana limestone was determined by MIP and shows that it has a quatrimodal pore size distribution. The majority of pores fall within the diameter range of 0.1 to 1 µm, and it also presents three smaller peaks, one of larger pores with diameters between 10 to 30 µm and another of smaller pores ranging between 0.01 to 0.03 µm and 0.01 to 0.02 µm (Fig 32). The overall porosity stone is 11.41 ($\pm$0.86) % and its density is 1.974 ($\pm$0.121) g/cm$^3$. This stone was cut into 50 x 50 x 50 mm cubes for testing.
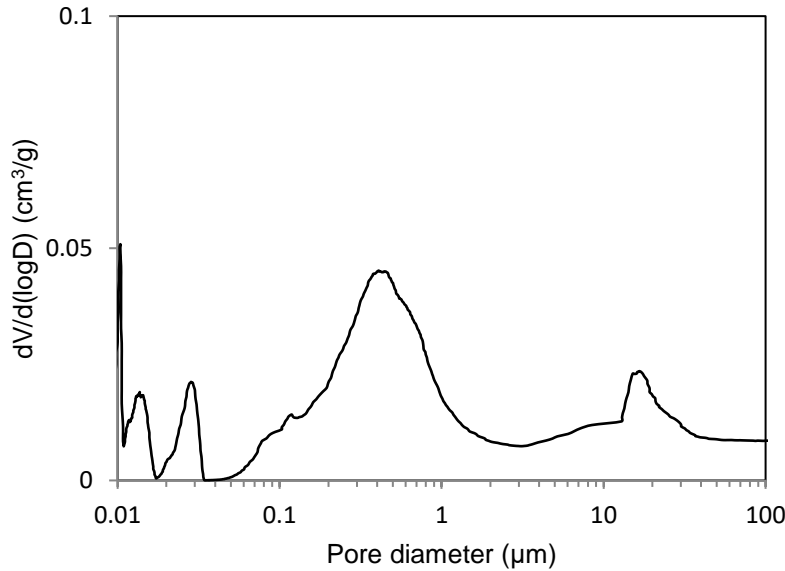
**Figure 32**. Pore size distribution (MIP) obtained from surface Indiana sample.

Each stone was cleaned with deionized water, cut and dried to constant mass at 60°C in a fan assisted oven and subsequently stored in a desiccator until the testing (5 < RH%, dry environment). All samples were weighed and labelled prior the treatment.

*3.1.4 Nanolime*

Three types of nanolime dispersions were used in this work:

–  **Nanorestore Plus Propanol 5®** (CSGI Consortium - University of Florence, Italy) [Nanorestore, 1996]: 5 g/L calcium hydroxide in 2-propanol. Particle size 100-300 nm. This dispersion is referred to as NAN.

–  **Calosil IP5®** (by IBZ Salzchemie GmbH & Co.KG, Germany) [Ziegenbalg, 2003]: 5 g/L calcium hydroxide in 2-propanol. Particle size 50-150 nm.  This dispersion is referred to as CAL.

–  **Nanolime synthesized through the method developed by Taglieri et. al. [Taglieri et. al., 2015] at the University of L'Aquila**: Particle size 20-80 nm.

This dispersion is referred to as LAQ. The synthesis process of this nanolime is described in the section 3.2.2. After the synthesis, the nanoparticles have been dispersed in different short-chain aliphatic solvents: ethanol (99.5%, Pharmco), 2-propanol (99.5% Sigma-Aldrich), Butanol-1 (99.5%, Fisher Scientific) and deionized water (purified by a Millipore Organex system [R≥18 MΩcm]).

Table 9 summarises the physico-chemical properties of the selected nanolimes.

**Table 9.** Physical-chemical properties of the selected nanolimes (B to WET are LAQ nanolimes)

| Code | Solvent | g/L | Boiling point (°C) | Surface tension (solvent/air) (N/m) |
|------|---------|-----|--------------------|-------------------------------------|
| NAN | Isopropanol | 5 | 82.6 | 0.0230 |
| CAL | Isopropanol | 5 | 82.6 | 0.0230 |
| B | Butanol | 5 | 117.7 | 0.0247 |
| IP | Isopropanol | 5 | 82.6 | 0.0230 |
| ET | Ethanol | 5 | 78.3 | 0.0221 |
| W | Water | 5 | 99.6 | 0.0728 |
| WIP | 50-50% Water-Isopropanol | 5 | 82.3 | 0.0247 |
| WIP | 50-50% Water-Isopropanol | 10 | 82.3 | 0.0247 |
| WET | 50-50% Water-Ethanol | 5 | 92 | 0.0281 |

### 3.1.5 Additives

The additives used in this work are:

- **Carbonated water**: the carbon dioxide gas was applied under pressure in deionized water by using a Sodastream machine®.
- **Urea**: 3% w/v of urea (($NH_2$)$_2CO_2$ Sigma Aldrich) was prepared in deionized water.
- **Sticky-rice powder**: Commercial pulverized sticky rice was used in this study. (Indica type, Enuo 6 variety). This was purchased from Erawan Marketing Co. TLD called *Farine de Riz Gluant* (product of Thailand).

## 3.2. Methods

### 3.2.1 Mortar preparation

Mortars were produced with a volumetric binder:sand ratio of 1:2.5 to a constant flow of 16 cm measured according to BS EN 1015-3:1999 (Fig. 33a). Although mix proportions are expressed by volume, mortars were batched by weight after accounting for component densities, which were measured in accordance with EN 1015-2:1998. The water:binder ratio to obtain the desired flow was 1.56. Mortars were produced by mixing the dry ingredients with water in a Hobart mixer. The mix protocol was as follows: 1) dry mix sand and lime for 2 minutes at 62 rpm; 2) add water while continuing mixing at 62 rpm for 30 s; 3) stop the mixer for 30 s and scrape the mixer bowl; 4) mix for 5 min at 125 rpm. Samples were cast in 40×40×160 mm steel moulds in two layers and vibration-compacted. Immediately upon floating off the fresh mortar, the moulds were covered with a plastic sheet and transferred to a temperature and humidity controlled room maintained at 20 ℃ and 65% RH (Fig. 33b). Mortar prism were de-moulded after 5 days and stored in the same room for the following 23 days. On the 28th day of curing, each prism was cut into approximately 4 40x40x40 mm cubes prior to curing for further 28 days in the same conditions.
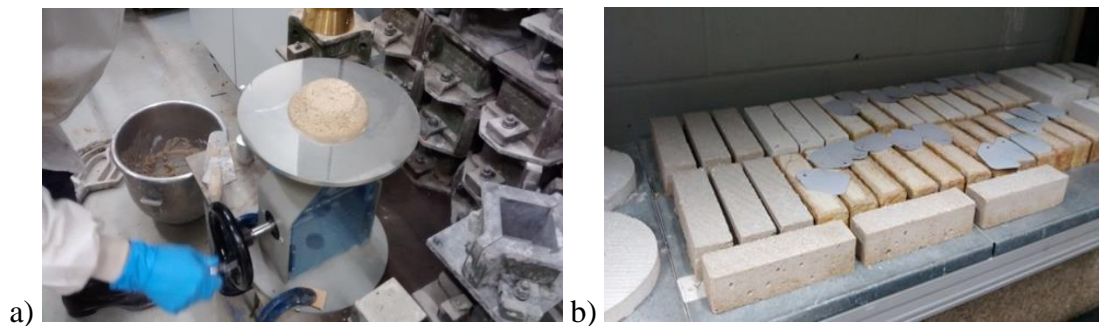


**Figure 33**. Mortar manufacturing process: a) Flow test; b) lime-mortars of size 40 x 40 x 160 mm.

### 3.2.2 Synthesis of nanolime

LAQ was synthesized through an anionic exchange process carried out at room temperature and ambient pressure by mixing under moderate stirring an anion exchange resin (Dowex Monosphere 550A OH from Dow Chemical) with an aqueous calcium

chloride solution following the methodology described by [Taglieri et. al. 2015; 2016; 2017a] and Volpe et. al. [Volpe et al, 2016]. When these two components are mixed together, the substitution of OH groups in the resin with chloride ions (Cl⁻) in solution leads, in conditions of supersaturation, to the formation of pure $Ca(OH)_2$ nanoparticles, following the reaction:
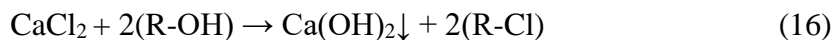
$$CaCl_2 + 2(R\text{-}OH) \rightarrow Ca(OH)_2\downarrow + 2(R\text{-}Cl) \tag{16}$$

The concentration of chloride was monitored during the process (Vernier Chloride Ion-Selective Electrode CL-BTA). The decrease rate of chloride content during the synthesis was very rapid, with about 97% of the reduction occurring within the first minute of the process (Fig. 34).
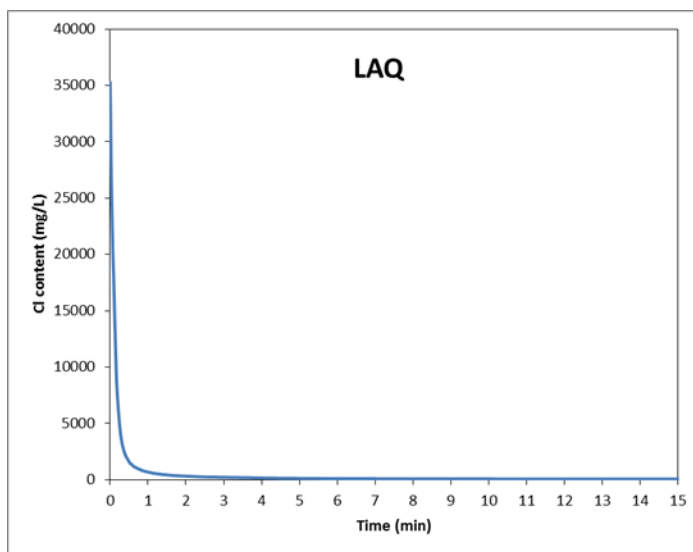


**Figure. 34**. Chloride content during the synthesis process

The synthesis was stopped after 15 minutes when the ion exchange process was completed (zero kinetic exchange), with a total reduction of chloride content of 99.82% and a residual chloride content of 0.18% (29.4 mg/L). Similar results have been reported in previous synthesis by Taglieri et. al. [Taglieri et al, 2015; 2016; 2017a,; 2017b]. When this reached a constant value below 30 mg/L, the stirring was stopped (Fig. 35b) and the aqueous suspension was separated from the resin by means of a sieve (80µm)

(Fig 35c). The supernatant water was then extracted with a pipette and replaced with alcohol maintaining the required concentration of 5, 10 and 25 g/L (Fig. 35d). Several formulations have been prepared following this procedure varying the type of the solvent and the concentration:

- 5 g/L in isopropanol (Water content = 5%). This dispersion is referred to as IP.
- 5 g/L in ethanol (Water content = 5%). This dispersion is referred to as ET.
- 5 g/L in water (Water content = 100%). This dispersion is referred to as W.
- 5 g/L in butanol (Water content = 5%). This dispersion is referred to as B.
- 5g/L in 50% isopropanol and 50% water. This dispersion is referred to as WIP.
- 5g/L in 50% ethanol and 50% water. This dispersion is referred to as WET.
- 10 g/L in 50% Isopropanol and 50% water. This dispersion is referred to as WIP*.
- 25 g g/L in ethanol (Water content = 5%). This dispersion is referred to as ET25.
- 25 g/L g/L in isopropanol (Water content = 5%). This dispersion is referred to as IP25.

All nanolime products were kept in a refrigerator (T< 5 °C) prior to the application to improve their effectiveness, as explained in the literature (section2.5.4) [Rodriguez-Navarro et al, 2016].



a)                                                    b)

c)        d)
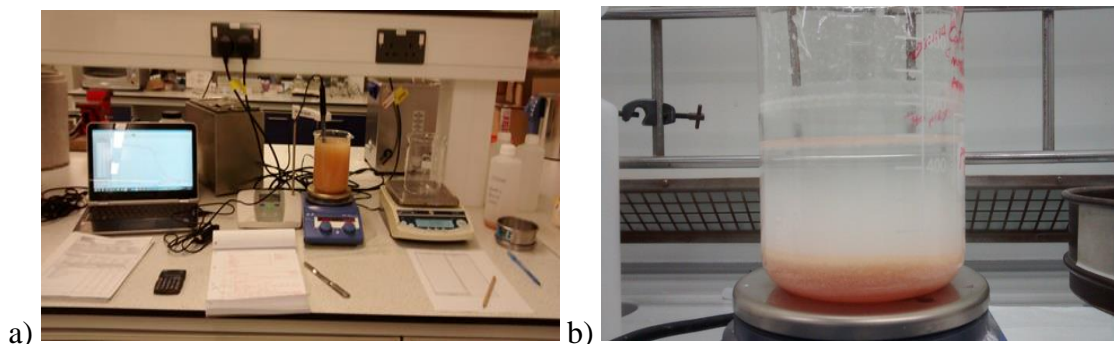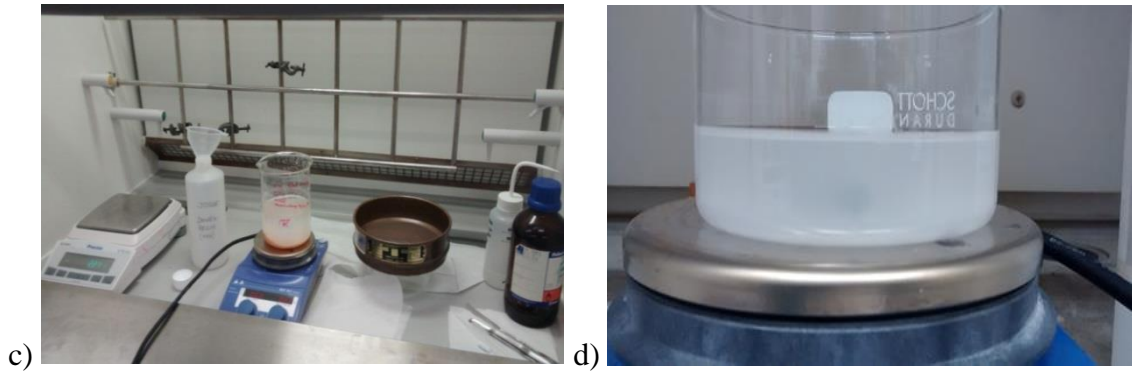
**Figure 35**. Nanolime synthesis process: a) mixture of $CaCl_2$ and the anion exchange resin, the anion exchange process is monitored with the ISE chloride system; b) When resin is exhausted (zero kinetic exchange), the stirrer is stopped; c) the resin and the aqueous suspension with $Ca(OH)_2$ nanoparticles are separated through a sieve (180 µm sieve); d) the nanoparticles are dispersed in the aqueous solvent.

### 3.2.3 Preparation of the additive sticky rice

A well-known approach was followed to prepare the sticky rice starch paste [Miller and Root, 1991; Yang et al, 2009; Yang et al, 2016b]. First, 2 g of pulverized sticky rice are added to 400 mL of deionized water (5 g/l or 5 wt%), and left to soak for an hour. The solution is then gradually heated (up to 100°C) and stirred for 4 hours. Afterwards, the resulting paste is left to cool to T ~ 30 ºC under vigorous stirring for approximately 1 hour. The solution was applied immediately after preparation.

### 3.2.4 Application methods
### 3.2.4.1 Application of nanolime

According to the literature, nanolime products have been applied following several methods (i.e., capillary absorption, spray, brush) [Chelazzi et. al., 2013; Pinto-Ferreiras and Delgado-Rodrigues, 2008a; Borsoi et al, 2015a]. In this work the nanolime was applied by brush following the application sequence described below:

Each of the nanolimes was agitated and applied by brush on the top face (as cast) of the mortar specimens, allowing the nanolime to be fully absorbed by the mortar between

two consecutive brushstrokes (Fig. 36a). Nanolimes were also agitated between each brushstroke. The treatment was continued until no further absorption was observed for a period of at least one minute after a brushstroke. At this time, the application was interrupted and was repeated 24 hours later when the specimen was dry. Samples were weighed before and after each application (after full evaporation of the solvent) to determine the total amount of nanolime absorbed by the mortar. The treatment was considered complete when each mortar cube absorbed 500mg of calcium hydroxide (approximately 100ml of nanolime). This required approximately 20 consecutive days of application for each nanolime, depending on the type of nanolime and substrate. Upon treatment completion, the samples were stored outdoor in a sheltered area for a period of 28 days (T ≈ 5–15°C, RH ≈ 60-80%) (Fig. 36b). A set of untreated control samples was also stored in the same conditions.

In order to estimate the amount of nanoparticles deposited within each specimen, the absorbed product was calculated. For this, specimens were weighted before and after each application. The amount of $Ca(OH)_2$ particles deposited in the sample is calculated following the formula:

$$\text{Volume of the absorbed nanolime (ml)} = \frac{Wf - Wo}{\rho} \qquad (17)$$

$$\text{Nanoparticles absorbed (g)} = \text{Vol of absorb. sol (ml)} * \text{conc. (g/L)} \qquad (18)$$

Where "Wo" is the weight before the treatment (g), "Wf" is the weight after the treatment (g), "ρ" is the density of the solution (which corresponds to 0.918 g/ml [Safety data sheet 50/50 Isopropyl Alcohol-Water (v/v) (703) 000000012660]) and "Conc" is the nanolime concentration (g/L).

The weight of the specimens was calculated after 28 days. The amount of dry matter (% w/w) was calculated as:

$$\text{Dry matter (\% w/w)} = \frac{Wc - Wo}{Wo} \, 100 \qquad (19)$$

Where "Wc" is the weight after 28 days (g) and "Wo" is the weight before the treatment (g).
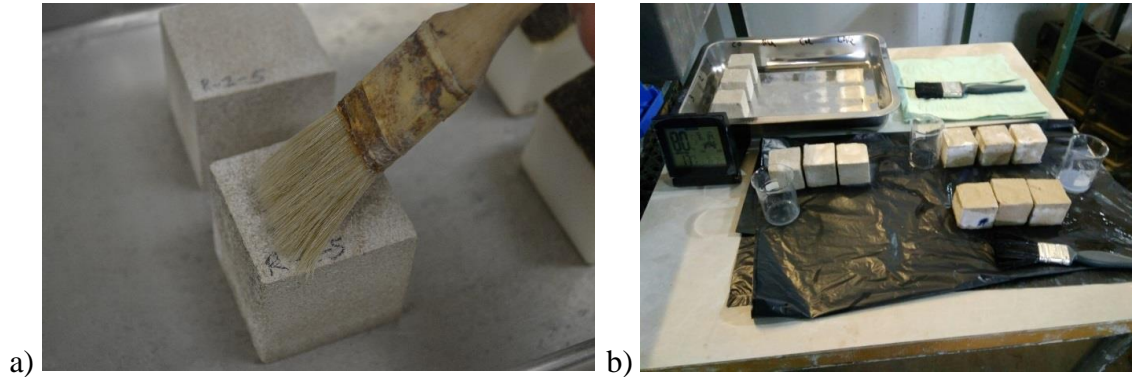


**Figure 36**. Nanolime application process: a) brushing the stone surface with nanolime; b) samples stored outdoor in a sheltered area (~75 (±5)% RH)

Two slightly different methods were used to apply the nanolimes on the biocalcarenite and the Indiana limestone and marble samples.

On the biocalcarenite the nanolimes were applied by brushing until stone saturation was achieved, by using about 100 mg of calcium hydroxide for each sample. The brushing was carried out on the largest and flattest face of the sample (approx. 10 cm$^2$ each). Straight after treatment, samples were wiped with a wet cloth to remove the excess of nanolime and to mitigate surface whitening. Stones were stored for 2 days at RH 75 ± 5 %. Then, the samples were oven-dried at 60°C until constant mass was reached, and then stored in a desiccator.

On the Indiana limestone and marble the nanolimes were applied by brushing until stones reached saturation. Before the application, the nanolime dispersions were placed in an ultrasonic bath (60 Hz) for 30 minutes to minimize nanoparticle aggregation. The nanolime dispersion was applied by brushing on two of the weathered faces of the marble specimens, whereas for Indiana limestone samples the dispersion was brushed on all faces. Both products were applied until saturation was reached. After treatment, to evaluate the influence of Relative Humidity on nanolime carbonation, two of the treated

marble samples were placed in two desiccators with two different relative humidity environments (one with a saturated solution of $Mg(NO_3)_2$ (RH~55%) and one with a saturated solution of NaCl (RH~75%)) (Fig. 37a). Additionally, two samples of treated marble and Indiana limestone were exposed to the room environment conditions (50±5% RH, T = 20±5°C) and finally two of each treated stone were sprayed daily with carbonated water at room conditions (Fig. 37b). A set of untreated control samples was also stored in the same room environment conditions.
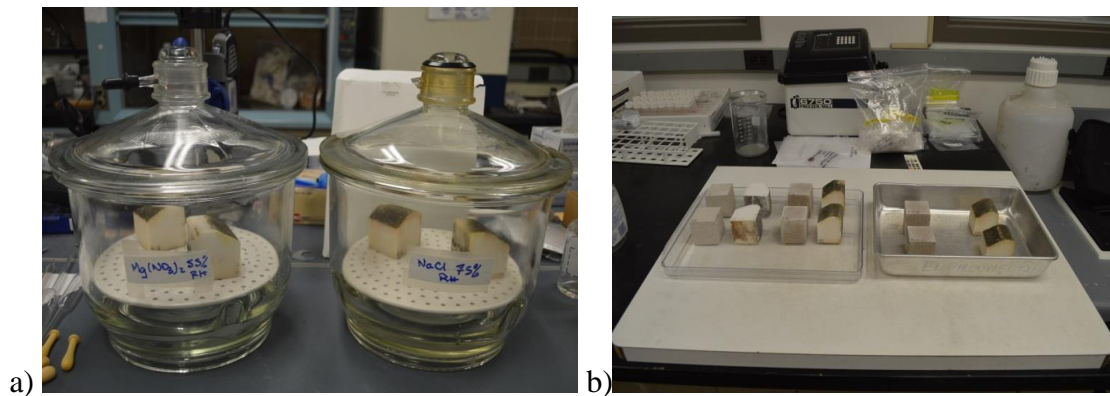


**Figure 37**. a) marble samples placed in desiccator with saturated solution of $Mg(NO_3)_2$ (RH~55%) and NaCl (RH~75%); b) Indiana limestone and marble samples were exposed to the room environment, the samples on the right were also sprayed daily with carbonated water.

*3.2.4.2* Application of sticky rice and nanolime

The sticky rice paste was used both as a consolidation treatment and as a pre-treatment before nanolime application. As a consolidation treatment, the sticky rice solution was applied by brush until no further absorption was observed for a period of at least five minutes between each brushstroke. At this time, the samples were dried in an oven at 40 ℃ until constant mass. Samples were weighed before and after each application (after full evaporation of the solvent) to determine the total amount of the absorbed sticky rice product by each substrate following the formula:

$$\text{Volume of the absorbed sticky rice (ml)} = \frac{Wf - Wo}{\rho} \qquad (20)$$

$$\text{Sticky rice absorbed (g)} = \text{Vol of absorb. sol (ml)} * \text{conc. (g/L)} \qquad (21)$$

Where "Wf" is the weight after treatment (g), "Wo" is the dry weight (g), "ρ" lis the density of the sticky rice solution and "Conc" is the concentration of sticky rice (g/L).

As a pre-treatment, in a sticky rice-nanolime combined application, the sticky rice paste was applied following the application process described above and then the nanolime was applied immediately after samples reached constant mass, following the application method described in section *3.2.4.1*

## 3.2.5 Analytical methodology

The characterisation of the nanolimes and the substrates, and the study of the effectiveness of the consolidation treatments were carried out by means of several analytical techniques and standardised methods which are described below.

### 3.2.5.1 *Characterisation of nanolime*

The two commercial nanolime products and the synthetised nanolimes were characterised in terms of size, morphology, reactivity, colloidal stability and evaporation rate by means of several techniques and standardised methods described below.

#### 3.2.5.1.1 Transmission Electron Microscopy (TEM)

This technique was used to determine the size, crystal phase, agglomeration phenomena and morphology of nanoparticles from both the commercial products (Calosil and Nanorestore) and the synthetised nanolime. TEM samples were prepared by dispersing 0.2 ml of nanolime suspensions in 20 ml of ethanol and placing a few drops of the resulting liquid on a carbon-coated copper grid (Fig. 38a) in nitrogen environment. This technique was also used to study the reactivity and particle growth of nanolimes. TEM samples for the study of reactivity were prepared by placing few drops (≈0.10 ml) of nanolime suspension on a carbon-coated copper grid and left in contact with the air at

laboratory room conditions (20°C, RH ≈ 50-60%). The analyses of the reactivity were carried out 1 minute immediately after solvent evaporation.

A Phillips CM200 Transmission Electron Microscope was used for this test (Fig. 38b). TEM images were obtained by working on 200Kv.
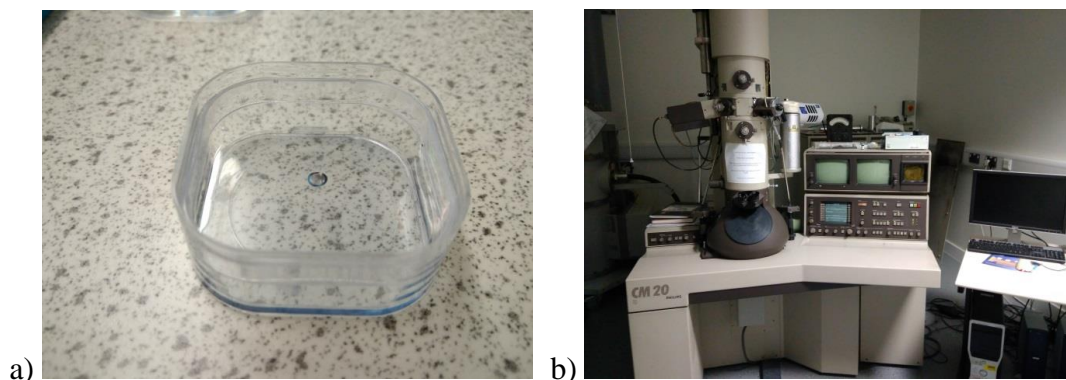


**Figure 38**. TEM. a) TEM copper grip sample; b) Phillips CM200 at Materials and Engineering Research Institute Labs.

*3.2.5.1.2 X-Ray Diffraction (XRD)*

This technique was used to determine the crystalline phase of nanoparticles in suspension. XRD samples were prepared by placing 0.10 ml of nanolime suspensions on a zero-background silica sample holder (Fig 39a). Samples were prepared in nitrogen atmosphere (99.99% nitrogen gas, 3ppm $O_2$ and 0.5 ppm $CH_4$ impurities) at 0% RH, to prevent lime carbonation (Fig. 39b).

It was also used to carry out a reactivity study of the nanoparticles carbonation process. For this purpose, XRD samples were prepared by exposing 0.10 ml of suspensions to outdoor conditions (T ≈ 5–15°C, RH ≈ 60-80%) for 1 hour, 1 day and 7 days prior to analysing by the diffractometer.

The samples were examined using a Philips X'Pert Pro MPD diffractometer with Cu detector Kα in the angular range from 15° to 75°2 θ (Fig. 39c). The XRD patterns were recorded with a step size of 0.026°2θ, in the angular range 5-70°2θ (Fig. 39d).

Quantitative analyses were carried out by means of Rietveld refinement [Rietveld, 1969; Bish, 1989]. X-ray data were fitted using the pseudo-Voigt profile function. Specimen displacement, polynomial coefficients for the background function, lattice parameters, profile parameters, and Gaussian and Lorentzian profile coefficients were refined. Each experimental diffraction pattern was elaborated by means of a Profile Fit Software (HighScorePlus, PANalytical), and each crystalline phase was identified using the ICSD and ICDD reference databases.
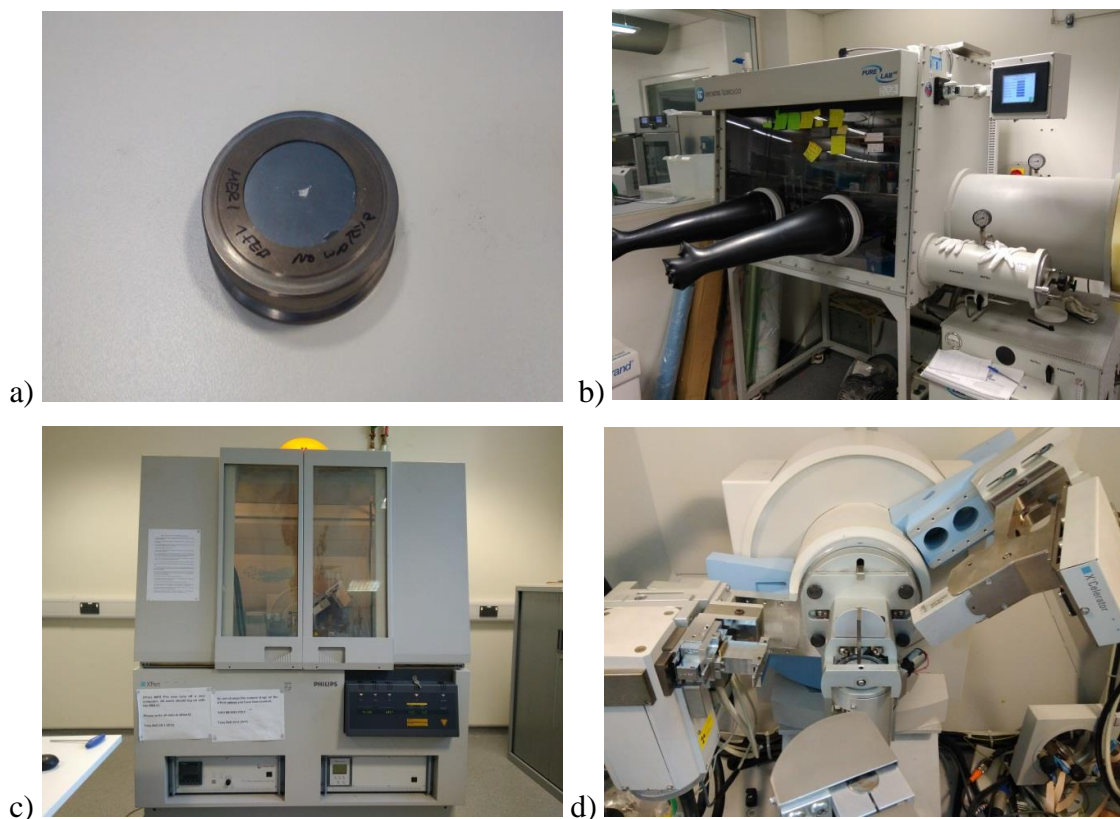


**Figure 39**. a) XRD silicon sample holder with the sample prior to analysis; b) Nitrogen chamber; c) XRD machine; d) details of the Cu detector Kα.

*3.2.5.1.3 Scanning Electron Microscopy (SEM)*

This technique was used to study the carbonation degree of nanoparticles. SEM samples were prepared by placing few drops (±0.10 ml) of nanolime suspensions on a carbon film on a copper SEM sample holder and exposing them to outdoor conditions in a

sheltered area (T ≈ 5–15°C, RH ≈ 60-80%) for 1 hour and 7 days prior to carrying out the observations (Fig. 40a).

A NOVA NANOSEM 200 instrument was used for this test (Fig. 40b). SEM micrographs were taken with an ETD detector, a working distance of ≈ 3mm, an accelerating voltage of ≈ 15 kV and a spot size of ≈ 30 nm in high vacuum (25 MPa). Specimens were coated with a 20 nm thick layer of gold using a Quorum Q150T coater unit at 10 MA sputter current and 420s sputter time, to prevent surface charging and to reduce loads (due to the low conductivity of the samples) which decrease the quality and resolution of images.
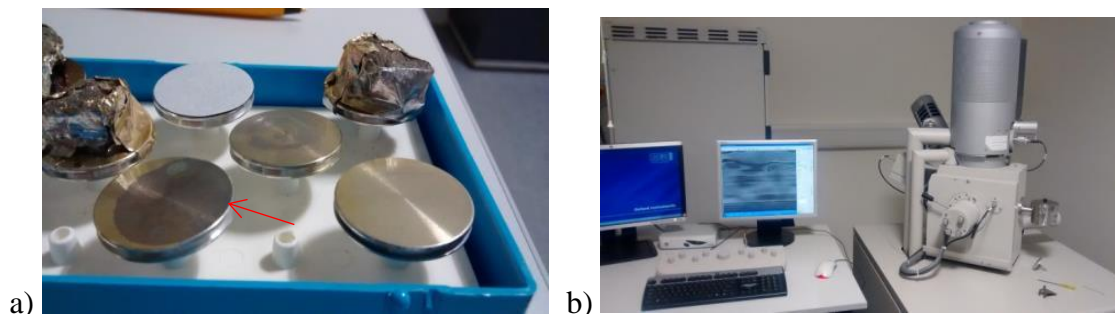


**Figure 40**. a) sample preparation after gold coating; b) NOVA NANOSEM 200;

*3.2.5.1.4 Ultraviolet-Visible Spectrophotometry (UV-VIS)*

The technique was used to determine the colloidal stability of the nanolime suspensions. Before the test, nanolimes were agitated instead of sonicated. Sonicating has been the normal practice in previous studies [Borsoi 2015a; 2016], however, agitation was preferred in this work to simulate in-situ conditions where conservators normally have no access to an Ultrasonic Bath. The kinetic stability (KS) of the nanolimes was determined by turbidity measurements, analysing their absorbance at $\lambda = 600$ nm by means of a UV/VIS Spectrophotometer (UV-VIS Spectrophotometer Varian 50SCAN, Fig.41). Measurements were taken over a period of up to 2 hours. The relative kinetic stability (KS %) was calculated using the following formula:

$$KS \% = 1 - [(A0 - At)/A0] \times 100 \tag{22}$$

Where "A0" is the starting absorbance and "At" the absorbance at time t, both at a wavelength of 600 nm [Ambrosi et al, 2001; Rodriguez-Navarro et al, 2013]. KS % decreases as a result of the nanoparticles settling; values range from 0 (unstable dispersion) to 100 (no deposition of nanoparticles).
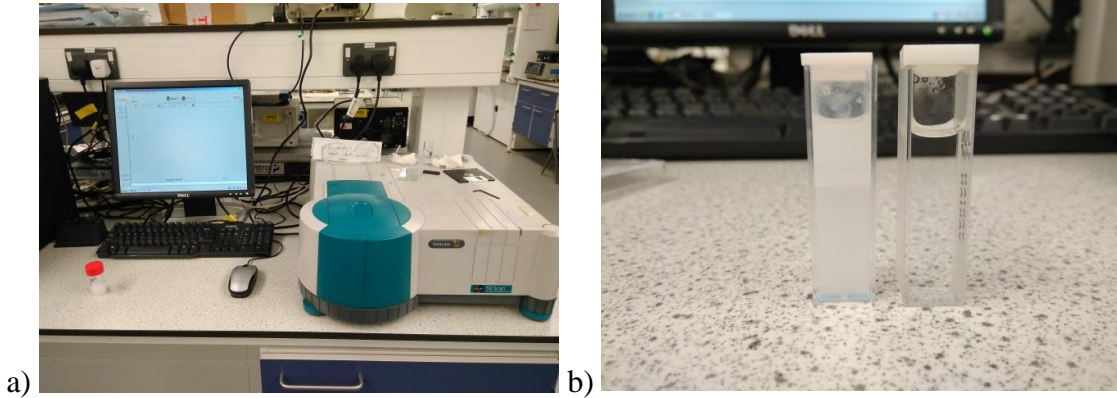


**Figure 41**. a) UV-VIS Spectrophotometer Varian 50SCAN; b) control and nanolime sample

*3.2.5.1.5 Drying rate*

The drying rate of the nanolime treatments was evaluated by measuring the weight loss over time after saturation of three treated samples, in accordance with EN 16322. This test measures the loss of weight by evaporation of solvent over time, recording their weight at different time (Wt) to reach the asymptotical value (Wa). The drying curves plot solvent content $\psi$ (Ut / Vs) [g / cm$^3$] as a function of time [h], where Ut = Wt - Wo and Vs is the specimen's volume. The initial straight section of the curve corresponds to the initial drying rate [g / cm$^3$ ·h].

The aim of this test is to study the correlation of the solvent evaporation rate and the in-depth deposition of the particles, as suggested by Borsoi et al [Borsoi, 2016]. The test was carried out following the same EN 16322 standard as used by Borsoi et al [Borsoi, 2016]. This test was carried out in outdoor conditions (T ≈ 5-15˚C, R.H ≈ 60-80%), using the same conditions as for the application process described in section 3.2.4.1.

### 3.2.5.2 Characterisation of substrates

The substrates were characterised in terms of porosity, chemical and mineralogical composition by means of the techniques described below:

### 3.2.5.2.1 Mercury Intrusion Porosimetry (MIP)

This test was used to characterise the porosity and pore structure of the substrates. The samples were examined using a PASCAL 140/240 Mercury Intrusion Porosimeter from CE Instruments (Fig. 42a). Mercury Porosimetry analysis measures the progressive intrusion of mercury into a porous structure under controlled pressures. From the pressure versus intrusion data, the instrument generates volume and pore size distributions using the Washburn equation:

$$P = \frac{2 \cdot \gamma \cdot \cos\theta}{r} \tag{23}$$

Where "P" is the applied pressure, $\gamma$ the mercury surface tension (at 25°C is 0.485 N·m$^{-1}$), "θ" the contact angle between mercury and the pore surface (at 25°C corresponds to 140º), and "r" is the radius of the pore.

Samples for MIP analyses consisted of fragments measuring approximately 5x5x10 mm which were dried in a fan-assisted oven at 60 ºC until constant weight prior to testing (Fig. 42b). Porosity (%) was calculated as an average of 3 measurements.
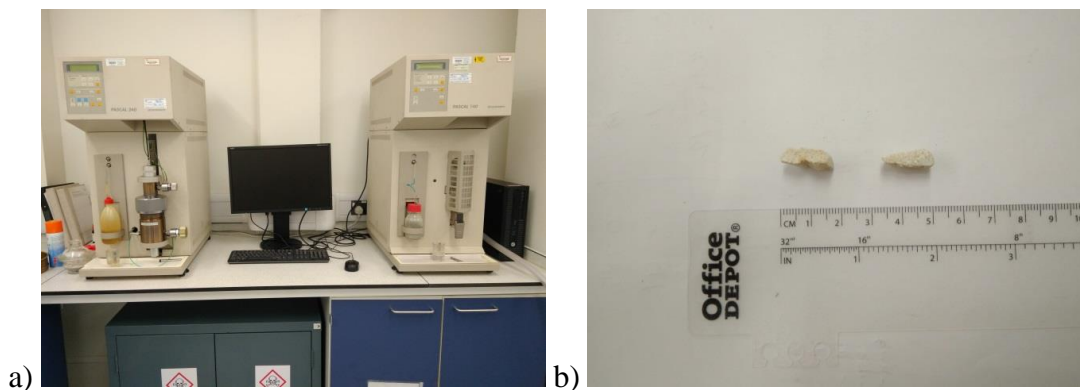
**Figure 42**. PASCAL 140/240; b) samples for MIP

*3.2.5.2.2 X-Ray Diffraction (XRD)*

This technique was used to identify the mineralogical composition of the substrates. XRD samples were prepared in two ways: 1) samples were ground and sieved through an 80 µm sieve mesh and placed over an XRD silicon sample holder (Fig 43a); 2) samples were ground, sieved (80 µm sieve mesh) and pressed in pellets (Fig 43b). XRD patterns were recorded with a step size of 0.026°2θ in the angular range 5-70°2θ using the same model, parameters and refinements as described in section 3.2.5.1.2.
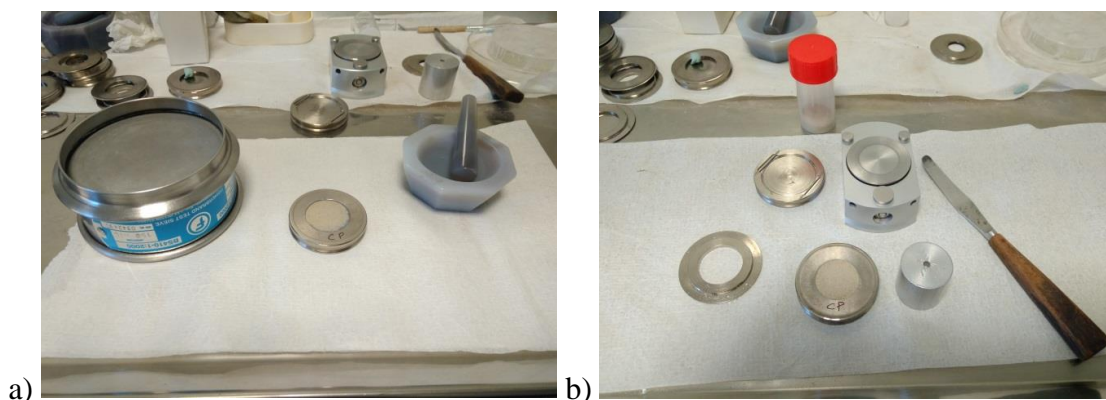


**Figure 43**. Sample preparation for XRD powder diffraction analysis. a) flat-plate XRD sample preparation; b) powder sample (<80 µm) sieved and placed over a XRD silicon sample holder.

*3.2.5.2.3 X-Ray Fluorescence (XRF)*

This technique was used to determine the elemental composition of the substrates. A PANalytical MagiX Pro X-ray Fluorescence (XRF, Fig 44a) was used, which analyses a

78

wide range of chemical elements from boron (B) to americium (Am) with concentration capabilities from few ppm to 100%. XRF samples were prepared as pressed powder samples. Samples were prepared by mixing approximately 0.1g of the sample with approximately 2g of cellulose binder on an aluminium boat. A mixture of approximately 0.1g of sample and approximately 0.1g of cellulose was then sprinkled on top of the 2g of cellulose. The aluminium boat was then compacted at 20 tons in a Retsch PP40 hydraulic press to form a pressed pellet (Fig. 44b). The pellet was loaded into the PANalytical MagiX Pro X-ray Fluorescence (XRF) spectrometer so that XRF spectra could be collected. This uses a Rhodium anode for the X-ray source, hence Rh lines can be observed in the XRF spectra. XRF can give information about the element composition of materials for Sodium and heavier elements, the emitted X-rays for elements lighter than Sodium are too weak to be easily detected by XRF, the binder material is composed of these lighter elements so this binder will not contribute significantly to the XRF spectra produced. XRF data for weight % concentration were analysed using PANalytical standardless "IQ+" software.



a)   b)
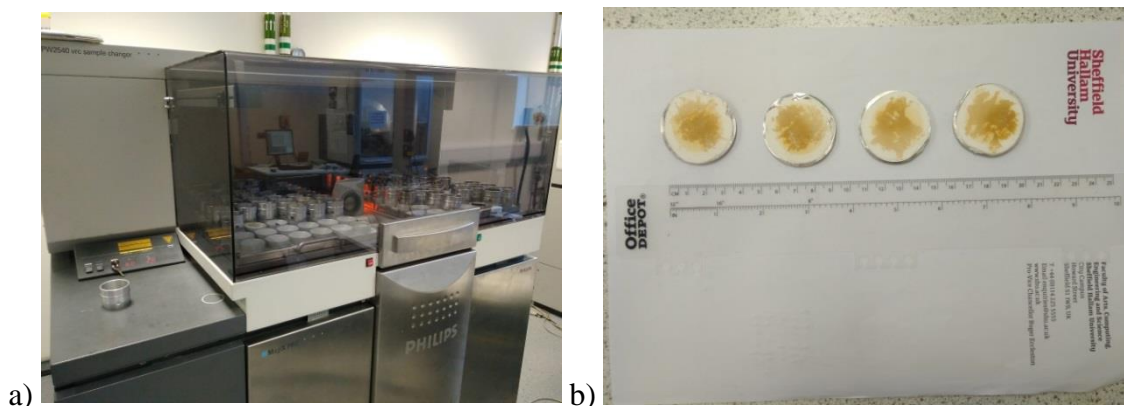
**Figure 44**. a) PANalytical MagiX Pro X-ray Fluorescence (XRF); b) XRF sample

*3.2.5.2.4 Fourier-Transform Infrared Spectroscopy (FTIR)*

This technique was used to determine the mineralogical composition of the substrates. An Attenuated Total Reflectance – Fourier Trans-form Infrared (ATR-FTIR, Thermo Nicolet Nexus instrument, Fig. 45a) was used in this work. The sample for ATR-FTIR

was ground (Ø < 150 µm), dried to constant mass at 60ºC and placed directly on the diamond crystal of the ATR accessory (Fig. 45b). FTIR spectra were collected by 64 scans in the range $400 - 4000$ cm$^{-1}$ at a spectral resolution of 4cm$^{-1}$. A piece of aluminum foil was used to back the sapphire anvil to eliminate any sapphire absorption in the IR spectrum. The obtained FTIR spectrum was identified using the IRUG (Infrared and Raman Users Group) libraries, the HR Hummel Polymer and Additives library as well as the ASTER mineral library.
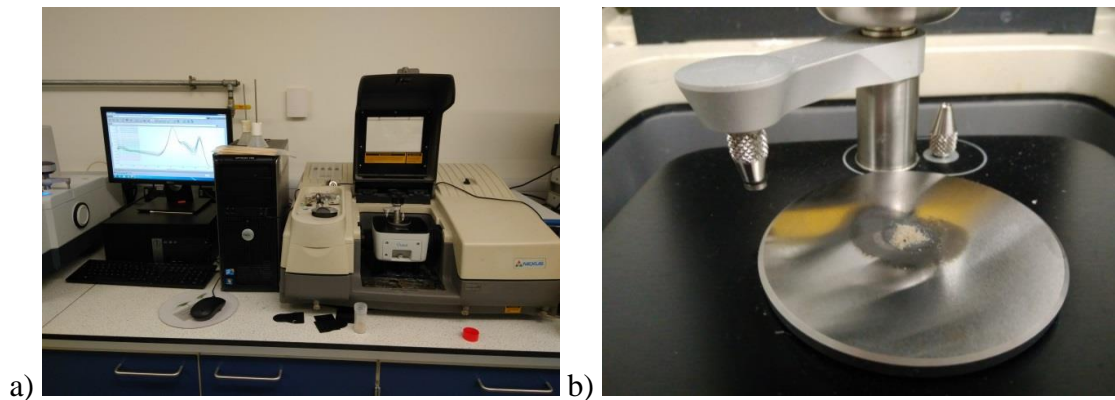


**Figure 45**. a) ATR-FTIR, Thermo Nicolet Nexus instrument; b) detail of the sapphire anvil and the sample prior to analysis.

*3.2.5.2.5 Optical Microscopy (OM)*

This technique was used to study the macroscopic morphology of substrates. A general examination was performed using a stereomicroscope (SM, Leica Stereozoom S8APO) with a Nikon DS-Fi1 digital camera.

*3.2.5.3 Evaluation of the treatments effectiveness*

The consolidation effectiveness of the treatments was assessed by the tests described below.

*3.2.5.3.1 Phenolphthalein test*

This test was carried out to assess the degree of carbonation of the nanolime absorbed by the treated samples. This test was carried out only in limestones, as a fully carbonated substrate was required to be able to detect any nanolime in the substrate that did not carbonate. Phenolphthalein is a chemical compound ($C_{20}H_{14}O_4$) which is a well-known pH indicator which remains colourless for pH <8.2, while it turns to pink/purple colour in pH conditions higher than 9.8 [Lahdensivu, 2016]. For this application, due to the alkalinity of the nanolime (pH ~12), it turns pink in basic solution (nanolime) and colourless in non-basic solutions ($CaCO_3$). 1% Phenolphthalein is dissolved in 100 ml of a hydro-alcoholic medium (70% ethanol - 30% water) [Borsoi et. al., 2015a]. For this test, the substrate cubes were split in half and the phenolphthalein solution was immediately sprayed onto one of the fresh split faces. The test was carried out immediately after saturation of the sample with nanolime and after 28 days curing.

*3.2.5.3.2 Contact angle*

This technique was used to determine the hydrophobicity behaviour of the treatments. A OCA 15 Plus (Dataphysics Instrument, Fig 46a) was used to determine the wettability of the substrates after treatments. The water drop contact angle which forms on a material's surface defines its hydrophobicity. The higher is the contact angle, the more hydrophobic is the material's surface.

For this test a water drop (5µl, deionised water) was placed over the substrate surface through a Hamilton 50µl DS 500/GT syringe (Fig. 46b). Pictures of the water drop on specimen's surfaces were taken after approximately 1 second after applying the water drop and the contact angle was calculated by the software. The static contact angle ($\theta$) has been calculated as the average of 10 measurements.
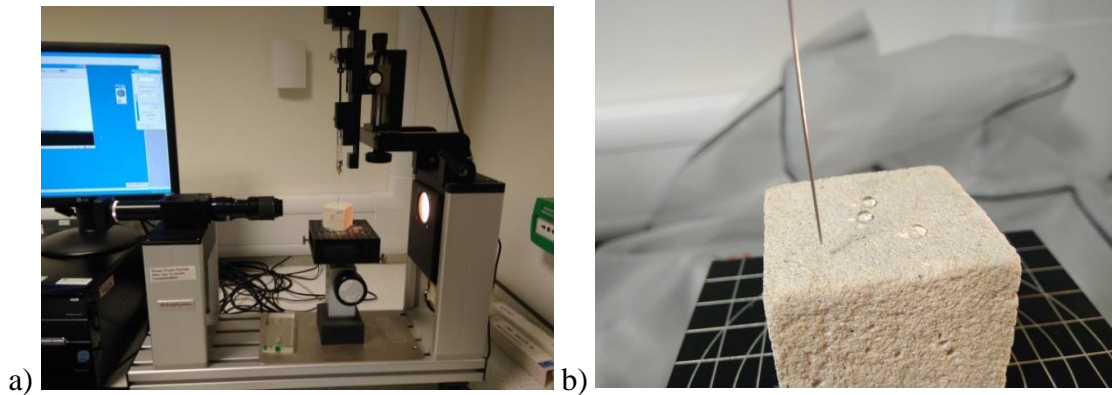
**Figure 46**. a) OCA 15 Plus (Dataphysics Instrument); b) details of the needle and drops of water on the sample.

### 3.2.5.3.3 Mercury Intrusion Porosimetry (MIP)

This technique was used to study the influence of nanolime treatments on the specimens pore structure. Pore size distribution has been determined by means of Mercury Intrusion Porosimetry (MIP) through a PASCAL 140/240 instrument, also described in section 3.2.5.2.1. MIP samples consisted of one fragment of each sample measuring approximately 5x5x10 mm which were dried in a fan-assisted oven at 60 ℃ until constant weight prior to testing. Samples were extracted from the surface (outer 5 mm) of treated and untreated samples to analyse the penetration and the effectiveness of the treatments.

### 3.2.5.3.4 Porosity, Water Absorption and Drying Characteristics

Water is involved in most of the stone weathering processes [Doehne and Price, 2009]. The water absorption coefficient by capillarity (WAC) of three treated and control samples were measured according to EN 13755. Before the test, samples were dried in an oven to constant mass, the dry weight (Wo) and the base area (S) were measured. Samples were placed on a dampened sponge cloth with deionized water, with only one face of the samples touching the dampened cloth (Fig. 47a-b). Weights were recorded at different times (Wt) until samples reached the asymptotical water absorption value (Wa). During the experiment, the water level is kept constant and the container is

hermetically closed throughout the experiment. The capillary water absorption curve plots the amount of water absorbed per unit area, (Ut/S) [g / cm$^2$] vs square root of time (sec $^{0.5}$), where Ut = Wt - Wo and S is the surface area. The initial straight section of the curve corresponds to the capillary water absorption coefficient WAC [g / m$^2$ sec$^{0.5}$]. The water absorption by capillarity test (WAC) was stopped when the difference between two consecutive weightings was no more than 0.1% of the amount of total water absorbed between two readings; which is considered the asymptotical value (Wa).

Upon completion of the WAC test, the samples were immersed in deionised water (Fig. 47c) for 24 hours and their apparent porosity at atmospheric pressure was calculated following ASTM C 97-96 (American Society for Testing and Materials, 1996). The immersion time was half of that recommended in this standard. Apparent porosity is the percent absorption by weight of water in open pores after immersion and is calculated following this formula:

$$\% \text{ Apparent porosity} = \frac{Ws - Wo}{Wo} \cdot 100 \qquad (24)$$

Where "Ws" is the saturation weight and "Wo" is the dry weight.

The open porosity is the percent absorption by the volume assuming that the density of water is practically 1 g/cm$^3$, and is calculated following the formula:

$$\% \text{ Open Porosity} = \frac{Ws - Wo}{Vs} \cdot 100 \qquad (25)$$

Where "Ws" is the saturation weight, "Wo" is the dry weight and "Vs" is the volume of the sample.

After calculating the apparent and open porosity, samples were monitored to assess their drying behaviour which was sequentially calculated according to CEN EN 16322 (Fig. 47d). This test measures the loss of weight by evaporation of water over time, recording their weight at different time (Wt) to reach the asymptotical value (Wa). The drying

curves plot moisture content $\psi$ (Ut / Vs) [g / cm$^3$] as a function of time [h]. The initial straight section of the curve corresponds to the initial drying rate [g / cm$^3$ ·h]. Critical moisture content corresponds to the residual water that remains in the sample after reaching the asymptotical value [g].

The behaviour of any stone with regard to water absorption and water loss is highly related with its decay processes. This sequence simulates a real situation in an outdoor condition (cycles of dry-wet-dry).
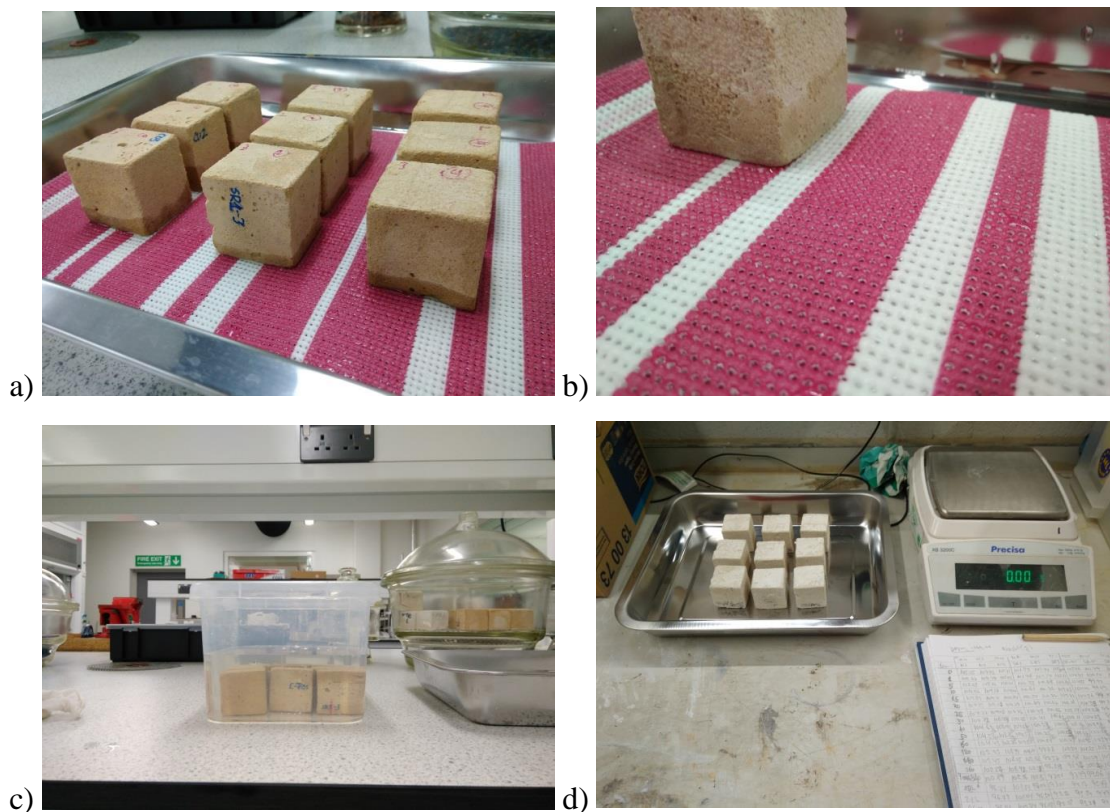


**Figure 47**. a) Water absorption by capillary test; b) detail of the absorption by capillary; c) 24 hours immersion in water; d) drying test.

The WAC test (Fig. 48) for the irregular biocalcarenite stones was carried out using a different method, which has been proposed by LNEC and was specifically developed for irregular substrates [Rosario et al, 2004]. The absorbed water is determined through the difference between the weights measured periodically and the initial weight. To measure the specimen irregular surface in contact with water, this surface is placed on a sheet of

millimetric paper and its contour is drawn and the area calculated (Fig. 48a). For each sample, the values of the coefficient of average absorption in 30 minutes (CA) was measured, as well as the amount of absorbed water at the end of the test (Qf) and the variation of CA values between untreated and treated stones ($\Delta$CA) was calculated. The effective protective efficacy ($E_p$), is defined as the percentage variation of Qf before and after treatment.
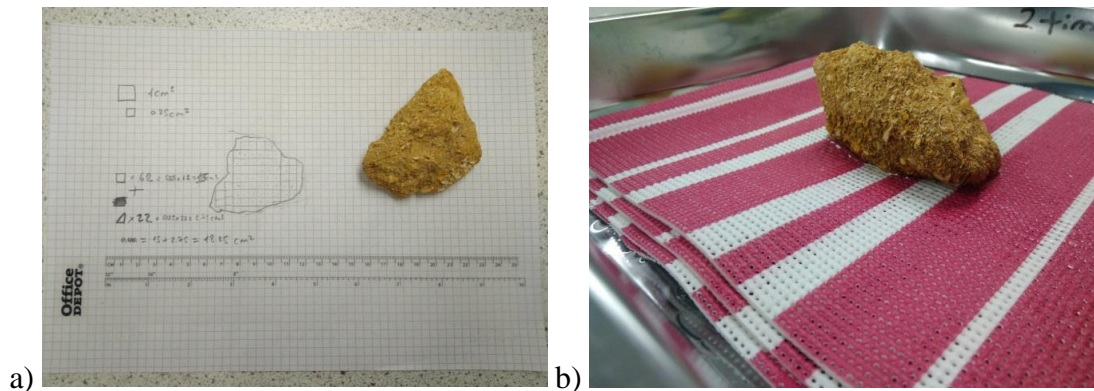


**Figure 48**. WAC following the method proposed by LNEC [Rosario, 2004], a) drawing of the contour and calculations of the area; b) water absorption by capillary test.

*3.2.5.3.5 Drilling Resistance Measurement System (DRMS)*

The consolidation effectiveness of the nanolimes was also assessed by means of a Drilling Resistance Measurement System (DRMS) from SINT-Technology (Fig. 49). The DRMS was specifically designed to evaluate the efficacy of consolidation treatments in historic mortar and stone substrates [Costa and Delgado-Rodrigues, 2012]. The DRMS measures the force required to drill a hole at constant rotation (rpm) and lateral feed rate (mm/min). It is generally considered the most suitable methodology for quantifying consolidation effectiveness and depth of penetration of consolidants, particularly in soft stones [Tiano 2001; 2006; Ferreira-Pinto and Delgado-Rodrigues, 2008a]. Tests were performed on both treated and control samples using drill bits of 5 mm diameter, a rotation speed of 200 rpm, a rate of penetration of 15 mm/min and a

drilling depth of 20 mm. Drilling resistance values per each treatment were calculated as the mean of 6 tests.
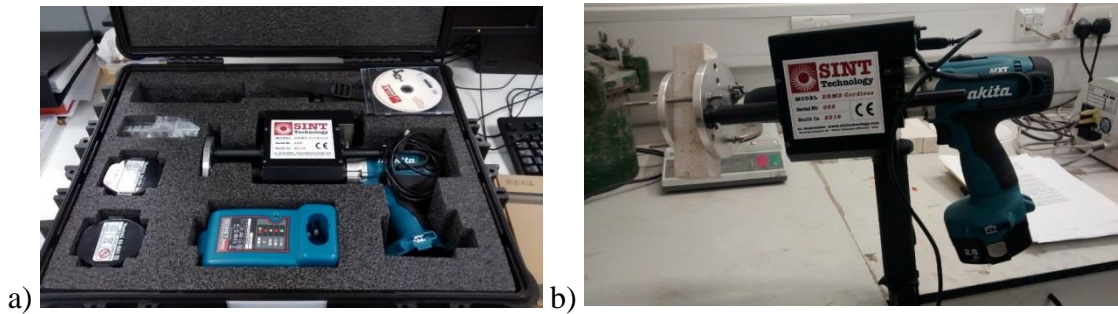


**Figure 49**. a) DRMS set; b) detail of drilling performance of DRMS.

The percentage of the increase of drilling resistance is calculated following the formula:

$$\Delta F\ (\%) = \frac{Fo - Ff}{Fo} * 100 \tag{26}$$

Where "Fo″ is the average of the strength before the treatment and "Ff″ is the average of the strength after the treatment.

### 3.2.5.3.6 *Scanning Electron Microscopy (SEM)*

The surfaces of both treated and control samples were observed under a Scanning Electron Microscope (Fig. 50a) in order to evaluate the morphology and distribution of the crystals resulting from the carbonation of nanolime within the pores. Samples were examined by the SEM as described in section 3.2.5.1.3, with TLD detector at an acceleration voltage between 2-7 kV, spot size 3 and WD 4-7mm in high vacuum (25 MPa). For SEM examinations, surfaces were observed after the treatments and cross-sectional samples of treated and control samples were also observed to assess the penetration and the surface pore structure. Samples were placed over a carbon film on a SEM aluminium sample holder. The samples were covered with foil from top to bottom with two or three copper tape strips placed from the specimen surface to its base (as it is

shown in Figure 50b). All samples were gold coated by "sputtering" with a conductive film of gold using a Quorum Q150T at sputter current 10mA and sputter time 420s.
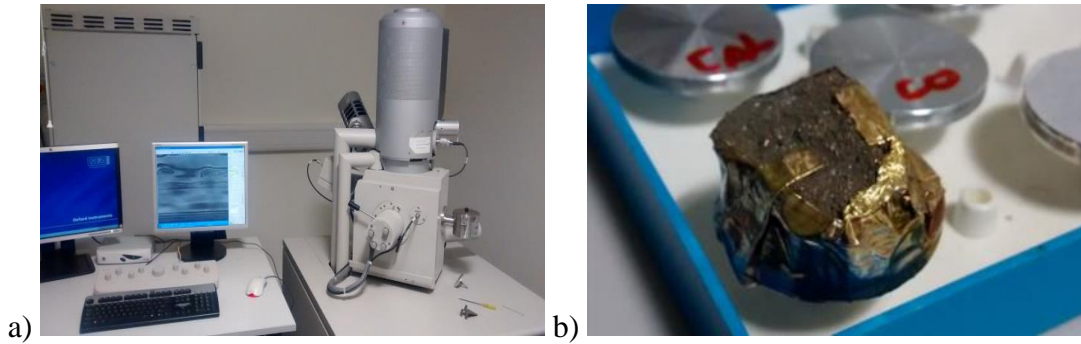


**Figure 50**. a) NOVA NANOSEM 200; b) example of one of the samples' preparation

*3.2.5.3.7 Colorimeter*

Any surface colour variations induced by the nanolime treatments were evaluated with a spectrophotometer (Minolta CM508D Colorimeter, Fig 51a) with the CIELab system [Rodriguez-Navarro et al, 2013]. 30 measurements were taken in different areas of the surface of each of the treated and control mortar cubes (Fig. 51b). Total colour variation (ΔE) was calculated by the formula:

$$\Delta E^* = \sqrt{\Delta L^{*2} + \Delta a^{*2} + \Delta b^{*2}} \tag{27}$$

Where "ΔL*", "Δa*" and "Δb*" are the change in luminosity for white-black, red-green and blue-yellow parameters, respectively.
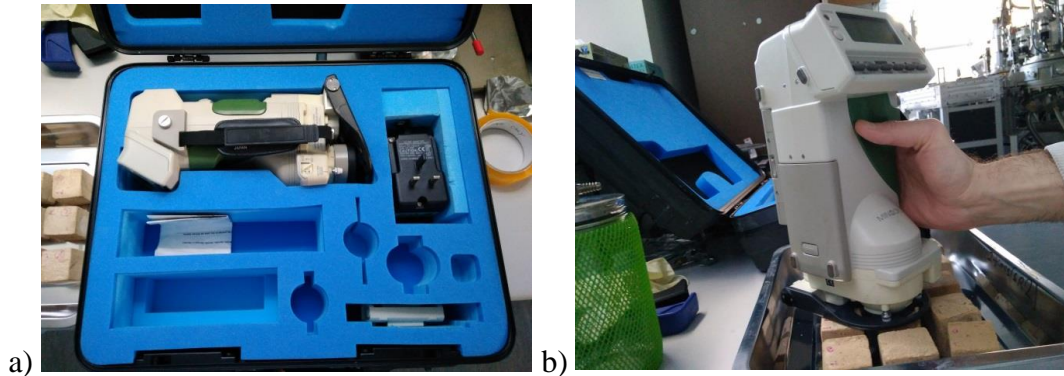
**Figure 51**. a) Minolta CM508D Colorimeter; b) test carried out in the laboratory on cubic samples.

### 3.2.5.3.8 Accelerated weathering testing

The durability of the nanolime treatments was evaluated using a QUV/SE Accelerated Weathering Tester from Q-Lab Europe Ltd (Fig. 52a). Both treated and control cubes were exposed to alternating cycles of UV light and moisture condensation at controlled temperatures in accordance to ASTM G154 CYCLE 6 for a period of 340 hours. Each cycle consisted of 8 hour exposure to UV light at an irradiance of 1.55 W/m2 and a temperature of 60 °C and 4 hour exposure to moisture condensation at 50 °C with no UV irradiation. This exposure conditions have been referred to as AWT 1 (see below).

The durability of the samples treated with sticky rice only and with the combined sticky rice - nanolime treatment was also evaluated using the accelerated weathering tester. Treated and control samples were exposed to alternating cycles of UV light and moisture condensation under two different exposure parameters:

- AWT 1: Step 1: 8 hours UV at 1.55 W/m2 irradiance and 60 °C; Step 2: 4 hours moisture condensation at 50 °C with no UV irradiation (ASTM G154 CYCLE 6). Duration 340 hours.
- AWT 2: Step1: 8 hours UV at 1.55 W/m2 irradiance and 40 °C; Step 2: 4 hours moisture condensation at 30 °C with no UV irradiation. Duration 340 hours.

After those weathering tests, the drilling resistance (DRMS), superficial cohesion (STT), colour (colorimeter) and hydrophobic properties (contact angle) were subsequently tested.



a)                                                         b)
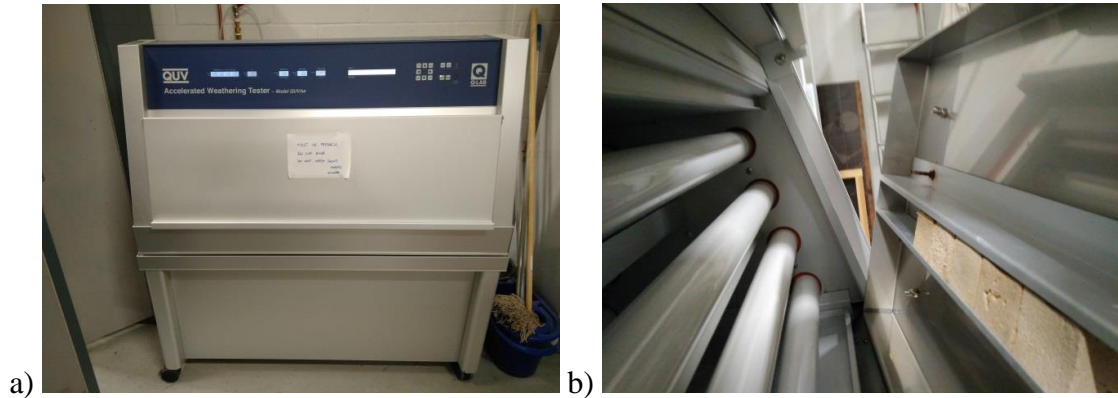
**Figure 52**. a) QUV/SE Accelerated Weathering Tester from Q-Lab Europe Ltd/; b) details of UV lamps and samples.

*3.2.5.3.9 Scotch Tape Test (STT)*

The influence of the nanolime treatments on the surface cohesion of the substrate was evaluated by means of the 'Scotch Tape Test' (STT) carried out in accordance with ASTM D3359-02. This Scotch Tape test (also known as 'peeling test') has been introduced into the field of conservation by P. Mora and G. Torraca in the 1960s [Mora and Torraca, 1965] and it has been widely used for more than 40 years in conservation practice for assessing the effectiveness of stone consolidation methods [Drdacky and Slizkova, 2015]. The method measures the amount of detached material that adheres to the scotch tape before and after the treatment. For this test, a small 3 M transparent scotch tape is cut into pieces (3 cm) with a contact surface of about 4 cm$^2$ (Fig. 53a) Then the one piece of the scotch tape is weighed (only the scotch tape), Fig. 53b) and pressed on to the substrate surface (Fig. 53c) and peeled off after three minutes and weighed with the released material attached to it (Fig. 53d). The amount of detached material is calculated in "mg/cm$^2$" following this formula:

$$\Delta W \ (g/cm^2) = \frac{Wf - Wo}{Wo} / a \tag{28}$$

Where "ΔW" is the detached material (mg/cm$^2$), "Wf" is the final weight, "Wo" is the initial Weight and "a" is the scotch tape area.

The percentage of the reduction of detached material is calculated following the formula:

$$\Delta W\ (\%) = \frac{Wo - Wf}{Wo} * 100 \qquad (29)$$

Where "ΔW (%)" is the percentage of the detached material, "Wo" is the initial weight; "Wf" is the final weight. The test was performed on both treated and control samples and results taken as the average of 10 measurements per sample.
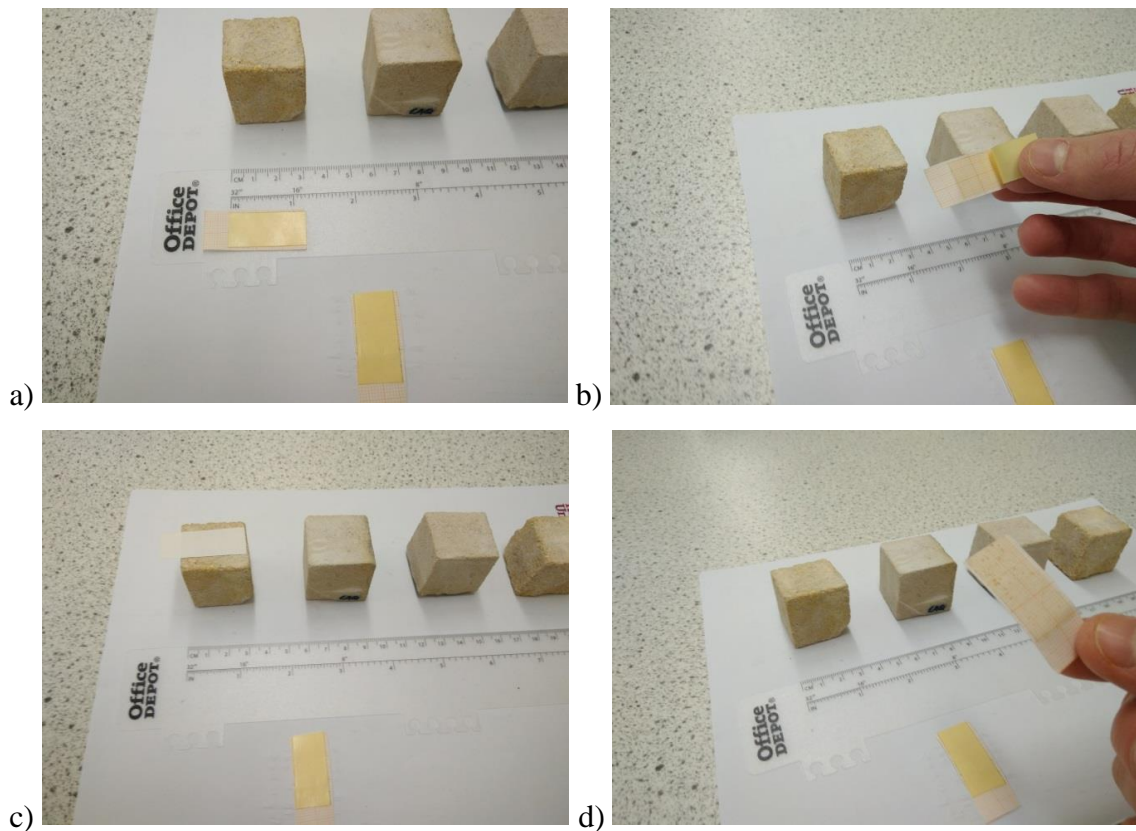


**Figure 53**. Scotch tape test, a) Cut the scotch in pieces (3 cm); b) remove the cover and weight the Scotch tape, c) contact with the surface and press; d) peeling off and weight the scotch.

*3.2.5.3.10 Resistance to wetting-drying cycles*

The resistance to wet-dry cycles of the samples treated with sticky rice was evaluated by conducting this experiment following a method described in the literature [Wei et al, 2012]. Three cubic samples both treated with sticky rice only and the sticky rice - nanolime combined treatment (SR and SR-LAQ, described in section 3.3.6) with dimensions 40 x 40 x 40 mm were used for this test. During the experiment, all the samples were immersed in the normal atmospheric-temperature deionized water for 8 h, with the water level 20 mm over the sample's upper surface. After thoroughly soaked, the samples were put into the fan-assisted oven (40º C) for 8 h, and then naturally cooled to the normal atmospheric temperature. This cycle was repeated 20 times.

After this weathering test, the drilling resistance (DRMS), superficial cohesion (STT) and hydrophobic properties (contact angle) were subsequently tested.

### *3.2.5.4 Characterisation of the additives: sticky rice*

The characterisation of the additives was carried out by the tests described below.

*3.2.5.4.1 Scanning Electron Microscope (SEM)*

The dried gelatinized sticky rice was observed by SEM to evaluate its morphology. Samples were prepared by placing few drops of the gelatinized sticky rice on carbon coated SEM sample holder and dried residue was coated with gold following the method as described in section 3.2.5.3.6.

*3.2.5.4.2 Fourier-transform infrared spectroscopy (FTIR)*

The FTIR technique was used to determine the chemical bonds of sticky rice. The dried gelatinized sticky rice was placed directly on the diamond crystal of the ATR accessory. FTIR spectra were collected by 64 scans in the range $400 - 4000$ cm$^{-1}$ at a spectral

resolution of $4\text{cm}^{-1}$. A piece of aluminium foil was used to back the sapphire anvil to eliminate any sapphire absorption in the IR spectrum. The obtained FTIR spectrum was identified using the IRUG (Infrared and Raman Users Group) libraries, the HR Hummel Polymer and Additives library as well as the ASTER mineral library.

*3.2.5.4.3 Iodine test*

Sticky rice starch is a mixture of two types of polysaccharides: amylose and amylopectin [Gadhave et al, 2017]. This test was used to characterize the type of polysaccharide of the sticky rice starch. Iodine reagent (KI) was prepared by dissolving 0.2 g of iodine in 100 ml of deionized water in the presence of 2.0 g of KI. The iodine-KI reagent was dropped into the sticky rice suspension. The suspension turns blue if there is presence of amylose or red if presence of amylopectin [Rundl et al, 1944].

*3.2.5.4.4 Rheology*

The depth and speed of penetration of the sticky rice in a porous material are related to the viscosity of the product. For this reason, the rheological behaviour of the gelatinized sticky rice solution has been assessed using a Rheometer Anton-Paar Physica MCR 301. The measurements were made at 40°C.

The obtained flow curves plot the shear stress (mPa) versus the velocity gradient ($s^{-1}$). The rheological behaviour of the sticky rice was compared to that of water.

*3.2.5.4.5 Surface tension*

The surface tension of the sticky rice solution was determined by the pendant drop-method by an OCA 15 Plus instrument (Dataphysics). The pendant drop-method is a universal method to measure surface tension. The surface tension of the sticky rice was calculated by measuring the shape of the pendant drop of the dosing needle. The shape

of the drop is the result of two forces: the gravitation elongates the drop and the surface tension is endeavouring to hold the drop in spherical form to minimize the exposed surface [Operating manual OCA]. The equilibrium state has a characteristic drop curvature. This force equilibrium is mathematically defined with the Young-Laplace equation, so once the drop shape has been calculated the surface tension can be calculated following the equation:

$$\Delta P = \gamma \left( \frac{1}{R1} + \frac{1}{R2} \right) \tag{30}$$

Where "$\Delta P$" is the difference in pressure across the interface, "$\gamma$" the surface tension, and "R1" and "R2" are the curvature radius.

For this test a sticky rice solution drop (5µl) was pending through a Hamilton 50µl DS 500/GT syringe. Pictures of the sticky rice solution were taken just before liquid dispensing. The software calculates the surface tension values according to the shape of a drop through the Young-Laplace equation.

## 3.3 Research Programmes

The literature review (section 2.5) elucidated several research point that required study to evaluate the effectiveness of nanolime as a consolidant in calcareous substrates. According to those needs, the following research programs were developed:

1. A comparison of three nanolime available products on highly porous substrates
2. Influence of different types of solvent on the effectiveness of nanolime treatments on highly porous substrates
3. Influence of substrate pore structure and nanolime particle size on the effectiveness of nanolime treatments
4. Case of study: Preliminary investigations of compatible nanolime treatments on Biocalcarenite from Agrigento, Italy
5. Case of study: Preliminary investigations of compatible nanolime treatments on Indiana limestone and weathered marble from the Smithsonian's building.
6. The use of additives to improve nanolime effectiveness
    6.1. Additives and their influence on carbonation
    6.2. Sticky rice
        6.2.1 Characterisation of sticky rice
        6.2.2 Consolidation effectiveness of sticky rice and a sticky-rice-nanolime treatment
        6.2.3 Durability of the sticky rice and sticky rice - nanolime consolidation effectiveness

**1**. **Nanolime for the consolidation of lime mortars: a comparison of three available products**

The results of this research have been accepted for publiscation in the Construction and Building Materials Journal (pending to be published). The aim of this work was to compare for the first time the consolidation effectiveness of the three available nanolime products on lime mortars and investigate their long term performance.

Three nanolime dispersions were used for this work:

- – **Nanorestore Plus Propanol 5**®. This nanolime is referred to as **NAN**.
- – **Calosil IP5**®. This nanolime is referred to as **CAL**.
- – **Nanolime synthesized through the method developed by the University of L'Aquila** [Taglieri et al, 2015; Volpe et al, 2016]. It has been selected the WIP nanolime (50% Water - 50% Isopropanol) for this test due to the promising preliminary results [Taglieri et al, 2016]. This nanolime is referred to as **LAQ**.

The size, morphology, reactivity and crystalline phase of the nanoparticles have been investigated by TEM, SEM and XRD. The colloidal stability of the nanolime products has been investigated by UV-VIS.

Each of the three nanolimes was applied on three 40x40x40 mm mortar cubes following an application method described in the section 3.2.4.1. Following 28-day outdoor exposure, the influence of the nanolime treatments on mortar have been investigated by assessing its superficial cohesion (STT), carbonation (phenolphthalein test), water absorption by capillarity (WAC), porosity by 24 hours immersion in water, drying rate, drilling resistance (DRMS), pore structure (MIP) and aesthetic properties (colorimetry).

The durability performance of the nanolime treatments has been investigated by exposing the mortar samples to Accelerated Weathering Testing (AWT) and measuring changes in the mortars surface colour and drilling resistance after the exposure.

**2. Influence of different types of solvent on the effectiveness of nanolime treatments on highly porous substrates**

The aim of this work was to study the influence of different types of solvent one the consolidation effectiveness of LAQ nanolime. This was carried out by dispersing the nanoparticles in different types of solvents. Furthermore, this research aimed to study a correlation between the solvent evaporation kinetics and the consolidation effectiveness which was described by Borsoi et al [Borsoi et al 2015a; Borsoi et al, 2016].

The nanolime was synthetised through the University of L'Aquila method (LAQ) and used in five nanolime formulations:

- 5 g/L dispersed in isopropanol (**IP**)
- 5 g/L dispersed in ethanol (**ET**)
- 5 g/L dispersed in water (**W**)
- 5 g/L dispersed in 50% isopropanol and 50 % water (**WIP**)
- 5 g/L dispersed in 50% ethanol and 50 % water (**WET**)

The size, shape, reactivity and crystalline phase of the nanoparticles have been investigated by TEM and XRD. The colloidal stability of the nanolime products has been investigated by UV-VIS. The solvent drying kinetic was calculated by EN16322.

Each of the five nanolimes was applied on three 40x40x40 mm mortar cubes following the application method described in section 3.2.4.1.

Following 28-day outdoor exposure, the consolidation effectiveness of nanolime treatments in lime mortar has been investigated by superficial cohesion (STT), water absorption by capillarity (WAC), porosity by 24 hours immersion in water, drying rate, drilling resistance (DRMS), pore structure (MIP) and aesthetic properties (colorimetry).

**3**. **Influence of substrate pore structure and nanolime particle size on the effectiveness of nanolime treatments**

According to the results of the research program 1 and the literature review (section 2.5), nanolimes which are synthetised from different routes (i.e. solvothermal reactions or anion exchange methods) present different particle size. Nanoparticles synthetised by solvothermal reactions (Nanorestore Plus) show a particle size of 150 - 300 nm, while nanoparticles synthetised by anion exchange resins (LAQ), have particle size of 20 - 80 nm. The aim of this work is to study the influence of the substrate pore structure and the nanolime particle size in the consolidation effectiveness. This study used two nanolimes with different particle size (LAQ and Nanorestore Plus®) and two substrates with different pore size distribution.

Two nanolime dispersions were used for this work:
- **Nanorestore Plus Propanol 5**®. Particle size **150-300** nm (**NAN**)
- 5g/L dispersed in 50% isopropanol and 50 % water. Particle size **20 - 80** nm (**LAQ**)

The size, shape, reactivity, crystalline phase and colloidal stability of both nanolimes have been characterised in the research program 1.

Each nanolime was applied on three 35 x 35 x 35 mm weathered Doulting limestones (**CP**) and on three 35 x 35 x 35 mm limestone (**LS**), following the application method described in the section 3.2.4.1. These limestones were selected because they present a different pore size distribution (section 3.1.3).

Following 28-day outdoor exposure, the consolidation effectiveness of nanolime treatments on the two limestones has been investigated by superficial cohesion (STT), water absorption by capillarity (WAC), porosity by 24 hours immersion in water, drying rate, drilling resistance (DRMS), pore structure (MIP) and aesthetic properties (colorimetry).

## 4. Case of study: Preliminary investigations of compatible nanolime treatments on biocalcarenite stone from Agrigento (Italy).

The results of this research were published in the Journal of Cultural Heritage (vol. 30 (2918) 92-99) as part of a research placement carried out in 2017 at the University of L'Aquila. As discussed in the research program 1, LAQ nanolime obtained promising consolidation properties in the laboratory. This project aimed to test the effectiveness of LAQ nanolime as a compatible treatment on biocalcarenite stones from Villaseta of the Temples (Agrigento, Italy), which are similar to the ones used for construction of the UNESCO Archaeological Site of *Valley of the Temples* in Agrigento (Sicily, Italy) and are characterised by a documented advanced decay Rossi-Manaresi 1982, Rossi-Manaresi 1991]. The aim of this research was to carry out preliminary investigations for the development of an in-situ compatible treatment.

Three synthesized nanolime dispersions were used for this work:
  - 5 g/L in butanol (**B**)
  - 5 g/L in 50% isopropanol and 50 % water (**WIP**).
  - 10 g/L in 50% isopropanol and 50 % water (**WIP\***).

The synthesis and characterisation of the nanolime was carried out at the University of L'Aquila (Italy) laboratories. The size, shape, reactivity and crystalline phase of the nanoparticles have been investigated by TEM and XRD. The colloidal stability of the nanolime products has been investigated by UV-VIS.

Each nanolime was applied following the application method described in section 3.2.4.1 on one irregular biocalcarenite stone (described in section 3.1.3):

  - **sample S1** was treated with WIP
  - **sample S2** was treated with WIP*
  - **sample S3** was treated with B

- **samples S4**, **S5** and **S6** were treated with WIP but the treatment was repeated three times for each sample, to increase the concentration of nanolime.

The use of irregularly shaped stone samples was considered to reproduce the real in situ application on irregular surfaces. Following 2-days at high Relative Humidity (75±5 % RH), the consolidation effectiveness of nanolime treatments in biocalcarenites has been investigated by superficial cohesion (STT), water absorption by capillarity (WAC), drilling resistance (DRMS), pore structure (MIP) and aesthetic properties (colorimetry).

**5. Case of study 2: Preliminary investigations of compatible nanolime treatments on American Indiana limestone and weathered marble stone.**

The results of this research have been attached in the Appendix A as part of a research placement carried out at the Smithsonian's Museum Conservation Institute in 2016. The aim of this work was to test the consolidation effectiveness of LAQ nanolime as a compatible treatment on Indiana limestones and on a weathered marble which was obtained from the Smithsonian Garber facility at the Smithsonian's Conservation Institute (MCI), Washington DC (USA) and represents a similar marble as the main constructive material of the *Smithsonian National Portrait Gallery and the Smithsonian American Art Museum*. The aim of this research is to carry out preliminary investigations for an in-situ compatible treatment for the weathered marble.

Two nanolime formulations were used for this work:

- 25 g/L dispersed in 90% isopropanol and 10 % water (**IP25**)
- 25 g/L dispersed in 90% ethanol and 10 % water (**E25**)

The synthesis and characterisation of the nanolime was carried out at the Smithsonian's Museum and Conservation Institute (MCI) following the procedure described in section 3.2.2.

IP25 nanolime was applied on 50 x 50 x 50 mm Indiana limestone samples and ET25 was applied on irregular weathered marble samples, following the application method described in section 3.2.4.1. Samples were kept in different environment conditions in order to study their influence on carbonation:

- Two marble samples were kept at 75% RH (**M75**)
- Two marble samples were kept at 55% RH (**M55**)
- Two marble samples were kept at room conditions ±50%RH (**MR**)

- Two marble samples were kept at room conditions ±50%RH but they were sprayed daily with carbonated water (**MRS**)
- Two Indiana limestone samples were kept at room conditions ±50%RH (**IR**)
- Two Indiana limestone samples were kept at room conditions ±50%RH but they were sprayed daily with carbonated water (**IRS**)

Following 28-days, the consolidation effectiveness of nanolime treatments in the different environments has been investigated by superficial cohesion (STT), water absorption by capillarity in cubic Indiana limestones (WAC), porosity by 24 hours immersion in water, drying rate, Drilling Measurement Resistance System (DRMS), colorimeter and micro-imaging (SEM).

## 6. The use of additives to improve nanolime effectiveness

*6.1 Additives and carbonation study*

Part of this research was also carried out at the Museum and Conservation Institute facilities, (Appendix 1). The aim of this experiment was to carry out a preliminary test of the influence of several additives in the carbonation of $Ca(OH)_2$ nanoparticles to study different ways to improve the nanolime performance.

Seven formulations were used for this experiment:

- 25 g/L dispersed in 90% isopropanol and 10 % water (**A**)
- 25 g/L dispersed in 100% deionised water (**B**)
- 25 g/L dispersed in 3%wt. urea $((NH_2)_2CO)$ in deionized water (**C**)
- 25 g/L dispersed in 100% sticky rice water (**D**)
- 25 g/L dispersed in deionized water with high concentration of residual NaCl (**E**)
- 25 g/L dispersed in 100% carbonated water (**F**)
- 25 g/L dispersed in tap water (**G**)

Following the synthesis, the nanoparticles were dispersed in the selected dispersions. After that, 20 ml of each sample was placed on a petri-dish and left to carbonate at room conditions (Fig.54). Following 14-days the morphology of the samples were observed by optical microscopy and SEM and their reactivity by XRD and FTIR.



**Figure 54**. Nanolime samples A-G in the fume hood cupboard at room conditions.

Carbonated water was expected to accelerate the carbonation process as carbonation occurs in presence of moisture and $CO_2$ [Lopez-Arce et al, 2011].The addition of urea to the water was expected to enhance the carbonation as urea decomposes according to the following reaction [Wu et al, 2009]:

$$(NH_2)_2CO + H_2O \rightarrow 2\ NH_3 + CO_2 \tag{31}$$

Sticky-rice soup (water from cooking sticky rice) has been used as an additive traditionally in China for the preparation of lime mortars to improve their resistance, durability and resistance to water [Yang et al, 2009]. The addition of sticky-rice produces a special inorganic-organic composite building material where the inorganic component is calcium carbonate, and the organic component is amylopectin, one of the components of starch from the sticky rice soup. The effect of small amounts of amylopectin plays a crucial role in the carbonation process increasing the specific area of the $Ca(OH)_2$ particles, inhibiting the growth of the $CaCO_3$ crystals that help to create dense and compact microstructure of mortars and reduces the penetration of water due to the inorganic-organic component (wetting-drying) [Wei et al, 2012, Yang et al. 2016b, Yang et al. 2009]. Starch have been patented as "waterproof adhesive" in 1938 [George et al , 1938] and it has also been tested as an effective adhesive providing excellent bonding strength as wood adhesive [Syed, 2000].

*6.2 Sticky rice*

*6.2.1. Characterisation of sticky rice*

The prepared sticky rice has been further characterised to obtain its composition (Iodine-KI reagent test and FTIR), morphology (SEM), viscosity (Rheology), and surface tension (contact angle) to study its properties.

*6.2.2. Consolidation effectiveness*

The aim of this work was to test, in a preliminary way, the consolidation effectiveness of sticky-rice by itself and in combination with a nanolime treatment. As the starch is not miscible in alcohol [Mitchell, 1977], the sticky rice was applied as a pre-treatment and nanolime has been applied immediately after the water of the sticky rice had evaporated. Two products were used for this experiment:

– 5 g/l of the **sticky rice** solution in deionised water. (**SR**)
– **LAQ** (5 g/L nanolime dispersed in 50% isopropanol and 50 % water).

The size, shape, reactivity, crystalline phase and colloidal stability of nanolime have been investigated in the research program 1 and the sticky rice in the research program 6.2.1.

The sticky rice and nanolime were applied on three 40 x 40 x 40 mm lime-mortar cubes following the application method described in section 3.2.4.2. Three cubic mortars were treated with nanolime (**LAQ**), three with sticky rice (**SR**) and three with a combination of sticky rice and nanolime (**SR-LAQ**).

Following 28-day outdoor exposure, the consolidation effectiveness of the sticky rice and nanolime treatments in lime mortar was investigated by superficial cohesion (STT), water absorption by capillarity (WAC), porosity by 24 hours immersion in water, drying rate, drilling resistance (DRMS), pore structure (MIP) and aesthetic properties (colorimetry).

*6.2.3 Durability of the consolidation effectiveness*

The durability of the sticky rice and sticky rice - nanolime treatments has been assessed by exposing three mortar samples treated with **SR** and three treated with **SR-LAQ** to the Accelerated Weathering Tester (AWT) under two different exposure conditions (see

section 3.2.5.3.8) and to wetting-drying cycles (see section 3.2.5.3.10). The durability of the treated samples has been investigated by measuring changes in the mortars superficial cohesion (STT), contact angle and drilling resistance (DRMS). A small amount of water used from the wetting-drying cycles was also analysed by FTIR to study its composition after the cycles.

# Results and Discussion

## 4.1 Nanolime for the consolidation of lime mortars: a comparison of three available products

### 4.1.1 Characterisation of the nanolime suspensions

Figure 55 shows TEM photomicrographs of the three nanolime products. Hexagonal Ca(OH)$_2$ nanoparticles with identical morphology can be observed in all of the three nanolimes. The crystals tend to agglomerate due to their high surface energy [Rodriguez-Navarro et al, 2013; Borsoi et al, 2016; Rodriguez-Navarro et al, 2016] (Figures 55). The size of the observed nanoparticles is 250 - 100 nm for NAN (Figure 55a), 150 - 80 nm for CAL (Figure 55b) and 80 - 20 nm for LAQ (Figure 55c). These results are in line with those reported by the developers of the three products [Ambrosi et al 2001, Baglioni et al, 2014, Taglieri et al, 2017b, Ziegenbalg et al, 2003].



a)



b)
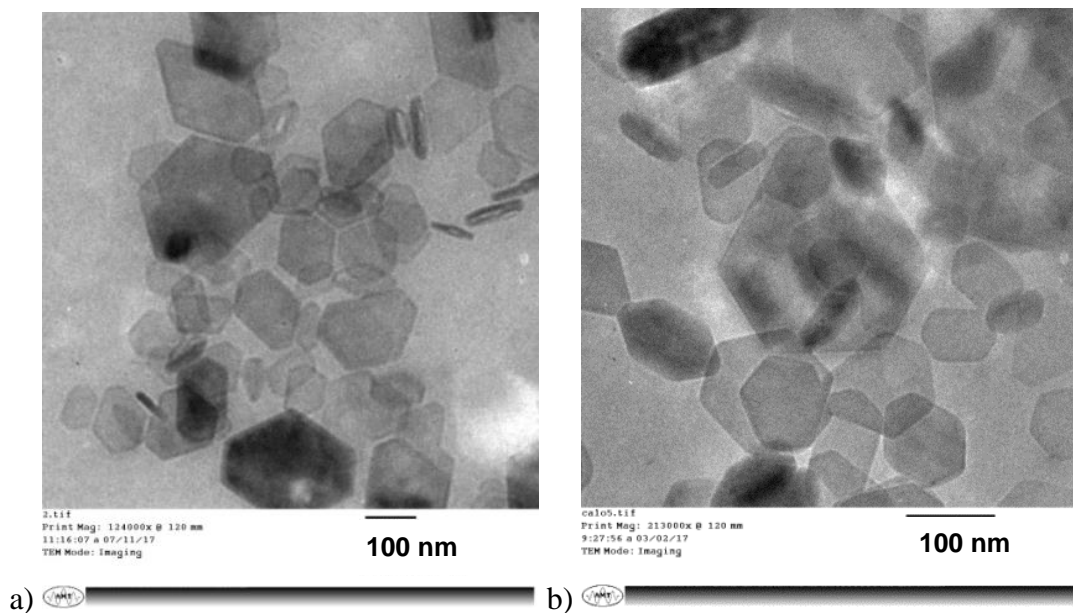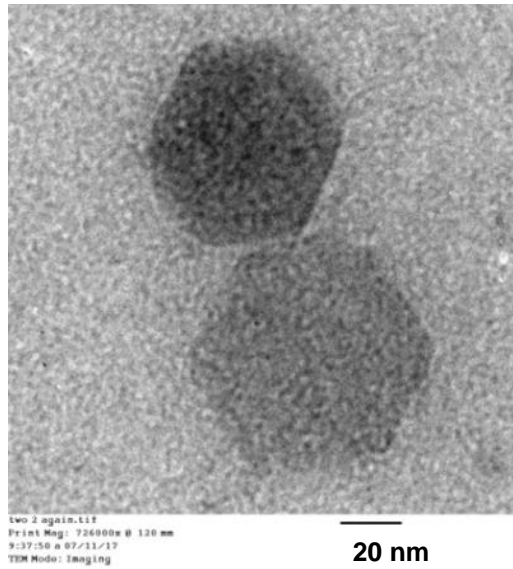
**Figure 55**. TEM images of: a) NAN; b) CAL; c) LAQ. Note that the magnification bar is 100 nm for NAN and CAL, and only 20 nm for LAQ.

The XRD analysis in nitrogen atmosphere (Fig. 56) shows that the only crystalline phase of the three nanolimes is Portlandite ($Ca(OH)_2$, ICSD #01-087-0674), confirming the results of the TEM observations. For the three samples the strongest peak corresponds to the {001} basal plane. However, XRD Rietveld refinements showed that LAQ $Ca(OH)_2$ particles have a preferred orientation to the side plane {010}. NAN and CAL did not show any significant preferred orientation. The Rietveld refinement factors are included in Table 10 (see section 4.1.2, page 109).

c)
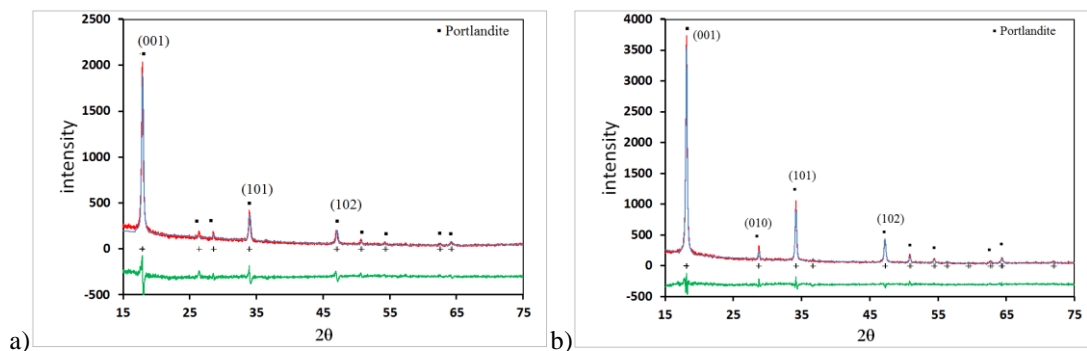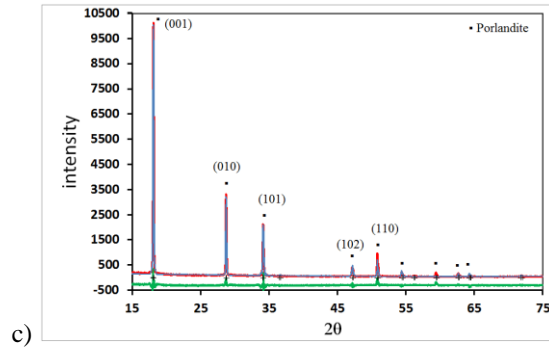
**Figure 56** . XRD patterns for NAN (a), CAL (b) and LAQ (c) samples dried in nitrogen atmosphere. Red line corresponds to Intensity observed, blue line to Intensity calculated and green line to the Intensity observed - Intensity calculated difference curve. The crystal phases are shown in brackets and the "+" symbol corresponds to the main peaks.

Figure 57 shows the absorbance (at 600nm) of NAN, CAL and LAQ dispersions over a period of 2 hours following a moderate agitation. A high colloidal stability was observed for NAN and CAL $Ca(OH)_2$ nanoparticles. Previous studies have shown that NAN and CAL nanolimes can keep the colloidal state for more than one week [Borsoi et al, 2015b]. In contrast, LAQ $Ca(OH)_2$ nanoparticles start to settle about 2 min after agitation (sedimentation rate $\approx$ 6% per h) and 12% of the particles settle after 2 hours. This sedimentation process is considerably slower than that occurring in limewater, where more than 90% of the particles settle in 2 hours [Giorgi et al, 2000]. The colloidal stability of LAQ dispersion during the first 2 minutes after agitation can be considered acceptable for practical purposes as most of the particles remain in colloidal state for the whole length of each application [Rodriguez-Navarro et al, 2013]. High colloidal stability is critical to prevent the formation of undesired surface whitening as colloidal particles penetrate better into the pores thus reducing accumulation on the surface [Giorgi et al, 2000].
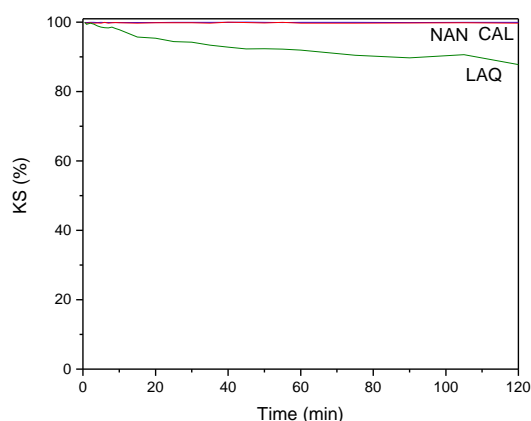
**Figure 57.** Kinetic stability KS (%) of NAN, CAL and LAQ dispersions

## 4.1.2 Nanolime carbonation process

The XRD patterns of nanolimes exposed to air for 1 hour (Fig. 58) show the LAQ nanoparticles to be the most reactive, with calcite (ICSD # 01-085-1108) being the only detected crystalline phase. NAN nanoparticles also showed good reactivity within the 1 hour of air exposure time, with 90.3% of the sample being composed of calcite (ICSD # 01-072-1652) and 9.7% of portlandite (ICSD # 01-087-0674). The only crystalline phase detected for CAL was portlandite (ICSD # 01-072-0156), indicating a slower carbonation process. The relatively high background combined with broad and weak Bragg peaks recorded for these samples suggest the presence of poorly crystalline phase(s) (Fig. 58).

c)
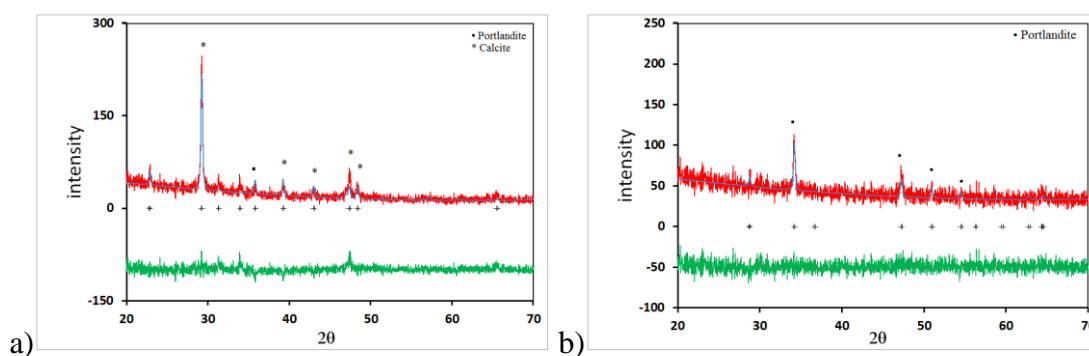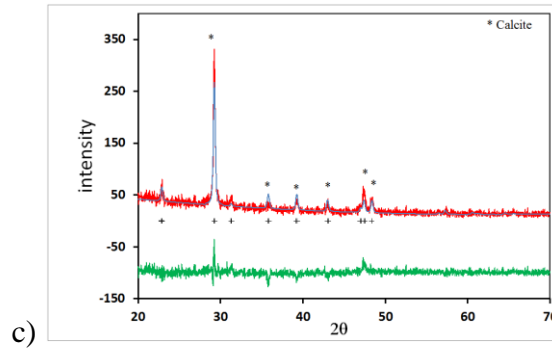
**Figure 58**. XRD patterns of NAN (a), CAL (b) and LAQ (c) samples exposed to air in outdoor conditions for 1 hour (60-80%RH). Red line corresponds to Intensity observed, blue line to Intensity calculated and green line to the Intensity observed - Intensity calculated difference curve. The crystal phases are shown in brackets and the "+" symbol corresponds to the main peaks.

XRD analysis after 7 days of air exposure shows a better defined crystalline structure for all three samples (Fig. 59) resulting from the completion of the carbonation process. Both NAN and LAQ samples consist entirely of calcite ($CaCO_3$, ICSD# 01-086-2334 and ICSD #01-083-0578 respectively) while CAL is composed of 75.8% of calcite ($CaCO_3$, ICSD# 01-081-2027) and 24.2% of vaterite (ICSD# 01-072-0506). Vaterite is the least stable polymorph of calcium carbonate, calcite being the most stable one [Lopez-Arce et al, 2010]. XRD-Rietveld shows the calcite crystals in LAQ are fully oriented to {104} while the crystals in NAN and CAL have no preferred orientation. The Rietveld refinement factors are included in Table 10.



a)                              b)

c)
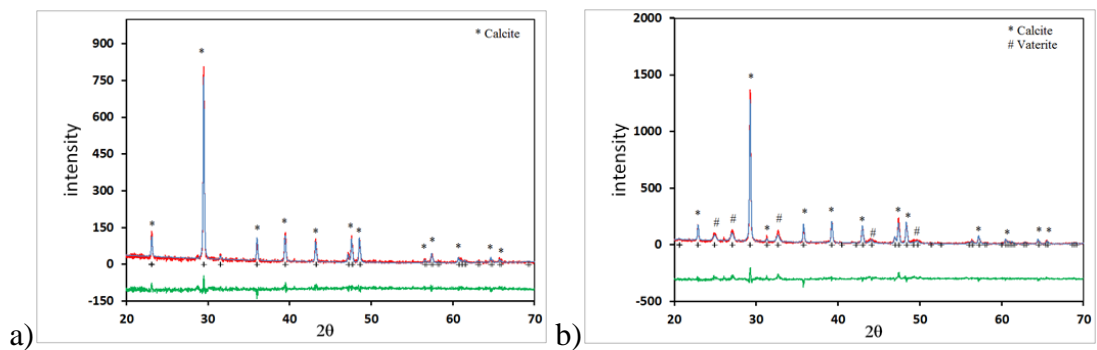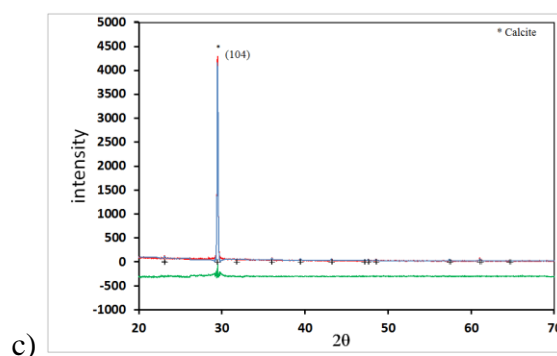
**Figure 59**. XRD patterns of NAN (a), CAL (b) and LAQ (c) samples exposed to air in outdoor conditions for 7 days (60-80%RH). Red line corresponds to Intensity observed, blue line to Intensity calculated and green line to the Intensity observed - Intensity calculated difference curve. The crystal phases are shown in brackets and the "+" symbol corresponds to the main peaks.

**Table 10**. Rietveld refinement factors of samples dried in Nitrogen atmosphere and exposed to air in outdoor conditions (60-80%RH) for 1h and 7 days.

|  | Nitrogen | | | 1 hour in air | | | 7 days in air | | |
|---|---|---|---|---|---|---|---|---|---|
|  | NAN | CAL | LAQ | NAN | CAL | LAQ | NAN | CAL | LAQ |
| R-expected | 10.1 | 9.3 | 13.8 | 20.2 | 20.2 | 20.0 | 19.5 | 15.6 | 20.0 |
| R-profile | 11.6 | 7.9 | 11.7 | 16.1 | 16.1 | 15.6 | 18.5 | 16.3 | 15.6 |
| Weighed R profile | 14.6 | 10.3 | 16.1 | 20.6 | 20.6 | 20.1 | 24.1 | 20.8 | 20.1 |
| Goodness of fit | 3.4 | 1.2 | 4.3 | 2.0 | 2.0 | 3.0 | 1.5 | 1.7 | 4.3 |
| Phase proportions | 100% P | 100% P | 100% P | 90.3% C 9.7% P | 100% P | 100% C | 100% C | 75.8%C 24.2% V | 100% C |
| Direction of preferred orientations | NPO | NPO | 010 | NPO | NPO | NPO | NPO | NPO | 104 |

NPO (No preferred orientation), P (Portlandite); C (Calcite); V(Vaterite)

TEM images taken after 1 minute of air exposure show that during the carbonation process NAN and CAL tend to grow mainly as hexagonal plates (Fig. 60 a, b) while LAQ nanoparticles can be seen to grow preferentially through the {010} side plane (Fig. 60c). SEM images taken after 7 days exposure to outdoor conditions show NAN and CAL being characterised by calcium carbonate crystals of irregular shape (Fig. 60d and e), while LAQ shows calcite in well-formed hexagonal prisms and parallelepiped shapes (Fig. 60f), presenting larger size (10µm) than NAN and CAL ones, despite the smaller original nanoparticle size. Prismatic calcite crystals with similar shape to that observed for LAQ have been described by Ukrainczyk et al

[Ukrainczyk et al, 2015] when examining the influence of additives on the growth of calcite crystals.
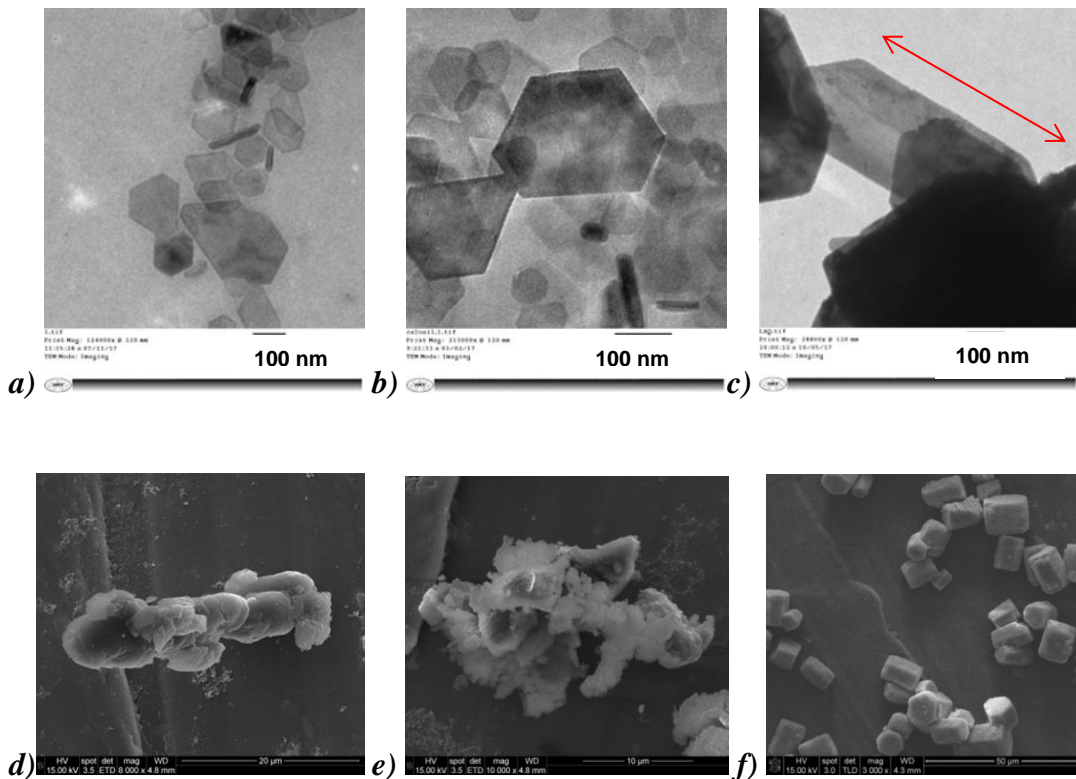


**Figure 60.** a) TEM image of NAN after 1 minute of air exposure at 124,000x; b) TEM image of CAL after 1 minute of air exposure at 213,000x; c) TEM image of LAQ after 1 minute of air exposure at 28,800x; d) SEM image of NAN after 7 days at 8,000x; e) SEM image of CAL after 7 days at 10,000 x; f) SEM image of LAQ after 7 days at 3,000x.

### 4.1.3 Effectiveness of the nanolime treatments

The phenolphthalein test was carried out to observe the penetration of nanolime in the samples immediately after treatment and the carbonation of nanolime in the pores after 28 days of outdoor exposure. Immediately after the application of nanolime (as described in section 3.2.4.1), the cubes were split in half and the phenolphthalein solution immediately sprayed onto one of the two fresh split faces as described in section 3.2.5.3.1. Results confirm that the three nanolimes fully penetrated the samples (pink colour on the split face indicates the presence of portlandite (Fig. 61 a, c, e). Results after 28 days show no presence of portlandite; therefore, it is confirmed that the three nanolimes are fully carbonated after 28 days even in the core of each sample (Fig. 61 b, d, f).
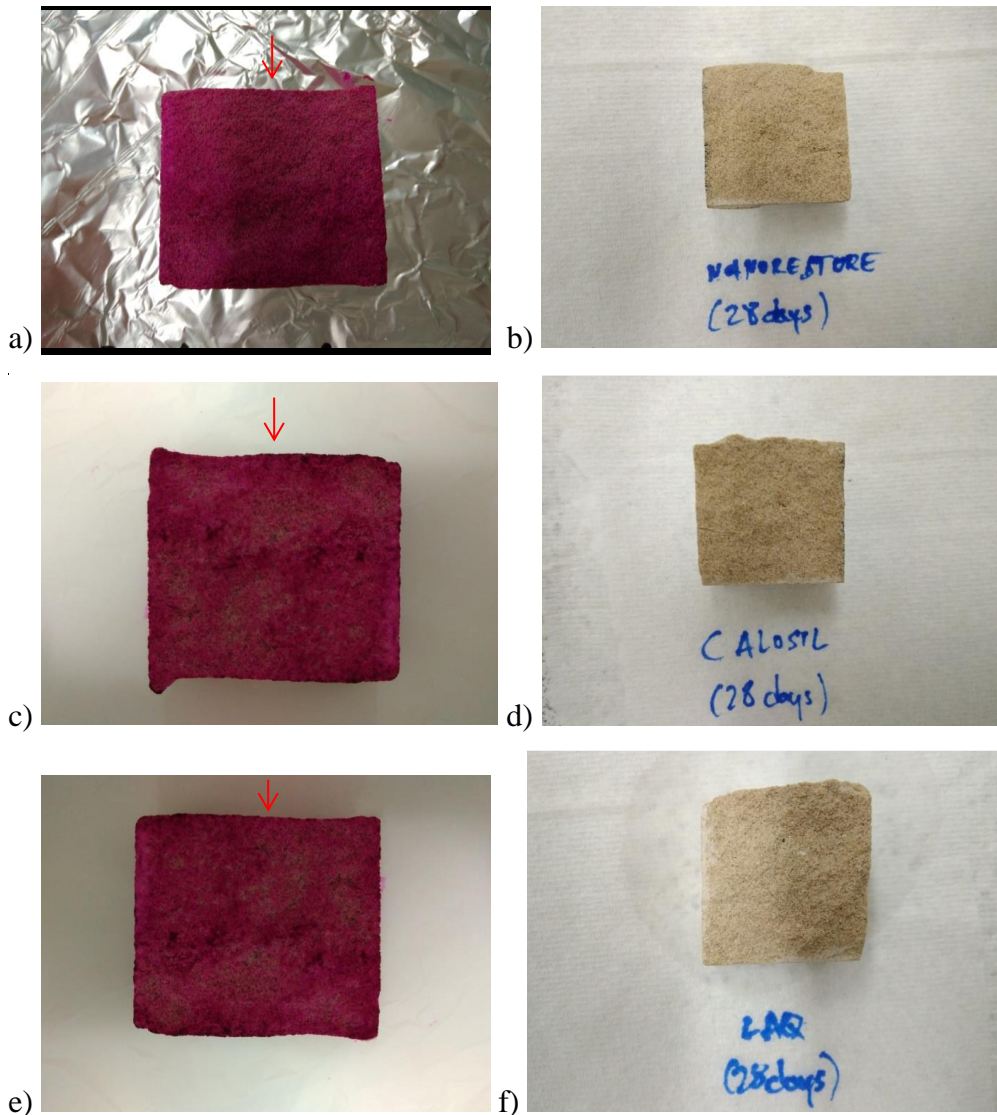
**Figure 61**. Phenolphthalein test carried out: a) immediately after Nanorestore treatment; b) 28-days of outdoor exposure after Nanorestore treatment; c) immediately after Calosil treatment; d) 28-days of outdoor exposure after Calosil treatment; e) immediately after LAQ treatment; f) 28-days of outdoor exposure after LAQ treatment. The red arrows show the face of the cube where nanolime was applied.

The pore structure properties of treated and control mortars are summarised in Table 11. It is evident that all three treatments affect the pore structure of the mortar by reducing the modal pore diameter and the porosity while increasing the total pore surface area. The highest porosity decrease was observed for the mortar treated with NAN (26% decrease), followed by those treated with LAQ (21%) and CAL (16%).

**Table 11.** Pore structure properties of treated and control mortar samples measured by MIP

| Sample | Porosity (%) | Modal pore diameter (μm) | Total pore surface area (m²/g) |
|--------|-------------|--------------------------|-------------------------------|
| Control | 22.63 | 18.09 | 0.45 |
| NAN | 16.75 | 15.23 | 0.575 |
| CAL | 18.92 | 13.55 | 0.585 |
| LAQ | 17.87 | 14.15 | 0.781 |

The pore size distributions of control and treated mortars are shown in Fig. 62. It can be seen that the control sample has a tri-modal pore size distribution, coarser pores with diameters between 25 μm and 100 μm, intermediate pores with diameters between 3 μm and 25 μm and finer pores with diameters between 0.06 μm and 0.7 μm. Following the treatments, a complete removal of the coarsest mode and enhancement of the intermediate mode can be observed (Fig. 62). Such enhancement is more prominent for the mortar treated with CAL (Fig. 62), which is in line with the lower decrease in porosity observed for this mortar.
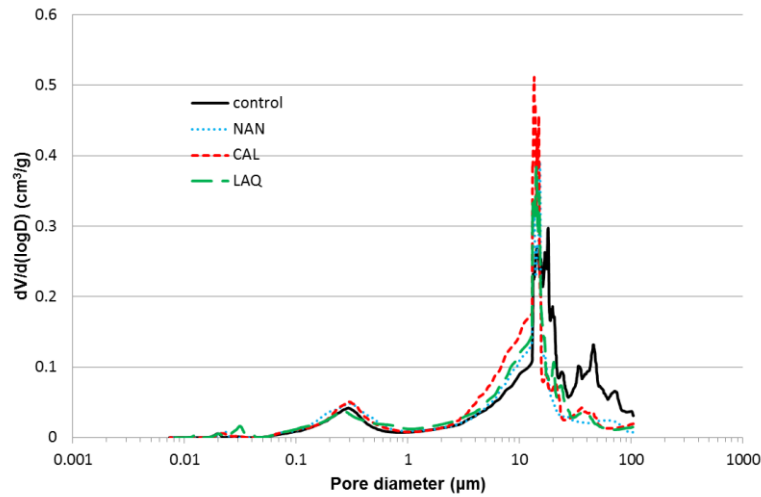


**Figure 62**. Differential volume of intruded mercury versus pore diameter of treated and control mortar samples

The water absorption and drying curves are reported in Fig. 63 and Fig. 64. Apparent porosity by immersion, water absorption and drying characteristics are reported in Table 12.

Capillary rise in a porous material is strongly influenced by pore size distribution. The pore diameter range affecting water capillary rise and transport could theoretically be considered to range between 1 mm and 1 µm diameter [Charola and Wendler, 2015]. It is shown that all three treatments yield a decrease of the capillary water absorption coefficient of the mortar. This decrease can be attributed to the reduction in the number of pores with diameters between 17 µm and 100 µm, which results from the applied treatments and was recorded by the MIP measurements. Figure 63 and Table 12 show that the NAN treatment yielded the biggest decrease in Water Absorption Coefficient (42%), followed by CAL (14%) and LAQ (4%). Control samples required about 7 hours of contact with water to reach asymptotic values while treated samples took nearly 9 hours (Fig. 63). The latter absorbed less water by both capillarity and 24-hour immersion, with the NAN treated sample showing the greatest decreases.
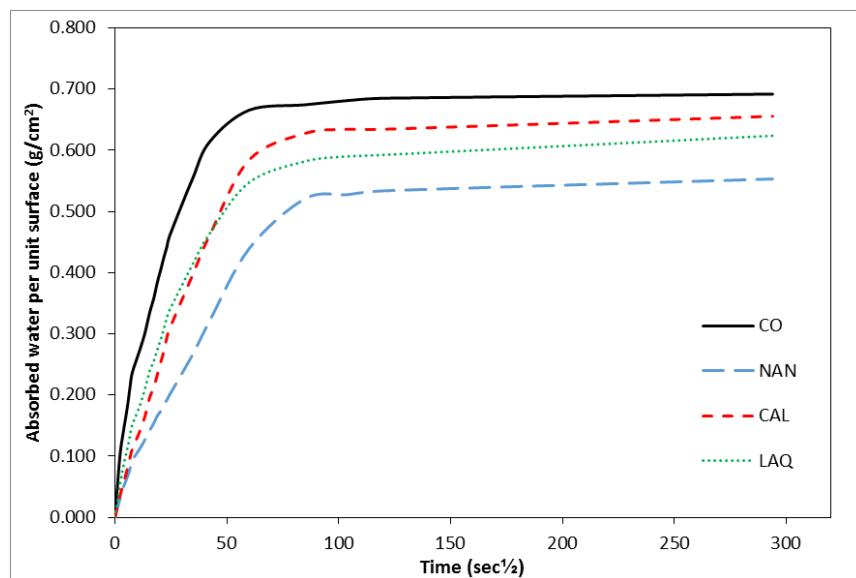


**Figure 63**. Capillary absorption for control and NAN, CAL and LAQ treated mortars

The treatments also tended to reduce the apparent porosity of the mortar, with the NAN treated samples showing the highest reduction (11.4%) followed by LAQ (5.7%) and CAL (2.1%) (Table 12). These results are fully compatible with the results of the MIP porosity measurements reported above.

**Table 12.** Apparent porosity by immersion, capillary water absorption and drying characteristics

| Parameter | CO | NAN | CAL | LAQ |
|---|---|---|---|---|
| Apparent porosity (%) | 11.84 ($\pm$ 0.20) | 10.49 ($\pm$ 1.63) | 11.60 ($\pm$ 0.40) | 11.17 ($\pm$ 0.65) |
| W. absorption coefficient ($10^{-3}$g/cm$^2$ s$^{0.5}$) | 9.5 ($\pm$ 0.78) | 5.5 ($\pm$ 1.7) | 8.2 ($\pm$ 2.5) | 9.1 ($\pm$ 0.5) |
| W. absorbed at asymptotic value (g) | 11.00 ($\pm$0.06) | 8.95 ($\pm$1.05) | 10.60 ($\pm$0.52) | 10.32 ($\pm$0.68) |
| W. absorbed after 24-hour immersion (g) | 11.57 ($\pm$ 0.16) | 10.34 ($\pm$ 1.61) | 11.49 ($\pm$ 0.38) | 11.07 ($\pm$ 0.50) |
| Initial drying rate ($10^{-3}$g/ cm$^3$ h) | 4.9 ($\pm$ 0.1) | 3.9 ($\pm$ 0.3) | 4.4 ($\pm$ 0.5) | 4.4 ($\pm$ 0.3) |
| Final drying rate ($10^{-3}$g/cm$^3$ h) | 1.0 ($\pm$ 0.3) | 1.0 ($\pm$ 1.0) | 1.2 ($\pm$0.6) | 1.2 ($\pm$ 0.5) |
| Moisture content after 72 hours (g/cm$^3$) | 0.01 ($\pm$0.01) | 1.81 ($\pm$0.01) | 1.94 ($\pm$0.02) | 2.02 ($\pm$0.02) |
| Time for total drying (h) | $\pm$50 | > 72 | > 72 | > 72 |

Values in parentheses are standard deviation of the three cubic samples. W (water)

The drying curves (Fig. 64) and the measured initial and final drying rates (Table 12) show that treated mortar samples take far more time to dry than the control ones. This is an undesirable behaviour as it increases the risk of spalling when the mortar is exposed to freeze-thaw cycles (limited to the external 1 cm plus where the nanolime precipitates) and / or biological attack [Charola et al, 2017]. The drying rate reduction is attributed to the finer pore structure of the mortar near the surface of the sample which results from the nanolime treatment. The smaller pores in the denser mortar layer reduce the liquid water transport towards the surface hence slowing down the drying kinetics [Charola et al, 2017]. The lowest initial drying rate was observed for the mortar treated with CAL while NAN and LAQ yielded similar rates. Whilst control samples were completely dry after 50 hours, treated samples still contained some residual moisture after 72h (Table 12).
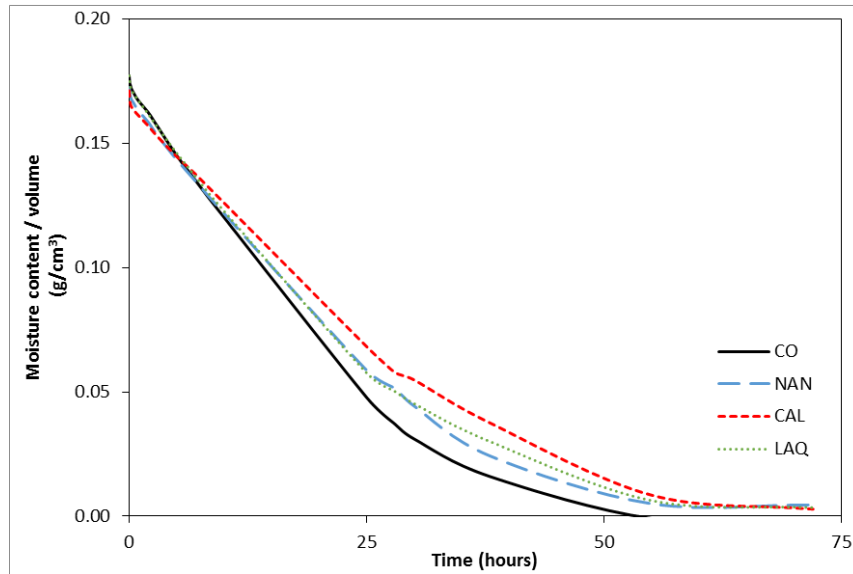
**Figure 64**. Drying curves for control and NAN, CAL and LAQ treated mortars

Table 13 shows the results of the Scotch Tape Test (STT). A significant decrease of removed material ($\Delta W \approx 90\%$) was observed for all treated mortars with no significant differences in the performance of the three nanolimes. The standard deviation of the $\Delta W$ (%) (SD) shown in the table confirms a good reliability for this test in the measuring of surface cohesion.

**Table 13.** Scotch tape test results. Values determined on 9 measurements.

| Treatment | Removed material (mg/cm²) | | $\Delta W$ (%) | SD |
|---|---|---|---|---|
| | **Before treatment** | **After treatment** | | |
| NAN | 26.85 (±1.24) | 2.54 (±3.96) | 90.54 | 5.1 |
| CAL | 26.71 (±1.56) | 1.71 (±0.73) | 93.6 | 2.3 |
| LAQ | 26.76 (±1.04) | 3.16 (±2.57) | 88.19 | 3.6 |

Scotch area: 3 x 1.5 cm; Values in parentheses are standard deviation for the nine measurements taken on each of the three cubic samples

Drilling resistance results are shown in Figure 65. It can be seen that whilst the control sample shows a steady drilling resistance throughout the drilling depth (average force $\approx 0.07$N), the treated samples show increased resistance within the first 10 mm from the surface (Fig. 65 a, c, e). The highest average drilling resistance

was observed for the mortar treated with NAN (average force ≈ 0.57N), followed by those treated with CAL (average force ≈ 0.32N) and LAQ (average force ≈ 0.27N). This is fully compatible with the results of the porosity measurements which showed a more marked decrease of porosity for NAN treated samples compared to those for CAL and LAQ treated samples. The average drilling resistance in the outer 5 mm is 0.09N for Control, 1.12 N for NAN, 0.68 N for CAL and 0.64 N for LAQ, which is also in line with the results of MIP measurements. The DRMS profiles in Figure 65 a, c, e show that the drilling resistance of the treated samples decreases with depth until it reaches the resistance of the control sample at about 10 mm for NAN and CAL and about 6 mm for LAQ. This data seems to indicate a deeper penetration into the mortar for NAN and CAL treatments compared to the LAQ treatment.

The drilling resistance tests were repeated after exposing the samples to alternating cycles of UV light and moisture (Fig. 65b, d, f) and the results show for the NAN and CAL treated samples a reduction of the depth at which the drilling resistance reaches that of the control samples. This could indicate that a certain amount of material got partially dissolved from the surface of these samples as a result of the exposure to the alternating cycles of UV light and moisture condensation at elevated temperatures in the tester. The presence of deposits of white powder material in the water pan just below the sample holder panel seems to support this interpretation. The DRMS profile of the LAQ treated sample (Fig. 65 f) is similar to that recorded before the accelerated weathering test (Fig. 65e), which seems to indicate that less or no material loss occurred on the surface of this sample. The apparent higher resistance to weathering of the LAQ treated sample compared to that of the NAN and CAL treated ones could be attributed to a better developed crystalline structure and larger crystals. As described in section 4.1.2, LAQ produces perfectly shaped prismatic and parallelepiped calcite crystals of a larger size compared to NAN and CAL, which present poorly crystallized ones. The "well-shaped" calcite crystals are more resistant to dissolution than irregular shaped crystals as is well known [Charola, 1988]. In the case of the CAL treated sample, a reduction of the drilling resistance was observed within the first millimeter of depth (Fig. 65e), which could be due to the solubility of metastable amorphous carbonate phases such as vaterite (see section 4.1.2).
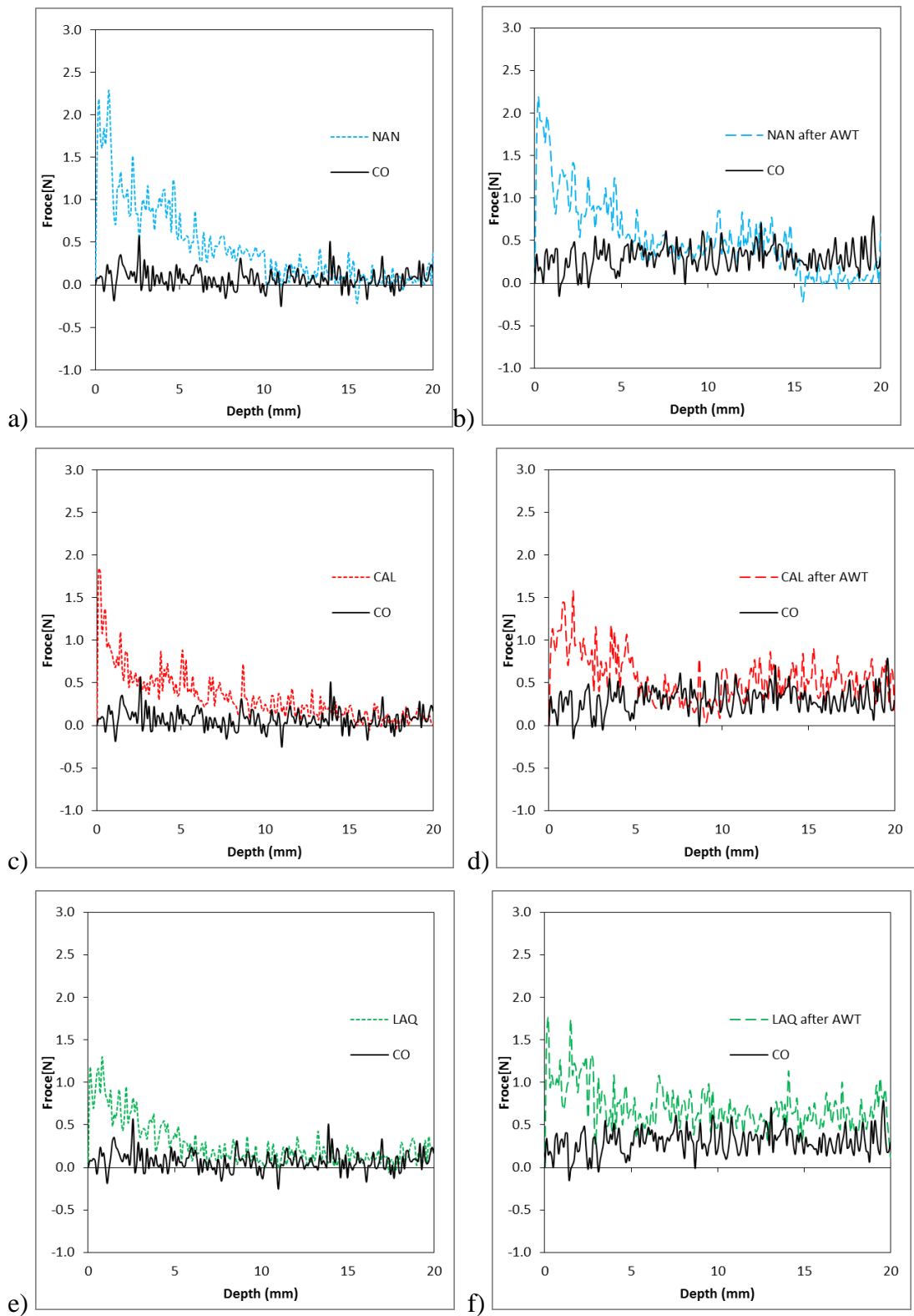
**Figure 65**. Drilling resistance of: a) NAN; b) NAN after AWT; c) CAL; d) CAL after AWT; e) LAQ; f) LAQ after AWT

Both treated and untreated mortar surfaces were observed by SEM in order to study the distribution of the nanolime in the pores and the morphology of the calcite

crystals. SEM micrographs showed for the control samples a great number of large pores (pore diameter >100 µm), which are outside of the measurement range of the used MIP technique (Fig. 66a). Following the treatments, the reduction of porosity and pore size due to the deposition of calcite inside the pores is clearly visible (Fig. 66 b-d).
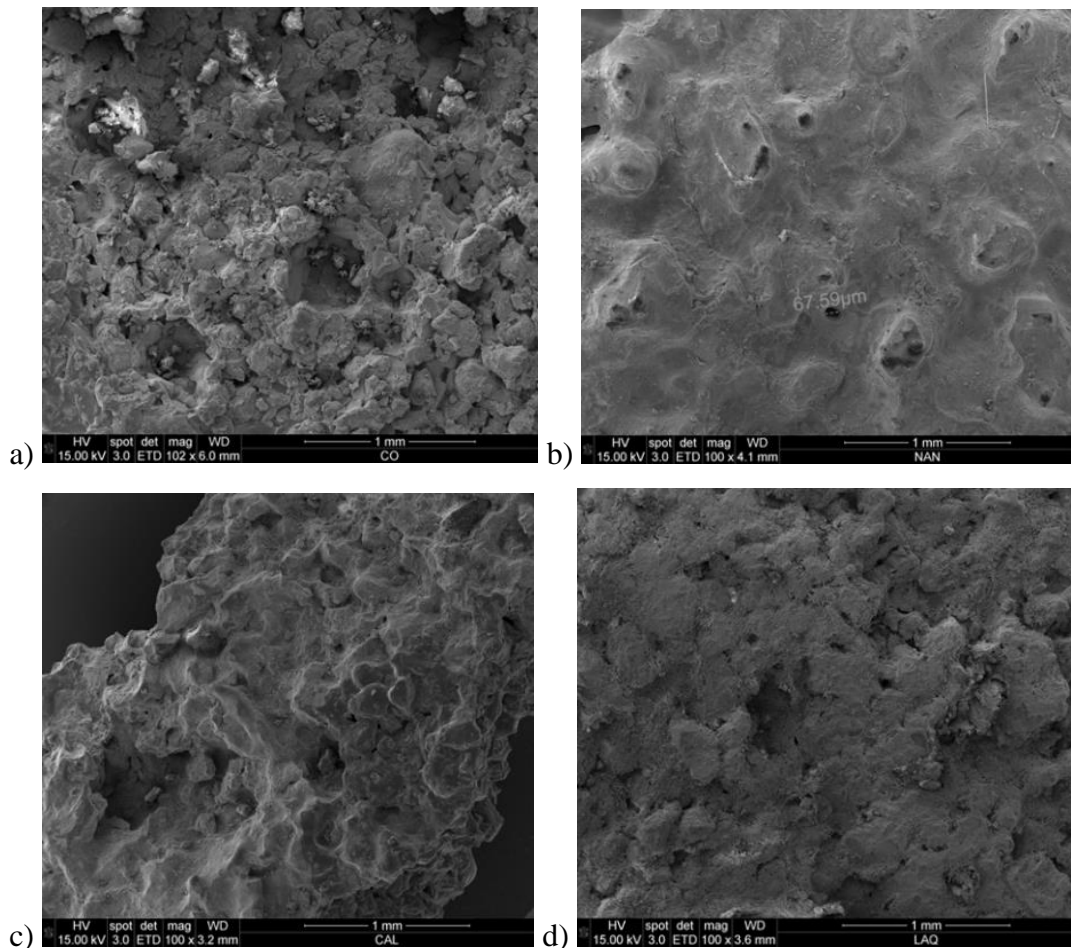


**Figure 66**. SEM micrographs of mortar samples (100 X): a) control sample; b) surface treated with NAN; c) surface treated with CAL; d) surface treated with LAQ.

In Figures 66 b-d it can be seen that the nanolime is distributed homogeneously in the pores of the mortar and seems to adhere well to the substrate to the point that it is not easy to distinguish between the mortar and the newly precipitated calcite which fills the pores reducing their size. Fig. 67a shows that the calcitic material resulting from the carbonation of NAN within the mortar presents a different variety of shapes (mostly rhombohedral with scalenohedral terminations), which were observed also in previous studies for the same nanolime [Arizzi et al, 2015]. CAL precipitated in the

form of calcite rhombohedra and some vaterite (Fig. 67b). Fig. 67c shows typical calcite prisms on the LAQ sample. These are larger than those formed by NAN and CAL hence resulting in a smaller specific surface which is associated with higher resistance to weathering [Charola, 1988]. This morphology is similar to that visible on the SEM images (section 4.1.2).
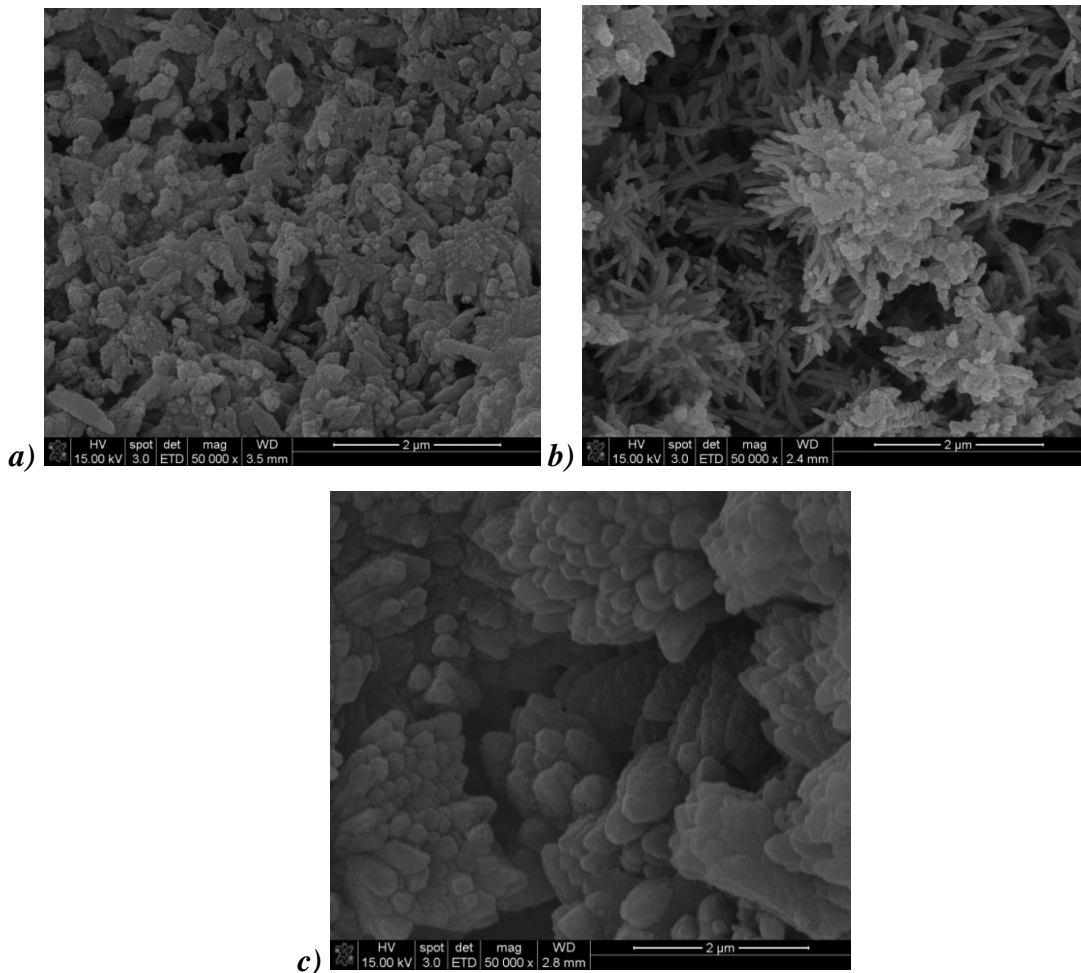


**Figure 67.** SEM detail micrographs of carbonated nanolime : a) NAN 50,000x; b) CAL 50,000x; c) LAQ 50,000x.

Ideally consolidation treatments should improve the physical-mechanical properties of the treated material without affecting its aesthetic appearance. However, a common side effect of the use of nanolime is a whitening of the surface following treatment. In order to investigate the occurrence of this phenomenon in association with the use of the tested nanolimes, spectrophotometric analyses were carried out to measure changes in L* (white-black parameter) and ΔE* (total colour variations)

following treatment. ΔE* values < 5 are considered suitable for practical conservation interventions and visually imperceptible [Rodriguez-Navarro et al, 2013]. The results (Table 14) show that all of the three treatments cause whitening of the surface with both ΔE and ΔL values above 5. NAN yielded the lowest whitening effect (ΔL* ≈ 6 and total colour alteration ΔE* ≈ 6). CAL and LAQ caused a more significant whitening effect with ΔL* ≈ 7.5 and ΔL* ≈ 11.94, respectively, and total colour change with ΔE* ≈ 9 and ΔE* ≈ 14, respectively. The lower colloidal stability of LAQ is considered responsible for the more significant formation of undesired surface whitening. Nonetheless, the observed whitening and total chromatic alterations are still lower than those caused by the lime-water technique, which normally vary between ΔL* ≈ 50 to 70 [Slizkova et al, 2015; Slizkova and Frankeova, 2012].

The whitening effect and total colour changes associated with the application of nanolime decreased after the samples were exposed to UV light and moisture cycles in the accelerated weathering test, with both ΔE* and ΔL* decreasing below 5. This could indicate that the induced weathering dissolved a certain amount of material from the surface of the samples, as also detected by DRMS for the NAN and CAL samples. It is apparent that in the case of the LAQ samples the amount of material that got dissolved from their surface during the accelerated weathering test was sufficient to reduce the whitening but too small to be detected by the DRMS.

**Table 14.** Chromatic alterations of treated samples before and after the Accelerated Weathering Test.

|  | ΔL* | | Δa* | | Δb* | | ΔE* | |
|---|---|---|---|---|---|---|---|---|
|  | **Treated** | **AWT** | **Treated** | **AWT** | **Treated** | **AWT** | **Treated** | **AWT** |
| NAN | 6.33 (±0.20) | 3.18 (±0.43) | -1.48 (±0.16) | -0.48 (±0.20) | -0.43 (±0.91) | -1.96 (±0.55) | 6.51 | 3.76 |
| CAL | 7.50 (±0.51) | 2.53 (±0.90) | -0.75 (±0.13) | -0.37 (±0.16) | -4.64 (±0.69) | -0.88 (±1.15) | 8.85 | 2.7 |
| LAQ | 11.94 (±0.96) | 4.04 (±0.63) | -1.25 (±0.15) | -0.55 (±0.0.26) | -6.96 (±1.07) | -1.17 (±1.45) | 13.87 | 4.24 |

Values determined on 30 measurements; AWT (Accelerated Weathering Test)

*4.1.4 Conclusions*

This study has shown that NAN, CAL and LAQ can be used effectively for the consolidation of highly porous calcareous materials such as lime mortars and represent a viable alternative to organic consolidants for their consolidation. It has been proven that repeated applications of low concentration dispersions of these nanolimes can restore the substrate superficial cohesion, improve its mechanical properties, reduce its porosity, number of micropores (10 - 100 µm) and water absorption coefficient.

It has been shown that:

- The $Ca(OH)_2$ nanoparticles of the three nanolimes consist of crystalline hexagonal plates with similar shapes. However, there is a difference in size: LAQ nanoparticles are smaller than both NAN and CAL. XRD-Rietveld refinements showed that LAQ $Ca(OH)_2$ particles tend to align in a preferential direction along the side plane {010} whereas NAN and CAL did not show any significant preferred orientation. Nanorestore Plus® and Calosil® are stable colloidal dispersions while LAQ nanoparticles start to settle about 2 min after agitation (sedimentation rate ≈ 6% per h) and the 12% of the particles has settled after 2 hours. This sedimentation rate is considered acceptable for practical purposes as most of the particles remain in colloidal state during the time of the application. However, a moderate agitation is highly recommended before the application of this nanolime. Moreover, the application should ideally be completed within the first 2 first minutes after the agitation, before the particles start to settle.

- Nanolime particles created by anion exchange synthesis (LAQ) are the most reactive with calcite being the only detected crystalline phase after 1 hour of air exposure. NAN particles also showed a good reactivity with 90% of the sample being composed of calcite following the same exposure time. CAL particles showed slower carbonation and no calcite had formed after 1 hour exposure. After 7 days both LAQ and NAN consisted entirely of calcite, while CAL was composed approximately of 75% of calcite and 25% of

vaterite, which is a metastable phase of calcium carbonate, less stable than calcite.

– During the carbonation process, NAN and CAL tend to grow mainly as hexagonal plates while LAQ nanoparticles seem to grow preferentially through the {010} side plane. After 7 days of carbonation, LAQ shows well-formed hexagonal calcite prismatic crystals with larger size than NAN and CAL, which consist of calcite crystals of irregular shape. XRD-Rietveld shows the calcite crystals in LAQ are fully oriented to {104} while the crystals in NAN and CAL have no preferred orientation.

– All treatments affect the pore structure by reducing the porosity of the superficial portion of the mortar. The reduction in porosity is attributed mainly to a reduction of the number of pores with diameter between 17µm and 100µm, which also decreases the capillary water absorption coefficient. Nanorestore Plus® presented the highest reduction of the porosity and water absorption by capillarity rate.

– All three nanolimes increase the drilling resistance of the mortar surface. The penetration depth of nanolime appears to be approximately 1 cm for NAN and CAL and 0.6 cm for LAQ. NAN treated mortars showed the highest increase in drilling resistance, which is in line with their highest reduction in porosity; followed by those treated with CAL and LAQ. Following an accelerated weathering test, the DRMS detected the loss of a certain amount of material from the surface of mortars treated with NAN and CAL. This was not observed for LAQ treated samples, possibly due to LAQ better developed crystalline structure providing higher resistance to dissolution processes during the accelerated weathering test. The detected loss is slightly more pronounced in Calosil® samples, possibly as a consequence of the dissolution of metastable vaterite. A study of the calcite morphology and structural features of LAQ nanolime must be addressed in future studies to better understand the performance of this nanolime.

- Following treatment, the samples take far more time to dry due to a finer pore structure of the mortar near the surface. This is an undesirable behaviour which may lead to deterioration processes. Specifically, spalling can occur where moisture is present and the mortar is exposed to freeze-thaw cycles. Furthermore, longer drying times can favour biological growth and the dissolution of poorly crystallised calcite and vaterite. A full study of the durability of mortars treated with the three nanolimes will be carried out in future research.

- All treatments produced an undesired whitening of the surface after application. LAQ treatment induced the highest whitening effect which can be attributed to the lower colloidal stability of this nanolime. The whitening effect associated with all treatments decreases to values which are imperceptible to the naked eye after exposing the samples to the Accelerated Weathering Test. This could indicate that a superficial layer of the consolidated mortar was partially dissolved during the accelerated weathering test, as also observed by DRMS. In the case of LAQ treated mortars the dissolution decreased the whitening without causing significant thickness reduction.

One final conclusion of this study is that substrates treated with the studied nanolimes will require regular maintenance (i.e. periodic application of nanolime) in order to achieve long term performance in terms of mechanical and physical properties.

## 4.2. Influence of different types of solvent on the effectiveness of nanolime treatments on highly porous substrates

*4.2.1 Characterisation of nanolime suspensions*

The nanolime suspensions (IP, ET, W, WIP and WET) are described in section 3.3.2 and the physical-chemical properties of the nanolimes are described in the section 3.1.4. The TEM photomicrograph (Fig.68) shows a plate-like hexagonal $Ca(OH)_2$ nanoparticle from the W suspension. This morphology is identical to particles observed in the previous work (section 4.1) and similar to other researches [Taglieri et al, 2017a; Taglieri et al 2017b; Taglieri et al, 2017c; Volpe et al, 2016]. $Ca(OH)_2$ nanoparticles are regularly shaped and have dimensions ranging from 20 to 80 nm diameter (Fig 68a), also similar to other researches [Taglieri et al, 2017a; Taglieri et al 2017b; Taglieri et al, 2017c; Volpe et al, 2016]. The selected area electron diffraction (SAED) clearly shows that these particles present a crystalline structure (Fig. 68b).
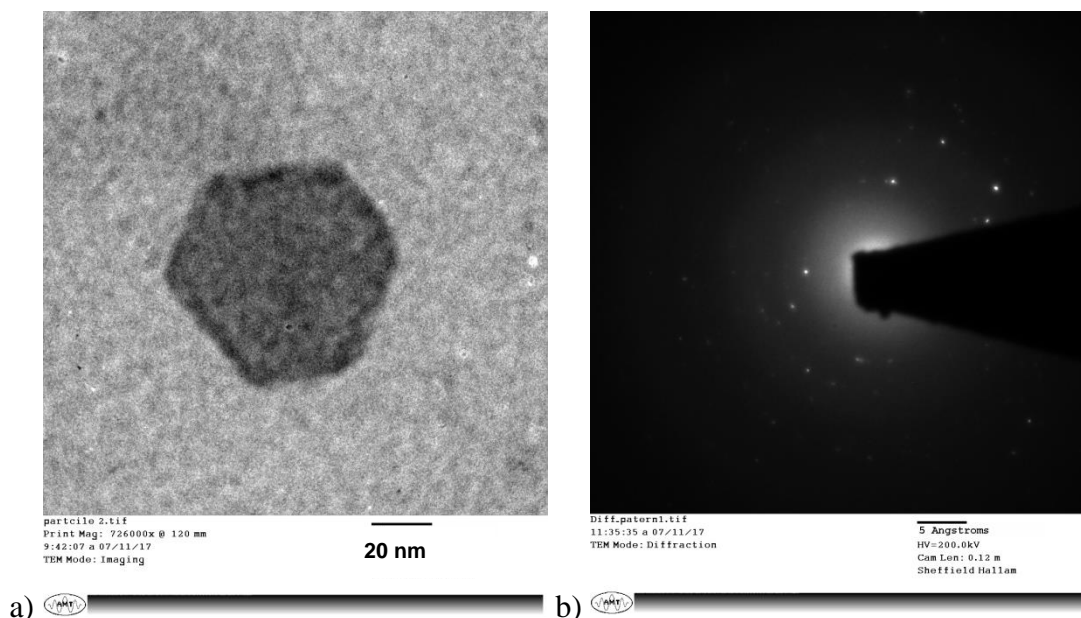


**Figure 68.** TEM image of: a) small single particle of synthetised nanolime (W, water); b) selected area electron diffraction images of W sample

XRD analysis of samples dried in nitrogen atmosphere (Fig.69) shows the only crystal phase present in each suspension corresponds to Portlandite ($Ca(OH)_2$, ICSD

#01-087-0674), apart from the W sample (nanolime in water) which contains a small amount of calcite (ICSD #01-072-1652). This is attributed to the higher reactivity of $Ca(OH)_2$ with $CO_2$ when dispersed in water. Rietveld refinement showed that the W sample consists of 79.3% Portlandite and 20.7% Calcite. For all samples, the strongest peak corresponds to the {001} basal plane. IP, ET, WIP and WEP particles have a preferred orientation to the planes {010} or {100}, which both are side planes. The Rietveld refinement factors are included in Table 15.

Table 15. Rietveld refinement factors of samples dried in Nitrogen atmosphere

| | Nitrogen | | | | |
| --- | --- | --- | --- | --- | --- |
| | IP | ET | W | WIP | WET |
| R-expected | 10.1 | 9.3 | 13.1 | 18.4 | 13.8 |
| R-profile | 11.6 | 7.9 | 14.5 | 15.4 | 11.7 |
| Weighed R profile | 14.6 | 10.3 | 12.7 | 11.1 | 16.1 |
| Goodness of fit | 3.4 | 3.3 | 4 | 4.1 | 4.3 |
| Phase proportions | 100% P | 100% P | 79.3%P 20.7%C | 100% P | 100% P |
| Direction of preferred orientations | 010 | 100 | NPO | 010 | 100 |

NPO (No preferred orientation), P (Portlandite); C Calcite)



a)

b)

c)

d)

e)
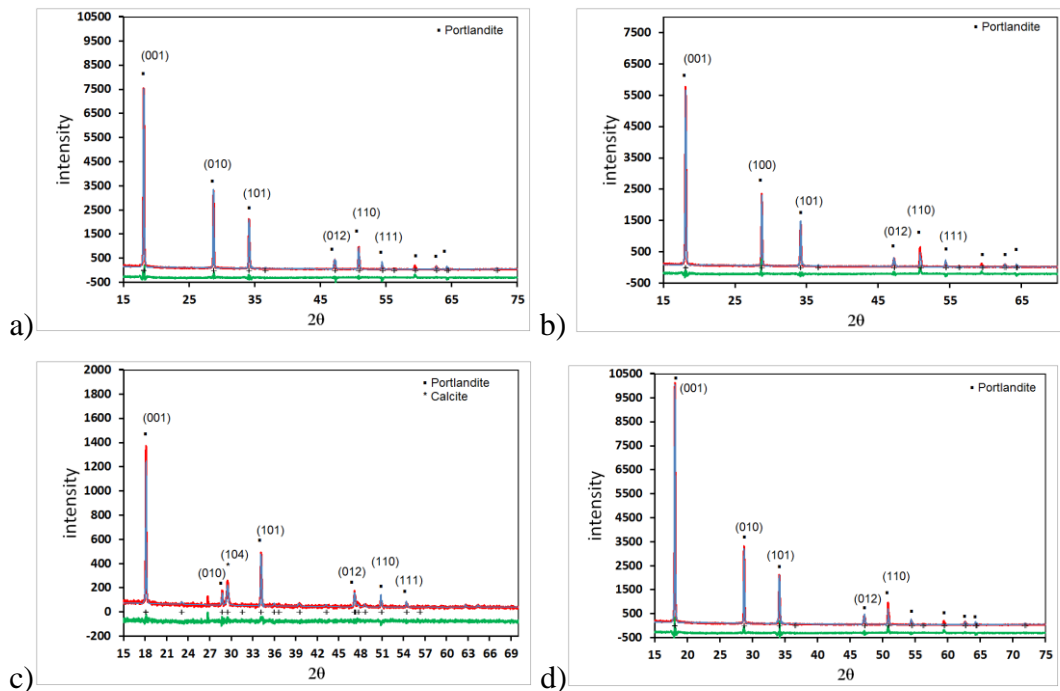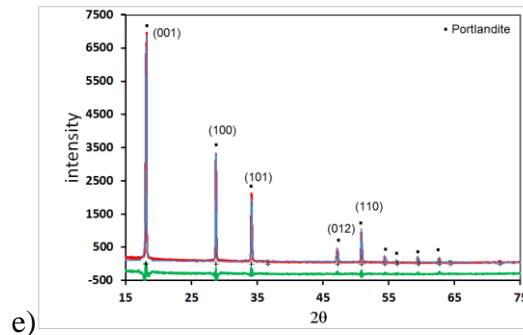
**Figure 69**. XRD patterns of samples dried under nitrogen atmosphere for; a) IP (Isopropanol); b) E (ethanol); c) W (water); d) WIP (50% Water and 50% Isopropanol); and e) WET (50% water and 50% Ethanol). Red line corresponds to Intensity observed, blue line to Intensity calculated and green line to the Intensity observed - Intensity calculated difference curve. The crystal phases are shown in brackets and the "+" symbol corresponds to the main peaks. In parentheses the portlandite peaks.

Figure 70 shows the colloidal stability of IP, ET, W, WIP and WET suspensions over a period of 2 hours following a moderate agitation. All nanolime suspensions tend to settle over time. WIP presented the highest colloidal stability (settling speed ≈ 5% per h). Similar results for this suspension were observed in the previous study (section 4.1) and in previous researches on LAQ nanolime [Taglieri et al 2016, Taglieri et al 2017a, Taglieri et al 2017b]. The colloidal stability of the nanoparticles synthetised by anionic exchange processes (LAQ) is lower than that of the nanoparticles synthetised by other synthesis routes (e.g. solvothermal reactions or drop-to-drop method), where nanoparticles remain in colloidal state for more than one week [Borsoi et al, 2016, Ambrosi et al,2001; Poggi et al, 2016]. Nevertheless, all dispersions showed a reasonable colloidal stability where most of the nanoparticles (>95%) remain in colloidal state during the first 5 minutes after agitation. This is considered acceptable in terms of practical purposes as most of the particles remain in colloidal state long enough to guarantee their penetration in the pores of the treated substrate [Rodriguez-Navarro et al, 2013].
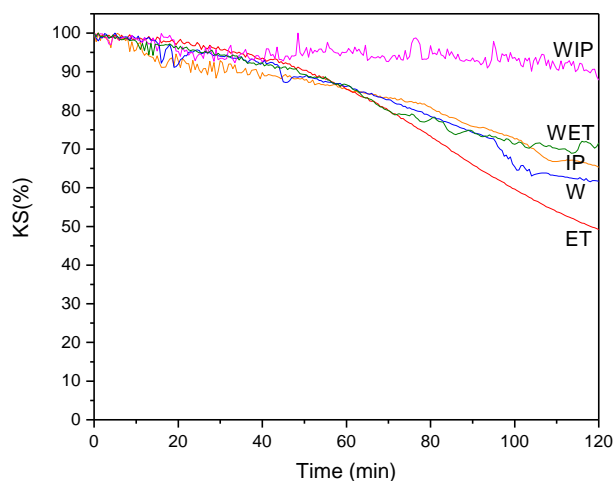
**Figure 70.** Kinetic stability KS (%) of IP (Isopropanol), E (Ethanol), W (Water), WIP (50% Water and 50% Isopropanol) and WET (50% Water and 50% Ethanol) samples

## 4.2.2 Nanolime carbonation characterisation

The XRD analysis of the studied nanolimes exposed to air for 1 hour (60-80% RH) proved the high reactivity of the nanoparticles (Fig. 71). Calcite (ICSD # 01-085-1108) is the only crystalline phase detected for all suspensions. W (Water) sample shows a reasonably well crystallised structure at only 1 hour of air exposure, suggesting higher reactivity than the other suspensions. The Rietveld refinement factors are included in Table 16.

**Table 16**. Rietveld refinement factors of samples dried in samples exposed to air in outdoor conditions (60-80%RH) for 1h and 7 days.

|  | 1 hour in air | | | | | 7 days in air | | | | |
|---|---|---|---|---|---|---|---|---|---|---|
|  | IP | ET | W | WIP | WET | IP | ET | W | WIP | WET |
| R-expected | 15.8 | 15.2 | 14.7 | 14.7 | 14.9 | 15.7 | 15.3 | 21.2 | 15.6 | 14.8 |
| R-profile | 11.3 | 10.7 | 12.3 | 11.4 | 9.9 | 11.1 | 11.3 | 16.1 | 16.3 | 10.8 |
| Weighed R profile | 14.3 | 13.6 | 16.2 | 14.5 | 12.7 | 14.1 | 14.1 | 20.8 | 20.8 | 13.7 |
| Goodness of fit | 1.8 | 1.8 | 1.2 | 1.9 | 1.7 | 1.8 | 1.8 | 1.9 | 1.7 | 1.8 |
| Phase proportions | 100 % C | 100 % C | 100 % C | 100 % C | 100 % C | 100 % C | 100 % C | 100 % C | 100 % C | 100 % C |
| Direction of preferred orientations | NPO | NPO | NPO | NPO | NPO | 104 | 104 | 104 | 104 | 104 |

NPO (No preferred orientation), P (Portlandite); C (Calcite)
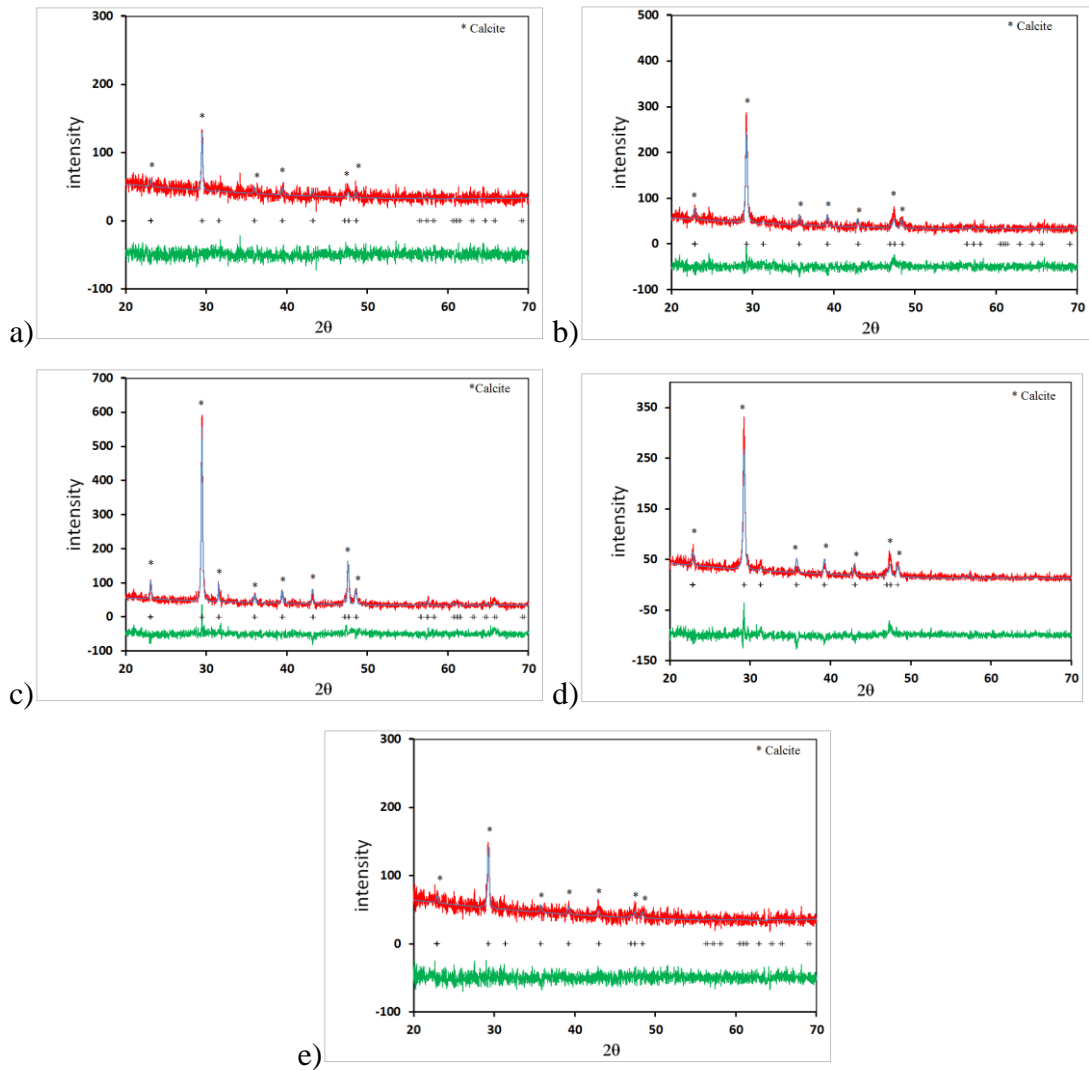
**Figure 71**. XRD patterns after 1 hour of air exposure (60-80%RH) for; a) IP (Isopropanol); b) E (ethanol); c) W (water); d) WIP (50% Water and 50% Isopropanol); and e) WET (50% water and 50% Ethanol). Red line corresponds to Intensity observed, blue line to Intensity calculated and green line to the Intensity observed - Intensity calculated difference curve. The crystal phases are shown in brackets and the "+" symbol corresponds to the main peaks. In parentheses the portlandite peaks.

The XRD results following 7 days of air exposure show that all suspensions present a better defined crystalline structure (Fig. 72). All samples are composed of pure calcite crystals ($CaCO_3$, ICSD# 01-086-2334) oriented to {104}, as reported in the previous research program (section 4.1). The relatively high background combined with broad and weak Bragg peaks recorded for the IP (Isopropanol) sample suggest this sample presents slightly poorer crystalline phase. The Rietveld refinement factors are included in Table 16.
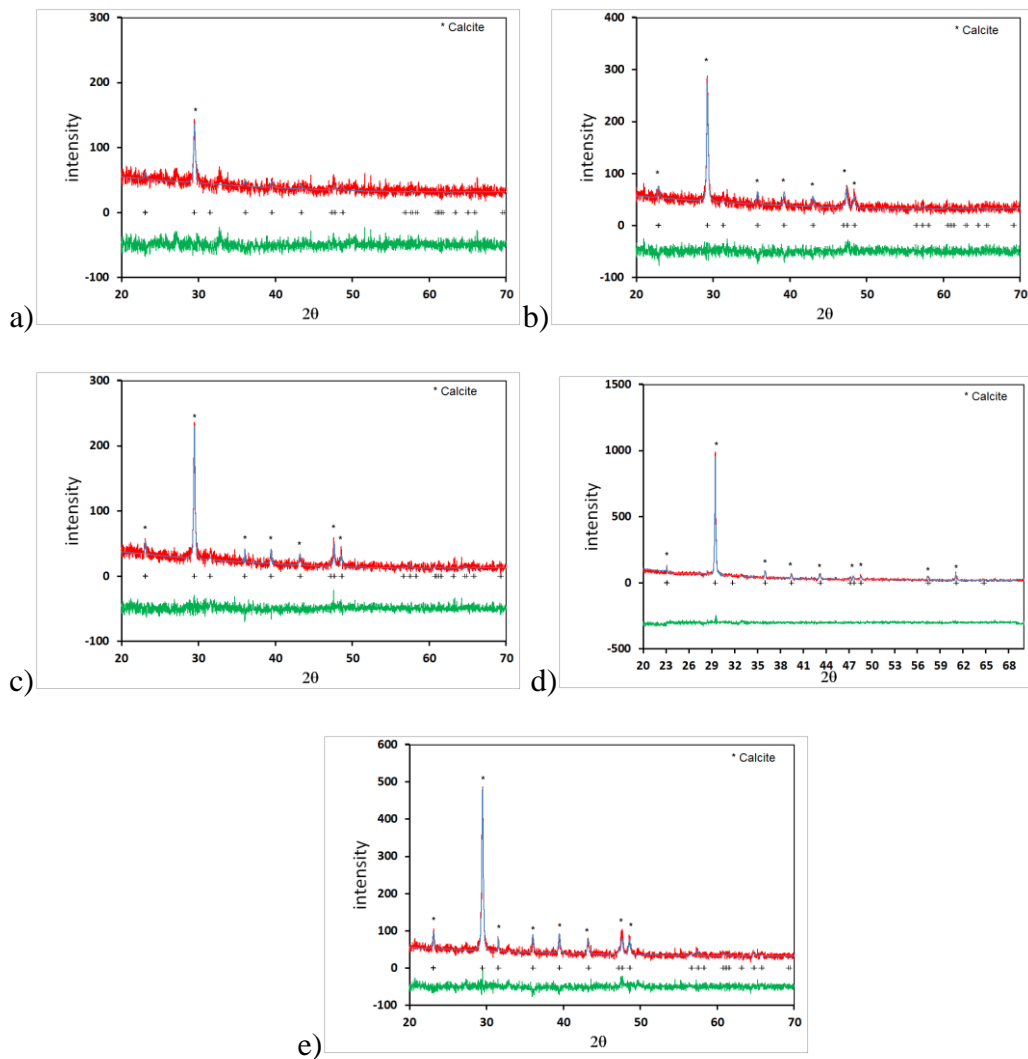
**Figure 72**. XRD patterns after 7 days of air exposure (60-80%RH) for; a) IP (Isopropanol); b) E (ethanol); c) W (water); d) WIP (50% Water and 50% Isopropanol); and e) WET (50% water and 50% Ethanol). Red line corresponds to Intensity observed, blue line to Intensity calculated and green line to the Intensity observed - Intensity calculated difference curve. The crystal phases are shown in brackets and the "+" symbol corresponds to the main peaks. In parentheses the portlandite peaks.

### 4.2.3 Solvent drying rate

Figure 73 shows the drying kinetics of the treated mortars after saturation with nanolime. ET and IP treatments evaporate faster; both solvents were completely evaporated in approximately 24 hours. This is attributed to the lower boiling point of ethanol and isopropanol (as shown in Table 9, section 3.1.4). WIP and WET treatments evaporate in approximately 28 hours, whereas W sample takes approximately 48 hours to dry. The evaporation of W treatment is slower due to the

higher surface tension of water that enhances its retention within the pore network, delaying the drying rate [Charola and Wendler, 2015; Borsoi el at, 2016].
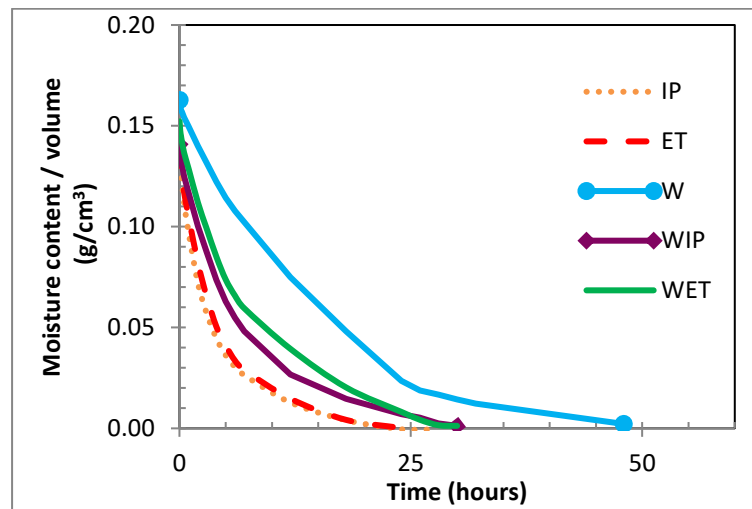


**Figure 73.** Drying curves of kinetics of the treated mortars IP (orange line), ET (red line), W (blue line), WIP (purple line), and WET (green line).

### 4.2.4 Consolidation effectiveness

The open porosity and pore structure properties of the control and treated mortars are summarised in Table 17. All treatments caused a noticeable reduction in the porosity near the surface (samples taken within 50 mm from the surface). WIP sample yields slightly higher reduction in the porosity (23% reduction) compared to the others treatments (from 6 to 17%). All samples showed an increased total pore surface area ($m^2/g$), suggesting a higher presence of smaller pores after treatment.

**Table 17.** Porosity properties of samples

|     | Porosity (vol.%) | Total pore surface area ($m^2/g$) |
| --- | --- | --- |
| CO | 23.34 | 0.674 |
| IP | 22.82 | 1.955 |
| ET | 21.85 | 1.227 |
| W | 19.36 | 1.393 |
| WIP | 17.87 | 1.328 |
| WET | 20.38 | 1.29 |

MIP curves (Fig.74) show that the porosity reduction in the samples treated with WIP and WET can be attributed mainly to the reduction in the population of pores

with larger diameter size (17 to 100 µm). The reduction in larger pores in both samples is also accompanied by an increase of the intermediate pores (diameters 1 to 10 µm). This effect is also observed for the sample treated with IP although this sample presents lower reduction of the pores with larger diameter size (17 to 100 µm). In contrast, IP and W nanolimes seem to be more effective in filling the pores with smaller size (0.05 to 0.7 µm). These results suggest that nanolime in a water-alcohol solvent tend to be more effective consolidating the larger pores than nanolime in alcohols only or in water only.
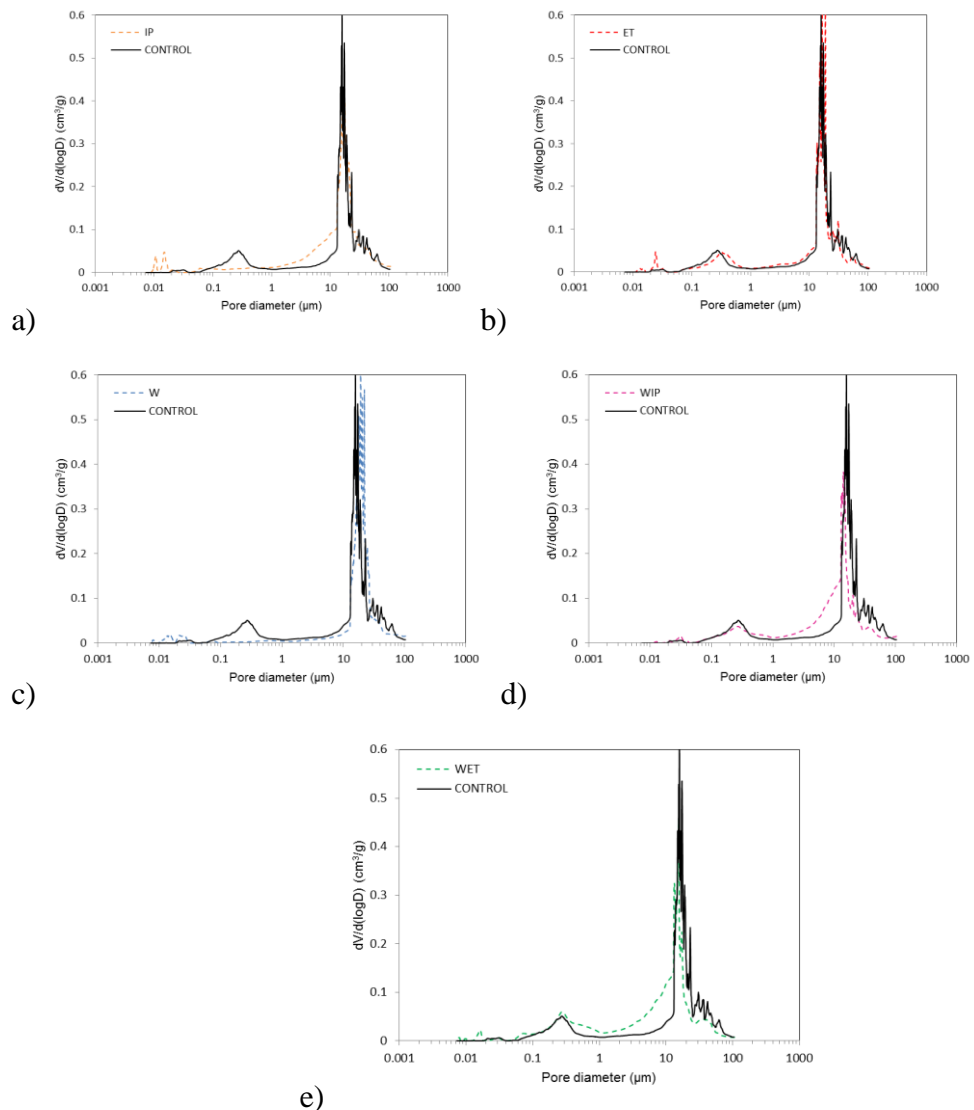


**Figure 74**. Pore size distribution of control and treated samples: a) IP; b) ET; c) W; d) WIP; and d) WET.

The water absorption and drying curves are reported in Fig. 75 and Fig. 76, and apparent porosity by immersion, water absorption and drying characteristics are

reported in Table 18. Results show that the denser pore structure obtained after treatments on the surface slightly affects the water absorption and drying kinetics of the samples. All nanolime treatments seem to have reduced the apparent porosity of the mortars. WIP and W seem to present slightly higher reduction of the apparent porosity than the others (Table 18), which is in the with the MIP results reported above.

**Table 18.** Apparent porosity by immersion, water absorption and drying characteristics

| Parameter | CO | IP | ET | W | WIP | WET |
|---|---|---|---|---|---|---|
| Apparent porosity (%) | 18.6 ($\pm$ 0.56) | 18.4 $\pm$0.25) | 17.9 ($\pm$ 1.18) | 17.7 ($\pm$0.57) | 17.8 ($\pm$ 0.98) | 18.4 ($\pm$ 0.32) |
| Capillary absorption coefficient ($10^{-3}$g/cm$^2$ s$^{0.5}$) | 17,1 ($\pm$ 2.74) | 15,8 ($\pm$8.46) | 13,7 ($\pm$2.24) | 13,2 ($\pm$5.18) | 12,1 ($\pm$2.28) | 15,2 ($\pm$2.22) |
| Water absorbed at asymptotic value (g) | 11.05 ($\pm$ 0.49) | 10.9 ($\pm$0.25) | 10.85 ($\pm$ 0.10) | 10.36 ($\pm$0.40) | 10.56 ($\pm$ 0.56) | 10.55 ($\pm$ 0.53) |
| Water absorbed after 24-hour immersion (g) | 11.89 ($\pm$ 0.33) | 11.80 ($\pm$0.23) | 11.48 ($\pm$ 0.75) | 11.36 ($\pm$0.36) | 11.37 ($\pm$ 0.63) | 11.81 ($\pm$ 0.20) |
| Initial drying rate ($10^{-3}$g/ cm$^3$ h) | 4,3 ($\pm$0.3) | 3,6 ($\pm$0. 3) | 3,5 ($\pm$0. 2) | 3,2 ($\pm$0. 2) | 2,7 ($\pm$0. 2) | 2,6 ($\pm$0. 2) |
| Final drying rate ($10^{-3}$g/cm$^3$ h) | 1,3 ($\pm$0. 7) | 1,7 ($\pm$0. 5) | 1,6 ($\pm$0. 2) | 1,5 ($\pm$0. 3) | 1,8 ($\pm$0. 2) | 1,7 ($\pm$0. 3) |
| Time for total drying (h) | $\pm$ 60 | $\pm$ 70 | $\pm$ 78 | $\pm$ 78 | $\pm$ 78 | $\pm$ 78 |

Control samples show, as expected, high and fast water absorption due to their coarse porosity network (see Section 3.1.2). All treated samples have lower water capillary absorption coefficients (WAC). This is due to a reduction of the porosity on the mortar's surface, which slows down the capillary rise [Charola and Wendler, 2015a]. WIP treatment yields the biggest decrease in capillary absorption coefficient, followed by the W treatment. Both samples also required more time (30 minutes more) to reach the asymptotic values (Fig.75) than the other treatments. These results are in line with the apparent porosity and MIP results which suggest that both treatments yielded higher reduction on porosity. All treated samples absorbed less water by capillarity than the control, which confirms that the samples have a denser pore structure after the treatment.
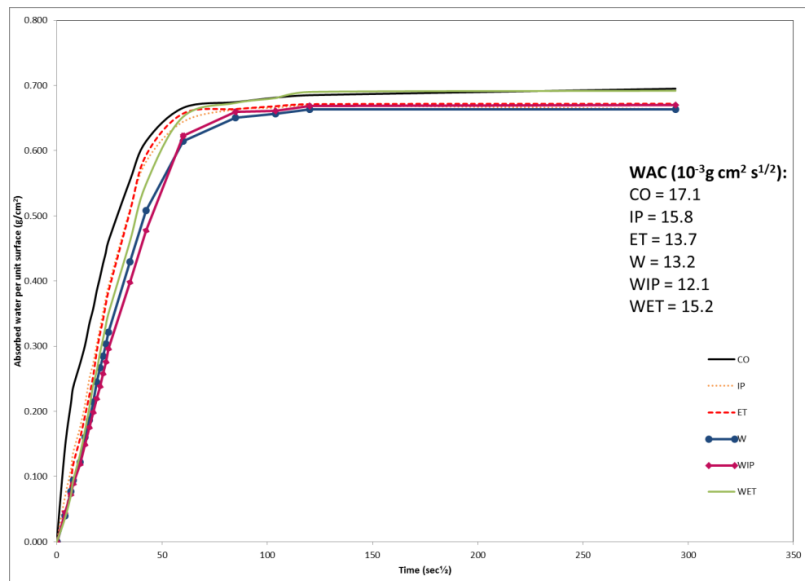
**Figure 75**. Capillary absorption curves of treated specimens (solvents).

The drying kinetics curves and the initial and final drying rates are shown in Fig.76 and Table 18. Results showed that all treatments slow the drying kinetics of the specimens. This result was also observed in the previous research program 1. This is attributed to the denser pore structure in the specimens' surface, which reduces the water transport towards the surface slowing down the drying kinetics. Control samples were completely dry after 60 hours. In contrast, IP sample needed approximately 70 hours to dry while ET, W, WIP and WET samples needed more than 75 hours.
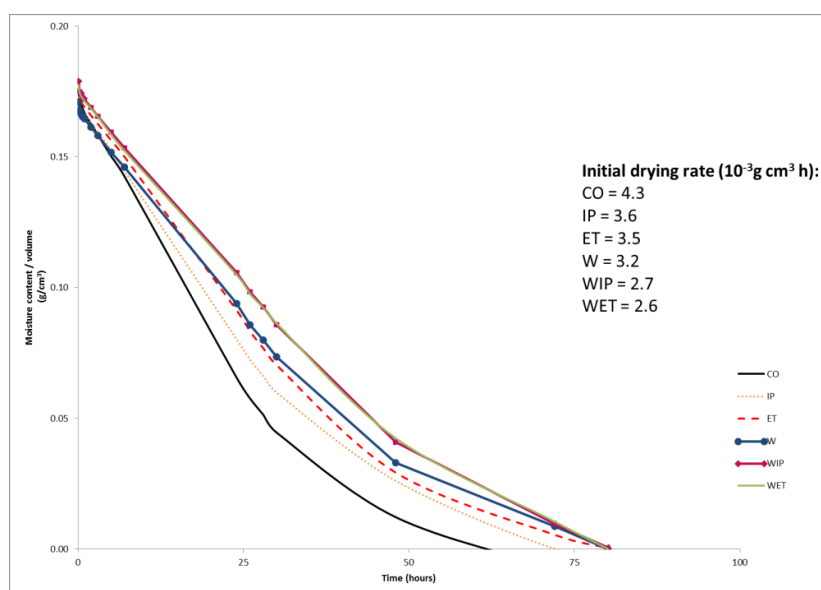


**Figure 76**. Drying curves of treated specimens (solvents).

The results of the Scotch Tape Test (STT) are shown in Table 19. All treatments obtained similar decreasing values of removed material after nanolime treatments ($\Delta W \approx 80\%$). These results confirm all surfaces are more compact after nanolime treatments.

Table 19. Scotch Tape Test (STT): experimental results

| Code ID | Released material (mg/cm²) | ΔW (%) | SD |
|---------|---------------------------|--------|-----|
| CO | 67.65 | - | 18.3 |
| IP | 9.42 | 86.1 | 3.6 |
| ET | 7.72 | 88.6 | 4.8 |
| W | 16.19 | 80.2 | 9.4 |
| WIP | 12.64 | 81.3 | 8.1 |
| WET | 15.8 | 80.9 | 6.2 |

Scotch area: 3 x 1.5 cm; SD (Standard Deviation) of released material

Drilling resistance results are shown in Figure 77. The control samples presented a constant drilling resistance (F ~ 0N (±0.12)) throughout the drilling depth (20 mm). It can be seen that IP, ET, W and WET treatments clearly increase the drilling resistance of the mortar within about 2-3 mm from the surface by approximately 1N. Additionally, a small consolidation effect (drilling resistance increased to F~ 0.35N) is also noticeable up to a depth of 6-9 mm for these samples. W sample yielded the highest increase in the drilling resistance in the outer 2-3 mm (>1.5 N (±0.32)). This is attributed to the high reactivity of these nanoparticles, which causes a quick carbonation on the surface. Moreover, this suspension presented low kinetic stability, which could facilitate the accumulation of the nanoparticles on the surface. In contrast, the consolidation effect of WIP appears to be more homogeneous within a depth of 6-7 mm (Fig. 77d). This is preferable as it does not result in the formation of a thin, excessively stronger superficial layer, which may increase the risk of spalling due to processes such as freeze-thaw or crystallization of salts occurring beneath this layer.

Recent studies carried out by Borsoi et. al. [Borsoi et al, 2015a, 2016] concluded that nanolime deposition in the pores can be influenced by the type of solvent. These researches concluded that nanoparticles tend to migrate back to the surface during

the evaporation of the solvent and thus solvents with slower evaporation rate can enhance the deposition of nanoparticles in the pores in highly porous substrates. In the present study, DRMS results did not indicate a clear correlation between the evaporation rate of the solvent and the consolidation in-depth. The addition of water to IP, which slows down the evaporation rate of the solvent, appears to have increased the penetration and degree of consolidation. However, this effect was not seen for the samples treated with ET and WET, where the addition of water to the ET solvent did not yield an increase in the penetration and consolidation degree. This could be attributed to the fact that the nanolime used by Borsoi et. al. was synthesised by solvothermal reactions while the nanolime used in this work was prepared by an anion exchange process. Nanolimes synthesised with these two methods present slightly different properties such as the colloidal stability, reactivity and morphology, as it was proven in the previous research programme 1.



a)

b)

c)

d)

e)
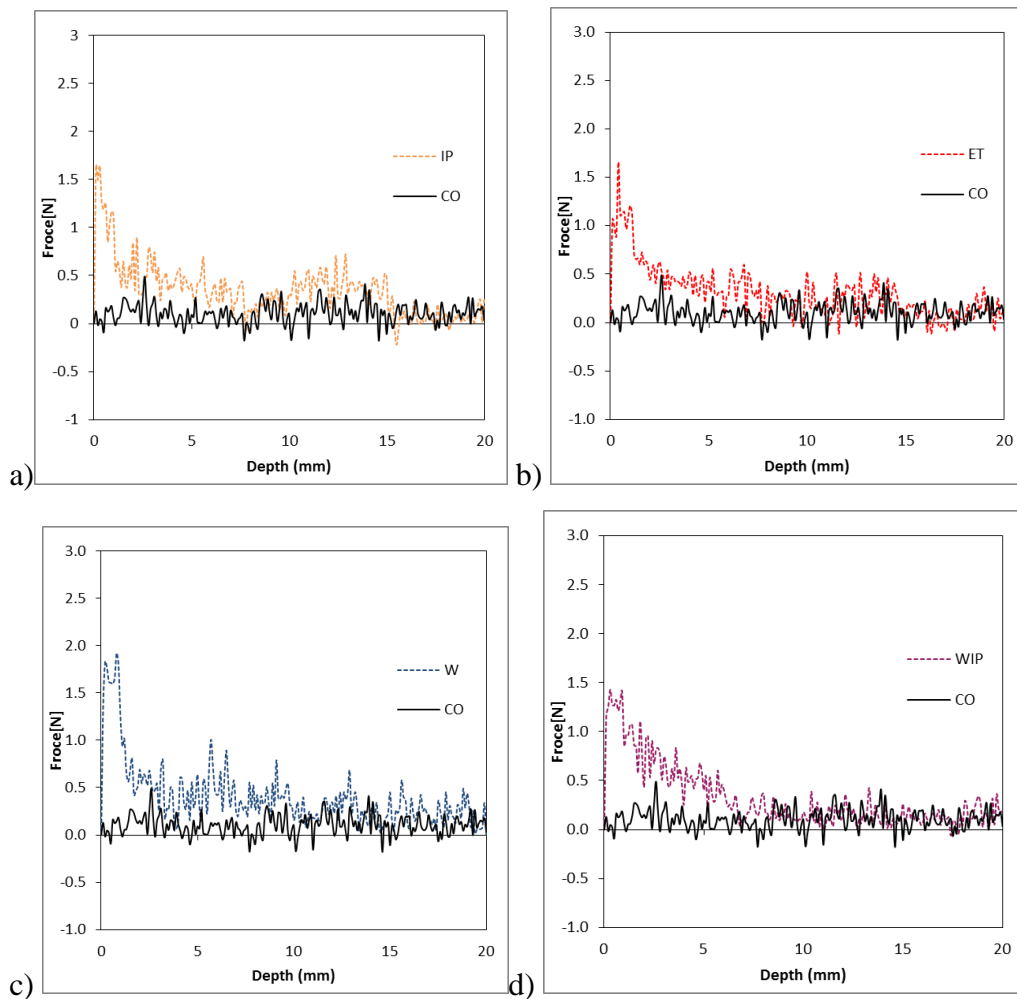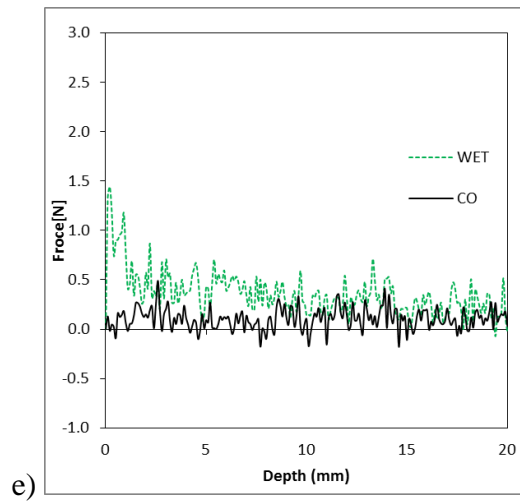
**Figure 77**. Drilling resistance profiles for control and treated samples: a) IP; b) ET; c) W; d) WIP; and e) WET.

The SEM images of control (Fig. 78a) and treated samples (Fig. 78b-f) show the new calcitic material filling the voids and reducing significantly the porosity of the surface of the mortar.



a)



b)



c)



d)
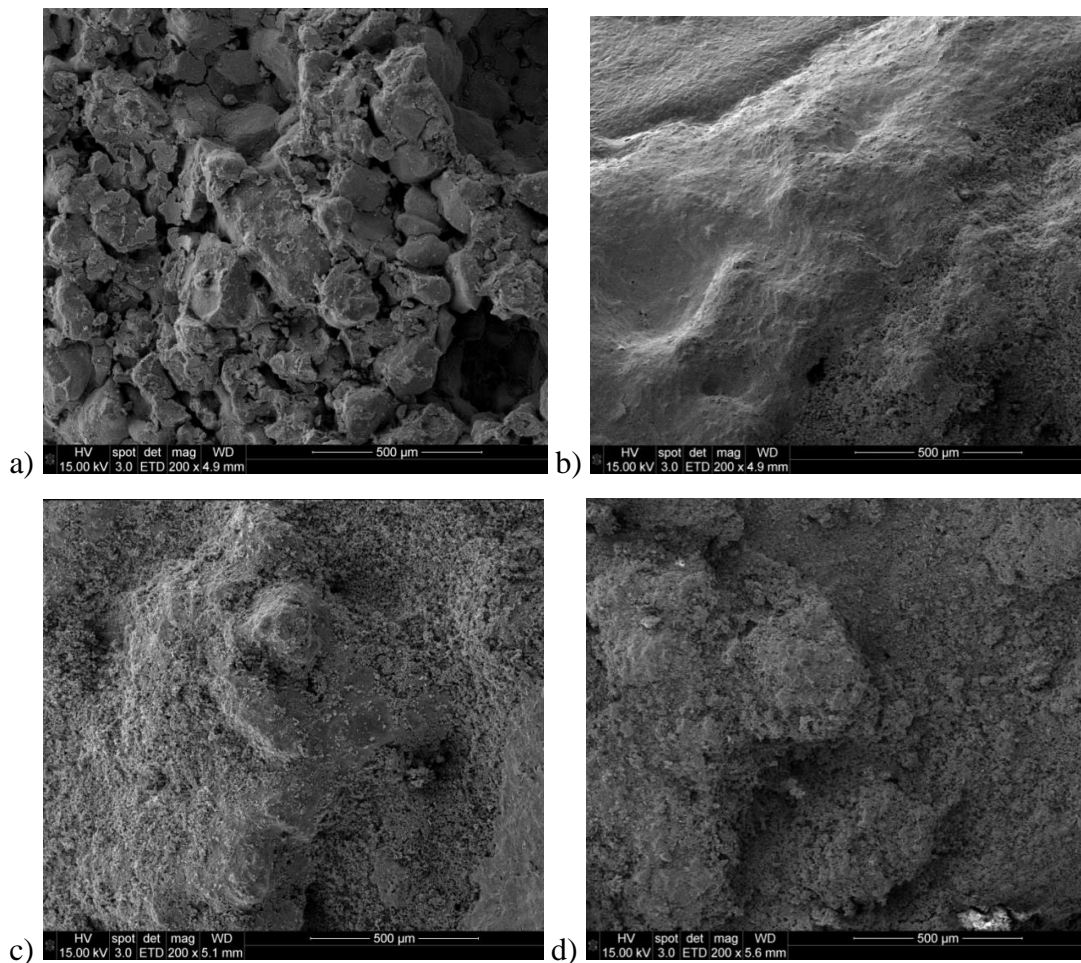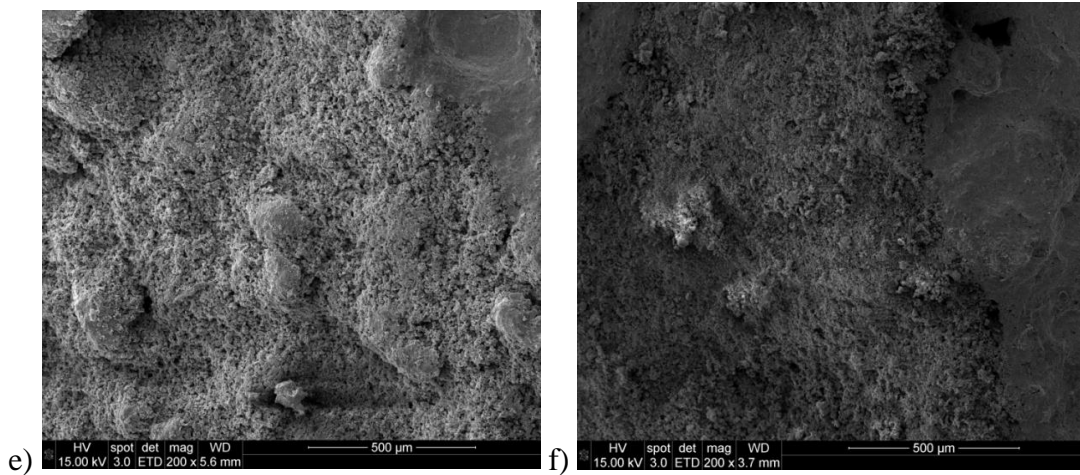
**Figure 78.** SEM micrographs of samples: a) control at 200x; b) IP sample at 200x; c) ET sample at 200x; d) W sample at 200x; e)WIP sample at 200x; f) WET sample at 200x.

Besides improving the physical-mechanical properties of the treated material, a conservation treatment must also not change its aesthetic appearance [Rodriguez-Navarro et al, 2013]. One of the most common side effects of nanolimes, which was already observed in the previous research programme (section 4.1), is the whitening of the surface after treatment [Baglioni et al, 2014]. Colorimetric results (Table 20) showed that all treatments certainly caused an undesired whitening of the specimen's surface. WIP yielded the lowest whitening and chromatic variations ($\Delta L^* \sim 7$ and $\Delta E^* \sim 10$ values). This could be attributed to the higher colloidal stability of this suspension which could facilitate the penetration of particles into the pores reducing the accumulation of the particles on the surface.

**Table 20.** Chromatic alterations for treated samples

|     | $\Delta L^*$ | $\Delta a^*$ | $\Delta b^*$ | $\Delta E^*$ |
|-----|-----------|-----------|-----------|-----------|
| IP  | 13.72 (±0.89) | -1.78 (±0.13) | -7.96 (±0.43) | 15.96 |
| ET  | 11.97 (±1.97) | -1.64 (±0.28) | -7.69 (±1.22) | 14.32 |
| W   | 11.92 (±1.87) | -1.65 (±0.31) | -8.12 (±1.13) | 14.52 |
| WIP | 7.81 (±1.78) | -0.18 (±3.92) | -6.79 (±1.12) | 10.35 |
| WET | 11.02 (±2.25) | 5.33 (±1.60) | -7.78 (±1.05) | 14.50 |

Mean values determined 30 measurements

*4.2.4 Conclusions*

This work has shown that Ca(OH)$_2$ nanoparticles synthetised by anion exchange resins and dispersed in various types of solvents can be used effectively for the consolidation of porous calcareous materials such as lime mortars.

This work has shown that:

- The synthetised Ca(OH)$_2$ nanoparticles consist of very small crystalline hexagonal plates. These are similar to the nanoparticles observed in the research programme 1 and in the literature [Taglieri et al, 2017b; Taglieri et al 2017c]. XRD confirm the presence of pure Ca(OH)$_2$ crystals for all suspensions. Nanoparticles dispersed in water present higher reactivity than nanoparticles dispersed in other solvents.

- All nanolime particles synthesised by anion exchange resins tend to settle with time. This sedimentation rate is higher than that observed by other researchers [Borsoi et al, 2015a, Ambrosi et al, 2001] for nanoparticles obtained through other synthesis routes (e.g. solvothermal reactions or drop to drop methods). The colloidal stability of nanoparticles in ethanol is significantly lower than that observed by other authors [Borsoi et al, 2016] for nanoparticles obtained from other synthesis routes (i.e. solvothermal reactions) and dispersed in the same solvent. A mixture of 50% of isopropanol and 50% water (WIP) presented the highest colloidal stability. All dispersions showed an acceptable colloidal stability (>95% nanoparticles in colloidal state) during the first 5 minutes after agitation, which it seems to be acceptable in terms of practical purposes as most of the particles remain in colloidal state for the duration of an application. An agitation is required before each brushstroke.

- XRD showed that the nanoparticles in all dispersions are very reactive. All suspensions are carbonated after only one hour of air exposure. W sample shows a reasonably well developed crystalline structure after only 1 hour of air exposure, suggesting higher reactivity than the other suspensions. After 7 days of air exposure, all samples are composed entirely of calcite crystals

with a better defined crystalline structure compared to those exposed for 1 day.

– ET and IP treatments evaporate faster than the other treatments. Both were completely dry after 24 hours. The evaporation of WIP and WET treatments was approximately 28 hours while for W treatment the evaporation was slower; they needed approximately 48 hours to dry.

– All treatments affect the pore structure by reducing the porosity of the superficial layer of the mortar. WIP and W seem to present slightly higher reduction of porosity followed by WET. The porosity reduction in samples WIP and WET can be attributed mainly to the reduction in the population of pores with larger diameter size (17 to 100 µm) while IP and W samples seem to be more effective in filling the pores with smaller size (0.05 to 0.7 µm).

– The denser pore structure on the surface decreases the capillary water absorption coefficient. WIP and W also presented the highest reduction of water absorption by capillarity rate, which is in the line with MIP results as both samples present the highest reduction in porosity. This confirms that both samples present pores with smaller size diameter on the surface that slow down the water absorption capillary rate.

– All treated samples present similar drying rate and all need more time to dry due to the denser pore network on the mortars' surface. This is not desirable as increases the risk of several decay processes (e.g. freeze-thaw or biocolonization).

– All nanolimes increase the drilling resistance of the mortar in the surface. DRMS results show that IP, ET, W and WET treatments clearly increase the drilling resistance of the mortar within about 2-3 mm from the surface by approximately, although, a small consolidation effect is also noticeable up to a depth of 6-9 mm for these samples. In contrast, the consolidation effect of WIP appears to be more homogeneous within a depth of 6-7 mm. This is preferable as it does not result in the formation of a thin, excessively stronger

superficial layer, which may increase the risk of spalling due to processes such as freeze-thaw or crystallization of salts occurring beneath this layer. W sample presents the highest increase in the drilling resistance in the outer 2-3 mm (>1.5 N). This could be attributed to the high reactivity of the nanoparticles when dispersed in water and low kinetic stability of this suspension which can facilitate the accumulation and precipitation of the particles on the surface.

– All treatments produced an undesired whitening of the surface after application. WIP yield the lowest whitening and chromatic variations.

– WIP sample is considered the optimal ratio as it shows slightly better consolidating properties in terms of increasing the drilling resistance, higher reduction of porosity, reduction of the WAC and lower impact on aesthetic properties.

Additionally, the results of this study did not indicate a clear correlation between the evaporation rate of the solvents and the consolidation in-depth in coarse materials, as it was found in previous works [Borsoi et al 2015a, Borsoi et. al, 2016]. This could be attributed to the fact that the nanolime used by Borsoi et. al. was synthesised by solvothermal reactions while the nanolime used in this work was prepared by an anion exchange process. Nanolimes synthesised with these two methods present slightly different properties such as the colloidal stability, reactivity and morphology, as it was proven in the previous research programme 1. More research needs to be done to fully understand the deposition of L'Aquila nanolime in the pores.

## 4.3 Influence of substrate pore structure and nanolime particle size on the effectiveness of nanolime treatments

### 4.3.1 Consolidation effectiveness

For the characterisation of the used limestones see section 3.1.3. The research programme methodology is described in section 3.3.3.

The pore structure properties of treated and control stones are summarised in Table 21. MIP results show that all treated samples have lower porosity than the control. In the case of LS stone, both treatments obtained a similar porosity reduction. In the case of CP stone, the NAN treatment yielded a higher porosity decrease than the LAQ one. Both treatments also reduced the modal pore diameter while increasing the total pore surface area in both stones. LAQ treatments yielded a higher increase in total pore surface and decrease in modal pore diameter in both stones, which suggests that samples treated with LAQ present finer pore network than samples treated with NAN (also observed in the research programme 1).

**Table 21**. Porosity properties of samples calculated by MIP

|  | Porosity (vol.%) | Modal Pore diameter (µm) | Total pore surface area (m$^2$/g) |
|---|---|---|---|
| LS-CO | 17.9 | 32.88 | 0.801 |
| LS-NAN | 15.7 | 32.10 | 1.081 |
| LS-LAQ | 15.5 | 30.15 | 1.433 |
| CP-CO | 14.1 | 34.47 | 0.502 |
| CP-NAN | 10.2 | 13.52 | 0.703 |
| CP-LAQ | 12.8 | 13.14 | 1.867 |

The pore size distributions of treated and control samples are shown in Figure 79. It is evident that both treatments affected the pore structure of both stones. NAN appears to have filled the pores with larger diameters in both stones. In the case of the LS stone, which has a higher population of pores with diameter between 10 µm to 50 µm compared to CP, the NAN treatment has reduced the amount of pores with

diameters between 10 and 40 µm (Fig 79a). Additionally, in this stone, MIP also recorded an increase of the pores with diameter between 40 to 100 µm. This is attributed to NAN reducing the number of pores with bigger diameters (>100 µm) which are outside of the measurement range of the used MIP technique. Moreover, as a result of this treatment, NAN caused a slight increase in the population of pores with diameters between 0.2 µm and 0.3 µm and between 0.01 µm and 0.03 µm. In the case of the CP stone, which presents a pore structure with large pores within the range 10-100 µm and intermediate pores between 0.1 to 6 µm, the treatment follows the same pattern. NAN treatment has clearly closed the large pores with diameter between 20 and 100 µm, and in this case the treatment has slightly reduced the amount of intermediate pores with diameters between 0.2 and 1 µm (Fig. 79b).

In contrast, MIP results show that LAQ treatment tends to fill both large and small pores more equally. LAQ treatment appears to partially fill the pores causing in both stones an increase in the population of smaller pores . In the case of LS stone, LAQ treatment clearly closed the large pores between 20 and 40 µm which is accompanied by an increase of the intermediate pores between 0.3 and 20 µm. This treatment also closed the pores with diameters of a smaller size (0.06 to 0.3 µm) which is accompanied by an increase of the finer pores size distribution (0.01 to 0.06 µm) (Fig. 79c). In the case of CP stone, the treatment follows the same pattern. LAQ treatment filled the pores with large pore size distribution (11 to 100 µm) while increasing the amount of intermediate pores (2 to 11 µm) and closed the pores with diameter 0.1 to 2 µm while increasing the amount of finer pores (0.01 to 0.03 µm) (Fig. 79d).

These results suggest that LAQ treatment could be more effective to consolidate fine pores than NAN. This is attributed to the small particle size of LAQ (particle size ~20-80nm), which may allow for a better penetration to reach pores with smaller size diameters when compared to NAN (particle size ~150-300nm). Nanoparticles tend to agglomerate and form clusters [Rodriguez-Navarro et al, 2013; Borsoi et al, 2016; Rodriguez-Navarro et al, 2016]. The clusters measure approximately 600nm for NAN [Rodriguez-Navarro et al, 2013] and 200nm for LAQ (see section 4.4.1, Fig. 83). Thus, the access of nanolime particles to the finer pores structure (0.01 - 1 µm), could be highly influenced by both the size of the particles and that of the clusters.
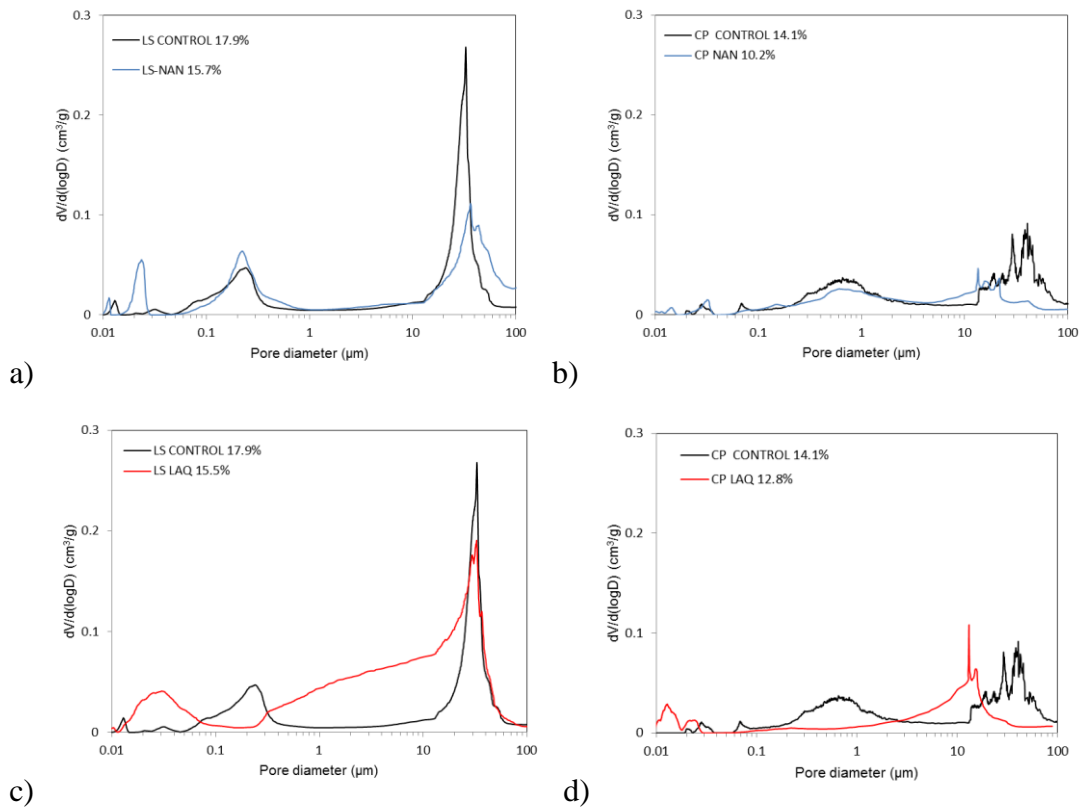
**Figure 79**. Pore size distribution of control and treated samples for: a) LS-NAN; b) CP-NAN; c) LS-LAQ; and d) CP-LAQ.

The water absorption and drying curves are reported in Fig 80 and Fig 81 and apparent porosity by immersion, water absorption and drying characteristics are reported in Table 22.

Table 22 shows that both nanolime treatments slightly reduced the apparent porosity of both stones. Table 22 also shows that the NAN treatment yielded a significant 77% decrease in the capillary absorption coefficient (WAC) in the LS limestone while LAQ only yielded in the same stone a 15.8 % decrease. This is attributed to the higher reduction of the large pores following the NAN treatment without increasing the intermediate pores, which clearly slows down the capillary rise [Charola and Wendler, 2015]. In the case of CP stone, both treatments slightly reduced the water absorption by capillary coefficient and both presented similar curves to each other. All treatments yielded similar reduction of the total water absorbed by capillarity in both stones.

**Table 22.** Water absorption and drying characteristics

| Parameter | LS-CO | LS-NAN | LS-LAQ | CP-CO | CP-NAN | CP-LAQ |
|---|---|---|---|---|---|---|
| Apparent Porosity (%) | 7.48 (±0.13) | 7.05 (±0.16) | 6.96 (±0.21) | 6.87 (±0.04) | 5.99 (±0.13) | 6.26 (±0.08) |
| W. absorption coefficient ($10^{-3}$g/cm$^2$ s$^{0.5}$) | 27.45 (± 0.5) | 6.14 (± 0.3) | 23.11 (± 0.3) | 13.95 (± 0.4) | 13.23 (± 0.3) | 13.82 (± 0.3) |
| W. absorbed at asymptotic value (g) | 5.25 (±0.07) | 5.17 (±0.08) | 5.11 (±0.17) | 4.12 (±0.11) | 3.9 (±0.13) | 4 (±0.09) |
| W. absorbed after 24-hour immersion (g) | 5.55 ±0.13) | 5.16 (±0.15) | 5.18 (±0.21) | 4.51 (±0.04) | 4.01 (±0.13) | 4.01 (±0.08) |
| Drying rate ($10^{-3}$g/ cm$^3$ h) | 5.9 (±0.2) | 5.8 (±0.4) | 5.2 (±0.5) | 4.4 (±0.10) | 3.9 (±0.2) | 3.7 (±0.3) |
| Time for total drying (h) | <50 | <50 | <50 | <50 | >50 | >50 |

All treated stones took more time to reach the asymptotical values (Fig. 80). LS stone control samples reached the asymptotical values in the first 20 minutes of contact with water. In contrast, LS samples treated with LAQ needed 35 minutes and NAN treated samples needed more than 90 minutes. In the case of CP stone, both treated samples reached the asymptotical value in the same time which was slightly higher than control samples.



a)

**b)**
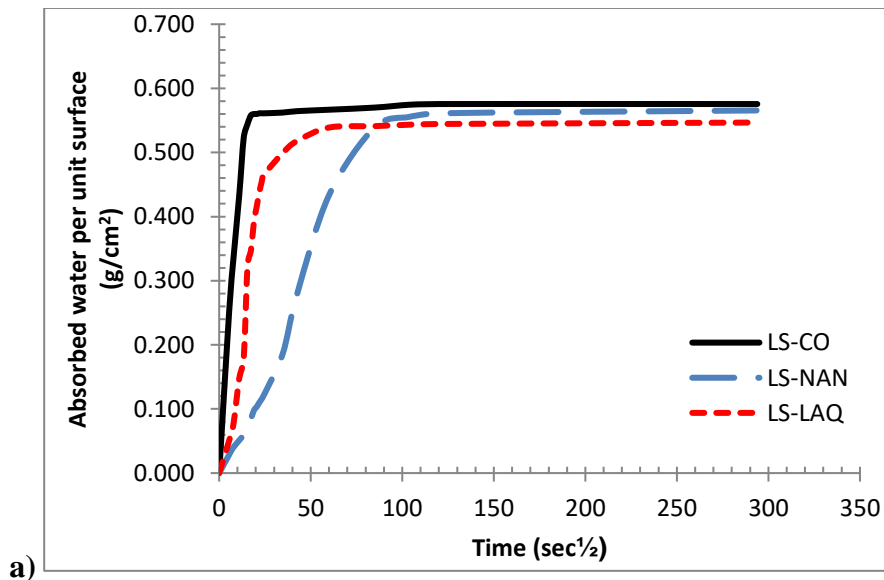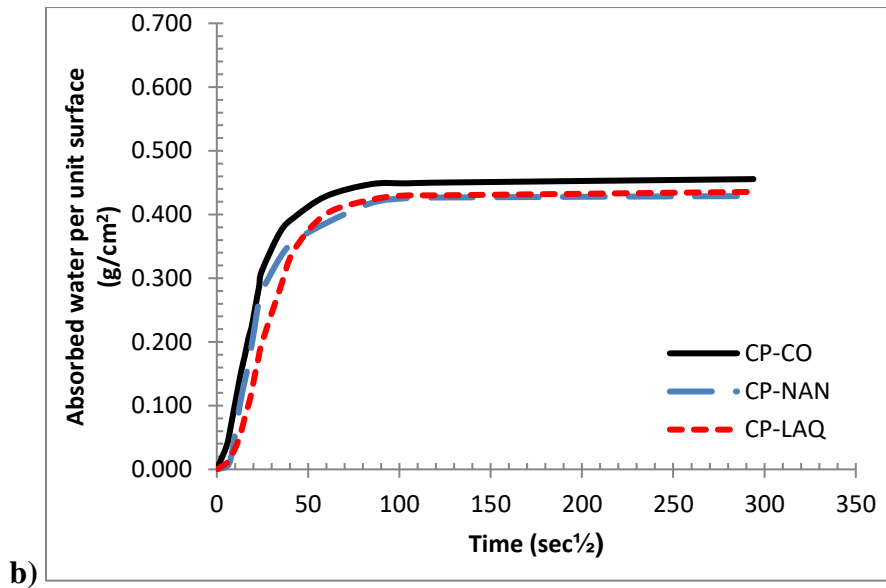
**Figure 80.** WAC curves for a) LS; b) CP.

The drying curves for both stones are shown in Fig 81. Drying curves for LS and CP show that the treated samples take slightly more time to dry than control samples (Table 22), similar as in the research programmes 1 and 2. Both treatments present similar drying rate and total drying time to each other in both stones. This is attributed to the more compact pore structure in the weathered layer which has been consolidated after nanolime treatments.



**a)**

**b)**
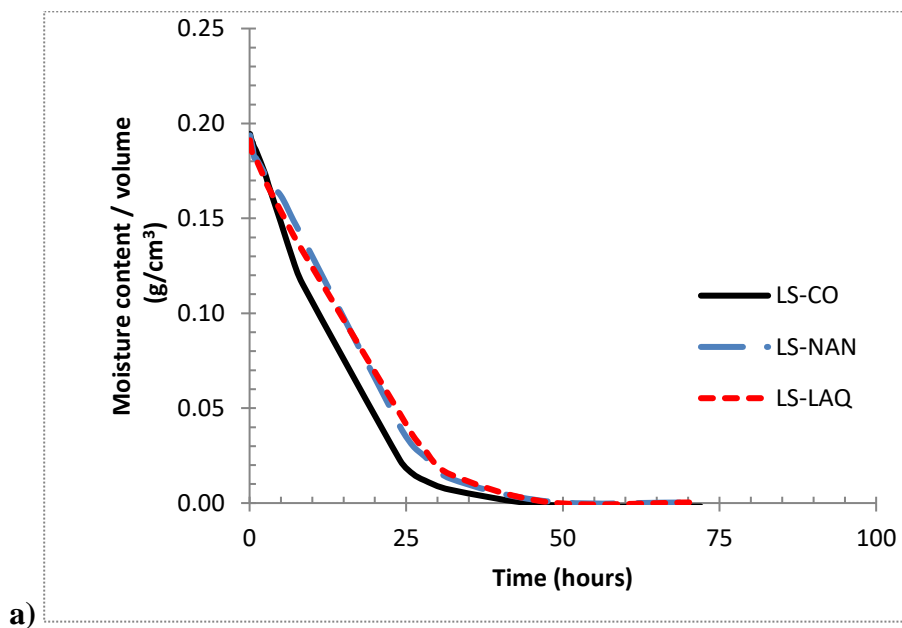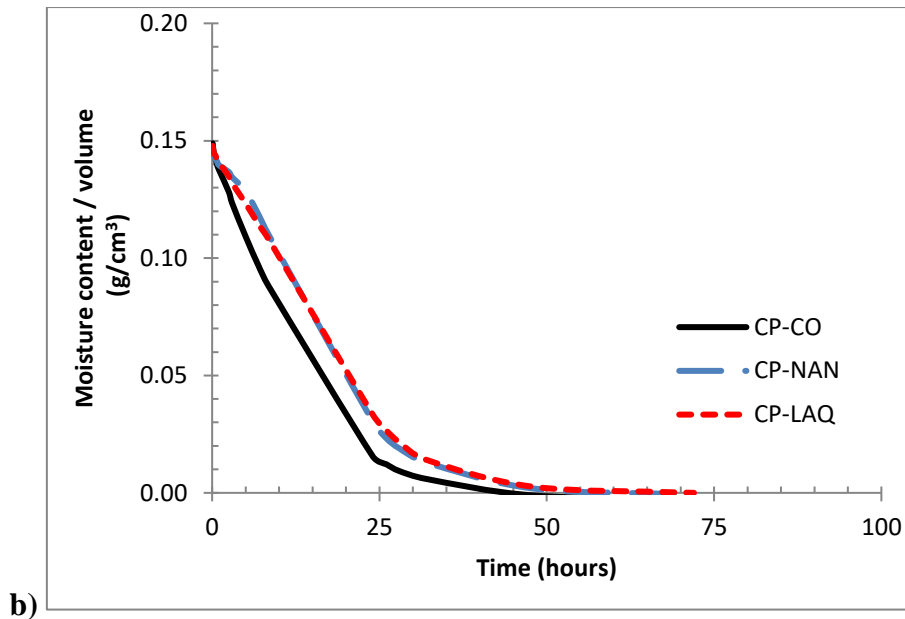
**Figure 81.** Drying curves for treated samples of: a) LS limestone; b) CP limestone

The results of the Scotch Tape Test (STT) are shown in Table 23. All treatments obtained lower values of removed material after nanolime treatments ($\Delta W \approx 62 - 88\%$). These results confirm that all surfaces are more compact after nanolime treatments. STT results confirm that the NAN treatment yielded the highest increase of surface cohesion in LS samples, which is in line with WAC and MIP results that show that this treatment is more effective in this type of stone. This is attributed to the higher reduction of the large pores of this treatment in this stone. In contrast, LAQ treatment yielded the highest increase in the surface cohesion in CP samples suggesting that the surface is more compact for this stone following this treatment.

**Table 23**. Scotch Tape Test (STT) results

| Code ID | Released material (mg/cm$^2$) | $\Delta W$ (%) | SD |
|---------|------------------------------|----------------|-----|
| LS-CO | 9.94 | - | 6.4 |
| LS-NAN | 1.64 | 83.5 | 0.5 |
| LS-LAQ | 3.28 | 67.0 | 2.1 |
| CP-CO | 17.74 | - | 6.6 |
| CP-NAN | 6.67 | 62.4 | 7.6 |
| CP-LAQ | 2.04 | 88.5 | 1.4 |

Scotch area: 3 x 1.5 cm; SD (Standard Deviation of released material)

Drilling resistance results for both limestone samples are shown in Figure 82. The drilling resistance of LS limestone is constant throughout the drilling depth (20 mm).

In contrast, the drilling resistance of CP limestone shows lower drilling resistance on the surface. This suggests that the external layer of this stone (Capital) has been affected by a weathering process, which decreased the compactness of the stone on the surface. The average drilling resistance of CP stone is F ~ 12.5N (±2.59), lower than LS stone (F ~ 18N (±1.47). Both treatments significantly increased the drilling resistance in both stones. In the case of the LS stone (Fig 82a), the samples treated with NAN recorded the highest increase in drilling resistance (ΔF ~ 50%), which was more pronounced in the outer 14 mm. This is in line with STT, WAC results that shows this treatment is more effective reducing the superficial cohesion and reducing the water absorption by capillarity. In the same stone, LAQ treatment also yielded an increase in the drilling resistance (ΔF ~ 22.2%), which was constant throughout the drilling depth. The higher increase of strength of NAN in this stone is attributed to the higher reduction of the large pores (20-40 µm), as the reduction of large pores delivers higher mechanical strength than reduction of small pores [Zhao et al, 2014]. In the case of CP stone (Fig. 82b), both treatments yielded similar drilling resistance which was constant throughout the drilling depth (20 mm). NAN and LAQ treatments yielded a strengthening of the weathered layer, where the drilling resistance increases considerably in the outer 14 mm (ΔF ~ 20.8% for NAN and ΔF ~ 18.4% for LAQ).

DRMS results of both stones show that the penetration of both nanolimes is significantly deeper than previous results on lime-mortars (2 – 6 mm). Furthermore, the increase of the drilling resistance is significantly higher in pure calcite-based materials (both limestones) than in lime-mortars (previous research programmes 1 and 2), which were composed of 82.3% quartz and 17.7% calcite. The higher mechanical strength in lime-based substrates is attributed to the fact that the amount of calcite in the matrix is higher facilitating the bonding of the newly formed calcite to the existing calcite crystals thus inducing a higher resistance due to chemical compatibility [Lanas et al, 2004]. Additionally, other authors also reported poor affinity of calcite with silicate-based materials [Lewins, 1982].

a)



` b)
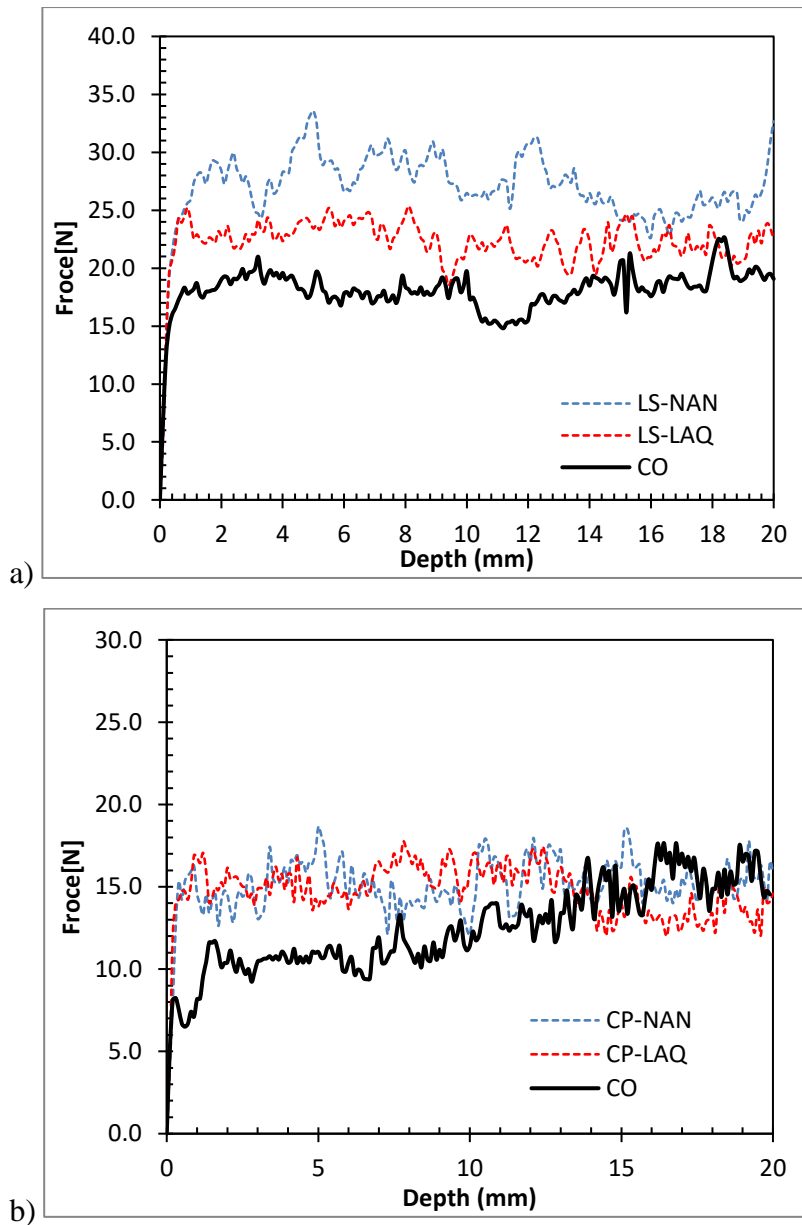
**Figure82.** DRMS measurements of: a) limestone (LS); b) weathered capital (CP).

The spectrophotometric analyses were carried out to measure changes in L* (white-black parameter) and $\Delta E^*$ (total colour variations) following the treatments. The results (Table 24) show that the treatments caused a whitening of the surface. Both treatments in both stones caused variations of both $\Delta E^*$ and $\Delta L^*$ with values above 5. The whitening is attributed as in previous research programmes to the accumulation of carbonated nanolime particles on the surface. The results are similar to the values obtained for lime-mortars in the research programmes 1 and 2.

**Table 24.** Chromatic alterations for treated samples

|  | ΔL* | Δa* | Δb* | ΔE* |
|---|---|---|---|---|
| LS-NAN | 8.23 (±.098) | -1.76 (±0.67) | -6.79 (±0.89) | 10.81 |
| LS-LAQ | 9.78 (±1.11) | -1.74 (±0.88) | -4.95 (±0.78) | 11.09 |
| - | - | - | - | - |
| CP-NAN | 11.15 (±1.40) | -2.56 (±0.87) | -13.48 (±1.21) | 17.68 |
| CP-LAQ | 10.28 (±1.52) | -0.61 (±0.56) | -4.43 (±0.87) | 11.21 |

Mean Values determined on 30 measurements

### 4.3.2 Conclusions

This work has shown that both nanolime products, NAN and LAQ, cause a significant consolidation of two different types of limestones with different porosity structure. Both types of nanolime are considered acceptable for a potential in-situ consolidation treatment on the weathered stone at the Cathedral of Wells or any historic structure built with Doulting stone.

It has been shown that:

- Both treatments reduced the porosity of both limestones. In the case of LS stone, both treatments obtained a similar porosity reduction. In the case of CP stone, the NAN treatment yielded a higher porosity decrease than the LAQ one. However, LAQ treatments yielded higher increase in total pore surface in both stones than NAN did, which suggests that LAQ treated samples present a finer pore network.

- The pore size distribution curves show that NAN treatment predominantly tends to close the pores with large pore sizes (20-100µm), while LAQ treatment tends to fill both large (20-100µm), and small pores (< 0.5µm) more equally. These results suggest that LAQ treatment could be more suitable to consolidate fine pores substrates than NAN. LAQ particles have better access to the smaller pores (<0.5 µm) due to the smaller particle size of LAQ (20-80nm) compared to NAN (150-300nm). Additionally, nanoparticles tend to agglomerate and form clusters. NAN product tends to form clusters of nanoparticles of size 600nm that reduce the penetration in the smaller pores [Rodriguez-Navarro et al, 2013]. However, L'Aquila nanoparticles present a

smaller particle size (20-80nm) and smaller clusters that could facilitate the access of the nanoparticles to the finer pore structure.

- Both treatments slow the water absorption by capillarity and drying rates due to the finer pore network in the stone's surface. NAN treatment yielded the largest decrease in capillary absorption rate for the LS limestone as this treatment yielded higher reduction of the large pores without increasing the intermediate pores. In the case of CP stone, both treatments reduced the water absorption by capillarity rate and both present similar water absorption curves.

- Scotch tape test confirm that both treatments successfully restore the surface cohesion of both limestones. NAN treatment yielded the highest increase in the surface cohesion in LS samples, where the treatment yielded higher reduction of the large pores.

- Both treatments clearly increase the drilling resistance of the stone after treatments. NAN treatment clearly yielded the highest increase of the drilling resistance ($\Delta F \sim 50\%$) in the LS stone, which is attributed to the higher reduction of the large pores. However, in the CP stone, both treatments yielded a similar drilling resistance as both obtained similar reduction of the large pores. Both treatments were able to consolidate the external weathered layer of the sample maintaining a constant drilling resistance throughout the stone.

- The increase of the drilling resistance due to nanolime treatments is significantly higher in pure calcite-based substrates (both limestones) than in lime-mortars (research programmes 1 and 2), which are composed of approximately 80% of quartz and 20% of calcite. This higher mechanical strength can be attributed to the fact that the bonding between calcite-calcite delivers higher resistance due to its higher chemical compatibility [Lanas et al, 2004].

- Finally, colorimeter results show that both treatments caused a considerable whitening of the surface of the limestones.

One final conclusion of this study is that the selection of a nanolime product for a consolidation treatment must be done in relation with the nanolime particle size and the substrate pore structure. Thus, Nanorestore Plus IP5® would be more suitable for consolidating stones with large pore sizes and L'Aquila nanolime for stones with fine pore sizes.

## 4.4 Case of study: Preliminary investigations of compatible nanolime treatments on Biocalcarenite from Agrigento, Italy

### 4.4.1 Characterisation of nanolime

The characterisation of the stone is reported in section 3.1.3 and the research programme is described in section 3.3.4. TEM examination of the synthetised nanolime (Fig. 83) showed nanoparticles with dimensions < 20 nm, with a tendency to agglomerate forming hexagonally shaped clusters of about 200-300nm.
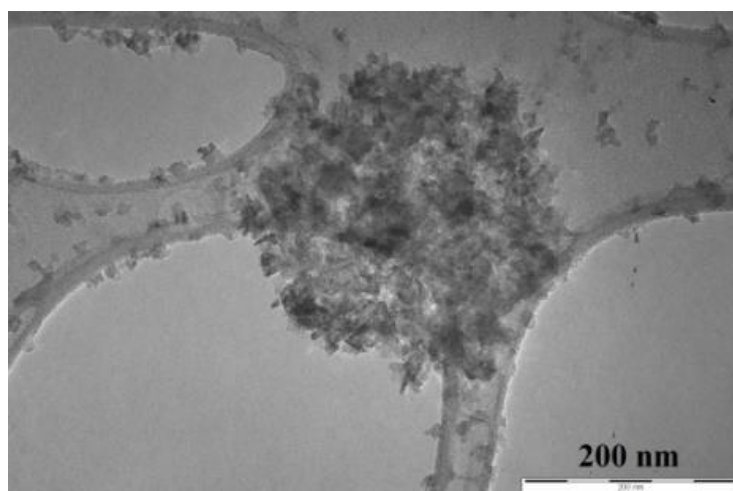


**Figure 83.** TEM micrograph of the W nanolime .

XRD results revealed that only pure $Ca(OH)_2$ was formed after synthesis (Fig.84).
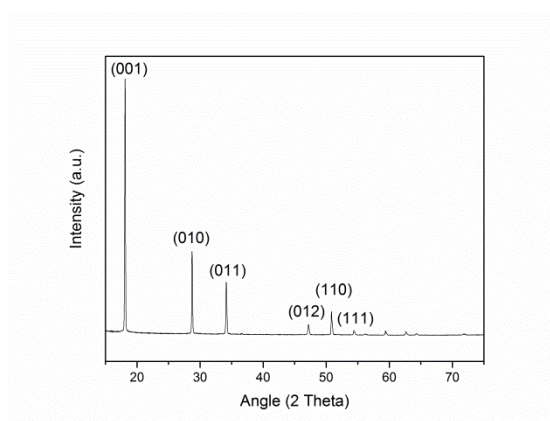


**Figure 84.** XRD pattern of dried particles from nanolime sample. Bragg peaks of $Ca(OH)_2$ pattern (ICSD#96-100-8782) were indexed.

From the analysis of the carbonation process we observed that **WIP** (5 g/L in 50% Water-50% Isopropanol) and **WIP\*** (10 g/L in 50% Water-50% Isopropanol) showed a completed carbonation process, i.e. only pure calcite ($CaCO_3$) formed. However, in the case of B (5 g/L in Butanol) only a partial conversion into calcite was observed (Fig. 85). In addition, an intermediate and metastable form, namely calcium carbonate hydroxide hydrate (CCH), was detected in samples WIP and B, as observed in previous studies [Taglieri et al., 2017a].
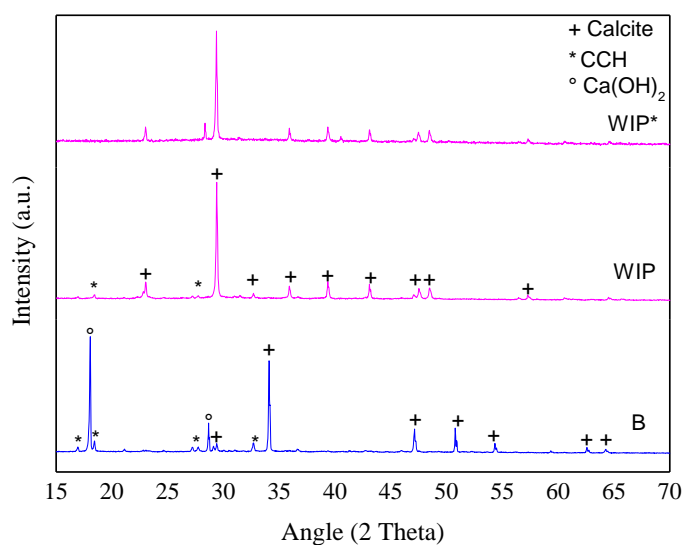


**Figure 85.** Analysis of the B, WIP and WIP\* suspensions, used for the treatments. The carbonation process in ambient air after solvent evaporation ($Ca(OH)_2$, ICSD #96-100-8782; Calcite, ICSD # 98-015-8258; CCH: calcium carbonate hydroxide hydrate, ICDD # 00-023-0107).

The kinetic stability of **WIP** and **WIP\*** samples was consistently stable in the first 2h (gradual settling process <10%), which is sufficient for practical purposes (Fig.86). **WIP\*** presented a rapid settling in the first 5 minutes but the KS parameters remained then stable, similarly to the other samples. The kinetic stability observed for WIP is similar to that detected by the previous research programme 2.
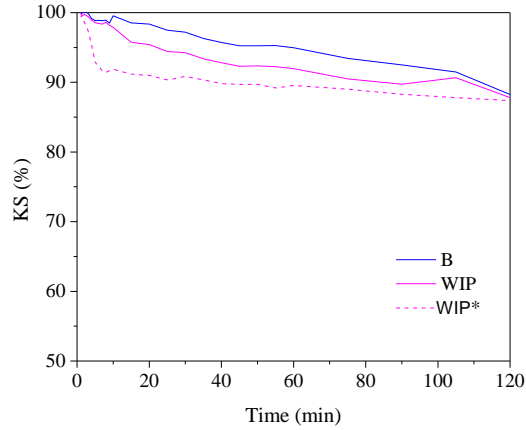
**Figure 86.** Kinetic stability (KS) of WIP*, WIP and B versus time, (at λ=600 nm).

## 4.4.2 Consolidation effectiveness

MIP measurements of the S1 (treated with WIP), S2 (treated with WIP*), S3 (treated with B) and S6 (treated with WIP*, repeated 3 times) samples, compared to the untreated ones, are reported in Fig. 87. As concerns S1 sample (Fig. 87a), the treatment yielded a reduction of the population of pores with diameter between 60 and 100 µm, similar to previous results, which is accompanied by an increase in the population of pores with diameters between 13 and 60 µm. Moreover, a reduction of the smallest pores (≤ 0,1 µm) was observed. For the S2 and S3 samples (Fig. 87b–c), both treatments reduced mainly the amount of pores with diameters between 30 and 100µm. MIP measurements carried out on S6 also confirms a clear reduction in the population of pores with diameters between 40 and 100 µm, together with a decrease in the average porosity of about 60% (Fig. 87d).



a)



b)
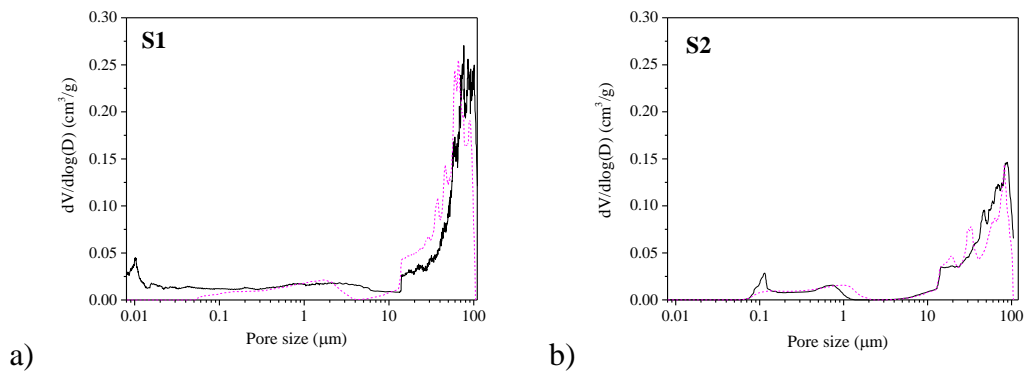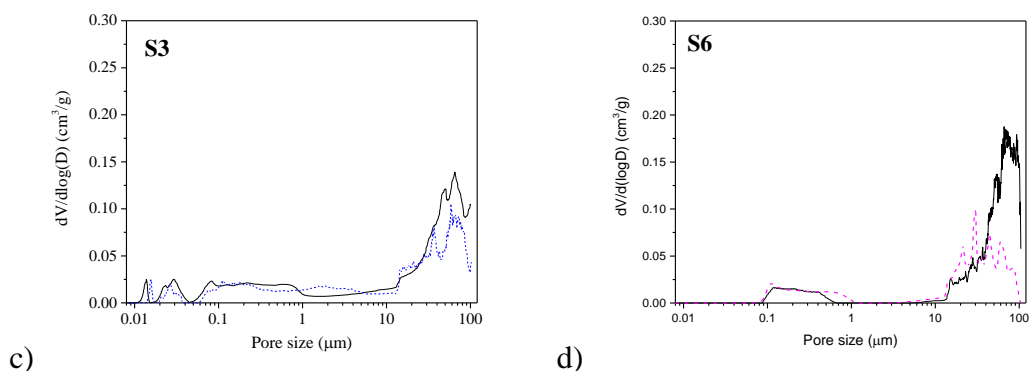
**Figure 87.** Differential volume of intruded mercury versus pore diameter of treated (dotlines) and untreated (continuous lines) stone samples: S1 (a), S2 (b), S3 (c), S6 (WIP* treatment repeated 3 times) (d).

The WAC was carried out following a method specifically developed for irregular substrates, which is described in the section 3.2.5.3.4. Table 25 shows the WAC results from the nanolime treatment on the irregular S1, S2 and S3 samples. It can be observed that, already after one treatment, all the samples showed a clear reduction both in the kinetics of capillary absorption ($\Delta CA$) and in the protective efficacy $E_p$. In particular, it was observed that the S1 sample showed the highest ability to absorb water both kinetically and in the saturation values, probably due to the higher porosity mainly related to the pores in the 10–100 µm range (Fig. 87a). In this case, the nanolime treatment seemed to have a greater influence on $\Delta CA$ than on $E_p$, and this could be due to the nanolime ability to reduce pore sizes by partially filling them, but without occluding them. In parallel, the samples treated using WIP* and B reached the highest efficacy (about 50%) in reducing water absorption.

**Table 25**. WAC results performed on irregularly shaped stone samples, before and after the nanolime treatment

|  | **Untreated (UT)** $Qf$ (mg / cm$^{-2}$) | **Treated (T)** $Qf$ (mg cm$^{-2}$) | $\Delta CA$ (%) | $E_p$ (%) |
|---|---|---|---|---|
| S1 | 1013 | 720 | 44 | 28 |
| S2 | 646 | 355 | 21 | 45 |
| S3 | 625 | 324 | 30 | 48 |

Fig.88, shows the WAC curves obtained for S4 and S5 (both samples treated with WIP*, repeated 3 times) before and after the nanolime treatment. WAC results show a higher reduction for the water absorption by capillarity compared to that obtained after only one treatment (Table 25).
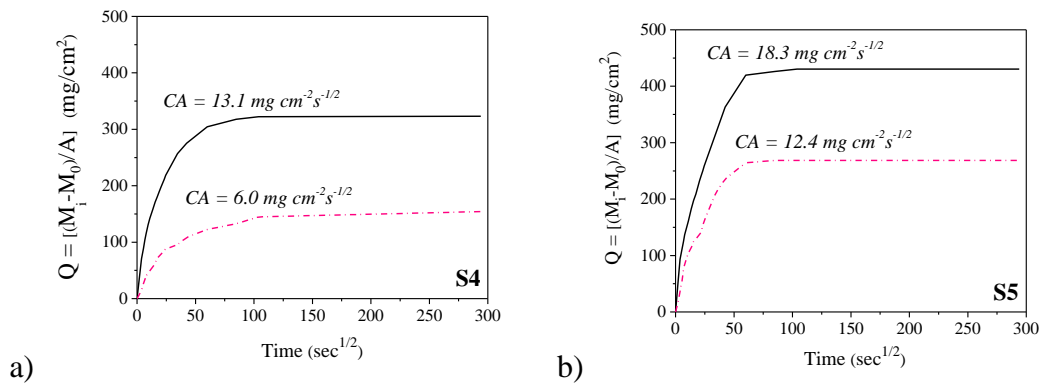


**Figure 88**. WAC curves before (continuous lines) and after (dotlines) the WIP*50% treatment, repeated 3 times. CA values were reported too, S4 (a), S5 (b)

In Table 26, the Scotch Tape Test (STT) results indicated that the nanolime treatments determined an increase of the surface cohesion of the treated stones, with a reduction in the percentage quantity of removed material ($\Delta W$) after one treatment of 10%, 14% and 30% for S1, S2 and S3 samples respectively. By repeating the treatment three times (S6) a clear $\Delta W$ improvement was obtained, reaching a mean value $\Delta W \approx 60\%$.

**Table 26**. Results of the STT performed on untreated and treated stones.

|  | UT (mg cm$^{-2}$) | T (mg cm$^{-2}$) | $\Delta W$ (%) |
|---|---|---|---|
| S1 | 1.92 (±0.34) | 1.69 (±0.65) | 9.5 |
| S2 | 3.15 (±0.17) | 2.65 (±0.11) | 14.3 |
| S3 | 1.17 (±0.46) | 0.57 (±0.25) | 29.6 |
| S6 | 10.25 (±0.30) | 4.05 (±0.64) | 60.5 |

Scotch area: 12.72 cm$^2$ (S1, S2 and S3) and 9.5 cm$^2$ (S6).

The drilling resistance profiles performed before and after the nanolime treatment, showed that a significant increase can be observed only when the treatment was repeated for three times (S6 sample). The results, reported in Fig. 89, showed that

before the treatment the S6 sample presented a value of resistance of $4 \pm 1$ N, slightly decreasing in the interior of the stone. After treatment, in addition to a small improvement at the surface, an increase of the resistance up to 10 mm from the surface with a medium value of $8 \pm 3$ N was observed.
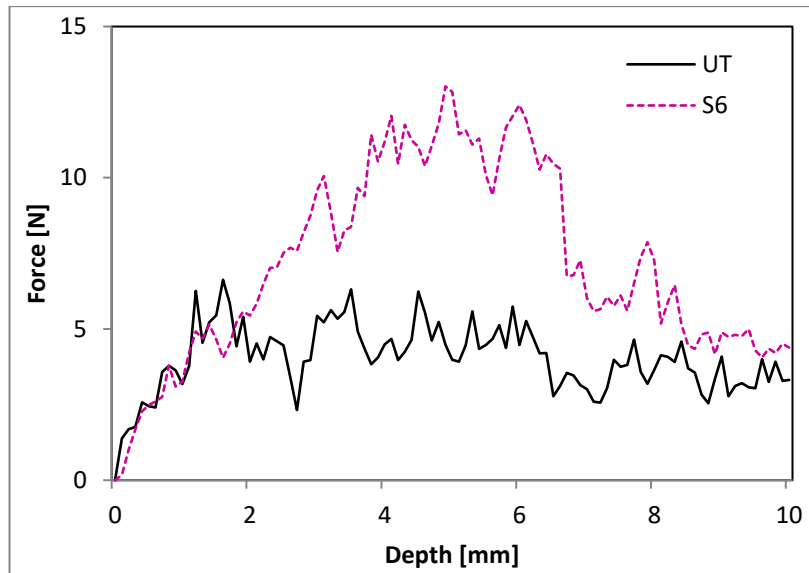


**Figure 89.** Drilling resistance profiles of untreated (continuous line) and treated (dotline) biocalcarenite (S6 sample).

The colorimetry results are reported in Table 27, showing that the nanolime treatments do not cause major aesthetic changes ($\Delta E^*$ 5–9) and do not cause a significant increase in luminosity ($\Delta L^*$1–5). In particular no significant white glazing was observed after the treatment for S1, S2 and S3 ($\Delta L^*$ 3, 5 and 1 respectively). S2 seemed to show the lowest chromatic alteration of the surface ($\Delta E^*$ 5) but the highest difference of luminosity ($\Delta L^*$ 5). S3 shows higher value with $\Delta E > 9$ due to a significant alteration with $b^* > 8$ (blue-yellow axis). S2 increases the $L^*$ parameter, probably due to the effect of higher concentration (10 g/L). The low chromatic changes for S1 and S2 (and $\Delta E^*$ 5–6) and their reduction over time as it has been seen in the research program 1, indicate that the nanolimes dispersions are suitable for practical conservation interventions.

**Table 27.** Results of the colorimetric analysis performed on the treated stones.

|    | ΔL* | Δa* | Δb* | ΔE* |
|----|------|------|------|------|
| S1 | 3.04 (±0.72) | -0.53 (±0.11) | -5.17 (±0.97) | 6.02 |
| S2 | 5.05 (±0.54) | 0.39 (±0.18) | -0.003 (±0.11) | 5.06 |
| S3 | 1.64 (±0.31) | 4.01 (±0.69) | 8.75 (±0.75) | 9.76 |

Mean values determined  30 measurements

*4.4.3 Conclusions*

This work has focused on testing the efficacy of a compatible conservative treatment for the biocalcarenite stones of the Valle dei Templi (Agrigento, Italy). It has been shown that:

- The characterisation analyses confirmed the high reactivity of the $Ca(OH)_2$ nanoparticles, reflecting a full carbonation process occurring, in ambient condition, in only the first 30 minutes. Moreover, the process led to the formation of calcite as pure and unique phase and this result is fundamental to guarantee a perfect compatibility with the treated surface, from a chemico-physical and mechanical point of view.

- As concerned the treatment efficacy, the best results were obtained by using the hydro-alcoholic nanolime suspension (50% water and 50% alcohol) at a concentration of 10 g/L, and by repeating the application for three times. This nanolime worked well as a superficial consolidant, increasing the surface cohesion, thus reducing the material loss from the surface, particularly in the first 10 mm beneath the surface. A decrease in water absorption by capillarity, up to 50%, was also observed and confirmed by a reduced porosity and a clear reduction in the population of pores with diameters between 40 and 100 µm. Nevertheless, the nanolime treatment caused some superficial whitening that needs to be removed by proper actions or examined in depth in a next study.

## 4.5 Case of study: Preliminary investigations of compatible nanolime treatments on Indiana limestone and weathered marble from the Smithsonian's building.

*4.5.1 Consolidation effectiveness*

The characterisation of both stones is described in section 3.1.3 and the research programme is described in section 3.3.5.

The porosity of cubic Indiana limestone samples (treated with ET25) was obtained by calculating their apparent porosity by immersing the samples for 24 hours in water at atmospheric pressure. Table 28 shows that both treated samples, IR (stored in room condition) and IRS (stored in room condition and regularly sprayed with carbonated water), have slightly lower porosity than the control. This confirms that a certain amount of nanolime penetrated and carbonated in the Indiana limestones.

**Table 28**. Calculated Apparent porosity (% g/g) and Open porosity ($cm^3/cm^3$)

| Sample | I-CO | IR | IRS |
|---|---|---|---|
| Apparent Porosity % w/w | 5.99 | 5.75 | 5.88 |
| Open Porosity % v/v | 13.44 | 12.96 | 13.04 |

The pore structure properties of the weathered marble (treated with IP25) and control samples were obtained by MIP and are summarised in Table 29. It is evident that all treatments affected the pore structure of the weathered marble by reducing the porosity. The highest porosity decrease was observed for the samples which have been treated and sprayed regularly with carbonated water, MRS (~60% decrease), followed by those treated and kept in a 75% RH environment, M75 (~50% decrease). This is in line with the literature, as is well-known; the carbonation process is strongly influenced by moisture and $CO_2$ exposure [Doehne and Price, 2009].

**Table 29.** Pore structure properties of treated and control marble samples measured by MIP

| Sample | Porosity (%) | Total pore surface area (m²/g) |
|---|---|---|
| M-CO | 6.00 | 3.49 |
| MR | 3.85 | 2.35 |
| MRS | 2.44 | 1.48 |
| M55 | 3.11 | 1.38 |
| M75 | 3.00 | 1.76 |

The pore size distributions of treated and untreated marble samples are shown in Figure 90. All treatments yielded a reduction in the population of pores with a wide range of diameters (between 0.02 µm and 30 µm), and such reduction is more pronounced for the samples treated with MRS, M-75 and M-55. The pore size regions of 0.1-0.2 µm and 30-50 µm seem to have been less affected by the treatments.
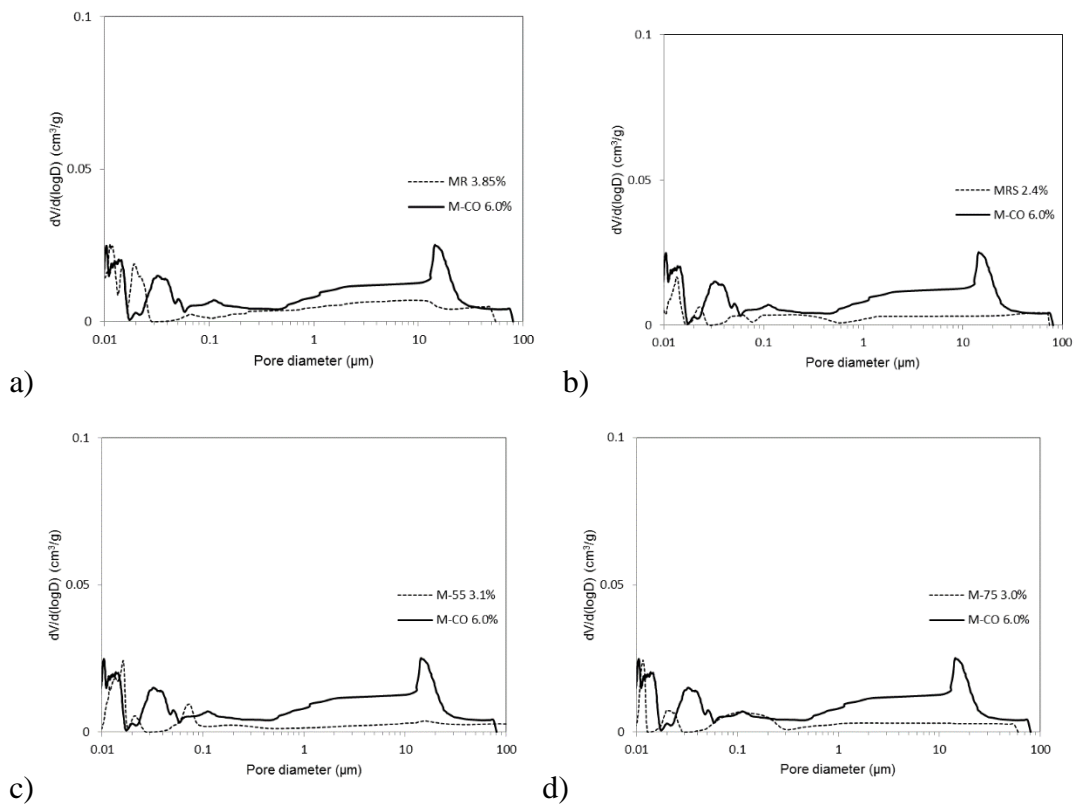


**Figure. 90**. Differential volume of intruded mercury versus pore diameter of treated and untreated marble samples : a) MR; b) MRS; c) M55; d) M75.

The results of the Scotch Tape Test (STT) for both Indiana limestone and weathered marble are shown in Table 30. All treatments yielded decreased values of removed material ($\Delta W \approx 54 - 83\%$). These results confirm that all surfaces are more compact after nanolime treatments in all environmental condition. The samples sprayed with carbonated water (IRS and MRS) yielded the highest increase in superficial cohesion ($\Delta W \approx 77.2$ and $82.8\%$, respectively). Marble samples stored at 75%RH (M75) yielded higher superficial cohesion than marble samples stored at 55%RH (M55), confirming that keeping samples in high relative humidity environments (~75%RH) increases the consolidation effectiveness [Lopez-Arce et al, 2010].

**Table 30.** Scotch Tape Test (STT): experimental results

| | Released material (mg/cm$^2$) | $\Delta W$ (%) | SD |
|---|---|---|---|
| ICO | 5.59 | - | 0.86 |
| IR | 2.55 | 54.3 | 0.93 |
| IRS | 1.28 | 77.2 | 0.19 |
| M-CO | 9.01 | - | 2.17 |
| MR | 3.56 | 60.5 | 1.66 |
| MRS | 1.56 | 82.8 | 1.47 |
| M55 | 4.52 | 49.9 | 1.78 |
| M75 | 2.9 | 67.9 | 1.54 |

Scotch area: 3 x 1.5 cm; SD (standard deviation of released material)

Drilling resistance results for the Indiana limestone samples are shown in Figure 91a. The Indiana limestone shows a constant drilling resistance throughout the 20 mm drilling depth (F ~ 15N ($\pm 1.34$)). The samples treated with ET25 stored in room conditions showed no increase in the drilling resistance. In contrast, the samples treated with ET25 and sprayed with carbonated water (IRS), showed an increase in the drilling resistance (F ~ 16.5 N ($\pm 1.43$)) within the outer 2-3 mm of the sample.

Drilling resistance results for the marble samples are shown in Figure 91b. It can be seen that the drilling resistance of the weathered layer (up to 10-12 mm deep) is lower than in the core of the sample. The drilling resistance average in the outer 10 mm of the stone is F ~ 37.4N ($\pm 11.35$), while for the inner 10 mm is F ~ 53.5 N ($\pm 1.36$). This result confirms that the formation of gypsum ($CaSO_4$) (see section 3.1.3) decreased the compactness of the stone on the surface. The treated marble

samples which were sprayed with carbonated water (MRS) yielded a significant increase in the drilling resistance of the external weathered layer ($\Delta F \sim 51.82\%$). In contrast, samples kept in the same room conditions (<50%RH) but not sprayed (MR), did not present any increase in the drilling resistance. This result clearly shows that a regular input of moisture enhances the carbonation of nanolime in low relative humidity environments. Marble samples which were treated and kept at 75%RH (M75), have obtained the highest increase in the drilling resistance on the external weathered layer ($\Delta F \sim 72.12$ %). This suggests that a high relative humidity environment seems to increase better the nanolime effectiveness by providing a constant supply of moisture which enhances the carbonation of nanolime particles, rather than a occasionally input of moisture. In contrast, samples kept at 55% RH (M55) did not present any increase in the drilling resistance.



a)



b)
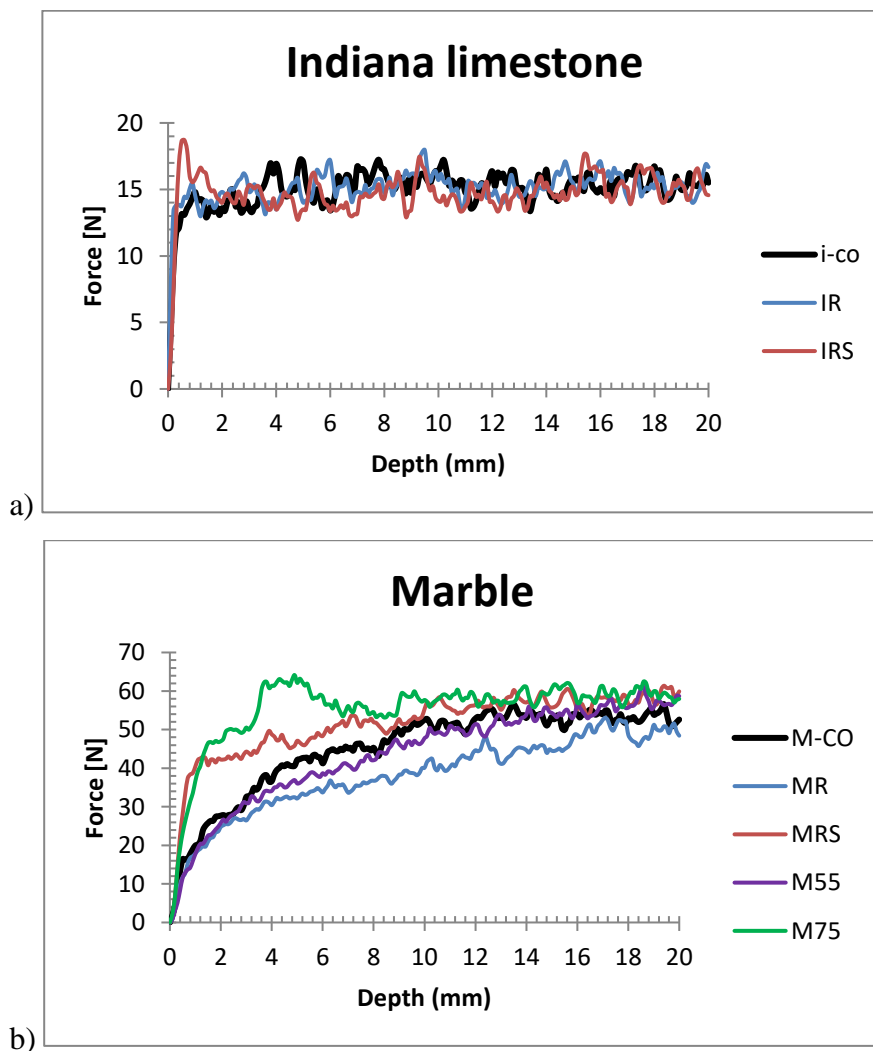
**Figure 91.** DRMS measurements of untreated (black line) and treated (colors) samples: a) Indiana limestone; b) marble

Cross-sections of treated samples were examined by SEM (Appendix 1). For the case of the Indiana limestone, treated and untreated samples presented no differences in terms of morphology. It was difficult to distinguish whether newly formed calcite crystals from nanolime have the same shape and size as the sparry calcite of the limestone, or whether there is no presence of nanolime in the samples observed by the SEM (Fig. 92).
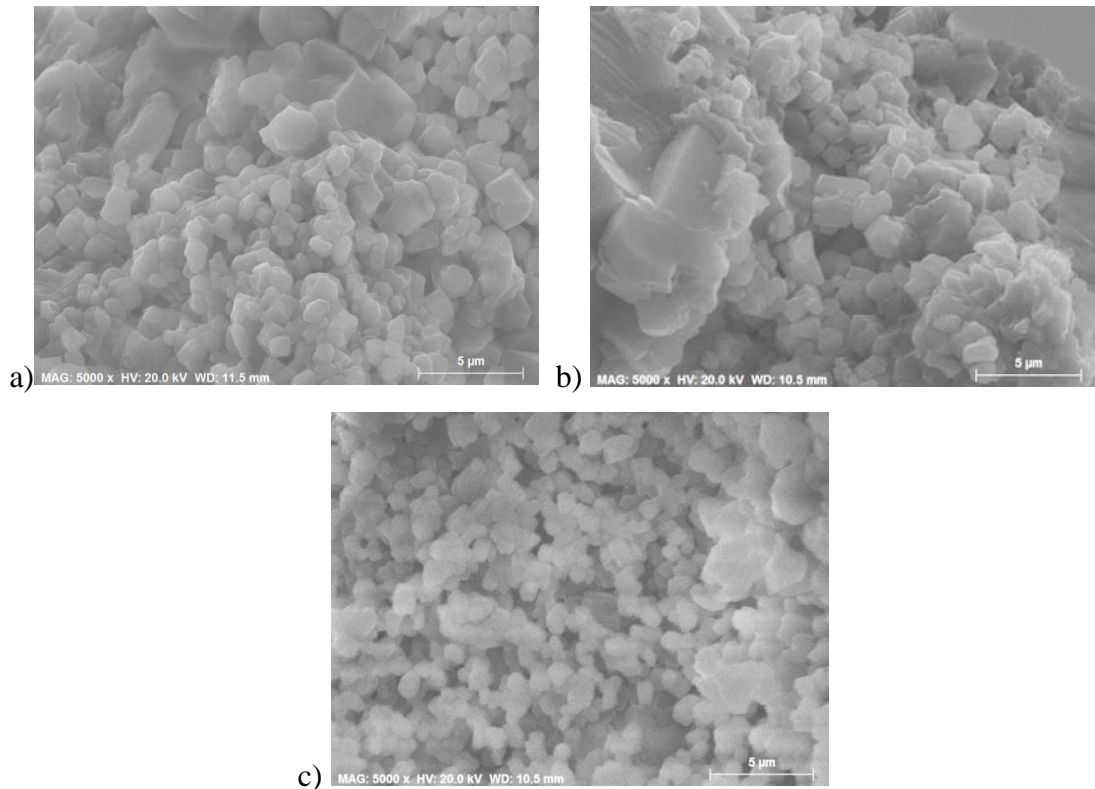


**Figure 92**. SEM images of Indiana Limestone a) I-CO; b) IR; c) IRS

SEM images of marble samples show some hexagonal plates of portlandite crystals in the core of the samples which were kept at room conditions (MR) and at 55%RH (M55) (Fig. 93b and 93c). In contrast, no portlandite crystals were observed in samples which were sprayed with carbonated water (MRS) or kept at 75%RH (M75). Furthermore, both MRS and M75 seem to have higher amount of calcite crystals in the pores (Fig 93d and 93e). These results suggest that the increase of the strength and the reduction of porosity of both samples (MRS and M75) could be attributed to a higher carbonation degree of the particles. Recent research studies showed that the carbonation of LAQ nanoparticles dispersed in pure alcohol solvents can take more

than a month to occur in low RH environments (<50%RH) and at high concentrations (i.e. 25 g/L) [Taglieri et al, 2017a].
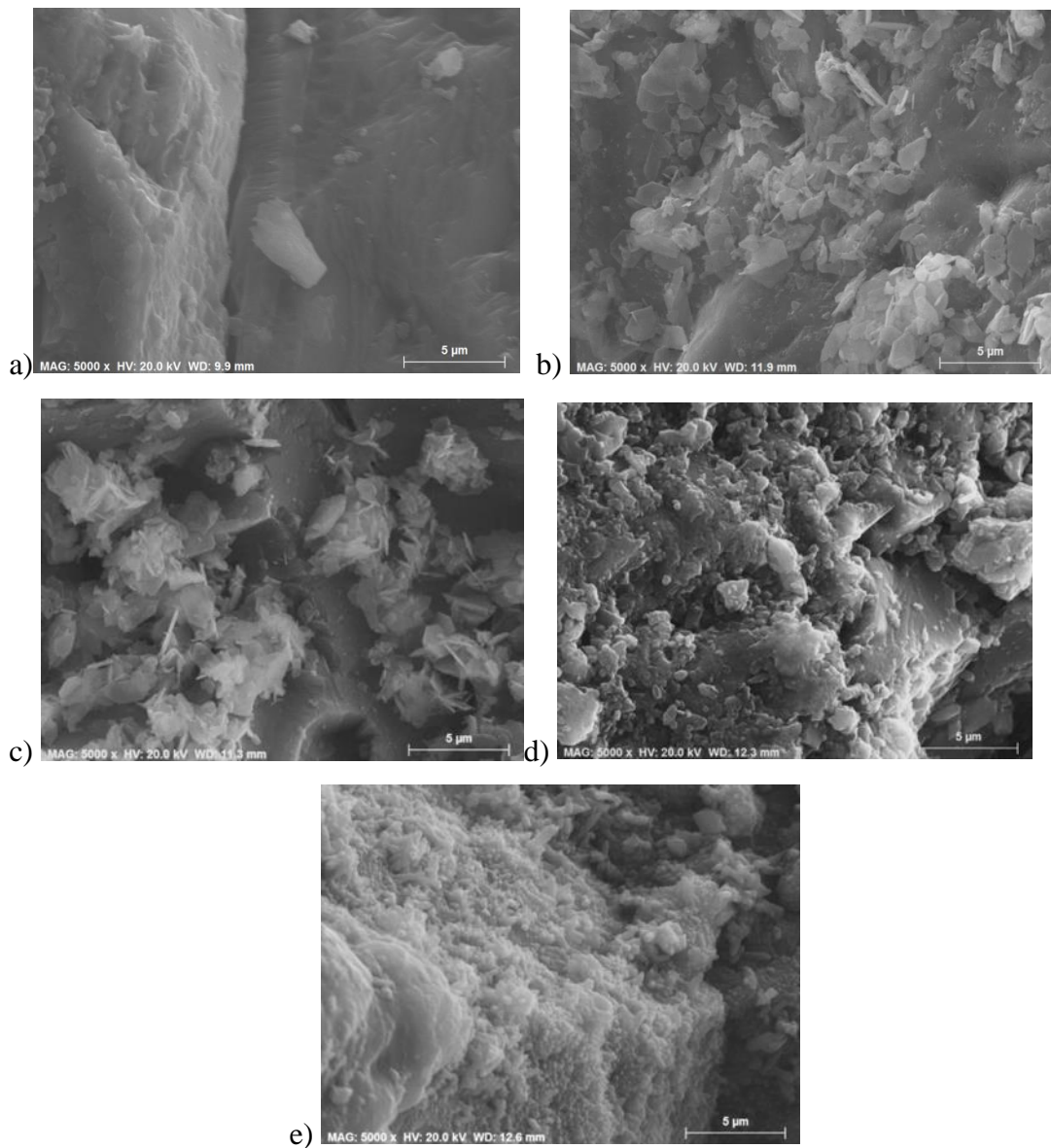


**Figure 93.** SEM images of treated marble samples; a) M-CO b) MR; c) M55; d) MRS; e) M75.

The water absorption by capillarity and drying curves of cubic Indiana limestone samples were also evaluated. Both tests were carried out in only one specimen per each sample, as there was only one sample available for the test. It can be seen that the water absorption curve of I-CO, IR and IRS samples are very similar (Fig 94). The water absorption by capillarity coefficients are reported in Table 31.

**Table 31.** Apparent porosity by immersion, water absorption and drying characteristics. Tests were carried out only in one specimen per each sample

| Parameter | I-CO | IR | IRS |
|---|---|---|---|
| Water absorption coefficient ($10^{-3}$ g/cm$^2$ s$^{0.5}$) | 5.55 | 5.01 | 5.54 |
| Water absorbed at asymptotic value (g/cm$^2$) | 0.66 | 0.64 | 0.64 |
| Initial drying rate ($10^{-3}$g/ cm$^3$ h) | 9.89 | 9.0 | 9.1 |
| Final drying rate ($10^{-3}$g/cm$^3$ h) | 0. 5 | 0. 6 | 0. 7 |
| Time for total drying (h) | ±60 | ±60 | ±60 |

The water absorption rate of IR samples is slightly slower than I-CO and IRS which are practically identical. The two treated samples absorbed a lower amount of water by capillarity.
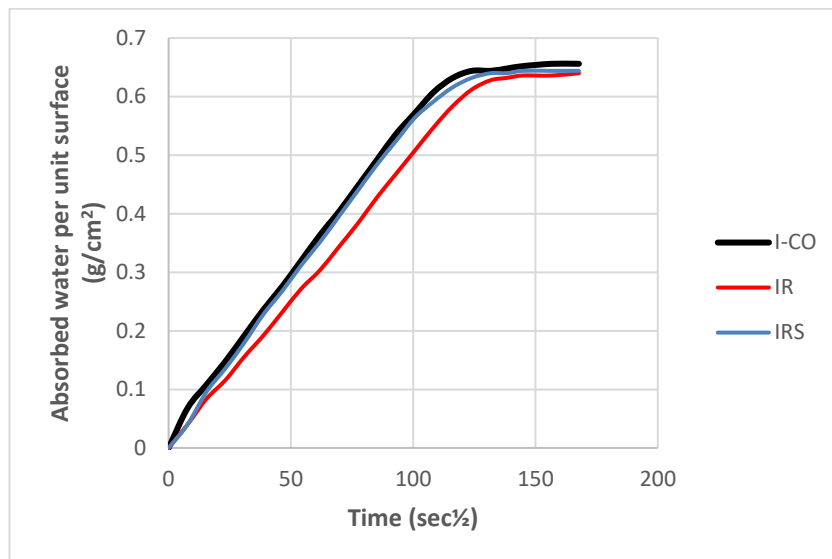


**Figure 94**. Capillary absorption curves for the three of treated and control samples, where I-CO is the untreated control, IR, is the treated sample, and IRS corresponds to treated and regularly sprayed sample.

The drying curves are shown below (Fig.95). The drying rate of the I-CO, IR and IRS samples are identical. The initial and final drying rates were calculated and are listed in Table 31. All treated and untreated samples were completely dried after 60 hours.
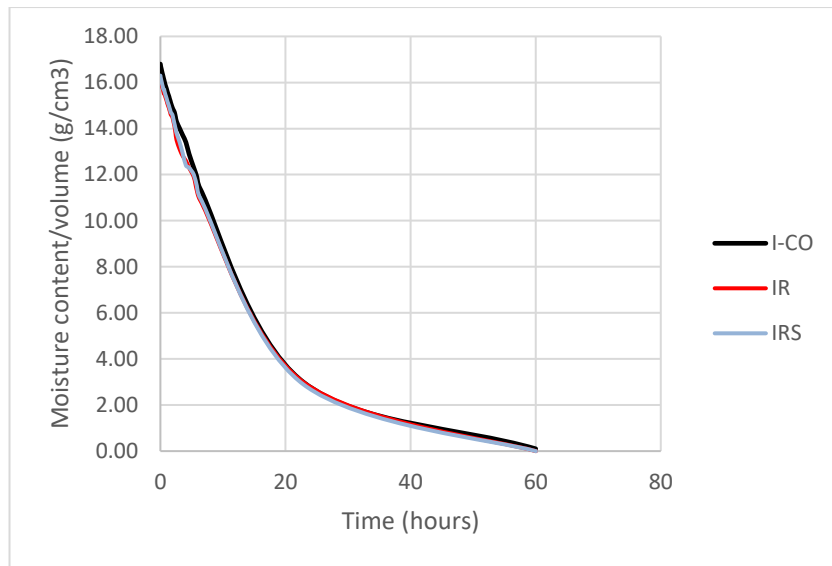
**Figure 95.** Drying curves for the three Indiana limestone samples showing practically identical behaviour.

The spectrophotometric analyses were carried out to measure changes in L* (white-black parameter) and $\Delta E^*$ (total colour variations) following treatment. Results (Table 32) show that all of the treatments caused minor whitening of the stone surface with both $\Delta E^*$ and $\Delta L^*$ values above 5, apart from IR sample which has obtained $\Delta E^*$ and $\Delta L^*$ values >5. The whitening effect was slightly lower than that in the previous research programs.

**Table 32.** Chromatic alterations for treated samples

|  | $\Delta L^*$ | $\Delta a^*$ | $\Delta b^*$ | $\Delta E^*$ |
|---|---|---|---|---|
| IR | 6.61 (±1.79) | -0.74 (±0.04) | -0.19 (±0.96) | 6.65 |
| IRS | 4.43 (±0.68) | -0.59 (±0.13) | -0.63 (±0.24) | 4.51 |
| MR | 2.26 (±0.43) | -0.05 (±0.0.19) | -1.37 (±3.46) | 2.64 |
| MRS | 2.95 (±3.31) | -0.46 (±0.20) | 1.81(±0.42) | 3.49 |
| M55 | 1.18 (±1.93) | -0.10 (±0.34) | 1.32 (±0.66) | 1.77 |
| M75 | 2.34 (±0.75) | -0.55 (±0.12) | 0.04 (±2.19) | 2.4 |

Mean Values determined on 30 measurements

### 4.5.2 Conclusions

This work has shown that nanolime can be used effectively for the consolidation of marble stones weathered due to the formation of gypsum. Thus, a solution of IP25 of L'Aquila nanolime is considered suitable for an in-situ application on the weathered marble stone used for the National Portrait Gallery and the Smithsonian American

Art Museum (USA). In the case of the Indiana Limestone, which was not weathered, only a slight superficial consolidation was observed.

In this research it has been shown that:

- The treatments reduced the porosity of both stones. In both stones the treatments that involved exposure to high relative humidity and spraying (IRS, MRS and M75) yielded a higher porosity decrease.

- Both treatments successfully recover the surface cohesion of the stones measured by Scotch Tape Test (STT). The treated samples which were sprayed with carbonated water (IRS and MRS) obtained a higher increase in the surface cohesion compared to samples kept in the same room conditions but without the addition of water by spraying. Marble samples kept at 75%RH obtained higher consolidating results than those kept at 55%RH which confirms that higher moisture conditions enhance the consolidation effectiveness.

- Drilling resistance results are in line with the STT results showed above. Samples which were sprayed with carbonated water (IRS and MRS) obtained a higher increase in the drilling resistance in both types of stone than samples kept in the same environment without the input of moisture. IRS obtained an increase only in the outer 2 mm of the sample, whereas the consolidation in MRS stones occurred throughout the sample but especially in the outer 8 mm, where the weathered layer was consolidated.

- Samples kept at 75%RH (M75) obtained the highest increase in drilling resistance of the external weathered layer. This suggests that a high relative humidity environment seems to increase the nanolime effectiveness by providing a constant supply of moisture which enhances the carbonation of nanolime particles more effectively than an intermittent input of moisture such as that provided with spraying.

– Samples stored at room conditions (50% RH) and samples kept at 55%RH obtained the lowest drilling resistance due to a poorer carbonation state. This is associated with the reactivity of the nanoparticles. Recent research showed that the carbonation of nanoparticles synthetised by anion exchange resins, which are dispersed at high concentration (i.e. 25g/L) in pure alcohol solvents, can take more than a month to carbonate in low RH environments [Taglieri et al, 2017a].

– No treatment caused any important change on the aesthetic properties. This could be attributed to the lower amount of nanolime particles applied into the samples (introduced approximately 150mg of $Ca(OH)_2$ nanoparticles), compared to treatments on research programme 1 and 2, where treatments consisted on 500 mg of $Ca(OH)_2$ particles.

## 4.6. The use of additives to improve nanolime effectiveness

*4.6.1 Additives and their influence on carbonation*

A description of the research programme, including a list of the used additives, can be found in section 3.3.6.

The reactivity of the $Ca(OH)_2$ nanoparticles dispersed in several solutions (isopropanol (A), deionised water (B), urea (C), sticky rice (D), and carbonated water (F)) has been investigated by X-Ray Diffraction (Fig. 96), and it is fully described in the attached in the Appendix 1. After 14 days of carbonation, samples A, D and F were composed entirely of calcite. In contrast, sample B (nanolime in deionised water) showed a small presence of vaterite and sample C (3%w/v of urea) showed a small amount of unreacted urea indicating that not all the urea decomposed during the carbonation process. No portlandite was found in any of the samples suggesting that all the nanolime solutions were fully carbonated after 14 days.



a)

b)

c)

d)
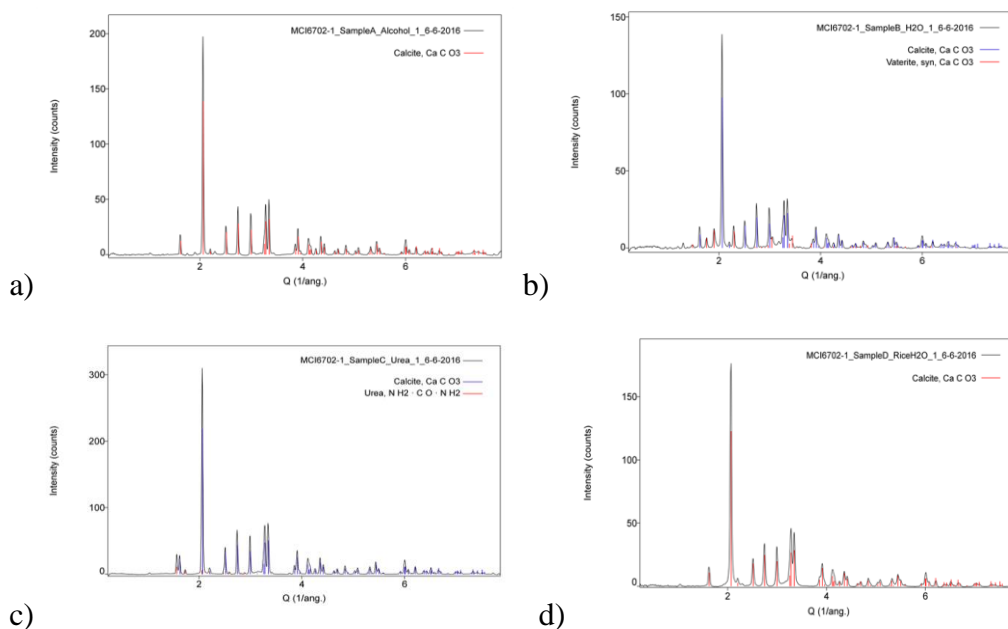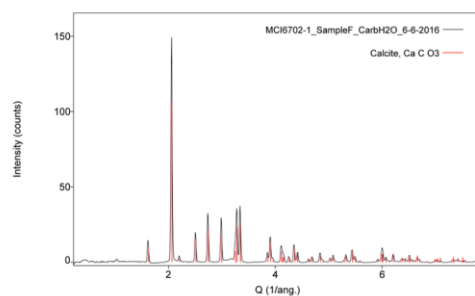
e)

**Figure 96**. XRD of experimental carbonation study: a) A (isopropanol); b) B (DI water); c) C (urea); d) D (sticky rice); e) F (carbonated water).

ATR-FTIR analysis was carried out to determine the presence of sticky rice in sample D, as sticky rice does not present crystalline structure that could be observed in XRD. ATR-FTIR analysis (Fig. 97) shows spectral features that may be attributed to the presence of sticky rice starch (2922, 1149, 1078, 1021, and 932 cm$^{-1}$), thus confirming its presence in the sample. In addition, some calcium carbonate (2507, 1792, 1405, 871, and 711 cm$^{-1}$) was also present. Additional peaks at 3567, 1584, and 859 cm$^{-1}$ could not be identified and may be attributed to other reaction products.
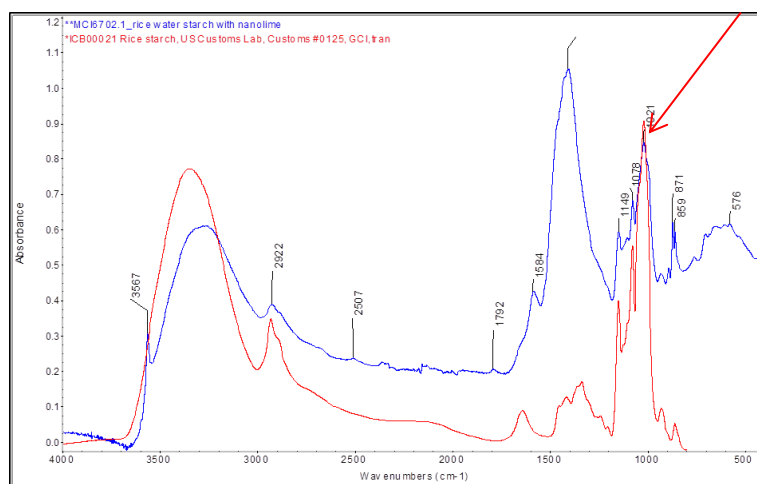


**Figure 97**. FTIR of sample D (sticky rice) after carbonation

All samples were also observed under optical microscope after carbonation. Samples dispersed in alcohol (A) and water (B-F) developed a very smooth surface on top (Fig. 98a and 99a). Sample F (nanolime in carbonated water) shows small cavities on the surface likely formed by carbon dioxide (Fig. 98b). Sample D (sticky rice) developed a yellowish tinge that can be attributed to the rice starch and showed a cracking pattern with flakes tending to curl up at the edges (Fig 98c and 98d).

172
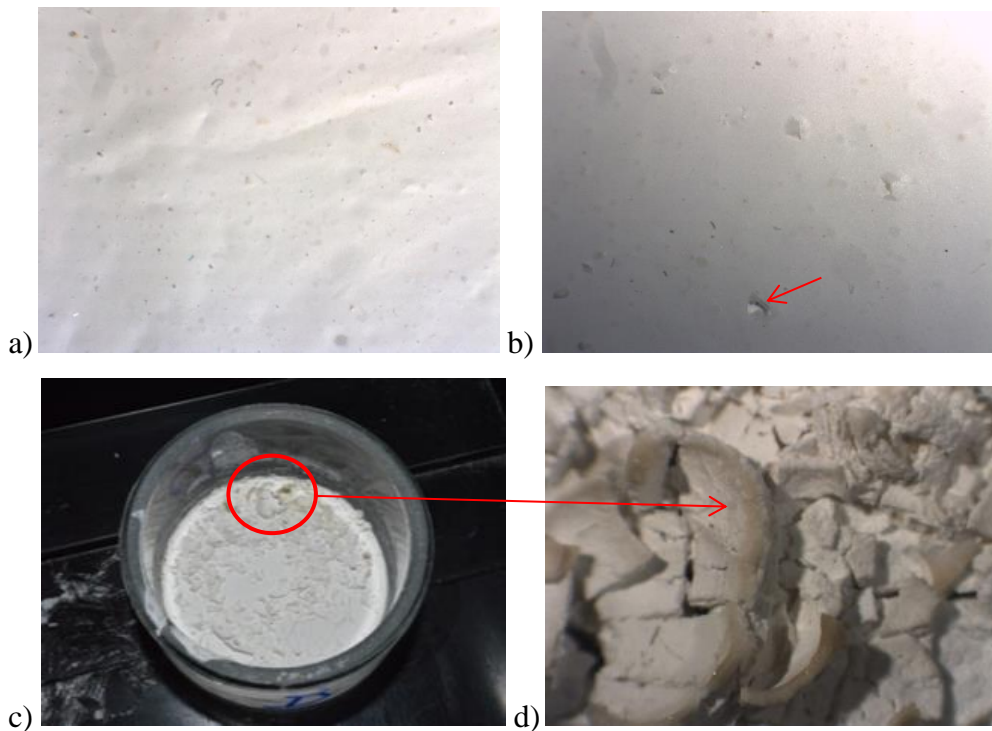
**Figure 98**. Optical microscope images. a) sample B (nanolime in water); b) sample F (nanolime in carbonated water); c) sample D (nanolime in sticky rice) and d) detail of sample D.

All samples were also observed in SEM. The images obtained showed that calcite is the main component for all samples (Fig 99a). In contrast, sample D (nanolime in sticky rice) presents different morphology (Fig 99b) where calcite crystals seem to be embedded in an organic film, which is attributed to the sticky-rice film creating an inorganic-organic composite. This is in the line with the literature that concluded this inorganic-organic composite may significantly increase the resistance to wetting-drying and water-repellence [Yang et al, 2009, Wei et al, 2012].
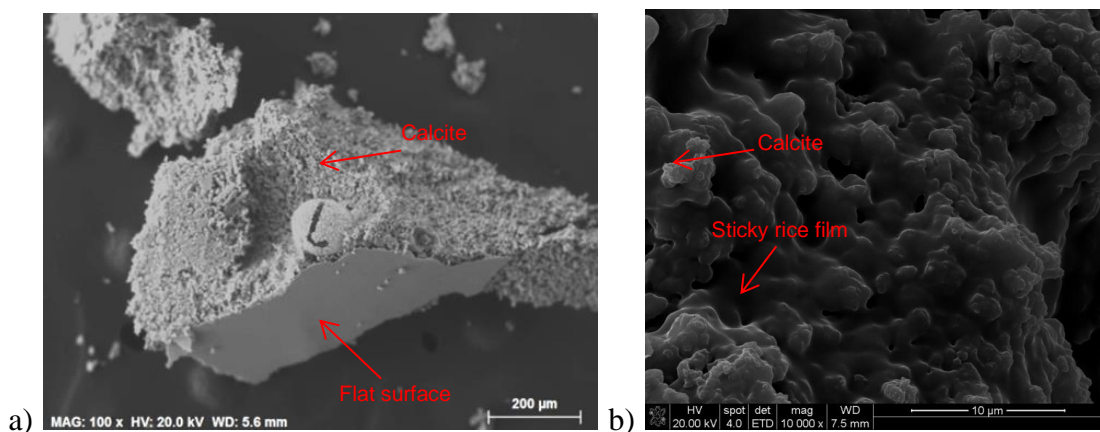


**Figure 99.** a) sample B (nanolime in water), it can be seen calcite crystals with a flat surface and a spheric dowex resin attach to it; b) calcites it can be seen calcite crystals are embedded in the sticky-rice starch film.

*4.6.2 Sticky rice*

It has been recently discovered that the addition of sticky rice soup (water from cooking sticky rice) was traditionally used as an additive in ancient Chinese architecture for the manufacturing of lime mortars to improve their strength, durability and resistance to water [Yang et al, 2009]. According to the literature, the addition of sticky-rice produces a special inorganic-organic composite building material where the inorganic component is calcium carbonate, and the organic component is amylopectin, one of the components of starch from the sticky rice soup. The effect of small amounts of amylopectin plays a crucial role in the carbonation process increasing the specific area of the $Ca(OH)_2$ particles, inhibiting the growth of the $CaCO_3$ crystals that help to create dense and compact microstructure of mortars that reduces the penetration of water and increases their durability [Yang et al. 2009, Wei et al, 2012, Yang et al. 2016a and Yang et al 2016b].

According to the promising results above (in section 4.6.1), the aim of this research is to study the influence of sticky rice solution on the strength and hydrophobicity in nanolime treatments.

4.6.2.1 Characterisation of the sticky rice solution

Sticky rice starch is a mixture of two types of polysaccharides: amylose and amylopectin. Natural sticky rice starches consist of about 10%–30% of amylose and 70%–90% of amylopectin [Gadhave et al, 2017]. Amylose is a linear polysaccharide composed entirely of D-glucose units joined by the α-1,4-glycosidic linkages while Amylopectin is a branched-chain polysaccharide composed of glucose units linked primarily by α-1,4-glycosidic bonds but with occasional α-1,6-glycosidic bonds [Gadhave et al, 2017; Alcazar-Alay and Almeida-Meireles, 2015].

The dried gelatinized sticky rice solution was first examined by SEM immediately after the water evaporation. The morphological properties of the dried gelatinized sticky rice show the rice starch presents uneven structure formed by a film with several hollows (Fig. 100a). The starch granules are tightly packed and clustered into

compound grains and these are surrounded by protein bodies (Fig. 100b). This micro-structure of sticky rice starch is similar to that described by other researchers [Wu et al, 2016; Rewthong et al, 2011].
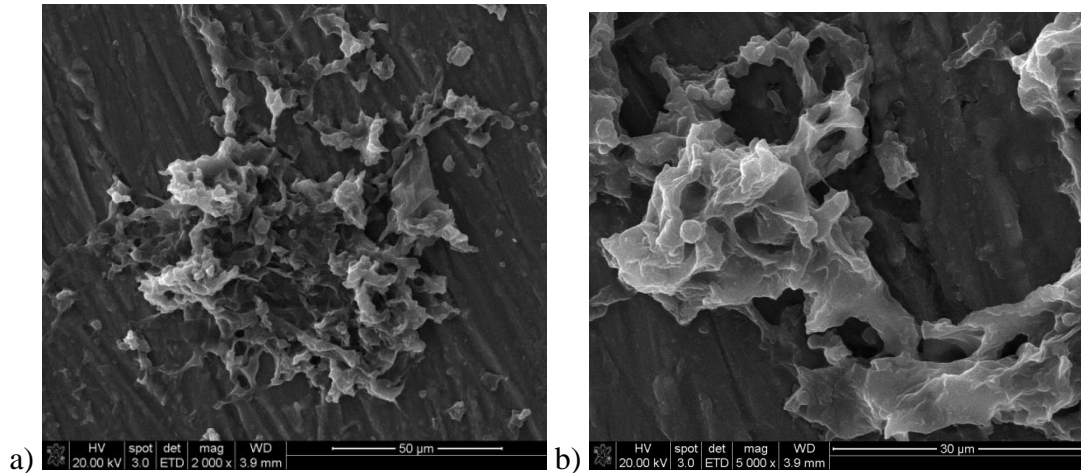


**Figure 100**. SEM images of the sticky rice. a) 2000x; b) 5000x

The FTIR result for the dried gelatinized sticky rice is shown in Figure 101. All absorbance bands registered by the ATR-FTIR can be attributed to rice starch [IRUG-ICB00021]. The absorbance band at 847 and 761 cm$^{-1}$ is attributed to the C-O group from the glucose anhydride ring, and the absorption bands at 3271 and 1654 cm$^{-1}$ can be attributed to the absorbance of the -OH groups in the starch [Yang et al, 2009; Pavlovic et al, 2003]. This rice starch spectrum is attributed to amylopectin patterns, as described by Pavlovic et al [Pavlovic et al, 2003].
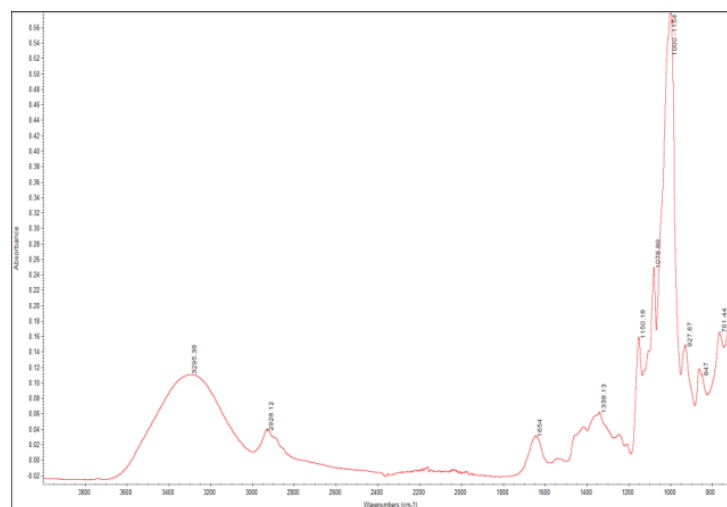


**Figure 101**. FTIR Analysis of the sticky rice powder

To further analyse the composition of the starch, a starch-iodine test was carried out. The red-brown colour was very evident after the addition of the iodine-KI reagent to the sticky rice solution [Rudl et al, 1944] which clearly indicates that the sticky rice starch is composed mainly of amylopectin (Fig. 102).



**Figure 102**. A red-brown color can be seen after the Iodine-KI reagent test due to the presence of amylopectin.

The rheological behaviour of sticky rice solutions was carried out to determine their viscosity. Rheological analysis shows that the sticky rice solution presents a constant complex viscosity between 0.002 and 0.001 mPas, presenting a similar behaviour to water (Fig. 103), and significantly lower viscosity than that other consolidation products used in Cultural Heritage such as PEG (poly(ethylene glycol)) or TEOS (Tetraethyl orthosilicate) [Walsh, et al, 2015].
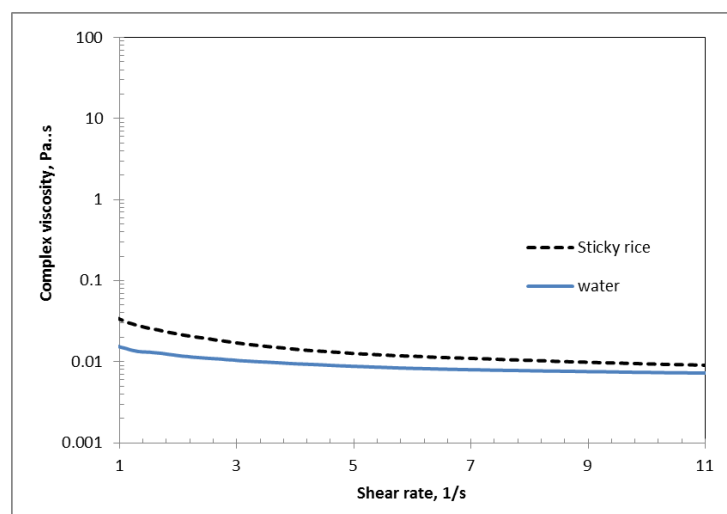


**Figure 103**. Rheological behaviour of the sticky rice solution compared to water.

To further investigate the penetration capability of the sticky rice solution into a pore structure, the surface tension of the sticky rice solution was measured using the pendant surface angle. The contact angle of sticky rice was 69.28 (±0.81) mN/m very similar to that of water (69.99 (±0.5) mN/m) (Fig. 104).



a)                                                  b)
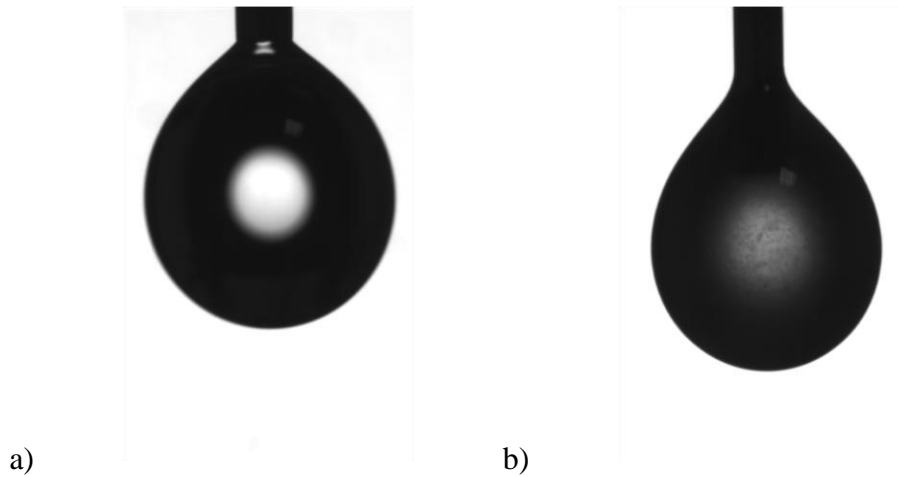
**Figure 104**. Analysis of the pendant surface angle of: a) water; b) sticky rice solution

The contact angle of the interaction between the sticky rice solution and the substrate surface (lime mortar, described in section 3.1.2) was calculated by placing one drop of the solution on the substrate and measuring the contact angle after 1 second. The static contact angle after 1 second is < 20° (Fig. 105). This indicates the sticky rice solution penetrates very easily a high porous structure like the lime mortar described in section 3.1.2.



**Figure 105**. Analysis of the contact angle of sticky rice and substrate

4.6.2.2 Consolidation effectiveness

The characterisation of lime-mortars is described in section 3.1.2, the preparation of sticky rice in section 3.2.3, the application treatment in section 3.2.4.2 and the research programme is described in section 3.3.6.

The porosity of treated and control samples was calculated by 24 hours immersion and MIP, which are summarised in Table 33. Results show that all treatments tend to reduce the porosity of the mortar. The highest decrease in apparent porosity and porosity by Hg intrusion seems to be for the samples treated with sticky rice and nanolime, SR-LAQ (~22.9% decrease), followed by those treated with nanolime only, LAQ, and sticky rice only, SR (13.14% and 12.8%, respectively).

**Table 33.** Calculated Apparent porosity (% g/g) and Open porosity ($cm^3/cm^3$), Porosity by Hg intrusion (%)

|  | CO | LAQ | SR | SR-LAQ |
|---|---|---|---|---|
| Apparent Porosity % w/w | 12.22 (±0.84) | 12.16 (±1.09) | 12.05 (±0.28) | 11.73 (±0.19) |
| Open Porosity % v/v | 17.26 (±0.56) | 17.01 (±1.71) | 16.82 (±0.63) | 16.88 (±0.14) |
| Porosity by Hg intrusion (%) | 18.8 | 16.33 | 16.44 | 14.46 |

The pore size distributions of treated and control samples are summarised in Figure 106. The MIP curves clearly shows that the reduction in porosity of all treatments can be attributed to a reduction in the population of pores with diameters between 2 and 11 µm. The nanolime only (LAQ) and sticky rice-nanolime (SR-LAQ) treatments also reduced the population of pores with diameters between 0.01 µm and 0.3 µm, the latter treatment yielding a slightly more marked decrease. LAQ treatment also slightly reduced the population of pores with diameters between 0.5 and 1 µm.
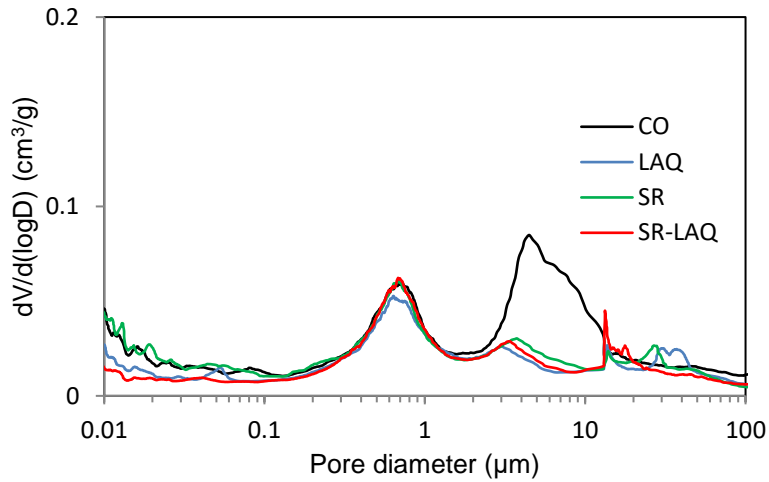
**Figure 106.** Differential volume of intruded mercury versus pore diameter of samples treated with LAQ, SR and SR-LAQ

The water contact angle of treated samples was carried out to investigate any hydrophobic properties induced to the mortar by the sticky rice and the sticky rice - nanolime treatments. The static contact angle ($\theta$) on samples treated with LAQ is 0. Fig. 107 shows the static contact angle ($\theta$) on the surfaces treated with SR and SR-LAQ. In both cases the application of sticky rice increases the hydrophobicity of the treated surface. The static contact angle on SR samples is 106º ($\pm$4.6), which confirms the surface of those samples has certain degree of hydrophobicity after treatment. The static contact angle on SR-LAQ is 66° ($\pm$5.41), which suggests that the hydrophobicity of the treated surface decreases when the application of sticky rice is followed by the application of nanolime.
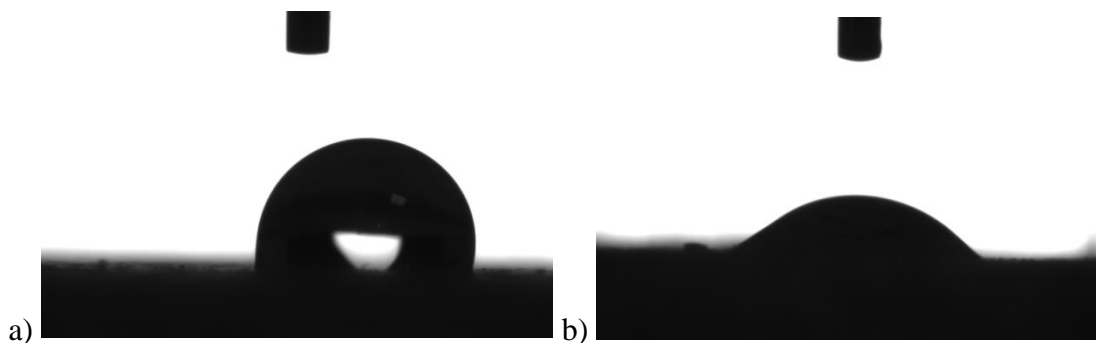


**Figure 107.** Static contact angle images after 1 second. a) SR (106º$\pm$4.6); b) SR-LAQ (66º$\pm$5.4).

A droplet of water remains for more than 3 minutes on the surface with a contact angle >80° in SR samples (Fig. 108). In contrast, the droplet of water is completely absorbed after 8 seconds in samples treated by SR-LAQ. The samples treated with LAQ and control present no static contact angle as water is absorbed before 1 second after placing the water drop over the substrates surface.
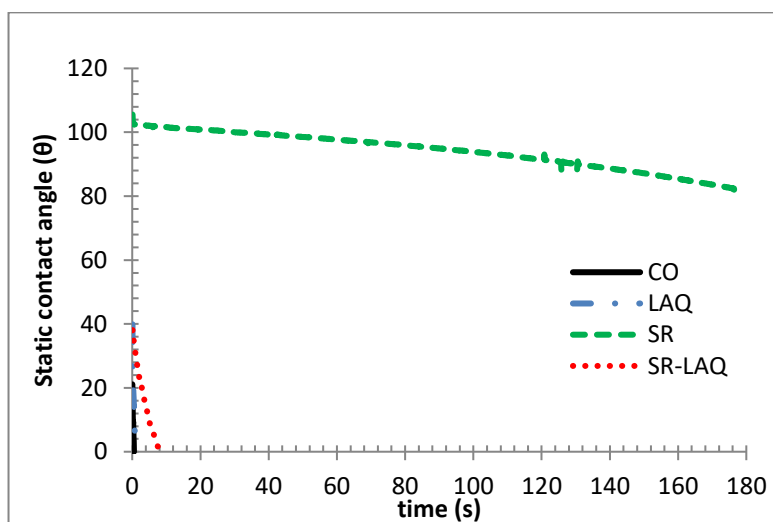


**Figure 108**. Contact angle on samples treated with LAQ (blue), sticky rice (green) and sticky rice and LAQ (red).

The water absorption by capillarity of treated samples is shown in Figure 109. All treated samples show a reduced water absorption by capillarity coefficient (Table 34). The highest decrease has been observed for the samples treated with sticky rice only (SR), followed by those treated with sticky rice and nanolime (SR-LAQ) and those treated with nanolime only (LAQ). Table 34 also showed that all treated samples tend to absorb less amount of water when saturated.

**Table 34.** water absorption and drying characteristics

| Parameter | CO | LAQ | SR | SR-LAQ |
|---|---|---|---|---|
| W.  absorption coefficient (10$^{-3}$g/cm$^2$ s$^{0.5}$) | 19.1 ($\pm$ 0.6) | 15.1 ($\pm$ 0.8) | 7.0 ($\pm$ 2.5) | 10.1 ($\pm$ 2.0) |
| W. absorbed at asymptotic value (g) | 10.32 ($\pm$0.70) | 10.17 ($\pm$0.92) | 9.59 ($\pm$0.80) | 10.05 ($\pm$0.10) |
| Initial drying rate (10$^{-3}$g/ cm$^3$ h) | 9.7 ($\pm$ 0.2) | 9.5 ($\pm$ 0.3) | 7.7 ($\pm$ 0.3) | 7.5 ($\pm$ 0.3) |
| Final drying rate (10$^{-3}$g/ cm$^3$ h) | 2.7 ($\pm$ 0.3) | 3.4 ($\pm$ 0.2) | 3.1 ($\pm$ 0.4) | 3.3 ($\pm$ 0.4) |
| Time for total drying (h) | $\pm$50 | $\pm$50 | $\pm$50 | $\pm$50 |

Values in parentheses are standard deviation of the three cubic samples. W (water)

Control and LAQ samples reached asymptotical absorption values after 20 minutes of contact with water, while samples treated with sticky rice only (SR) and sticky rice and nanolime (SR-LAQ) needed approximately 2 hours (Fig 109).
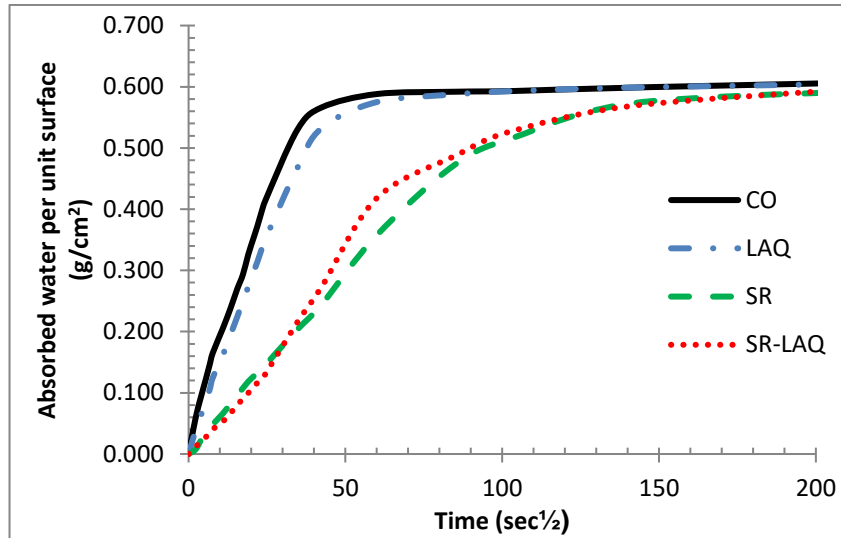


**Figure 109**. WAC curves of treated and control samples of sticky rice samples

The drying curves are shown in Fig.110. All treated samples present slightly different initial drying rate (from 0 to 30 hours) and similar final drying kinetics (from 30 to 50 hours). LAQ presents slightly slower initial drying rate followed by SR and SR-LAQ (Table 34). All treated samples were completely dry after 50 hours, which is similar to control samples.
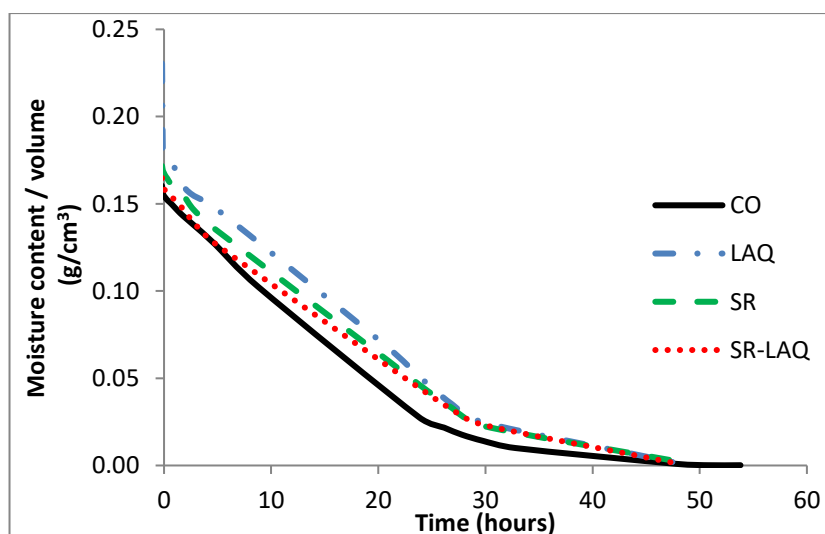


**Figure 110**. Drying curves curves of treated and control samples of sticky rice samples

The results of the Scotch Tape Test (STT) are shown in Table 35. All treatments yielded decreasing values of removed material ($\Delta W \approx 66 - 96\%$). These results confirm that all surfaces are more compact after treatments. The samples treated with sticky rice only and with sticky rice and nanolime showed a higher increase in surface cohesion ($\Delta W \approx 96\%$ and $\Delta W \approx 93\%$, respectively) than those treated by nanolime only ($\Delta W \approx 74\%$).

**Table 35.** Scotch Tape Test (STT): experimental results

|  | Released material (mg/cm²) | ΔW (%) | SD |
|---|---|---|---|
| CO | 84.59 | - | 12.01 |
| LAQ | 21.9 | 74.12 | 6.09 |
| SR | 3.04 | 96.41 | 3.5 |
| SR-LAQ | 5.77 | 93.18 | 5.6 |

Scotch area: 3 x 1.5 cm; SD (standard deviation of released material)

Drilling resistance results for treated and untreated samples are shown in Figure 111. The samples treated with nanolime only (LAQ) show a slightly increased drilling resistance (F ~ 0.13 (±0.19) N, ΔF ~ 62 %) within about 6 mm from the surface, which is in line with the results previously obtained for this nanolime (research programme 1 and 2) for the same substrates. Drilling resistance of the samples treated with sticky rice only (SR) and with sticky rice and nanolime (SR-LAQ) is higher than that of the control and of the sample treated with nanolime only, and it has a fairly constant value throughout the drilling depth (Fig. 111). This seems to indicate that sticky rice provides a deeper consolidation of the mortar independent of the use of nanolime in combination with it. These results cannot confirm whether the increase of the in-depth strength in the SR-LAQ treatment is due to the effect of sticky rice on its own, or that the sticky rice has improved the penetration of nanolime. Further research is required to elucidate this hypothesis.
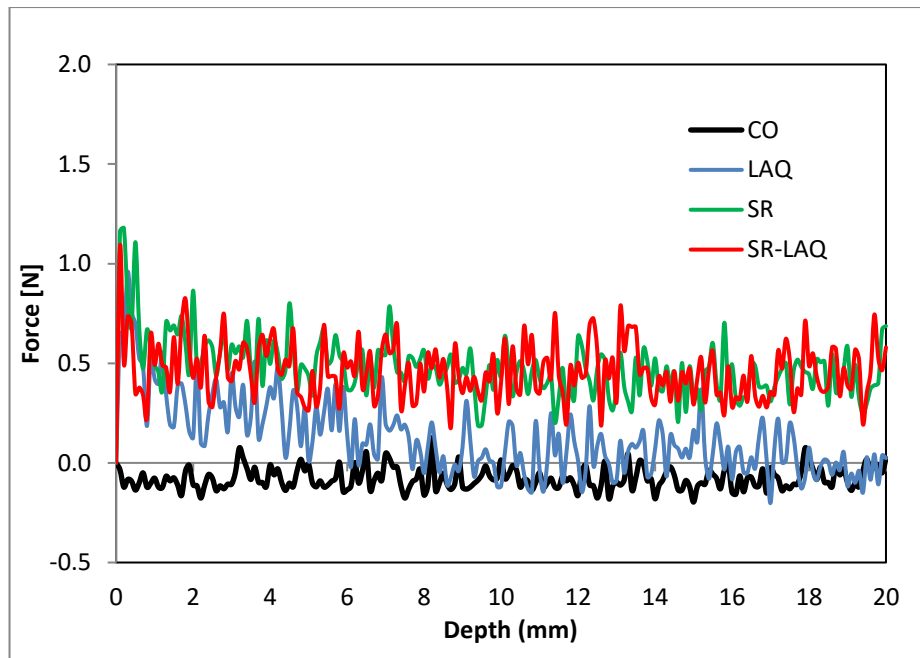
**Figure 111**. DRMS of treated and untreated samples

A cross-section of each treated samples was examined by SEM (Fig. 112). Samples were taken at a depth of approximately 5 mm from the treated surface. SEM images show morphological differences between the sample treated with sticky rice only and that treated with sticky rice and nanolime. SR samples show that the sticky rice is distributed homogeneously over the mortar as a film on top of the grains (Fig. 112a and Fig. 112b). In contrast, SR-LAQ samples show that the calcite crystals of LAQ embed into this film as they crystallise upon carbonation (Fig 112c, 112d). The morphology and size of those calcite crystals are very similar to the ones observed in the research programme 1 (section 4.1.2, Fig. 60f) without the influence of the sticky rice. Thus, this result suggests that the calcite crystals that grew into the sticky rice film have not reduced in size as in the case of the ancient Chinese lime-mortars with sticky rice [Yang et al, 2009].
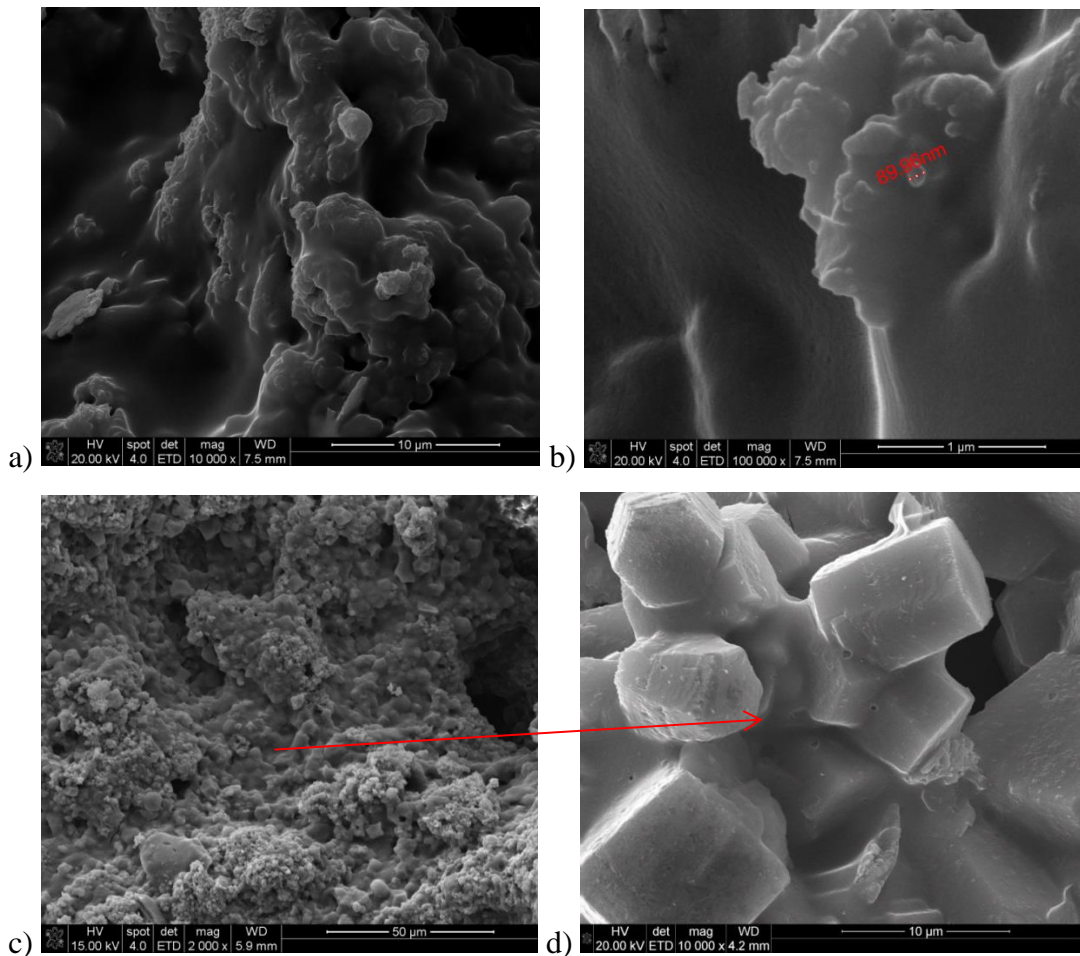
**Figure 112**. SEM images of a) SR at 10000X; b) SR at 100,000X; c) SR-LAQ at 2,000X; d) SR-LAQ at 10,000X.

Spectrophotometric analyses were carried out to measure changes in colour following treatments. Results (Table 36) show that the treatments involving nanolime (LAQ and SR-LAQ) caused a minor whitening effect on the surface, with both $\Delta E^*$ and $\Delta L^*$ values above 5. The increase in whitening is attributed to the accumulation of nanolime particles on the surface, as described in previous programmes (1, 2, and 3). SR samples (treated with sticky rice only) do not show any aesthetic alterations.

**Table 36.** Chromatic alterations for treated samples

|  | $\Delta L^*$ | $\Delta a^*$ | $\Delta b^*$ | $\Delta E^*$ |
|---|---|---|---|---|
| LAQ | 11.94 ($\pm$0.97) | -1.25 ($\pm$0.26) | -6.96 ($\pm$1.04) | 13.87 |
| SR | 2.19 ($\pm$2.35) | -0.56 ($\pm$0.24) | -1.20 ($\pm$0.74) | 2.55 |
| SR-LAQ | 7.99 ($\pm$1.72) | -0.59 ($\pm$0.48) | -1.91 ($\pm$0.83) | 8.23 |

Mean values determined 30 measurements

4.6.2.3 Durability of the consolidation treatments

The durability of the sticky rice treatments (SR and SR-LAQ) was studied by exposing the samples to the accelerated weathering tester (AWT) under two weathering programmes (with different temperature range), and by exposing the samples to wetting and drying cycles at room conditions. After those weathering tests, the strength and hydrophobic properties were subsequently tested.

The two weathering programmes of AWT are described in section 3.2.5.3.8 and the resistance to wetting and drying cycles is described in section 3.2.5.3.10. The results are summarised below.

4.6.2.3.1 *Influence of the exposure to weathering condition AWT 1 (8 hours UV at 1.55 W/m2 irradiance and 60 ºC; Step 2: 4 hours moisture condensation at 50 ºC with no UV irradiation (ASTM G154 CYCLE 6). Duration 340 hours)*

A Scotch Tape Test was carried out on the samples before and after exposing them to the accelerated weathering. The results are shown in Table 37. It can be seen that the surface cohesion obtained during the consolidation treatment, decreased for SR and SR-LAQ samples. The decrease is more pronounced in the samples treated with only sticky rice, i.e. SR, therefore, it seems that this treatment has reduced more their surface cohesion than SR-LAQ samples after the AWT.

**Table 37.** Results of the Scotch Tape Test (STT) after AWT (Programme 1)

| | Released material (mg/cm$^2$) | | ΔW (%) | | SD | |
|---|---|---|---|---|---|---|
| | **Before AWT** | **After AWT** | **Before AWT** | **After AWT** | **Before AWT** | **After AWT** |
| CO | 84.59 | 83.12 | - | - | 12.01 | 15.70 |
| SR | 3.04 | 18.64 | 96.41 | 77.6 | 3.50 | 3.21 |
| SR-LAQ | 5.77 | 12.88 | 93.18 | 84.51 | 5.60 | 1.08 |

Scotch area: 3 x 1.5 cm; SD (standard deviation of released material)

The water contact angle measured on the samples after AWT shows that the hydrophobicity of the samples treated with SR and SR-LAQ is significantly reduced. Following the accelerated weathering, the contact angle is 0º on the sample treated

with SR-LAQ, and 20.6º (±3.14) on the sample treated with SR (Fig. 113). These results clearly suggest that the sticky rice, which was the responsible for the hydrophobicity effect, is removed from the surface during the AWT process.
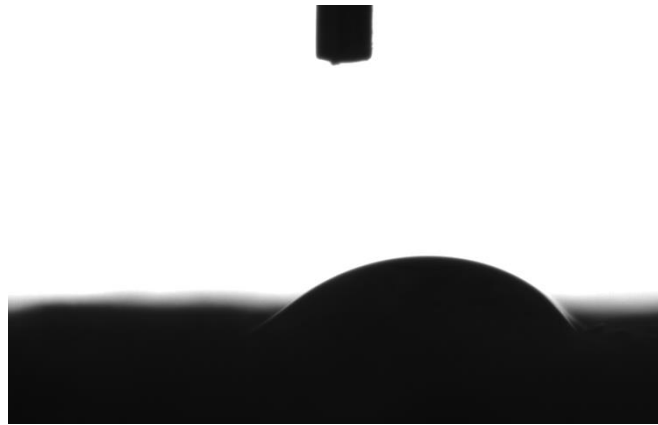


**Figure 113**. Water contact angle on a sample treated with SR (20.6º±3.14) after AWT (Programme 1)

Drilling resistance results for samples treated with sticky rice (SR) and sticky rice and nanolime (SR-LAQ) after AWT are shown in Figure 114. It can be seen that the drilling resistance of both samples has significantly decreased after the AWT, which is in line with the scotch tape test and the contact angle results described above. The drilling resistance of SR samples significantly decreased to values near those of the control sample. In contrast, the drilling resistance of SR-LAQ remained similar to that recorded before the AWT within about 2 mm from the surface and decreased to values slightly above those of the control throughout the remaining drilling depth. The higher consolidation effect on the SR-LAQ samples compared to SR samples could be attributed to the effect of nanolime on this sample.

Results of STT, contact angle and DRMS clearly show that the consolidating effect of the sticky rice is lost during the AWT. This can be attributed to the exposure to the alternating cycles of UV light and moisture condensation at elevated temperatures (T=60 to 50ºC) in the tester, which may have degraded the sticky rice starch. Starch in presence of water and heat undergoes a starch gelatinization process, which is an irreversible process where the water dissolves starch granules by breaking down the intermolecular bonds of starch molecules [Chandroth and Tholath,

2008]. This gelatinization process especially occurs at temperatures above 55ºC [Hans-Dieter, et al, 2004]. Thus, in the case of both samples (SR and SR-LAQ), the sticky rice is probably solubilized and partially washed out of the sample during the AWT programme.
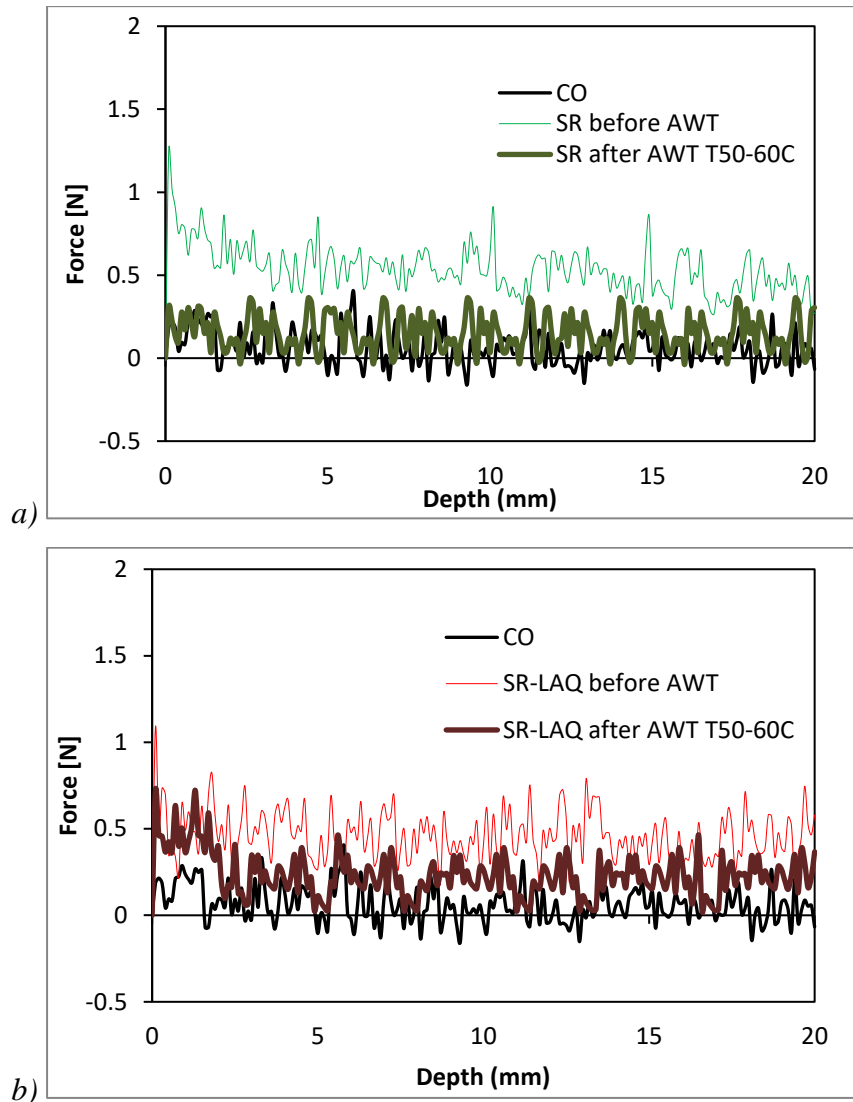


**Figure 114**. DRMS of samples before and after AWT (T=50-60ºC) of: a) sticky rice (SR); and b) sticky rice and LAQ (SR-LAQ).

Spectrophotometric analyses were carried out on samples before and after the AWT to investigate the development of any yellowish tinge on the treated surfaces (observed in previous results, section 4.6.1). Results (Table 38) indicate that following the accelerated weathering the treated surfaces show a decrease of the lightness ($\Delta L^*$) and an increase of the red ($\Delta a^*$, positive number indicates red) and yellow ($\Delta b^*$, positive number indicates yellow) colour. The total colour difference

values for both, i.e., SR and SR-LAQ, samples are ΔE* ~ 5, which is considered a low aesthetic change [Rodriguez-Navarro et al, 2013].

**Table 38.** Chromatic alterations for treated samples

| | ΔL* | | Δa* | | Δb* | | ΔE* | |
|---|---|---|---|---|---|---|---|---|
| | Before AWT | After AWT | Before AWT | After AWT | Before AWT | After AWT | Before AWT | After AWT |
| SR | 2.19 (±2.35) | -4.27 (±0.16) | -0.56 (±0.24) | 0.93 (±0.38) | -1.2 (±0.74) | 2.55 (±0.17) | 2.55 | 5.06 |
| SR-LAQ | 7.99 (±1.72) | 2.28 (±0.15) | -0.59 (±0.48) | 1.13 (±0.43) | -1.91 (±0.83) | 2.63 (±0.29) | 8.23 | 4.15 |

Values determined on 30 measurements

4.6.2.3.2 *Influence of the exposure to weathering condition AWT 2 (8 hours UV at 1.55 W/m2 irradiance and 40 ºC; Step 2: 4 hours moisture condensation at 30 ºC with no UV irradiation. Duration: 340 hours.)*

The durability of the sticky rice treatment was also evaluated by exposing the samples to the accelerated weathering tester (AWT) under a programme with lower temperature (T ~ 40 to 30 ºC instead of T ~ 60 to 50 ºC) to assess the influence of temperature on the degradation of sticky rice.

The superficial cohesion of treated and control samples was measured by means of STT before and after exposing the samples to an accelerated weathering programme 2. The results are summarised in Table 39 and it can be seen that both surfaces (SR and SR-LAQ) have a lower cohesion following the weathering exposure, what suggests that the starch degradation process still occurs at T~ 40 to 30 ºC. Samples treated with SR showed a more pronounced decrease of the superficial cohesion, similarly to what was observed for the samples exposed to the previous accelerated weathering programme at higher temperature (T=60-50ºC). The decrease of the surface cohesion in both samples is lower than in the previous weathering programme 1, what suggests that high temperatures increase the degradation of the sticky rice.

**Table 39.** Results of the Scotch Tape Test (STT) after AWT (Programme 2)

| | Released material (mg/cm$^2$) | | ΔW (%) | | SD | |
|---|---|---|---|---|---|---|
| | Before AWT | After AWT | Before AWT | After AWT | Before AWT | After AWT |
| CO | 84.59 | 83.12 | - | - | 12.01 | 15.70 |
| SR | 3.04 | 11.10 | 96.41 | 86.65 | 3.50 | 1.44 |
| SR-LAQ | 5.77 | 8.74 | 93.18 | 89.49 | 5.60 | 0.88 |

Scotch area: 3 x 1.5 cm; SD (standard deviation of released material)

The water contact angle on treated samples shows that samples have preserved some hydrophobic properties after the accelerated weathering at lower temperatures. The contact angles after AWT on the samples treated with SR and SR-LAQ are 80.16º (±3.18) and 69.26º (±8.83) respectively (Fig. 115). This clearly indicates that the sticky rice is still present on the sample surface. The static contact angle clearly decreased in SR samples from approximately 106º (before AWT) to 80º (after AWT), while for SR-LAQ samples did not change significantly, from approximately 66º (before AWT) to about 69º (after AWT).



a)      b)
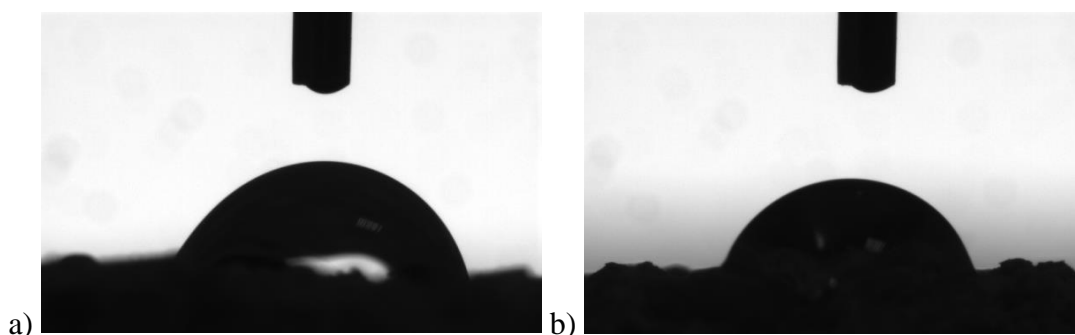
**Figure 115**. Static contact angle of treated samples after AWT (T=40-30°C) of: a) SR (80.2º±8.83); d) SR-LAQ (69.26º±8.83).

Drilling resistance results after AWT of both treated samples are shown in Figure 116. Both drilling resistance profiles show a decrease in the resistance of both samples what clearly shows that the starch degrades even at T~40-30ºC, confirming the results of STT. This decrease in drilling resistance is significantly more pronounced on samples exposed to higher temperature (T=60-50ºC) than at T~40-30ºC, which in the line with STT. Furthermore, the decrease in the drilling resistance is significantly more pronounced in SR samples than in SR-LAQ samples, which is also in the line with the results showed above of contact angle and Scotch tape test.

These results suggest that the degradation of sticky rice is higher when it is applied on its own rather than when it is applied in a combination with nanolime treatment. This could be attributed to the fact that when sticky rice is applied with nanolime, the calcite crystals from nanolime grow up and get embedded in the sticky rice film (as shown in Fig 112d). This might increase the adhesion to the mortar as both calcite and starch film may bond to the grains and matrix physically and chemically due to the calcite-calcite bonding. This may have made the sticky rice slightly more resistant to solubilisation. In contrast, when the sticky rice solution is applied without nanolime, it appears to form a film on top over the substrate grains (as shown in Fig. 112a), which may suggests that this film only adheres to the mortar grains physically. Thus, it is more likely to solubilise as it does not present any chemical bond to the mortar.
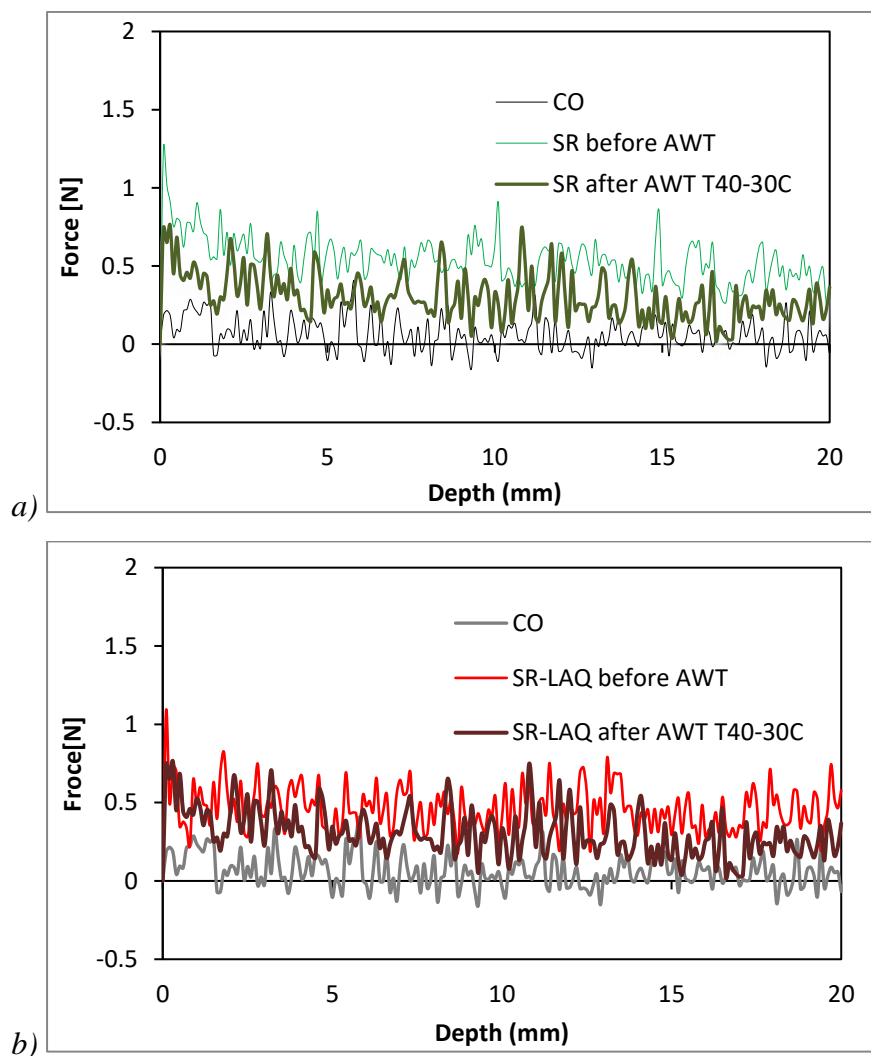


**Figure 116.** DRMS of samples before and after AWT (T=40-30ºC) of: a) sticky rice (SR); and b) sticky rice and LAQ (SR-LAQ).

*4.6.2.3.2 Resistance to wetting-drying cycles*

The durability of the sticky rice samples was also evaluated by exposing the samples to wetting and drying cycles, to study if the starch degradation process occurs at room temperature.

The superficial cohesion was measured by means of STT before and after exposing the samples to the wetting-drying cycles, results are shown in Table 40. It can be seen that all surfaces have a slightly decreased superficial cohesion. Decreasing values are similar to the samples exposed to the AWT at T=40-30ºC, and lower than samples exposed to the AWT at T=50 - 60ºC. SR and SR-LAQ samples yielded similar decreasing values. These results suggest that the degradation of starch is also noticeable at room conditions.

**Table 40.** Results of the Scotch Tape Test (STT) after wetting-drying cycles

| | Released material (mg/cm²) | | ΔW (%) | | SD | |
|---|---|---|---|---|---|---|
| | Before AWT | After AWT | Before AWT | After AWT | Before AWT | After AWT |
| CO | 84.59 | 83.12 | - | - | 12.01 | 15.70 |
| SR | 3.04 | 9.92 | 96.41 | 88.07 | 3.50 | 0.98 |
| SR-LAQ | 5.77 | 10.02 | 93.18 | 87.73 | 5.60 | 1.45 |

Scotch area: 3 x 1.5 cm; SD (standard deviation of released material)

The water contact angle measurements indicate that the hydrophobic properties of SR and SR-LAQ are reduced during the wetting-drying cycles (Fig. 117). The contact angle on samples treated with SR was 71.1º (±6.12) after the wetting and drying, which is lower than before the wetting and drying cycles (~106º). This is similar to the contact angle measured on the same samples exposed to AWT at T=40-30ºC (~80º). These results suggest than both obtained similar reduction on hydrophobic properties. In contrast, SR-LAQ obtained slightly higher decrease in static contact angle (42.8º ±5.15) compared to samples exposed to AWT T=40-30ºC (~69º) and before the AWT (~66º). Thus, these results confirm that the sticky rice was partially washed from the surface of both samples even at room temperature conditions.
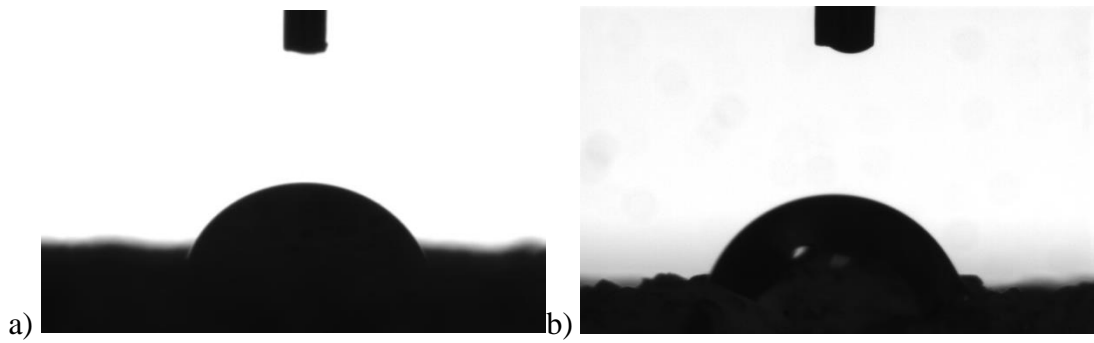
**Figure 117**. Static contact angle after wetting and drying cycles of treated samples of: a) SR (71.1° ±6.12); b) SR-LAQ (42.8°±5.15)

Drilling resistance results after wetting-drying cycles are shown in Figure 118. Both drilling resistance profiles show a decrease in drilling resistance after wetting-drying cycles, what confirms that the sticky rice still degrades at room temperature conditions. Drilling profiles are similar to that observed for samples exposed to the AWT at T=30-40ºC where treated samples with SR samples presents higher decrease in drilling resistance than SR-LAQ.



*a)*

*b)*
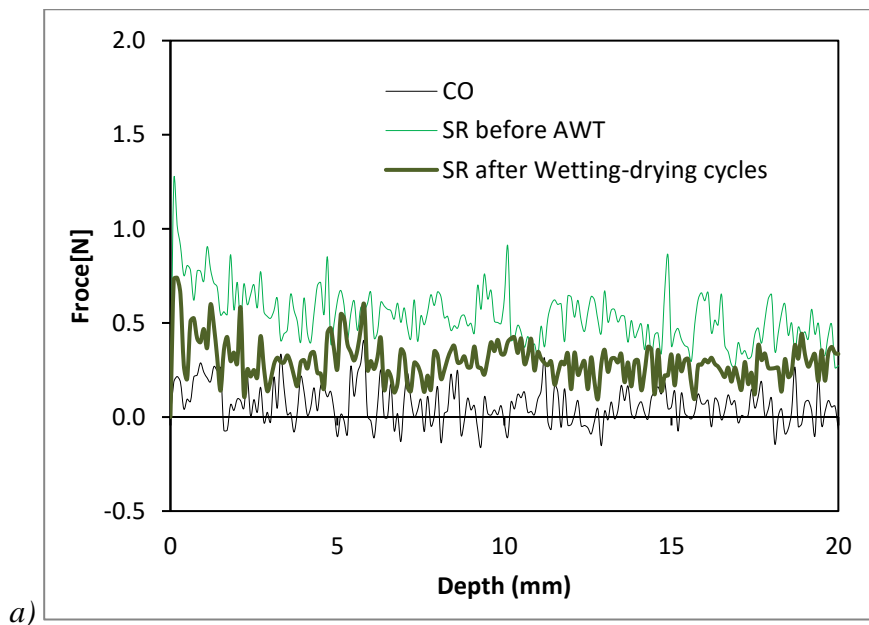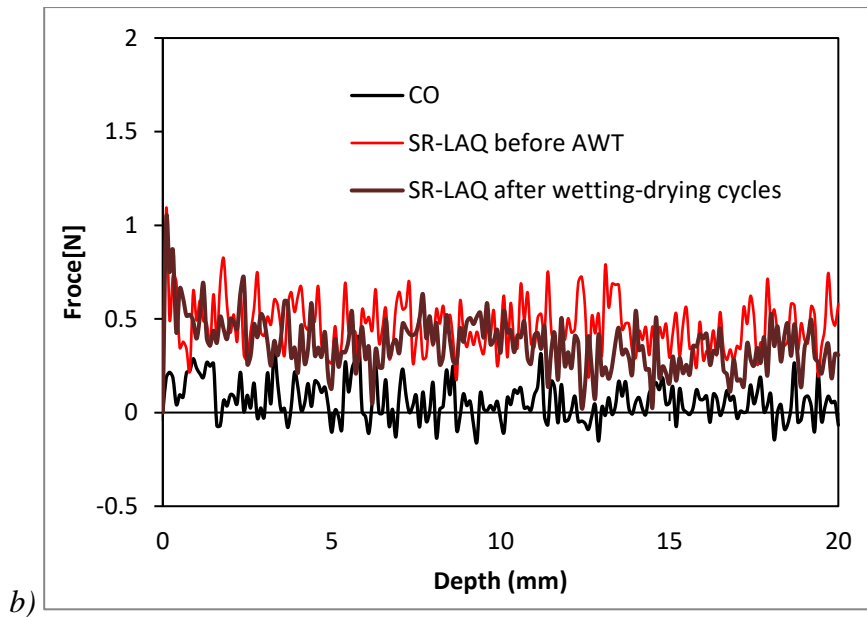
**Figure 118**. DRMS of samples before and after wetting-drying cycles of: a) sticky rice (SR); and b) sticky rice and LAQ (SR-LAQ).

To confirm the solubilisation of the sticky rice, ATR-FTIR analysis was carried out of the water used for the wetting-drying cycles. This analysis clearly shows that the water contains some small presence of the sticky rice. Thus, this confirms that some of the starch is dissolved into the water during the wetting cycle. The absorbance band between 1000 - 1500 cm$^{-1}$ is attributed to sticky rice (Fig. 119).
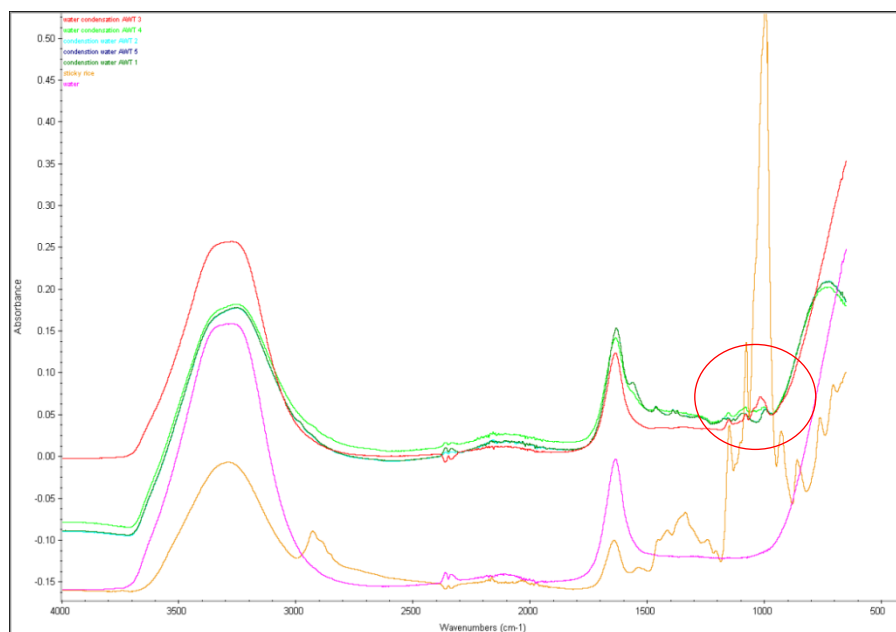


**Figure 119**. FTIR analysis of the water sample taken from the surface of samples treated with sticky rice during the wetting-drying cycles. The curve purple corresponds to water, orange to sticky rice, and the three patterns (red, green and dark green) corresponds to the water taken by the wetting-drying cycles.

193

*6.2.3 Conclusions*

This experimental programme studied the influence of the use of several additives in nanolime treatments. Results show that the use of sticky rice alone or in combination with LAQ nanolime yields a higher degree of consolidation than that produced by LAQ when used alone. However, the consolidation effectiveness of sticky rice decreases considerably when the treated samples are exposed to accelerating weathering processes.

This research has shown that:

- Among the additives added to nanolime, *sticky rice* obtained the most promising results in terms of the microstructure formed by sticky rice and nanolime. SEM images showed that the calcite crystals from nanolime seem to grow and embed in the sticky-rice film creating an inorganic-organic composite. This morphology is similar to ancient Chinese lime mortars that have sticky rice in their composition. Most of the literature about the sticky-rice-lime-mortars concludes that this inorganic-organic composite significantly increases the resistance to wetting-drying and water-repellence [Yang et al, 2009, Wei et al, 2012, Yang et al, 2016a].

- The gelatinous solution of sticky rice presents low viscosity which allows a good penetration into the porous substrate. The dried gelatinized sticky rice starch, which is composed mainly of amylopectin, is an uneven film with several hollows where the starch granules are surrounded by protein bodies forming a paste, similar to that described in the literature in other researches [Wu et al, 2016].

- Treated samples with nanolime (LAQ), sticky rice (SR) and sticky rice and nanolime (SR-LAQ) reduced the porosity after treatment. The highest porosity decrease was observed for the samples treated with sticky rice and nanolime (~22.9% decrease), followed by those treated with sticky rice only (12.8%). MIP results clearly show that the reduction in porosity can be attributed to a reduction in the population of pores with diameters between 2 to 11 µm in all treatments. Both treated samples involving nanolime, i.e LAQ and SR-LAQ, also showed a reduction on the small pores with the diameter

between 0.01 µm and 0.3 µm. This result also confirms the good access of the L'Aquila nanolime to the fine pores (observed in the research programme 3).

–  Both treatments involving sticky rice, i.e., SR and SR-LAQ, endow a certain degree of the hydrophobicity of the surface of treated samples. The hydrophobicity of the treated sample decreases when the sticky rice is applied in combination with nanolime.

–  Both treatments involving sticky rice (SR and SR-LAQ) showed a significant reduction of the water absorption by capillarity coefficient (approximately a 60% reduction) without affecting the drying rate.

–  Both treatments involving sticky rice (SR and SR-LAQ), significantly increase the surface cohesion. The samples treated with only sticky rice showed the highest increase in the superficial cohesion followed by samples treated with sticky rice and nanolime.

–  Both treatments involving sticky rice (SR and SR-LAQ), have clearly increased the drilling resistance which is fairly constant throughout the drilling depth. This result confirms that sticky rice starch increases the mechanical resistance of samples. However, the results cannot confirm whether the increase of the in-depth strength in the SR-LAQ treatment is due to the effect of sticky rice on its own, or that the sticky rice has improved the penetration of nanolime. Further research is required to elucidate this hypothesis.

–  SEM images of the treated samples show morphological differences between both treatments involving sticky rice (SR and SR-LAQ). SR samples show the sticky rice appears to form a film on top over the substrate grains. In contrast, SR-LAQ samples show calcite crystals from nanolime grow up and get embedded in the sticky rice film. The size of the calcite crystals embedded into this film has not reduced, as in the case of ancient Chinese lime-mortars with sticky rice [Yang et al, 2009, Yang et al, 2016a, Yang et al,

2016b]. This is a significant difference as when the sticky rice is added during the mortar manufacturing process, the amylopectin was found that plays a crucial role in the carbonation process of $Ca(OH)_2$ inhibiting the growth of the $CaCO_3$ crystals that help to precipitate smaller calcite crystals that create dense and compact microstructure of mortars that reduces the penetration of water and increases their durability [Yang et al, 2009, Yang et al, 2016]. However, this reduction in size can definitely not be obtained when sticky rice is applied as a treatment on a hardened mortar

– Colorimetric results show that both samples involving nanolime (LAQ and SR-LAQ) caused a slight whitening of the surface with both $\Delta E^*$ and $\Delta L^*$ values above 5. The increase in whitening is attributed to the accumulation of nanolime particles on the surface, as described in previous programmes 1-5.

– The surface cohesion, hydrophobicity and drilling resistance of sticky rice samples significantly decreased after exposing the samples to the weathering tester at high temperatures (T=40-60ºC). This decrease in the consolidating properties is attributed to the high temperature values (T=60-50ºC) and moisture cycles exposed during the AWT, which have degraded the sticky rice starch. Starch in presence of water and heat undergoes starch gelatinization, which is an irreversible process where the water dissolves starch granule by breaking down the intermolecular bonds of starch molecules [Chandroth and Tholath, 2008]. This gelatinization process especially occurs with temperatures above 55ºC [Hans-Dieter, et al, 2004]. During this degradation process the sticky rice samples acquired a yellowish tinge, which was measured by colorimetric analysis.

– The decrease of consolidating properties (surface cohesion, hydrophobicity and drilling resistance) is also noticeable after exposing the samples to the weathering tester at lower temperatures (T=40-30ºC) and after exposing samples to wetting and drying cycles. These results confirm that starch still degrades at medium or room temperatures after several moisture cycles. Therefore, the use of sticky rice or a combined treatment of sticky rice and nanolime is considered not appropriate for any outdoor consolidation

treatment. Additionally, the weathering results also confirm that the starch degradation is significantly more pronounced in samples exposed to high temperatures (T=60-50ºC), which clearly confirms that heat accelerates the starch breakdown.

– The decrease of surface cohesion, hydrophobicity and drilling resistance after weathering process is more pronounced in SR samples than in SR-LAQ. This is attributed to the different morphology of both treatments. The calcite crystals from nanolime that grow up in the sticky rice film might increase the adhesion to the matrix of both calcite and starch film, as both may bond to the matrix physically and chemically due to the calcite-calcite bonding. This may have made the sticky rice more resistant to solubilisation. In contrast, when the sticky rice is applied on its own, it forms film on top over the substrate grains which may suggest that this film only adheres to the mortar grains physically. Thus, it appears to be more likely to solubilise as it does not present any chemical bond to the structure.

– The FTIR analysis of the water from wetting-drying cycles shows a small amount of sticky rice starch was dissolved in the water during the wetting-drying cycles. This result confirms that the sticky rice starch solubilizes in the water during the wetting and drying cycles at room temperature.

– The above results clearly show that the consolidation effect of sticky rice as a treatment or a treatment in combination with nanolime decreases after exposing the samples to several durability cycles involving moisture. However, it is important to highlight that the addition of sticky rice during the lime mortar manufacturing process significantly increases the resistance towards wetting-drying, strength and water-repellence [Wei et al, 2012, Yang et al, 2016a, Yang et al, 2009]. This can be attributed to the fact that during the manufacturing process the sticky rice is completely chemically bonded to the matrix. However, these effects can definitely not be obtained when sticky rice is applied as a treatment on a hardened mortar.

- Further studies with sticky rice are needed to understand changes in pH, any damage caused by the swelling phenomenon as part of the starch hydrolysis and the long-term bio-degradation effect. Sticky rice is a polysaccharide, thus in the right environment can be a source of nutrients for microorganisms. Further studies will need to understand the effect microorganisms.

- Although more research needs to be done, it could be preliminary concluded that sticky rice could be used to repair weathered calcareous materials in very dry environments (e.g. Mediterranean Eastern countries) or in places where there is controlled humidity (e.g. Museums).

# Chapter 5
# Conclusions

This Ph.D. has shown that different nanolime products can be used effectively for the consolidation of different types of calcareous substrates. Firstly, this Ph.D. has reviewed existing knowledge of nanolime to produce an overview-paper for publication about the synthesis, applications and factors influencing the performance of nanolime. Additionally, the results of the six research programmes have contributed to the understanding of different nanolime products and their consolidation effectiveness.

This Ph.D. has been shown that:

- The decrease of chloride content during the synthesis of L'Aquila nanolime was 99.82%, leaving 0.18 % (29.4 mg/L) residual chloride content. This residual content was significantly less than the concentration of chlorides reported in previous synthesis by Taglieri et. al. (which was approximately 1%) [Taglieri et al, 2015]. The concentration of chloride was monitored during the synthesis by means of a Vernier Chloride Ion-Selective Electrode CL-BTA, which presents better reliability than the chloride strips used at the University of L'Aquila and at the Smithsonian Museum Conservation Institute.

- Nanorestore Plus IP5® (NAN), Calosil IP5® (CAL) and a nanolime synthesised following an anion exchange synthesis method (University of L'Aquila, LAQ) can be used effectively for the consolidation of highly porous calcareous materials such as limestones or lime mortars to reduce their porosity and increase their strength.

- Nanoparticles following anion exchange synthesis (LAQ) are more reactive than the commercial products and tend to form well-formed hexagonal prismatic and parallelepiped calcite crystals fully oriented to {104}, while NAN and CAL present calcite crystals of irregular shape which have no

preferred orientation. Calosil particles are the least reactive nanoparticles and show a lower level of crystallinity after carbonation.

– NAN presents the highest consolidation results of the three nanolimes - giving greater reduction of porosity, water absorption by capillarity and higher strength increase in both lime mortars and limestones. However, following an accelerated weathering test, the DRMS detected the dissolution of a certain amount of material from the surface of samples treated with NAN and CAL which was not observed for LAQ treated samples. This was attributed to the dissolution of calcium carbonate during the moisture condensation intervals at high temperature in the tester. LAQ appears to have higher resistance to dissolution compared to the commercial products due to its better developed crystalline structure and larger crystal size, which provides higher resistance to dissolution. The loss of material was slightly more pronounced in samples treated with Calosil®, possibly as a consequence of the dissolution of the metastable vaterite, which is produced in the carbonation of this nanolime.

– All nanolime treatments affect the pore structure by reducing the porosity of the superficial portion of the substrate (approximately the outer 1 cm). In general terms, all nanolime treatments tends to reduce the number of pores with large diameter, predominantly between 10µm and 100µm. However, MIP results in research programme 3 showed that NAN tends to close predominantly large sized pores while LAQ tends to fill both large and small pores more equally. This is attributed to the reduced particle size of LAQ particles (size ~20-80 nm) which might facilitate higher access to the smaller pores (<0.5 µm) than NAN particles (size ~150-300nm). Thus, these results suggest that LAQ treatment could be more suitable to consolidate substrates with fine pores than NAN while NAN treatment could be more suitable to consolidate substrates with large pores.

– As a result of the finer pore structure of the superficial portion of the substrate, treated samples tends to take more time to dry. The denser pore structure in the superficial layer reduces the water transport towards the

surface, slowing drying [Charola, et al, 2017]. This is an undesirable behaviour as it increases the risk of biological growth and spalling when the mortar is exposed to freeze-thaw cycles and could also exacerbate the dissolution of poorly crystallised calcium carbonates such as vaterite.

- The used nanolimes have reached different penetration depths depending on the type of substrate and nanolime product. In mortar samples the penetration of both commercial products, Nanorestore and Calosil, was approximately 10mm. L'Aquila nanolime obtained slightly different penetration depths depending on the solvent. Dispersions in isopropanol, ethanol, water and 50% water and 50% ethanol mix clearly increased the drilling resistance of the mortar within about 2-3 mm from the surface, although a small consolidation effect was also noticeable up to a depth of 6-9 mm for those samples. Nanolime dispersed in 50% water and 50% isopropanol (WIP) yielded a more homogeneous consolidation in the outer 6-7 mm. In the case of stones samples, nanolime treatments have obtained higher penetration depths. Nanorestore and LAQ reached a penetration depth of up to 14-20 mm in the weathered stones (weathered limestone, marble and weathered Doulting stone). In contrast, in the case of Indiana limestone, which was not weathered, the penetration depth of LAQ (ET) was only 2-3 mm. These results clearly show that nanolime presents higher penetration in weathered calcareous stones than in lime mortars with silica sand aggregates. Further work should study the penetration of different nanolime products in different substrates.

- Nanolimes have also obtained different increase of strength depending on the substrate and nanolime product. The increased drilling resistance in lime mortars was approximately 1.5N in the outer 1 cm for each of the samples treated with NAN and CAL or LAQ, using any type of solvents. However, in the case of stones, the increased drilling resistance was significantly more pronounced. All treated stones (e.g. weathered limestone, the capital of Doulting stone, the biocalcarenite and Indiana limestone) have increased the drilling resistance between 5 - 18N after the application of either NAN or LAQ (WIP or ET). Moreover, it must be highlighted that LAQ (IP25)

significantly increased the drilling resistance on the weathered marble surface by approximately 30N. On the basis of these results, it can be concluded that the increased drilling resistance is significantly higher in pure calcite based materials (e.g. limestones or marble) than in lime-mortars with silica sand aggregate (~80% Quartz). The higher mechanical strength can be attributed to the higher calcite content of the substrate facilitating bonding of the newly formed calcite to the existing calcite crystals, thus inducing a higher resistance due to chemical compatibility [Lanas et al, 2004].

- All nanolime treatments tend to induce an undesired whitening of the substrates surface after application. LAQ treatment produced the more whitening than the commercial products, which can be attributed to LAQ's lower colloidal stability.

- Nanoparticles synthesised by anion exchange resins (LAQ) give slightly better consolidation effectiveness when dispersed in a 50% water - 50% isopropanol (WIP) solvent than when dispersed in other solvents. WIP has obtained better colloidal stability of the particles, higher reduction of the porosity, more homogeneous distribution in the substrate and the lowest colour variations. The higher consolidating effectiveness is attributed to the higher colloidal stability of the particles, which may have reduced the deposition of the particles on the surface and enhanced its penetration. LAQ nanoparticles are more reactive when dispersed in water than in other solvents.

- A high relative humidity environment or a regular spray with carbonated water enhances the consolidation effectiveness by decreasing the porosity and increasing the drilling resistance. This is in line with the literature that shows that nanolime is more effective in highly relative humidity environments [Arizzi et al, 2012; Lopez-Arce et al, 2011]. In contrast, low relative humidity environments (~50%RH), clearly reduce the consolidation effectiveness due to the lower carbonation degree of the particles. Thus, it can be concluded that nanolime must be applied in high RH environments, or when not possible, treated surfaces could be regularly sprayed with

carbonated water to enhance the carbonation effectiveness in dry environments.

– Results demonstrated that both nanolimes, Nanorestore Plus (5g/L) and LAQ (5 g/L, 50%water and 50% isopropanol) can be used effectively for the consolidation of weathered Doulting Stone (CP). Therefore, both nanolime products can be considered suitable for an in-situ consolidation treatment on the Cathedral of Wells or in any historical structure built with this type of stone.

– Results demonstrated that L'Aquila nanolime can be used effectively for the consolidation of biocalcarenite from Agrigento which is the main building material of the UNESCO's *Archaeological site of Valle Dei Templi* structures (Agrigento, Italy). Therefore, this nanolime is considered suitable for an in-situ consolidation treatment at the historic building. The optimal treatment for biocalcarenite stone was WIP*, i.e., nanoparticles are suspended in a 50% water - 50% isopropanol solvent (WIP) at a concentration of 10 g/L, repeating the application three times.

– Results demonstrated that LAQ (IP, 25 g/L), in high relative humidity environments (~75% RH or regularly sprayed with carbonated water) can be used effectively for the consolidation of marble stones weathered due to the formation of gypsum. Therefore, this nanolime can be considered suitable for an in-situ application on the weathered marble of the National Portrait Gallery and the Smithsonian American Art Museum (Washington D.C, USA).

– Results show that a sticky rice solution and a combined treatment of sticky rice and nanolime can be used to increase the strength, to reduce the water absorption by capillarity and to endow with hydrophobic properties porous inorganic materials.

– Hydrophobic behaviour and the increased strength attributed to the sticky rice significantly decreases after exposing the samples to several accelerating weathering cycles. The decrease of both properties is attributed to the starch

solubilisation process in water during the weathering cycles. Starch in the presence of water undergoes starch hydrolysis, which is an irreversible process where the water dissolves starch granules by breaking down the intermolecular bonds of starch molecules [Chandroth and Tholath, 2008]. The breakdown is most pronounced in high temperatures (T >50ºC), although it is still noticeable at room temperature [Hans-Dieter, et al, 2004]. Degradation was more pronounced in samples where the sticky rice was applied alone and not in combination with nanolime. When sticky rice and nanolime are applied together, calcite crystals of nanolime form and embed on the sticky rice film. Both sticky rice and nanolime can bond to the mortar physically and chemically due to calcite-calcite bonding, which may have made the sticky rice more resistant to solubilisation. On the contrary, when the sticky rice solution is applied without the nanolime, it appears to form a film on top over the substrate grains, suggesting that the film only adheres to the mortar grains physically, appearing more likely to solubilise as it does not present any chemical bond to the structure.

- Although more research needs to be done, it could be preliminarily concluded that sticky rice could be used to repair weathered calcareous materials in very dry environments (e.g. Mediterranean Eastern countries) or in places where there is controlled humidity (e.g. Museums).

One final and important conclusion of this study is that substrates treated with nanolimes will require regular maintenance (i.e. periodic application of nanolime) in order to achieve long term performance in terms of mechanical and physical properties.

# Future works

- Nanolimes yielded different penetration depths depending on the substrate and product. Further studies could measure the penetration depth of different nanolime products into several calcareous substrates with different pore size distributions.

- Related to the proposed study above, further work could focus on the correlation between the type of solvent, nanolime concentration and the penetration and consolidation effectiveness of nanolime.

- Further work should be carried out to understand the morphology of calcite crystals precipitated from L'Aquila nanolime, accounting for changes in relative humidity, concentrations, and type of solvent. This could identify variations in morphology and degree of crystallinity to be correlated with consolidation effectiveness and modification of the pore structure.

- Further work should be carried out to assess the durability of commercial products and LAQ nanolime. This must be carried out in several substrates through several durability tests (e.g. resistance to freeze-thaw cycles and to salt crystallization cycles).

- Further studies are needed with sticky rice to understand changes in pH, any damage caused by the swelling phenomenon as part of the starch hydrolysis and the long-term bio-degradation effect. Sticky rice (polysaccharide) in the right environment can be a food source for microorganisms. Further studies are needed to understand the effect microorganisms may have on it and how to reduce the starch solubilisation process.

# References

Alcazar-Alay S. C., Almeida-Meireles, M. A, (2015), "Physicochemical properties, modifications and applications of starches from different botanical sources", Food Sicence and Thecnology, vol. 35, No.2. http://dx.doi.org/10.1590/1678-457X.6749

Ambrosi, M., Dei L., Giorgi R., et al., (2001), "Colloidal particles of $Ca(OH)_2$: Properties and applications to restoration of frescoes", Langmuir, 17(14), pp.4251–4255.

Arizzi, A., Gomez-Villalba L. S., Lopez-Arce P., et al., (2015), "Lime mortar consolidation with nanostructured calcium hydroxide dispersions: the efficacy of different consolidating products for heritage conservation". European Journal of Mineralogy, 27(3), pp.311–323.

Arnold, A., Zehnder, K. (1987), "Monitoring Wall Paintings Affected by Soluble Salts", The Conservation of Wall Paintings: Proceedings of a Symposium organized by the Courtauld Institute of Art and the Getty Conservation Institute, London, July 13-16 pp.119-149.

ASTM C97-96 Standard Test Methods for Absorption and Bulk Specific Gravity of Dimension Stone, (2000), ASTM International, West Conshohocken, PA,https://doi.org/10.1520/C0097-96E01.

ASTM D3359-02: Standard Test Methods for Measuring Adhesion by Tape Test, (2002), ASTM International, 10 August.

ASTM 6154 -4. Standard Test Method for the Accelerated Weathering test Method for QUV QUV/BASIC Weathering Tester.

Baglioni, P., Carretti, E., Dei, L., et al., (2003), "Nanotechnology in wall painting conservation". Self-Assembly, ed. B.H. Robinson, (IOS-Press), pp.32–41.

Baglioni P., Carrasco-Vargas R., Chelazzi D., et. al., (2006a), The maya site of Calakmul: In situ preservation of wall painting and limestone using nanotechnology, Sudies in Conservation, 51:2, 162-169, DOI: 10.1179/sic.2006.51.Supplement-2.162,

Baglioni, P. and Giorgi, R., (2006b), "Soft and hard nanomaterials for restoration and conservation of cultural heritage". Soft Matter Journal, Royal Society of Chemistry, pp.293–303.

Baglioni, P., Chelazzi D., Giorgi R., et al, (2014), "Commercial $Ca(OH)_2$ nanoparticles for the consolidation of immovable works of art". Applied physics. A, Materials science & Processing, 114(3), pp.723–732.

Banfill, PFG, Szadurski, E & Forster, A.M,. (2016) Deterioration of natural hydraulic lime mortars, II: Effects of chemically accelerated leaching on physical and mechanical properties of carbonated materials Construction and Building Materials 111, 182-190. doi:10.1016/j.conbuildmat.2016.02.055.

Bennardo, C., Meli P., Bisconti N, et al, (2000), "Comparative study of different methods for gap filling applications and use of adhesive on the biocalcarenite surfaces of the "Tempio della Concordia" in Agrigento", 9th Intern. Congress on deterioration and conservation of stone, Elsevier, 2000.

Biçer-Simsir, B., Griffin I., Palazzo-Bertholon, B., et. al., (2009), "Lime-based injection grouts for the conservation of architectural surfaces", Reviews in Conservation Vol. 10. http://www.getty.edu/conservation/field_projects/grouts/index. html

Bish D. L. and Post J. E., (1989), Modern powder diffraction. Mineralogical Society of America, Crystal Reasearch & Technology, Washington. ISBN 0‑939950‑24‑3.

Borsoi, G., Lubelli B., Van Hees R., et al., (2012), "Microstructural characterization of consolidant products for historical renders: an innovative nanostructured lime dispersion and a more traditional ethyl silicate limewater solution". Journal of Microscopy Society of America, 18(5), pp.1181–9.

Borsoi, G., Lubelli B., Van Hees R. et al., (2015a), "Understanding the transport of nanolime consolidants within Maastricht limestone". Journal of Cultural Heritage, pp.1–8.

Borsoi, G., Lubelli, B., van Hees, R., et. al., (2015b). Deposition of modified nanolimes within calcareous substrates. 1-2. Abstract from Green Conservation of Cultural Heritage, 27-28 October 2015, Rome, Italy.

Borsoi, G., Lubelli B., Van Hees R. et al., (2016), "Effect of solvent on nanolime transport within limestone: How to improve in-depth deposition". Colloids and Surfaces A: Physicochemical and Engineering Aspects, 497, pp.171–181.

Bracci, S., Sacchi, B., Pinto, A. F., et. al., (2008), "Inorganic consolidants on stone artifacts: optimization of application procedures for marble and limestones". International Symposium "Stone consolidation in cultural heritage: research and practice", Lisbon 6-7 May, 2008. Proceedings, J. Delgado Rodrigues & João Manuel Mimoso (Eds.), pp. 81-90.

Brajer I. and Kalsbeek N., (1999), "Limewater absorption and calcite crystal formation on a limewater-impregnated secco wall-painting", Studies in Conservation vol. 44 (3), pp. 145–156.

BS EN 14617-5:2012, (2012), Agglomerated stone. Test methods. Determination of freeze and thaw resistance.

BS EN 13139:2002, (2002), Aggregates for mortar.

BS EN 459-1:2015, (2015), Building lime, Part 1: Definitions, specifications and conformity criteria.

Camuffo, D. (1998), "Micro-climate for cultural heritage", Developments in Atmospheric science, 23, Elsevier, Amsterdam, pp.425.

Campbell, A., Hamilton A., Stratford, T., et al., (2011), "Calcium hydroxide nanoparticles for limestone conservation: Imbibition and adhesion". Proceedings of symposium, adhesives and consolidants for conservation, Ottawa, pp.1–16.

Chandroth K. S. and Tholath E., A., (2008), "Physicochemical Rheological and Thermal Properties of Njavara Rice (oryza sativa) starch", Journal of Agricultural and foos chemistry, 56, 12105-12113.

Charola A. E. and Tucci A., (1986), "On the reversibility of treatments with acrilic/silicone resin mixtures", Journal of the American Institute for Conservation, Vol. 25, pp. 83–92.

Charola, A. E., (1988), "Chemical-physical factors in stone deterioration", Durability of Building Materials vol. 5, pp. 309-316

Charola A. E., (1995), "Water-repellent treatments for building stones : A practical Overview", Association for Preservation Technology International (APT), vol. 26 (2), pp.10–17. Available at: http://www.jstor.org/stable/1504480.

Charola, A. E., (2000), "Salts in the Deterioration of Porous Materials: An Overview", Journal of the American Institute for Conservation (JAIC). 39, Vol. 3, pp. 327-343.

Charola A. E. and Ware R., (2002), "Acid deposition and the deterioration of stone: a brief review of a broad topic", Geological society, London, Special Publication, 205, 393-406. DOI: https://doi.org/10.1144/GSL.SP.2002.205.01.28

Charola, A.E., Pühringer, J. and Steiger, M. (2007). "Gypsum: a review of its role in the deterioration of building materials", Environ. Geol. (2007) 52:339-352

Charola A. E., Magallan M. L., Korth G. M. A., et. at., (2009), "Manual Básico de Conservacion para las misiones Jesuíticas guaraníes", UNESCO World Heritage Fund, pp.40-52.

Charola A. E., Centeno S. A., Normandin K., (2010), The New York Public L:ibrary, "protective treatment for sugaring marble, Journal of Architectural Conservation, Vol. 16, Issue 2, 00 29-44.

Charola A. E. and Wendler E., (2015), "An overview of the water-Porous building materials interactions",  Restoration of building and monuments Journal, vol. 21(2-3), pp. 55-63.

Charola A. E. and Blauer C., (2015), "Salts in Masonry: An overview of the problem", Restoration of buildings and monuments, vol. 21 (4-6):119-135.

Charola A. E., Vicenzi E. P., Grissom C. A., et. al., (2017), "Composition and characteristics of Kasorta limestons on the exterior of the National Museum of the American Indian Building", pp.17-26. J.Sledge, A. E. Charola, P. T. DePriest and R. Koestler, eds. Conservation of the Exterior of the National Museum of the American Indian Building, Smithsonian Contributions to Museum Conservation, No. 6. ISSN 1949-2359.

Chelazzi D., Poggi G., Jaidar Y., et al (2013), "Hydroxide nanoparticles for cultural heritage: consolidation and protection of wall paintings and carbonate materials", Journal of colloid and interface Science, 392 (2013), 42-49.

Costa D., Delgado-Rodrigues J., (2012), "Consolidation of a porous limestone with nano-lime", in: G. Wheeler (Ed.), 12th International congress on the deterioration and conservation of stone, New York, pp. 10–19.

Daehne, A., Herm, C., (2013), "Calcium hydroxide nanosols for the consolidation of porous building materials", results from EU-STONECORE. Heritage Science, 1(1), p.11. Available at: http://www.heritagesciencejournal.com/content/1/1/11.

Daniele, V., Taglieri, G., Quaresima R., (2008), "The nanolimes in cultural heritage conservation: Characterisation and analysis of the carbonatation process". Journal of Cultural Heritage, 9(3), pp.294–301.

Daniele, V., Taglieri, G., (2010), "Nanolime suspensions applied on natural lithotypes: The influence of concentration and residual water content on carbonatation process and on treatment effectiveness". Journal of Cultural Heritage, 11(1), pp.102–106.

Daniele, V., Taglieri, G., (2011), "$Ca(OH)_2$ nanoparticle characterization: microscopic investigation of their application on natural stones". Materials Characterisation, 72, pp.55–66.

Daniele, V. and Taglieri, G., (2012), "Synthesis of $Ca(OH)_2$ nanoparticles with the addition of Triton X-100. Protective treatments on natural stones: Preliminary results". Journal of Cultural Heritage, 13(1), pp.40–46.

De Rosario I., Feijoo Conde, J., (2016), "Alteración de las rocas y otros materiales de construcción en los monumentos. Técnicas de conservación", University of Vigo IBSN: 978-84-8158-720-3.

Dei, L., and Giorgi, R., (2001), "Stable dispersions of $Ca(OH)_2$ in aliphatic alcohols: properties and application in cultural heritage conservation". Progress in Colloid and Polymer Science, 118, pp.68–72.

Dei, L., and Salvadori, B., (2006), "Nanotechnology in cultural heritage conservation: nanometric slaked lime saves architectonic and artistic surfaces from decay". Journal of Cultural Heritage, 7(2), pp.110–115.

Delfort, B., Born M., Chive A., et al, (1997), "Colloidal calcium hydroxide in organic medium: Synthesis and analysis". J Colloid Interface Science, 157(189), pp.151–157.

Delgado-Rodrigues J, & Grossi A, (2007), Indicators and ratings for the compatibility assessment of conservation actions. Journal of Cultural Heritage, 8:32-4.

Delgado-Rodrigues J., Ferreira-Pinto A. P., (2016), "Laboratory and onsite study of barium hydroxide as a consolidant for high porosity limestones", Journal of cultural heritage, 19 467-476.

Doehne E., Price C. A., (2009), "Stone Conservation: An Overview of Current Research", Research in conservation Series, Getty Conservation Institute, USA.

Drdácký, M., Slizkova Z., Ziegenbalg G., (2009), "A Nano approach to consolidation of degraded historic lime mortars". Journal of Nano Research, 8, pp. 13-22.

Drdacky M., Slizkova Z., (2015), "In situ peeling test for assessing the cohesion and consolidation characteristics of historic plaster and renders surfaces", Studies in Conservation, 60:2, 121-130, DOI: 10.1179/2047058413Y.0000000116
Dunham R. J., (1962), "Classification of carbonate rocks according to depositional texture. In Ham, W.E. classification of carbonate rocks", Am. Assoc. Petroleum Geologists Mem. 1 108–121

Embry, Ashton F., Klovan, J. Edward (1971-12-01). "A late Devonian reef tract on northeastern Banks Island, N.W.T". Bulletin of Canadian Petroleum Geology. 19 (4): 730–781. ISSN 0007-4802

EN 1015-3:1990, (1990), Methods of test for mortar for masonry. Determination of consistence of fresh mortar (by flow table).

EN 1015-2:1998, (1998), The European Standard, Methods of test for mortar for masonry. Bulk sampling of mortars and preparation of test mortars.

EN 12370: (1999) Natural stone test methods. Determination of resistance to salt crystallization Physical weathering of building stones induced by freeze–thaw action: a laboratory long-term study

EN 13755, (2008), The English Standard for Natural stone test methods. Determination of water absorption at atmospheric pressure.

EN 16322. (2013), The European Standard CEN - Conservation of Cultural Heritage - Test methods - determination of drying properties.

EN 1015-19:1999. Methods of test for mortar for masonry, Part 19: Determination of Water Vapor Permeability of Hardened Rendering and Plastering Mortars

English Heritage, (2012a), "Practical Building Conservation: Stones", Ashgate Publishing limited, ISBN: 9780754645528.

English Heritage, (2012b), "Practical Building Conservation: Mortars, Renders and Plasters", Ashgate Publishing limited, ISBN10: 0754645592.

Ferreira-Pinto, A. P. and Delgado-Rodrigues, J. (2008a), "Stone consolidation: The role of treatment procedures", Journal of Cultural Heritage, 9 (1), pp.38–53. Available at: http://linkinghub.elsevier.com/retrieve/pii/S1296207407001458

Ferreira-Pinto, A. P. and Delgado-Rodrigues J., (2008b), "Hydroxylating conversion treatment and alkoxysilane coupling agent as pre-treatment for the consolidation of limestones with ethyl silicate". In Stone Consolidation in Cultural Heritage: Research and Practice; Proceedings of the International Symposium, Lisbon, 6-7 May 2008, ed. J. Delgado-Rodriguez and J. M. Mimoso, 41-52. Lisbon: LNEC (Laboratorio National de Engenheria Civil).

Folk R. L., (1959), "Practical petrographic classification of limestone", Am. Assoc. Pet. Geol. Bull. 43 (1) 1–38.

Forster, A.M, Szadurski, E and Banfill, P.F.G., (2014), Deterioration of natural hydraulic lime mortars, I: Effects of chemically accelerated leaching on physical and mechanical properties of uncarbonated materials Construction and Building Materials 72, 199-207.

Gadhave, R. V., Mahanwar P. A., Gadekar P. T., (2017), "starch-Based Adhesives for Wood/Wood Composite Bonding: Review",Open Journal of polymer Chemistry, vol. 7, pp. 19-32.

Geoffrey, A., (2003), "Hydraulic Lime Mortar for Stone, Brick, and Block Masonry", Shaftesbury: Donhead Publishing Ltd. 1-873394-64-0.

George H. O., Russel G. P., Tacoma W., et. al. (1938), "Waterproof starch-base adhesive", United states patent office, Dec 27, 1938, patent number 2.141.313.

Giorgi R., Dei L., Baglioni P., (2000), "A new method for consolidating wall paintings based on dispersions of lime in alcohol", Studies in Conservation, vol. 45, no 3, pp 154-161.

Giorgi, R., Ambrosi M., Toccafondi N., et al., (2010), "Nanoparticles for cultural heritage conservation: Calcium and barium hydroxide nanoparticles for wall painting consolidation". Chemistry - A European Journal, 16(31), pp.9374–9382.

Gomez-Heras, M. (2005), "Procesos y formas de deterioro termico en piedra natural del patrimonio arquitectonico", Doctoral Thesis. University of Complutense of Madrid. ISBN: 84-669-2801-4, 399p.

Gottardi, V., I Leganti, Appunti dalle lezioni di tecnologia dei materiali e chimica applicata, Editor: Pàtron, Bologna (1978).

Goudie, A. S. and Viles, H. A. (1997) "Salt weathering hazard", Wiley, Chichester, New York, vii, 241 pp.

Grabau, A.W. (1904), "On the Classification of Sedimentary Rocks", American Geologist, 33, 228-247

Grossi, C. M., Brimblecombe P., Menéndez B., et al., (2008), "Long term change in salt weathering of stone monuments in north-west France", In Proceedings of the 11th

Hall, C, Hamilton, A, Hoff, W. D, Viles, H. A, Eklund, J. A., (2010), 'Moisture dynamics in walls: response to micro-environment and climate change' Proc R Soc Aug 2010.

Hall-Stoodley L,, Costerton J. W,, Stoodley P (February 2004). "Bacterial biofilms: from the natural environment to infectious diseases". Nature Reviews Microbiology. 2 (2): 95–108. doi:10.1038/nrmicro821.

Hans-Dieter B., Werner G., Schieberle P., (2004), "Food chemistry", Edition 3, Springer, page: 318-323, ISBN 3-540-40818-5.

Hansen E., Doehne E., Fidler J. A., (2003), "A review of selected inorganic consolidants and protective treatments for porous calcareous materials", Studied in Conservation 4, 13-25.  https://doi.org/10.1179/sic.2003.48.Supplement-1.13

Henriques, F. and Charola, A. E., (1996), "A comparative study of standard test procedures for mortars", Proceedings of the 8th International Congress on Deterioration and Conservation of Stone, pp. 1521-1528.

Historic England. "Wells Cathedral", (2011), PastScape. Retrieved 4 196971

Hunter, R. S., and Harold, R. W, (1987), "The Measurement of Appearance", 2nd ed., John Wiley and Sons, Inc. New York, NY USA. CIE

ICOMOS, (1931), "Carta del Restauro", the First International Congress of Architects and Technicians of Historic Monuments, Athens.

ICOMOS, (1964), "The Venice Charter", International Charter for the Conservation and Restoration of Monuments and Sites.

ICOMOS, (2008), "Illustrated glossary on stone deterioration patterns glossaire illustré sur les formes d'altération de la pierre", ICOMOS international scientific committee for stone (iscs). Comité scientifique international "pierre" de l'icomos. ISBN : 9782-918086-00-0. 78 p.

International Commission on Illumination, Recommendations on Uniform Color Spaces, Color-Difference Equations, Psychometric Color Terms, Supplement No. 2 to CIE Publication No. 15, Colorimetry, 1971 and 1978.

Istituto Superiore per la Protezione e la Ricerca Ambientale, Servizio Geologico d'Italia. Note Illustrative della Carta Geologica d'Italia alla scala 1:50.000, Foglio 636 Agrigento.

IRUG (Infrared & Raman Users Group) data base, Rice starch, Getty Conservation Institute, 2018.

Jenkins, P J, and A M. Donald. (1998), "Gelatinisation of Starch: a Combined Saxs/waxs/dsc and Sans Study." Carbohydrate Research. 308: 133-147.

Lahdensivu, J. (2016) Cement Concrete Composites Vol. 65, p 29.

Lanas J, Perez-Bernal M. A., Bell M. A. et al, (2004), "Mechanical Properties of hydraulic lime based mortars", Cement and Concrete Research 34:2191-2201.

Lewin, S.Z., 'X-Ray Diffraction and Scanning Electron Microscope Analysis of Conventional Mortars'. In Mortars, Cements and Grouts Used in the Conservation of Historic Buildings, ICCROM, Rome, proceedings of conference held on 3–6 November 1981 (1982), p. 106.

Liu, T., Zhu Y., Zhang X., et al., (2010), "Synthesis and characterization of calcium hydroxide nanoparticles by hydrogen plasma-metal reaction method". Materials Letters, 64(23), pp.2575–2577.

López-Arce, P., Gomez-Villalba L.S., Pinho L., et al., (2010), "Influence of porosity and relative humidity on consolidation of dolostone with calcium hydroxide nanoparticles: Effectiveness assessment with non-destructive techniques". Materials Characterization, 61(2), pp.168–184.

Lopez-Arce, P., Zornoza-Indart, A., (2015), "Carbonation acceleration of calcium hydroxide nanoparticles: induced by yeast fermentation". Applied Physics A, 120(4), pp.1475–1495.

Lopes-Margalha, M. G., Santos Silva, A., Rosario Veiga, M., de Brito, J., Ball, R. J., Allen, G. C., (2013), "Microstructural Changes of Lime Putty during Aging", Journal of Materials in Civil Engineering, 25, 1524-1532

Lubelli, B., van Hess, R.P.J., Groot, C.J.W.P., (2004), "The role of sea salts in the occurrence of different damage mechanisms and decay patterns on brick masonry". Construction and Building Materials 18, 119-124.

Lubelli, B., (2006), "Sodium chloride damage to porous building material", Ph.D. Thesis. Dottore in Architettura, Politecnico di Milano, Italy.

Mariani, E., (1976), "I leganti aerei e idraulici", Ambrosiana, Milano.

Miller B. F., Root W., (1991), "Long-term storage of wheat starch paste", Stud. Conserv. 36 (2) 85–92.

Mitchell, W. A., (1977), "Starch solubility", Journal of Chemical Education, 54 (2), p 1932. DOI: 10.1021/ed054p132.3.

Mitchell, D. J., Searle D. E., (2004), "Stone deterioration in polluted Urban environments", Land Reconstruction and Management Series 3. Enfield, NH:Science Publisher.

Mora P., Torraca G., (1965), Bollettino Instituto Centrale del Restauro (Rome) pp 109-32.

Mortensen, H. (1933), Die "Salzsprengung" und ihre Bedeutung für die Regionalklimatische Gliederung der Wüsten. Dr. A. Petermanns Mitteilungen. Gotha: Justus Perthes. 79:130–35.

Mtani, I. W., (2016), "Salt Deterioration of Historic Mortars in Tropical Climate: Analysis and Characterisation", kassel university press, ISBN: 978-3-7376-0074-3, P. 231 , DOI: 10.19211/KUP9783737600750

Nanni, A., Dei, L., (2003), "$Ca(OH)_2$ nanoparticles from W/O microemulsions". Langmuir, 19(13), pp.933–938.

Nanorestore®, CSGI Consortium - University of Florence, Italian Patent No. FI/96/A/000255, filed on 31/10/1996.

Newman, B., (2017), "Building Conservation Directory, Special Report on Historic Churches: The Conservation and Repair of ecclesiastical buildings, Building Conservation Directory Special Report", Cathedral Communications Limited, ISBN 978 1 900915 830, pp. 18-23.

Nuño, M., Pesce G. L., Bowen C. R., et al., (2015), "Environmental performance of nano-structured $Ca(OH)_2/TiO_2$ photocatalytic coatings for buildings". Building and Environment, 92, pp.734–742.

Operating Manual OCA 20. DataPhysics OCA. © Copyright 2006 por DataPhysics Instruments GmbH, Fiderstadt.

Otero, J., Charola, A. E., Grissom, et al, (2017), "An overview of nanolime as a consolidant for calcareous substrates". Submitted to Proceedings of the 5th

International Conference Youth in Conservation of Cultural Heritage, Museo Nacional Centro de Arte Reina Sofia.

Pavlovic, S., Brandao, P., (2003), "Adsorption of starch, amylose, amylopectin and alucose monomer and their effect the flotation of hematite and quartz". Miner. Eng. 16, 1117-1122

Pe, L. A., Wang, L., Matijevic, E., et al., (1998), "Nanosize indium hydroxide by peptization of colloidal precipitates". Langmuir, 7463(8), pp.4397–4401.

Pecchioni, E., Fratini, F., Cantisani, E., (2008), "Le malte antiche e moderne tra tradizione e innovazione", Pàtron, Bologna.

Piaszczynski, E., Wolf, V. (2011), "The combination of nano-lime and silicic acid ester for stone conservation", Proceedings of the European Workshop on Cultural Heritage Preservation, Berlin 2011, Fraunhofer IRB:Verlag, 254.

Pliny, (1971), Natural History, W. Heinemann LTD, London,  Book XXXVI.

Poggi, G., Toccafondi N., Chelazzi D., et al, (2016), "Calcium hydroxide nanoparticles from solvothermal reaction for the deacidification of degraded waterlogged wood". Journal of Colloid and Interface Science, 473, pp.1–8.

Price, C., Ross, K., White, G., (1988), "A further appraisal of the 'Lime Technique' for limestone consolidation, using a radioactive tracer". IIC journal.Studies in Conservation, vol. 33 (4), pp.178–186.

Price, C., (1989), "Conservation de la Façade ouest de la cathedrale de Wells, In L'Ornementation architecturale en pierres dans les monuments historiques: Chateau de Fontaineableau", October 1988. Actes des colloques de la direction du Patrimoine, 1989, 38-40. Reviews consolidation of limestone with Alkoxysilanes and lime treatments.

Rewthong, O., Soponronnarit, S., Taechapairoj, C., et al , (2011), "Effects of cooking, drying and pretreatment methods on texture and starch digestibility of instant rice", J .Food Eng,103, 258-264

Rietveld H.M., (1969), "A profile refinement method for nuclear and magnetic structures", Journal Applied Crystallography, 10, 65.

Rodriguez-Navarro C., Suzuki A., Ruiz-Agudo E., (2013), "Alcohol dispersions of calcium hydroxide nanoparticles for stone conservation", Langmuir vol. 29, pp. 11457−11470.

Rodriguez-Navarro, C., Bettori I., Ruiz-Agudo E., (2016), "Kinetics and mechanism of calcium hydroxide conversion into calcium alkoxides: Implications in heritage conservation using nanolimes", Langmuir, 32(20), pp. 5183-5194.

Rosario Veiga, M., Magalhaes A. C., Bokan-Bosilikov V., (2004), "Capillary test on historic mortar samples extracted from site", Methodology and compared results, in: 13th International Brick and Block Masonry Conference, Amsterdam, July 4-7.

Rossi-Manaresi, R., Forsythe C., Omexinsky D., (1982), "scientific investigation in relation to the conservation of stone, science and technology in the service of conservation", Washington congress, 3-9 September 1982, p.39-45 (1982).

Rossi Manaresi R., Charola A. E., Tucci A., et al., (1984), "Study of accelerated weathering of limestones treated with an acryilic-silicone mixture", ICOM 7th Triennial Meeting, Copenhagen. pp. 84.10.1-84.10.4. Paris: ICOM-J. Paul Getty Trust.

Rossi-Manaresi, R., Tucci, A., (1991), "Pore structure and the disruptive or cementing effect of salt crystallization in various types of stone", Stud Conserv 36 (1) 53–58.

Roy, A., Bhattacharya, J., (2010). "Synthesis of $Ca(OH)_2$ nanoparticles by wet chemical method". Micro & Nano letters,(3), pp.131–134.Scherer, G. W.,

Crystallization in pores, (1999), Cement and concrete research, vol.29, Issue 8 pp.1347-1358.

Ruffolo, S., La Russa M., Aloise P., et al, (2014), "Efficacy of nanolime in restoration procedures of salt weathered limestone rock". Applied Physics A: Materials Science and Processing, 114, pp.753–758.

Rundl, R. E., Foster, J. F., Baldwin, R. R, (1944), "On the Nature of the Starch-Iodine Complex". J. Am. Chem. Soc., 66, 2116–2120.

Safety data sheet, Honeywell, 50/50 Isopropyl Alcohol-Water (v/v) (703) 000000012660.

Salvadori, B., Dei, L., (2001), "Synthesis of $Ca(OH)_2$ nanoparticles from diols". Langmuir, 17(8), pp.2371–2374.

Samanta, A., Chanda D. K., Das P. S., et al., (2016), "Synthesis of nano calcium hydroxide in aqueous medium". Journal American Ceramic Society, 795(37004), pp.787–795.

Scherer, G. W. (2004), "Stresses from crystallization of salt", Cement and Concrete Research 34 (9) 1613-1624.

Schueremans L, Cizer O, Janssens E, Serre G, Van Balen K., (2011), Characterization of repair mortars for the assessment of their compatibility in restoration projects: Research and practice. Construction and Building Materials, 25:4338-4350.

Sequeira, S., Casanova C., Cabrita E. J., (2006), "Deacidification of paper using dispersions of $Ca(OH)_2$ nanoparticles in isopropanol", Journal Cultural Heritage, 7, pp.264–272.

Slizkova Z., Frankeova D., (2012), "Consolidation of a porous limestone with nanolime". Proceedings of the 12th International Congress on the Deterioration and Conservation of Stone, New York.

Slizkova, Z., Dracky M., Viani A., (2015), "Consolidation of weak mortars by means of saturated solution of calcium hydroxide or barium hydroxide", Journal of Cultural Heritage, vol. 16, No. 4, pp. 420-460.

Syed H. I., (2000), "Stuck on starch: a new wood adhesive, Agricultural research magazine", US Department of Agriculture.
https://agresearchmag.ars.usda.gov/2000/apr/wood/

Şengün N., Demirdag S., Akbay D., (2014), Investigation of The Relationships Between Capillary Water Absorption Coefficients And Other Rock Properties of Some Natural Stones, V. Dünya Doğaltaş Kongresi (Globalstone 2014), Antalya-Türkiye, pp. 22–25.

Taglieri, G., Daniele V. Del Re, et al, (2015), "A new and original method to produce $Ca(OH)_2$ nanoparticles by using an anion exchange resin". Advances in Nanoparticles, 4, pp.17–24.

Taglieri G., Felice B., Daniele V., et al., (2016), "Analysis of the carbonisation process of nanosized $Ca(OH)_2$ particles synthesized by exchange ion process", Proceedings of the Institution of Mechanical Engineers, Part N: Journal of Nanoengineering and Nanosystems vol. 230 (1), pp. 25-31.

Taglieri G., Daniele V., Macera L., et al., (2017a), "Nano $Ca(OH)_2$ synthesis using a cost-effective and innovative method: Reactivity study", J.Am Ceram Soc. 2017;100:5766–5778.

Taglieri G., Otero J., Daniele V., et. al., (2017b), "The biocalcarenite stone of Agrigento (Italy): Preliminary investigations of compatible nanolime treatments", Journal of Cultural Heritage, https://doi.org/10.1016/j.culher.2017.11.003.

Taglieri G., Daniele V., Macera L., et al (2017c), "Eco-compatible protective treatments on an Italian historic mortar (XIV century)", Journal of Cultural Heritage 25, 135–141.

Tiano, P., (2001), "Biodegradation of Cultural Heritage: Decay Mechanisms and Control Methods", CNR-Centro di Studio Sulle Cause Deperimento e Metodi Conservazione Opere d'Arte, 9, pp.1–37. Available at: http://www.arcchip.cz/w09/w09_tiano.pdf.

Tiano P., (2006), "A new portable system for determining the state of conservation of monumental stones". Materials and Structures Journal Vol. 39 Issue 2, pp.139–147.

Thomson M., Lindqvist J. E., Elsen J., et al, (2007), "Chapter 2.5: Porosity of mortars", Characterisation of Old Mortars with Respect to their Repair, RILEM publications SARL, Editors: C.Groot, G.Ashall, J.Hughes, pp.75—103.

Tucker, M. E., (2003), Sedimentary rocks in the field, Wiley Editions, Department of Geological Sciences, University of Durham, University Press, ISBN:0-470-85123-6.

Ukrainczyk, M., Greiner M., Elts E., et. al., (2015), Simulating preferential sorption of tartrate on prismatic calcite surfaces, CrystEngComm Journal, vol. 17, 149-159. DOI: 10.1039/c4ce01447b.

UNI 10924 Norma, (2001), Cultural heritage - Mortars for building and decorative elements - Classification and terminology, UNI Ente Nazionale Italiano Unificazione, Milan (2001).

Villegas R., Baglioni, R., Sameno, M. (2003), "Tipología de materiales para tratamiento, Metodología de diagnóstico y evaluación de tratamiento para la conservación de los edificios históricos", Instituto Andaluz de Patrimonio Histórico ISBN: 84-8266-370-4. pp 168-193.

Vitruvius, On Architecture, W. Heinemann LTD, London, (1962), Book VII

Volpe R., Taglieri G., Daniele V., et. al., (2016), "A process for the synthesis of $Ca(OH)_2$ nanoparticles by means of ionic exchange resin", European patent EP2880101.

Walsh Z., Janecek, E. R., Jones M., et al, (2015), "Natural polymers as alternative consolidants for the preservation of waterlogged archaeological wood", Studies in Conservation, Vol 62, issue 4.

Watnick, P., Kolter, R. (2000). "Biofilm, city of microbes". Journal of Bacteriology. 182 (10): 2675–2679.

Watt J. Tidblad J., Kucera V., (2009), "The effect of air pollution on cultural heritage", Springer, 6, 10, 12, 14-16, 22-23, 138.

Wei G., Zhang H., Wang H., et al, (2012), "An experimental study on application of sticky rice–lime mortar in conservation", Construction and Building materials, vol. 28, pp. 624-632.

Wheeler G., (2005), "Alkoxysilanes and Consolidation of stone", Research in conservation Series, Getty Conservation Institute, USA.

Wheeler G., (2008), "Alkoxysilanes and the consolidation of stone: Where we are now. In Stone Consolidation in Cultural Heritage: Research and Practice", Proceedings of the International Symposium, Lisbon, 6-7 May 2008, ed. J. delgado-Rodriguez and J. M. Mimoso, 41-52. Lisbon: LNEC (Laboratorio National de Engeneria Civil).

Winkler, E. M., Wilhelm, E. J. (1970), "Salt burst by hydration in architectural stone in urban atmosphere", GSA Bulletin 81 (1970) 567-572.

Winkler, E. M., (1979), "Weathering of molasse sandstone on monuments and natural outcrops", Proceedings of the 3rd International Congress Deterioration and Preservation of stones, Venice, 24-27.

Wu, Y., Lee, Y., Chang, H., (2009), "Preparation and characteristics of nanosized carbonated apatite by urea addition with precipitation method", Materials Science & Engineering C, 29, pp.237–241.
Available at: http://dx.doi.org/10.1016/j.msec.2008.06.018.

Wu J., Chen J., Liu C., et al, (2016), "Effect of aleurone layer on rice cooking: A historical investigation", Food chemistry, Volume 191, pp. 28-35.

Yang F., Zhang B., Ma Q., (2009), "Study of Sticky rice - Lime mortar technology for the restoration of historical masonry construction", Accounts of Chemical research, vol. 43 No 6, pp. 936-944.

Yang, R.  Li K., Wang L, et al., (2016a), "A micro-experimental insight into the mechanical behaviour of sticky rice slurry-lime mortar subject to wetting-drying cycles", Journal of Materials Science, 51(18), pp.8422–8433. Available at: "http://dx.doi.org/10.1007/s10853-016-0099-x.

Yang, T. Ma, X., Zhang B., et al., (2016b), "Investigations into the function of sticky rice on the microstructures of hydrated lime putties", Construction and Building Materials, Vol 102, Part 1, pp.105–112.

Young, M., Murray M., and Cordiner P., (1999), Stone consolidants and chemical treatments in Scotland. Report to Historic Scotland.

Zhao H., Xiao Q., Huang D., et al, (2014), Influence of Pore Structure on Compressive Strength of Cement Mortar, Scientific World Journal. 2014; 247058. DOI: 10.1155/2014/247058.

Ziegenbalg, G., (2003), "Verfahren zur verfestigenden Behandlung von mineralischen anorganischen Baustoffen", Patent number: DE:10327514 B3.

Zobel, H., (1988), "Starch crystal transformations and their Industrial importance", Biosynthesis Nutrition Biomedical, Vol. 40, Issue 1, p.p. 1-7.

# Appendix 1

Smithsonian's Museum Conservation Institute Report

**Nanolime for consolidation of deteriorated calcareous stones:**

**Report on its preparation, application, and related studies**

**Jorge Otero**

## 1. Nanolime synthesis

Two nanolimes dispersions were synthetized following a newly developed method (Taglieri et al., 2015) based on an ion exchange process between an anionic resin and a calcium chloride aqueous solution, at room temperature, following the reaction:

$$CaCl_2 + 2R\text{-}OH \rightarrow Ca(OH)_2\downarrow + 2R\text{-}Cl$$
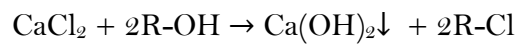
First, in order to obtain colloidal dispersions with an equivalent concentration of 25 g/L (calculations can be found in Appendix 1.), a 400 ml aqueous solution of 0.3M calcium chloride dihydrate ($Ca(OH)_2 \bullet 2H_2O$, Sigma-Aldrich) was prepared. The solution was added to 300 ml of Dowex anion ($OH^-$) exchange resin in the hydroxyl form (Dowex Monosphere 550A (OH), Dow Chemical), at room temperature, and kept under moderate stirring for about 60 minutes. At this point, few drops were collected and used to check for the presence of chlorides in the solution by means of selective chloride ion strips (Hach-Quantab 30-600ppm $Cl^-$) ( fig. 1).
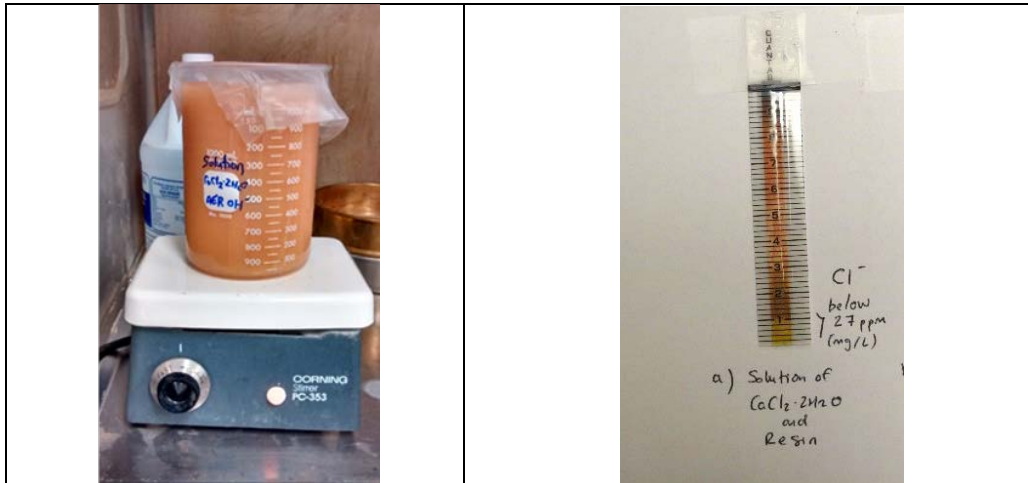


Figure 1. Left. Preparation of the nanolime aqueous suspension and resin. Right: chloride test strip used to test the chloride content in the nanolime suspension after 60 minutes (<27 ppm).

Once the chloride concentration fell below 30 ppm, the stirrer was stopped, the resin was separated from the nanolime suspension using a sieve (180 μm mesh opening) and put into an airtight container to prevent carbonation. The exhausted resin was stored in a sealed bottle for its regeneration. Since a certain amount of water is retained by the resin, the aqueous nanolime

suspension was weighed after the separation, the final volume noted and the volume weight loss calculated. The final volume was 260mL, thus nearly 35% of initial volume is retained by the resin during the synthesis.

To prepare the aqueous-alcoholic dispersion, the aqueous suspension was centrifuged (IEC clinical centrifuge) for 15 minutes at high speed (fig. 2). The supernatant water was subsequently extracted with a syringe and replaced with 230 mL of a short-chain aliphatic alcohol, either ethanol (99.5%, Pharmco) or isopropanol (99.5%, Fisher Scientific) maintaining the concentration at 25 g/L. The dispersion was sealed with Parafilm M (Bemis NA, USA) to avoid carbonation and evaporation of the solvent. As reported in the literature (Dei and Salvadori 2006), the final dispersions were prepared using a hydro-alcohol medium, with a water/alcohol ratio (W/A) of 1:10 considering the final volume and were kept under moderate stirring for 30 minutes. The final dispersions were stored into an air tight container. This procedure was used to prepare two nanolime dispersions, one in ethanol-water, identified as E25; and another in isopropanol-water, identified as I25 (fig. 2).



Figure 2. Left: centrifugation process. Center: nanolime dispersion in alcohol under stirring. Right: initial and final concentration of Cl⁻ for the resin regeneration process
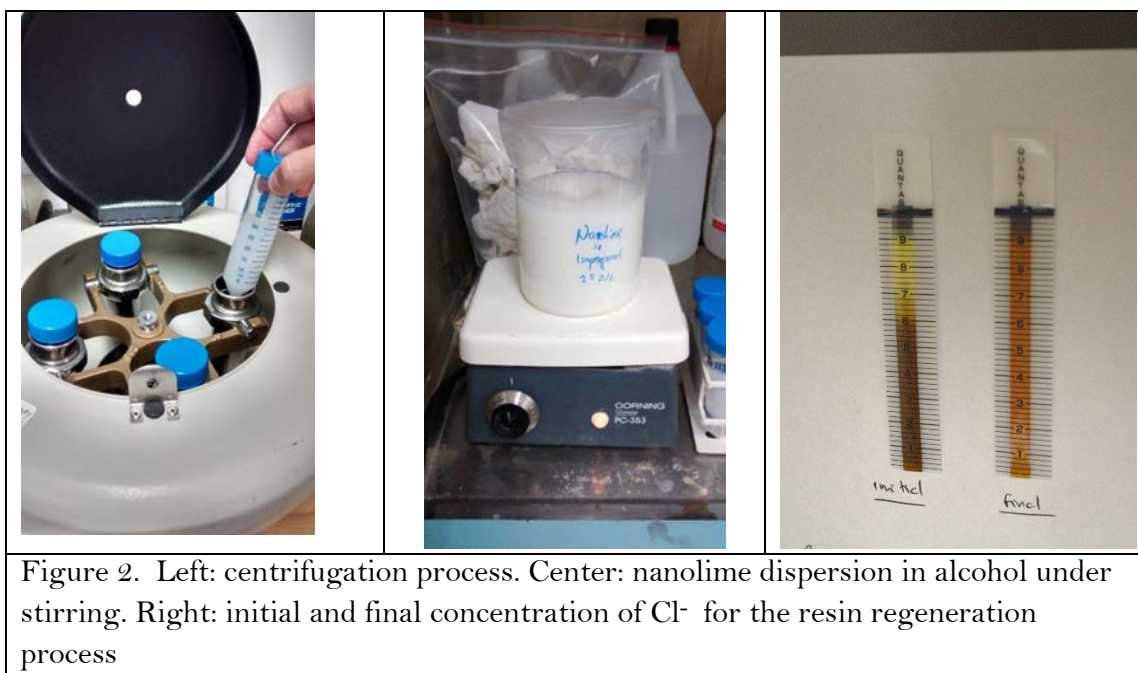
After the synthesis process, the exhausted resin was regenerated in a batch approach by adding a 1 M NaOH (p.a. 99.5% Fisher Scientific) solution and stirring for 15 minutes. The resin regeneration follows the reaction:

$$Na(OH) + R\text{-}Cl \rightarrow R\text{-}OH + NaCl$$
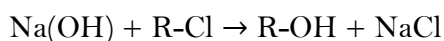
At the end of the regeneration, the chloride concentration of the solution was checked with chloride ion selective strips (substitution of Cl- ions with OH- groups on the resin). To remove the NaCl produced, several deionized water washings were performed until the chloride concentration was below the 30 ppm as shown in figure 2, and finally a vacuum filtration (Millipore Express 0.1μm) was used to separate the solid product from the liquid solvent.

## 2. Specimen preparation

Two carbonate stone types were used, a weathered marble and Indiana limestone. The marble block, possibly the cornice of a building, was taken from a pile of architectural marble blocks among the stone deposits at the Smithsonian Garber facility. It is a fine-grained marble with two weathered surfaces, and a third one that apparently still has some mortar attached to it. The block was cut into 5 cm thick slices as shown in figure 3. The approximate dimensions are: two weathered faces: 5 x 5 cm one of them curved (fig.3); one with mortar rests: 5 x 5.5 cm; three sawn surfaces, two of which are 5 x 5.5 cm, and the last one 4 x 5 cm. A very weathered specimen of this same marble was examined under optical and scanning electron microscopy and some EDS analyses were carried out (Appendix 2).

The Indiana limestone is a clastic oolitic limestone commonly used as building material in USA. It has >97% $CaCO_3$, density = 1.75 to 2.05 g/cm3, the open porosity is around 23% and the pore size distribution is bimodal, the highest volume of smaller pores (0.2 μm) is about 1.5 times the volume of the larger pores (4 mm) (Rossi Manaresi et al., 1984). The samples were cut from a sound block into 5 x 5 x 5 cm blocks (fig. 3).
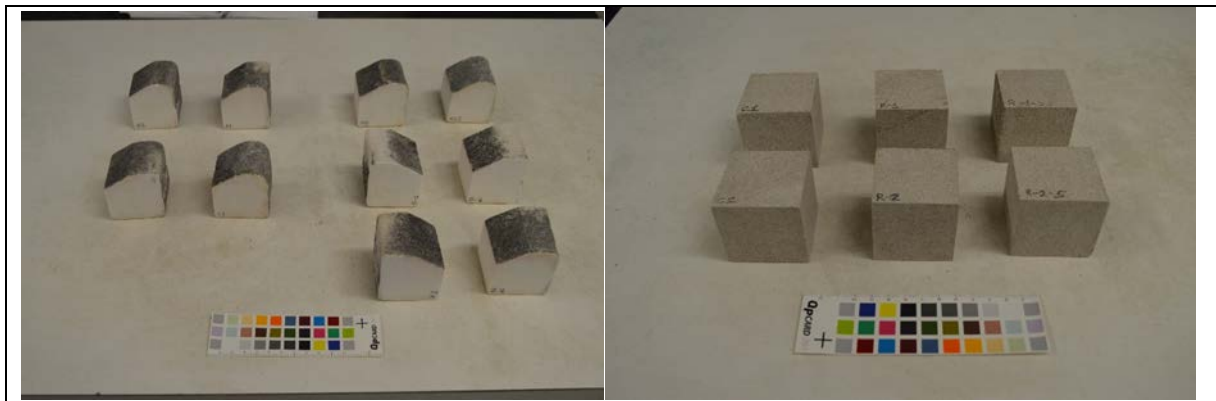


Figure 3. Left: weathered marble samples. Right: Indiana limestone samples.

All samples were weighed and labelled prior to treatment. Since the samples had been in the laboratory for at least a month prior to the experiment, they were not oven dried as it was assumed that they were in equilibrium with the environment. The samples weight and their codes are listed in Table 1.

Two specimens from each of the two samples (marble and Indiana limestone) were used as control. The ethanol-water nanolime dispersion (E25) was applied to eight of the marble specimens while the isopropanol-water nanolime dispersion (I25) was applied to four of the Indiana limestone. Ethanol was chosen for application on the marble samples because of their lower porosity, while isopropanol was selected for the Indiana limestone because of its higher porosity (Borsoi et al, 2016).

Table 1. Weathered marble and Indiana limestone samples and their initial weight prior to treatment. (Balance sensitivity ± 0.1g).

| Environmental Conditions | Weathered marble | | Indiana Limestone | |
|---|---|---|---|---|
| | Code | Weight (g) | Code | Weight (g) |
| Control | C-1 | 353.4 | C-1 | 293.1 |
| Control | C-2 | 363.8 | C-2 | 280.6 |
| Room | R-1 | 360.7 | R-1 | 282.3 |
| Room | R-2 | 348.5 | R-2 | 281.9 |
| Room + spray | R-1-S | 347.1 | R-1-S | 284.1 |
| Room + spray | R-2-S | 372.9 | R-2-S | 277.4 |
| Desiccator 55%RH | 5-1 | 371.2 | - | - |
| Desiccator 55%RH | 5-2 | 378.6 | - | - |
| Desiccator 75%RH | 7-1 | 371.4 | - | - |
| Desiccator 75%RH | 7-2 | 366.6 | - | - |

Before the application, the nanolime dispersions (E25 and I25) were placed in an ultrasonic bath (60 Hz) for 30 minutes to minimize nanoparticle aggregation. The nanolime dispersion E25 was applied by brushing on two of weathered faces of the marble specimens (fig. 4), whereas the I25 dispersion was brush applied on all faces of the Indiana limestone samples. Both products were applied until surface saturation was reached, i.e., when the surface remained wet for 1 minute in a total of 15 applications for marble and 30 for limestone. This operation was carried out within the fume hood because alcohols are VOCs. The specimens were placed on a metallic tray (fig. 4).



Figure 4. Nanolime I25 brush application to the limestone.

To evaluate the influence of RH on carbonation, a pair of treated marble samples was placed in each of the two desiccators with saturated solution of $Mg(NO3)_2$ (RH~55%) and NaCl (RH~75%) respectively. However, while this approach appears reasonable, the fact that the desiccators have a limited volume (approximately 6L) the amount of $CO_2$ present is limited and estimated calculations as to how much lime had been applied on the weathered marble surfaces suggest that they would not carbonate totally (Appendix 1). Therefore, two other samples were exposed to the room environment (50±5% RH, T = 20±5°C) and for comparison, a pair was sprayed daily with carbonated water.
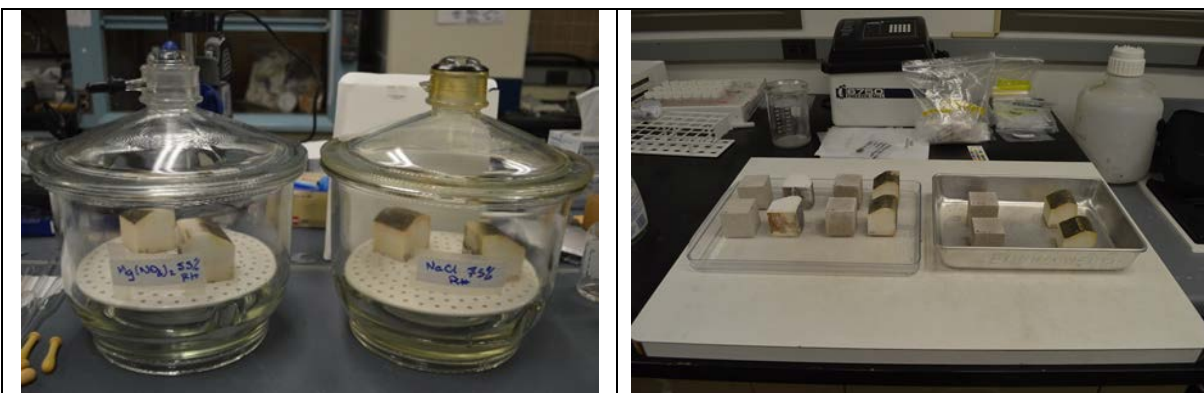


Figure 5. Left: desiccators conditioned to 55% RH (saturated solution of $Mg(NO3)_2$) and 75% RH (s.s. NaCl). Right: control and treated samples at room conditions in left tray; samples sprayed daily with carbonated water (right tray).

The treated marble specimens were kept under the following conditions for 28 days:
- 2 at 75% RH (in a desiccator);
- 2 at 55% RH (in a desiccator);
- 4 at room environment (~55%RH and 20°C).

Of these four, one pair was sprayed daily with carbonated water to enhance carbonation.

The four Indiana specimens were kept at room environment for 28 days, and one pair was sprayed daily with carbonated water (fig.5).

After conditioning for 28 days, the samples were reweighed. None of them showed an increase in weight, except for the two weathered marble samples kept at 75% RH. These increased each by 0.1 g, (7-1 from 371.4 to 371.5; 7-2 from 366.6 to 366.7), most likely reflecting the moisture absorbed in the more humid environment. It is to be taken into account that the samples had received a single application of nanolime and for the case of the weathered marble, only two surfaces received the treatment.

### 3. Experimental carbonation study

The goal of the experiment was to evaluate the carbonation of $Ca(OH)_2$ nanoparticles when other materials are present in the solution. A total of 7 samples (A-G) were prepared using the I25 as the starting dispersion. Their composition is given in Table 2. Sample A corresponds to straight nanolime I25. The nanoparticles used to prepare samples B, C, D and F were extracted from nanolime I25 and the alcohol was replaced by different solvents, such as deionized water, rice water; a 3% w/v urea (Sigma Aldrich, $(NH_2)_2CO$). For samples E and G, the nanoparticles were extracted from a dispersion of nanoparticles still containing chlorides.

Table 2. Nanolime dispersions, where DI stands for deionized water.

| Nanolime | Solvent | Origin of nanoparticles |
|----------|---------|-------------------------|
| A | Isopropanol | I25 |
| B | DI water | I25 |
| C | % w/v Urea in DI water | I25 |
| D | Rice water | I25 |
| E | NaCl solution | Nanoparticles with Cl- |
| F | Carbonated water | I25 |
| G | Water | Nanoparticles with Cl- |

The objective in modifying the solvent was to determine their influence on the carbonation of the nanolime particles. For example, the addition of urea to the water should in principle aid carbonation as urea decomposes according to the following reaction:

$$(NH_2)_2CO + H_2O \quad \rightarrow \quad 2\,NH_3 + CO_2$$
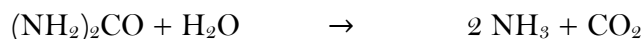
And carbonated water should also, in principle improve the rate of carbonation. Rice water has been used traditionally in China for the preparation of mortars with improved resistance.

The nanolime A sample (I25 dispersion) was first stirred for 10 min, and some milliliters were extracted with a syringe and placed into a small Petri dish.

For the case of samples B-G, the I25 nanolime dispersion was centrifuged for 10 minutes, the i.e., di-ionized water (B), urea solution (C), rice water (D), carbonated water (F), and residual solutions from resin regeneration containing chlorides and some nanoparticles, where (E) had a higher concentration of chlorides than (G). After addition of the solvent, each of the samples was stirred for few minutes and then placed in their corresponding dishes. These were placed on a plastic tray which was protected by a polyurethane board on top to diminish the chance of contamination from suspended air particles in the fume hood falling into them. The samples were left to carbonate for 14 days at room RH and T conditions as shown on fig 5. The samples were sprayed regularly (once a day during working weekdays) with carbonated water to stimulate the carbonation process.

It was observed that the samples that contained water, such as B (DI water) and F (carbonated water) developed a very smooth surface, however, the latter shows small cavities likely formed by carbon dioxide evaporation. On the other hand, sample A (isopropanol) showed a rougher surface; sample C (urea 3% w/v) showed a creep phenomenon (fig 10); and D (rice water) developed a yellowish tinge that can be attributed to the starch in the rice water and showed a cracking pattern similar to that of mud, with the flakes tending to curl up at the edges. Samples E and G had residual chlorides and nanoparticles included and therefore were not analyzed.



Figure 6. Nanolime samples A-G in the fume hood cupboard.

The surfaces of the various petri dishes were examined under a microscope as shown in fig.s 7-10.
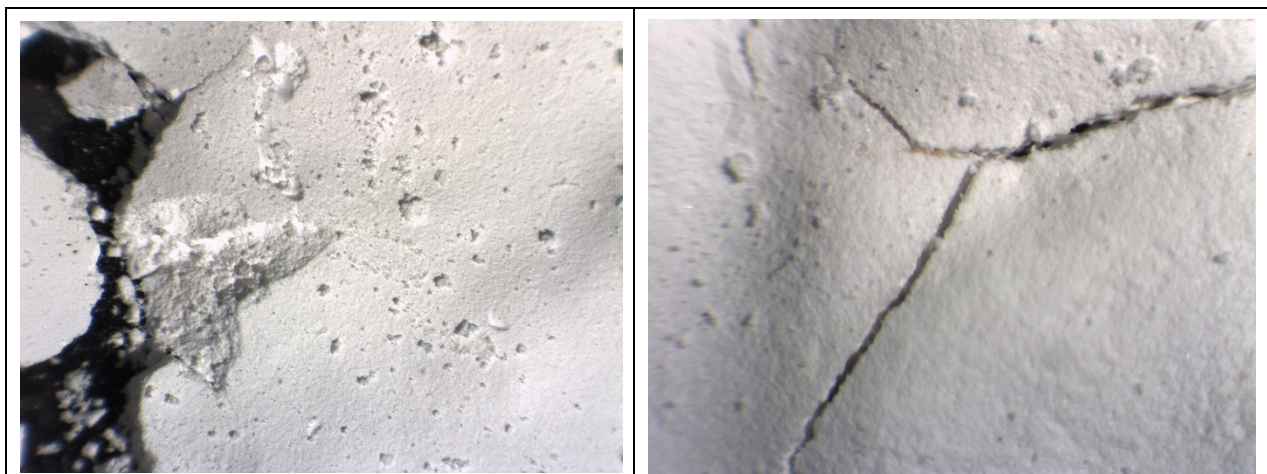


Figure 7. Microphotographs of sample A (I25). Left: details at 12x magnification. Right: Details of a crack at 50x magnification.
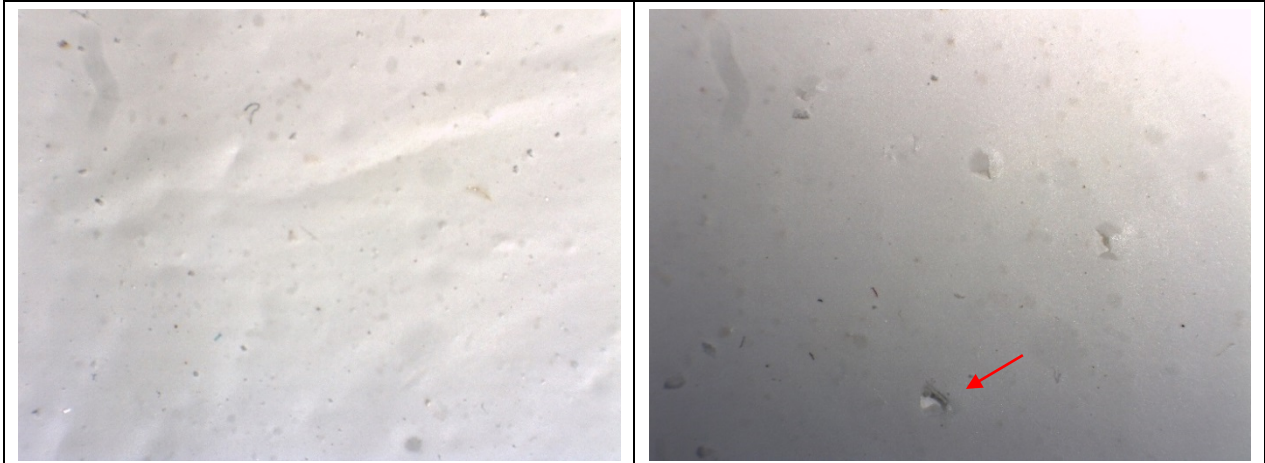
Figure 8. Microphotographs at 10x magnification. Left: sample B (DI) shows a very smooth surface without any cracks. Right: sample F (carbonated water), the smooth surface shows pitting likely to have formed by the evaporation of the CO2 in the carbonated water.
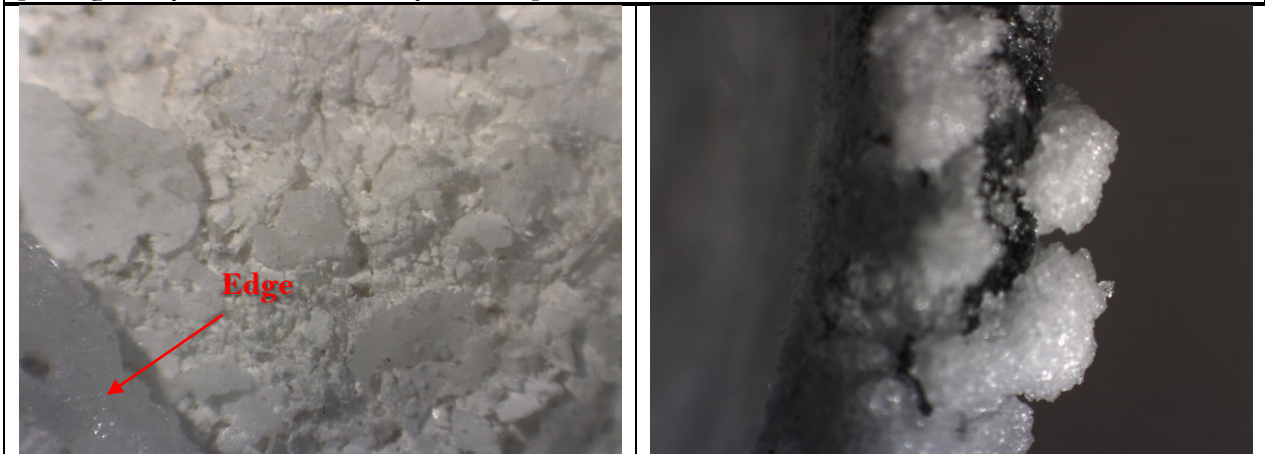


Fig. 9. Cracked surface of sample C (urea) some with a shiny gloss (*left*); and a detail of creep phenomena of urea on to the glass edge of the Petri dish (*right*).
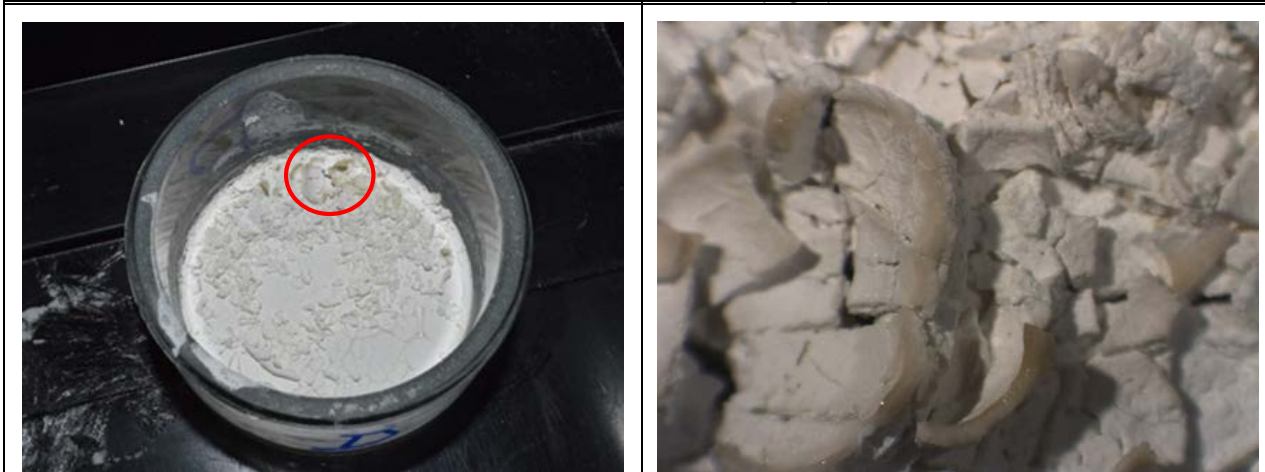


Figure 10. Left: Sample D (rice-water) after 14 days. The surface, with a slightly yellowish tinge, cracked similarly to drying mud and tended to curve. Right: Detail of the curling flakes at 12x magnification.

### *3.1 Mineralogical characterization by XRD*

After 14 days the nanoparticles in samples A-D and F, were analyzed by X-Ray Diffraction (Rigaku D/Max Rapid Micro X-ray Diffractometer) with the collaboration of Nicole Little.

A minuscule sample was taken with a scalper and attached to a glass fiber. The XRD patterns were run from $2\theta$ angle 15° to 60°. Settings and patterns are reported in Appendix 3. All samples contained calcite, except for samples B (DI water), where vaterite was also found, and C (3%w/v urea) where a small peak for urea was found, indicating that not all the urea had decomposed. No portlandite was found suggesting that either all the nanolime had fully carbonated that after 14 days, or that the amount remaining was below 5%, or that the particles were too small to be properly identified.

### *3.2 SEM microscopy*

The morphology of the samples was examined by Hitachi 3700-N SEM with the collaboration of Thomas Lam. Two specimens were taken from each samples (A-D and F), on from the exposed surface, and one from beneath it. They were deposited on a carbon film stuck to a stub and then carbon coated. The samples were observed in at 100, 500, 1000 and 2000x, mostly in backscattered mode (BS), and occasionally in secondary electron mode (SE) on the surface (in contact with atmospheric air) and underneath the sample (Appendix 4).

The particles, presumably calcite, their distribution, morphology and aggregation is very similar for all samples. Interesting was the extremely flat surface of sample B (DI water) (fig. 11) which also had a Dowex resin bead with particles attached to its surface.
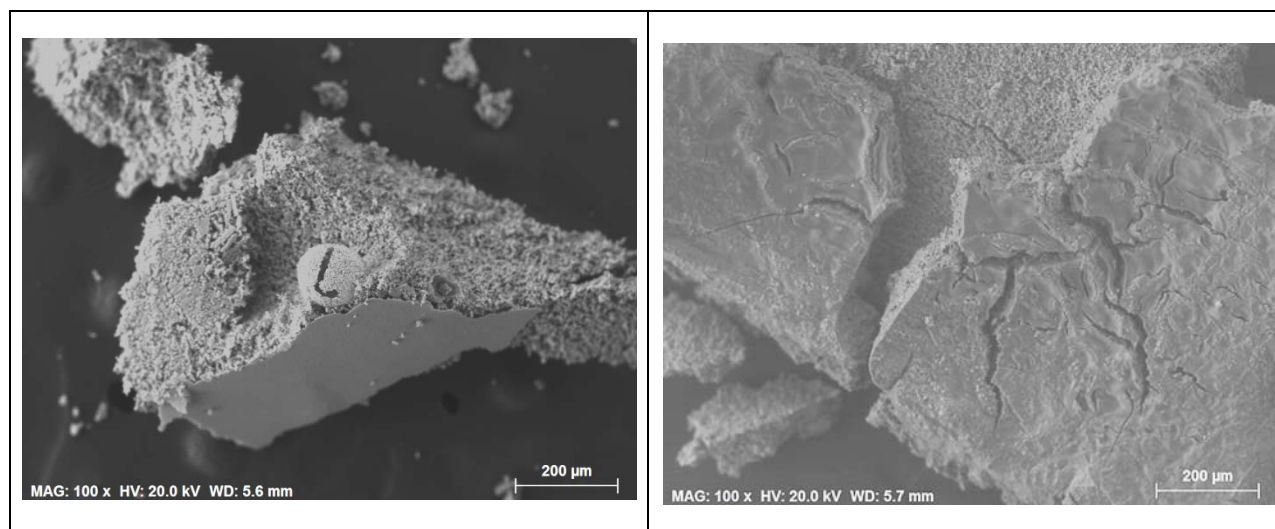


Figure 11. *Left,*BSE image of sample A (DI water) showing the very smooth exterior surface that formed as the sample dried out and carbonated. *Right,* SE image of the cracked surface of sample D (rice water) showing the curling of the flakes. Both figures at 100x (photomicrographs T.F. Lam).

## 4. Specimens treated with nanolime

### 4.1 SEM microscopy

The morphology of the marble and Indiana limestone after application of the nanolime was examined by SEM. For the case of the weathered marble, a surface chip was taken from the corner between the top weathered surface (where the nanolime dispersion had been applied) and two untreated cut surfaces. All specimens of the treated marble, as well as a control, were examined under the SEM. In the case of the Indiana limestone, since all surfaces had received the treatment, a corner chip was removed but the interior fractured surface was examined. The samples were mounted by Thomas Lam so that the surfaces to be examined were flat and they were gold coated. The examination was carried out with Hitachi 3700-N SEM, mostly in secondary electron mode (SE) at three different depths from surface, near surface, medium and lower area with the collaboration of Thomas Lam (Appendix 5).

Of the marble samples, the one kept in the desiccator at 75%RH (7-1) appeared to show some nanolime particles among calcite particles (Figure 12) while at that at 55% RH (5-2) there appeared to be framboidal particles of vaterite (Figure 12), both of these were found right next to the treated weathered surface. Those kept at room conditions (R-2), showed also what appear to be some unreacted nanolime particles, i.e., portlandite (Figure 13), while those sprayed with carbonated water (R-2-S) showed mostly what appear to be calcite crystals.

For the case of the Indiana limestone, it was difficult to see whether new particles had formed, given its heterogeneous texture (Appendix 5).
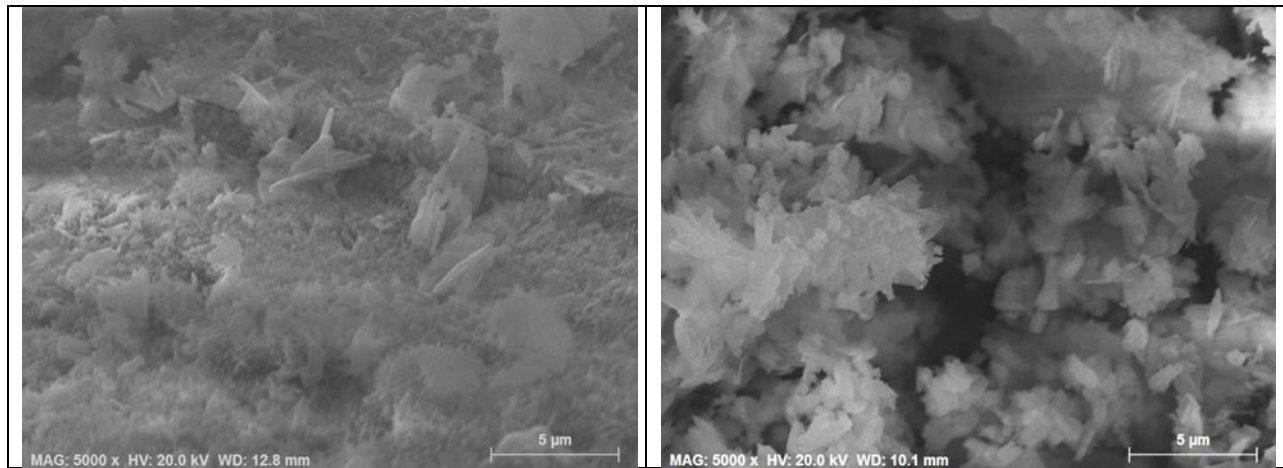


Figure 12. Both photographs were taken close to the weathered surface area. *Left*, sample kept at 75%RH showing some portlandite; *right*, sample kept at 55% RH, showing what appears to be vaterite. (photomicrographs T.F. Lam).
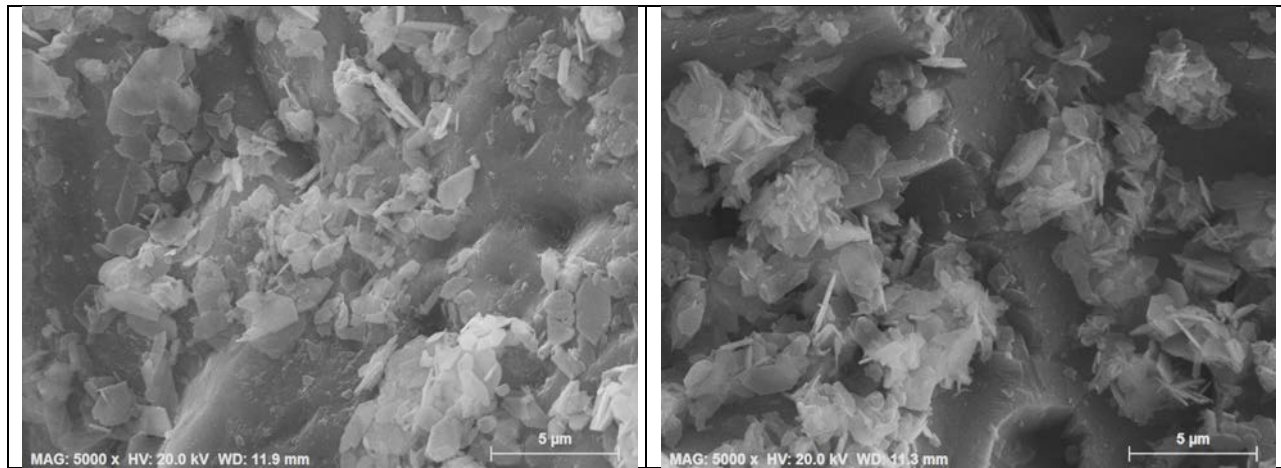
Figure 13. Treated marble specimen, kept at room condition [R-2]. Left, next to the surface; right, an area further away. The hexagonal crystals of what appear to be portlandite are found in both figures, but in the one at right, there are other smaller crystals that could be calcite.
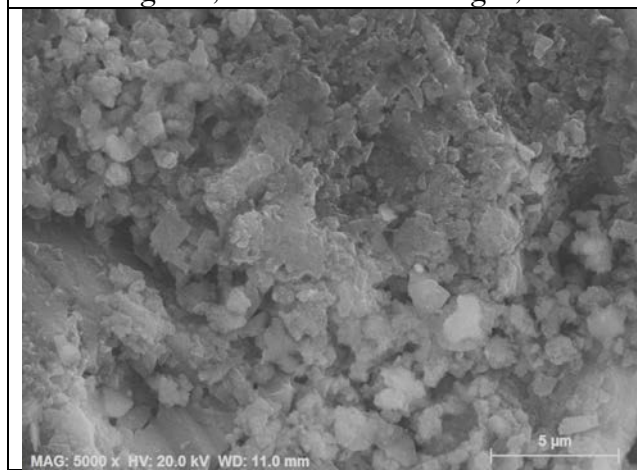


Right, an area further down in the same specimen shows mainly what appear to be calcite crystals. (photomicrographs T.F. Lam).
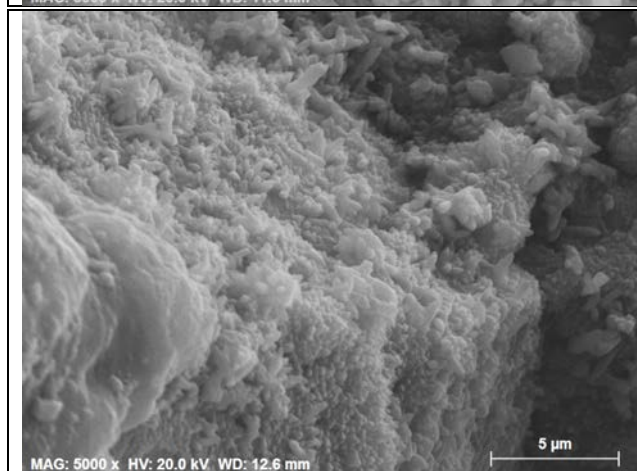




Figure 14. Treated marble at room condition and sprayed with carbonated water [R-2-S]. *Left*, near the treated surface. Mostly calcite crystals are seen with some framboidal vaterite. Right, an area further down showing apparently new calcite crystals but there are fewer of them (photomicrographs T.F. Lam).

## 4.2 Water absorption and drying of the Indiana limestone

To evaluate any change in the porosity of the stone, the cubic Indiana limestone samples were tested following an approach developed by A. Elena Charola (Appendix 6). This approach is based on sequencing existing standards (Normal 11/85 and 29/88; ASTM C67-97 and ASTM C948-94; UNI 10859, 2000; DIN EN 16322, 2013; Borelli, 1999). This approach has proved practical to evaluate the behavior of untreated and treated stone, so ensure that they are compatible with regards to the absorption and release of water, this being one of the key factors in the deterioration of porous inorganic materials.

The test is done in three sections:

1. Capillary water absorption
2. Total immersion in water for 24 hours.
3. Drying behavior.

Since the samples had been in the laboratory for at least a month prior to the experiment, they were not oven dried as it was assumed that they were in equilibrium with the environment. The results of the water absorption show how the water is introduced on the specimens.

The capillary absorption curve obtained for the three samples tested: control (C2); treated and kept at room conditions (R-2); and that treated, kept at room conditioned and sprayed with carbonated water is shown below (fig. 15). It can be seen that the three samples are fairly similar. Sample R-2 is slightly different and that can be attributed to that particular specimen since the three other specimens were practically identical to the C2 and R-2-S specimen. The initial slope of the curve corresponds to the capillary absorption coefficient which ranges from 0.0055 for C2 and R-2-S, to 0.0050 for R-2. The correlation factor for all three values is 0.999.
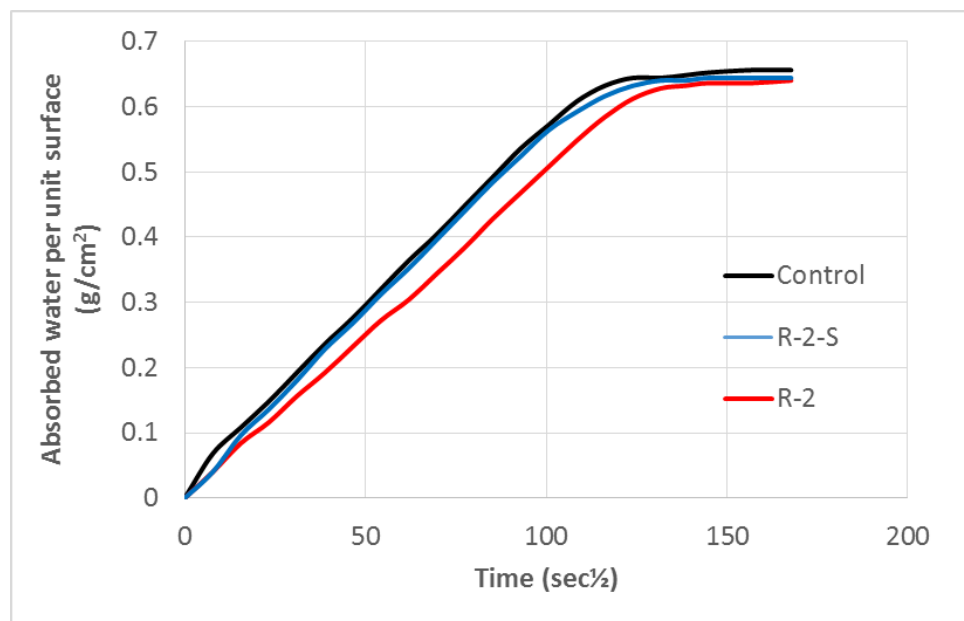


Figure 15. Capillary absorption curves for the three samples, where C2 is the untreated control, R-2, is the treated sample, and R-2-S corresponds to treated and regularly sprayed sample.

Once the sample reached the asymptotical value, ranging from 0.656 (C2), through 0.644 (R-2-S), to 0.640 (R-2), it was taken out and totally immersed in deionized water. From the amount of water absorbed, the apparent porosity as well as the open porosity can be calculated. Table 3 lists these values and shows that the treated samples have a lower porosity than the control confirming that a certain amount of nanolime was introduced and presumably carbonated.

Table 3. Calculated Apparent porosity (% g/g) and Open porosity (cm3/cm3)

| Sample | C-2 | R-2 | R-2-S |
|---|---|---|---|
| Apparent Porosity % w/w | 5.99 | 5.75 | 5.88 |
| Open Porosity % v/v | 13.44 | 12.96 | 13.04 |

The drying curves are shown below (fig.16). They show that all three samples dry at similar rates. The straight initial and final drying rates were calculated and are listed in Table 4. The rates are very similar but both treated samples had a slightly faster initial drying rate.
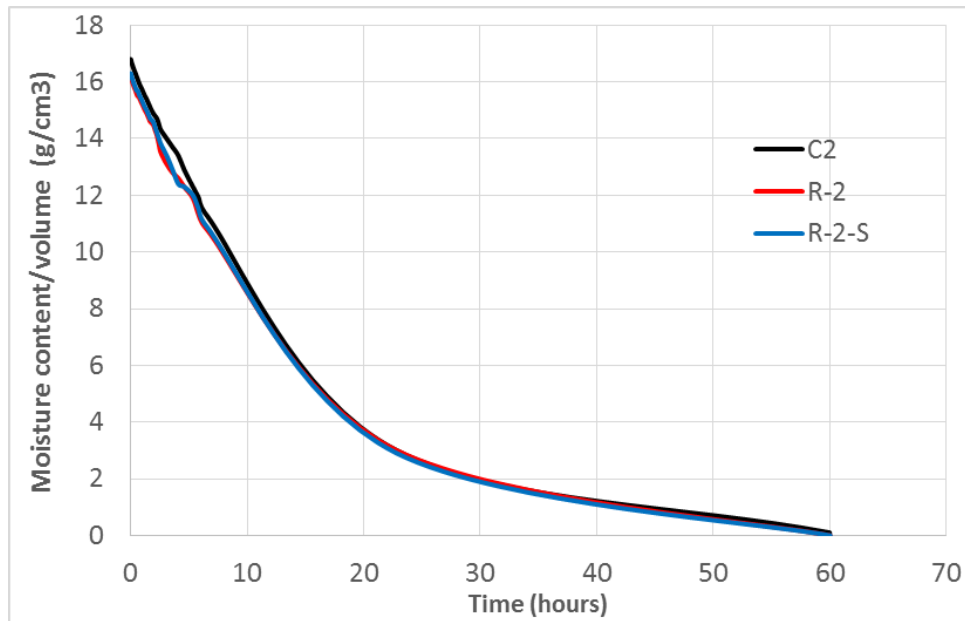


Figure 16. Drying curves for the three Indiana limestone samples. Their behavior is practically identical.

Table 4. Initial and final drying rates for the three samples. Correlation factors are 0.997 or higher.

| Drying rate (g/cm³.h) | C-2 | R-2 | R-2-S |
|---|---|---|---|
| Initial | 0.98 | 0.90 | 0.91 |
| Final | 0.05 | 0.06 | 0.06 |

## 4.3 Infrared spectroscopy

The surface of sample D, nanolime dispersion in rice water, that showed a yellowish tint was analyzed by ATR-FTIR Method (Attenuated Total Reflectance-Fourier Transform Infrared Spectroscopy) using a Thermo Nicolet 6700 a FTIR spectrometer by Gwénaëlle Kavich (Appendix 7). FTIR analysis confirmed the presence of rice starch in the sample as well as calcium carbonate, as expected. No portlandite or vaterite were found. Some extra peaks were also present that could not be attributed.

## 4.4 Tape test (TT)

The consolidation effectiveness with regards to increasing surface cohesion was evaluated by the tape test (TT) for weathered marble after application. For this purpose, the ASTM Standard D 3359 – 09 was used as a guide. The test was carried out over the two weathered surfaces that had been treated on the marble specimens. The test was carried out for samples C1, R-1, R-2-S, 5-1 and 7-1 following the procedure below:

1. A piece of regular tape (2-cm width) is cut to a length of approx. 5.5 cm for each sample.
2. The tape is glued to the weathered area on top and side surfaces.
3. The glued tape is pressed down moderately 5 times uniformly with the thumb.
4. The tape is withdrawn from one side.
5. The tape is stick to a transparent sheet and is labelled.
6. All samples are photographic recorded.

The resulting photographs show the material removed from the surface for all samples (Appendix 8). Macroscopically the results do not show a difference in surface cohesion between the control and the various treated samples and therefore no clear conclusions can be drawn regarding the surface consolidation effect. A photo-analysis is required to obtain a more accurate evaluation and this will be carried out in the near future.

## 5. Conclusions

The undertaken experiments resulted in some interesting observations. For the case of the weathered marble samples, the conditions under which they "cured" was critical: when kept in a desiccator at 75% RH they apparently had not carbonated completely, while those kept at 55% RH showed what appeared to be framboidal vaterite crystals. Kept at laboratory environment, some uncarbonated lime particles were seen; however, when regularly sprayed with carbonated water, mainly calcite crystals were observed. On the other hand, nanoparticles were not clearly evident in the treated Indiana limestone, though from the porosity of the stone evaluation it appears that some nanolime was introduced, and presumably carbonated within this stone.

The experimental carbonation of pure nanolime with different solvents also yielded some interesting results: calcite was found for all samples but no portlandite was found. Vaterite was found in the sample where most alcohol was replaced by de-ionized water, mimicking the situation that would be found in a treated specimen, since the alcohol would be eliminated first.

These are preliminary results and further tests will be required to understand the mechanisms underlying the carbonation process.

An extra supply of an aqueous-ethanol dispersion of nanolime was prepared for testing on deteriorated marble columns or window sills at the former Patent Office Building, now the D.W. Reynolds Center that houses the National Portrait Gallery and the Smithsonian American Art Museum.

# References

ASTM C67-00. *Standard Test Methods for Sampling and Testing Brick and Structural Clay Tile.* West Conshohoken, PA: American Society for Testing Materials, 2000

ASTM C97/C97M-09. *Absorption and Bulk Specific Gravity of Dimension Stone.* West Conshohoken, PA: American Society for Testing Materials, 2009.

ASTM D3359-09. Standard Test Methods for Measuring Adhesion by Tape Test. West Conshohoken, PA: American Society for Testing Materials, 1996.

Borelli E.1999. *Porosity. ARC Laboratory Manual.* Rome: ICCROM. 1999. Available at http://www.iccrom.org/ifrcdn/pdf/ICCROM_14_ARCLabHandbook00_en.pdf

Borsoi G., Lubelli B., van Hees R., Veiga R., Santos Silva A. 2016. *Understanding the transport of nanolime consolidants within Maastricht limestone.* Journal of Cultural Heritage 18:242-249.

Dei L.,Salvadori B. 2006. *Nanotechnology in cultural heritage conservation: nanometric slaked lime saves architectonic and artistic surfaces from decay.* Journal of Cultural Heritage 7[2]:110–115. Available at: http://linkinghub.elsevier.com/retrieve/pii/S1296207406000021

DIN EN 16322. 2013. *Erhaltung des kulturellen Erbes −Prüfverfahren −Trocknungsverhalten.* Berlin: Deutsches Institut für Normung e.V.

NORMAL 11/85. 1985. Capillary water absorption and capillary absorption Coefficient.  Rome: CNR-ICR.

NORMAL 29/88. 1988. Measurement of the drying index.  Rome: CNR-ICR.

Rossi Manaresi R., Charola A.E., Tucci A., Koestler, R.J., Wheeler G.E. 1984. *Study of accelerated weathering of limestones treated with an acryilic-silicone mixture.* ICOM 7th Triennial Meeting, Copenhagen. pp. 84.10.1-84.10.4. Paris: ICOM-J. Paul Getty Trust.

Taglieri G., Daniele V., Del Re G., Volpe R. 2015. *A new and original method to produce Ca(OH)2 nanoparticles by using an anion exchange resin.* Advances in Nanoparticles 4:17-24.

UNI 10859. 2000. *Beni culturali. Materiali lapidei naturale ed artificiali. Determinazione dell'assorbimento d'acque per capillaritá.* Milan: Ente Nazionale Italiano di Unificazione.

## Calculations

### 1. Nanolime concentration in dispersion

To obtain a concentration of 25g/L nanolime, the following amounts of calcium chloride and water were used:

20g $CaCl_2$ $2H_2O$ were dissolved in 400 ml $pH_2O$ (0.4 L)

Since the MW of $CaCl_2$ $2H_2O$ (Molecular weight) = 147 g/mol, the number of moles in a given amount of this compound is calculated by:

$$n = \frac{g}{MW}$$

Thererefore $\quad n = \frac{20\ g}{147g/mol} = 0.13$ moles

Consequently the molar concentration $M = \frac{n}{v} = \frac{0.13\ moles}{0.4\ L} = 0.34$ M

After the synthesis, the original volume is reduced due to absorption by the resin, and it was measured to be final volume 260 mL (0.26L)

The number of moles of nanolime can be estimated from the original Molar concentration of the solution (0.34 M) and the final volume (0.26 mL) obtained, as follows:

$0.34$ M $= \frac{n}{0.26\ L} = 0.0884$ moles of $Ca(OH)_2$

And knowing that the molecular weight of $Ca(OH)_2$ is 74 g/mole the number of grams of $Ca(OH)_2$ obtained can be calculated

$0.884$ moles $= \frac{g}{74\ g/mol}$ therefore $\quad g = 6.54$ g of $Ca(OH)_2$

Final concentration $= \frac{g}{l}$

Final concentration $= \frac{6.54\ g}{0.26\ L} = \mathbf{25.16\ g/L}$ of $Ca(OH)_2$

## 2. Amount of calcite and gypsum on very weathered marble

To determine the % of gypsum and calcite from the results obtained by EDS (Appendix 2). Note that samples 1 and 2 are similar but different from the others. Samples 3 and 6 are similar, having the highest content of gypsum. Samples 4, 5 and 7 are similar and have the highest content of Ca.

Table 1. Mass percent (%)

| Spectrum | C | N | O | F | Na | Mg | Al | Si | P | S | Cl | K | Ca |
|---|---|---|---|---|---|---|---|---|---|---|---|---|---|
| 1 | 16.79066 | 1.540845 | 47.3325 | | 2.152108 | 0.230122 | 9.105668 | 9.29043 | 0.05758 | 0.057228 | | 0.7241 | 12.71876 |
| 2 | 15.25814 | 1.272749 | 49.40926 | | 0.350346 | 0.314648 | 7.695298 | 9.547754 | 0.087822 | 0.129327 | | 3.036463 | 12.8982 |
| 3 | 35.24375 | 4.354829 | 38.13419 | | 0.209832 | 0.16926 | 1.377084 | 0.234551 | 0.393739 | 1.125226 | 0.172288 | 0.49422 | 18.09103 |
| 4 | 18.16784 | 1.698172 | 48.24814 | | 0.091324 | 0.085476 | 1.391571 | 0.180358 | 0.150642 | 0.139643 | | | 29.84683 |
| 5 | 15.90634 | | 50.05432 | 0.596348 | 0.12322 | 0.074712 | 1.185629 | 0.110812 | 1.847587 | 0.150378 | 0.063436 | | 29.88722 |
| 6 | 36.19084 | 3.811274 | 39.70218 | | 0.163009 | 0.164786 | 1.032975 | 0.12963 | 0.133428 | 0.236415 | 0.035089 | 0.384327 | 18.01605 |
| 7 | 17.86048 | 2.113561 | 49.37093 | | 0.03559 | 0.060253 | 1.018554 | 0.110506 | 0.413669 | 0.097523 | 0.089052 | | 28.82989 |
| | | | | | | | | | | | | | |
| Mean value: | 22.20258 | 2.465238 | 46.03593 | 0.596348 | 0.44649 | 0.157037 | 3.258111 | 2.800577 | 0.440638 | 0.276534 | 0.089966 | 1.159777 | 21.46971 |
| Sigma: | 9.291872 | 1.293906 | 4.962825 | 0 | 0.758752 | 0.092788 | 3.539463 | 4.522129 | 0.636674 | 0.378231 | 0.059141 | 1.259107 | 7.837898 |
| Sigma mean | 3.511997 | 0.489051 | 1.875771 | 0 | 0.286781 | 0.035071 | 1.337791 | 1.709204 | 0.24064 | 0.142958 | 0.022353 | 0.475898 | 2.962447 |

To determine the % mass of gypsum, we select the sample with highest amount of S, which is the sample 3 (Table 1), and we calculate the grams of $CaSO_4$ in base on the S mass percent (%). After this, we calculate the grams of $CaCO_3$.

Where:   $CaSO_4.2H_2O$ MW=172.17 (Ca=23.28; S=18.62; O=55.76; H=2.34)

$CaCO_3$ = 100.08 (Ca=23.28; C=12; O=48)

In sample 3:   S = 1.125 g     and  Ca= 18.091

$CaSO_4.2H_2O$ (Ca = 1 mol; S= 1mol; O= 6moles; H= 2 mol)

$CaCO_3$ (Ca = 1 mol; C= 1mol; O= 3moles)

| | 3 | Gypsum | |
|---|---|---|---|
| | G | M | g |
| S | 1.125226 | 0.035163 | 1.125226 |
| | | 0.21098 | 3.375677 |
| Ca | | 0.035163 | 1.406532 |
| | | | 5.907434 |

| | 3 | Calcite | |
|---|---|---|---|
| | G | M | G |
| C | | 0.417112 | 5.005349 |
| O | | 1.251337 | 20.02139 |
| Ca | 16.6845 | 0.417112 | 16.6845 |
| | | | 41.71124 |

**Sample 3** has an estimated amount of  **~5-6 %w/w gypsum** and **~ 40-42%w/w calcite.**

**Sample 7** has the lowest sulfur content  >0.1%w/w, and since these calculations are merely approximations, only the amount of calcite can be estimated. The amount of Ca 28.83% w/w, corresponds to (28.83g/40 g/mol) = 0.72 moles of Ca, and since there is 1 mol of Ca in 1 mol of CaCO3, this means that there are 0.72 moles of calcite.

Calcite %w/w = (0.72 moles*100 g/mol) = 72 %w/w

**Sample 7** has an estimated amount of **70-72 %w/w calcite**.

## 3. Estimation of carbon dioxide (CO₂) within the desiccators and amount of nanolime applied to the specimens.

Since the desiccators have a limited volume, the amount of $CO_2$ available for lime carbonation is constrained. The concentration of $CO_2$ available within desiccators was calculated as follows:

### 3.1 Volume in the desiccator
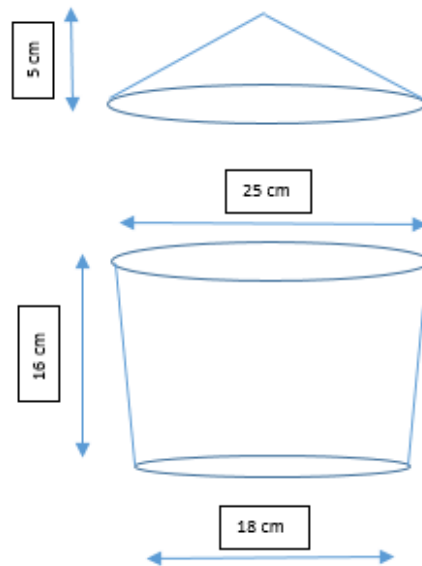


Figure 1. Desiccator's approximate measurements

The total desiccator volume is calculated as the sum of the two conical structures volumes ($V_T$), a regular cone and a truncated cone, calculated by the following formulas:
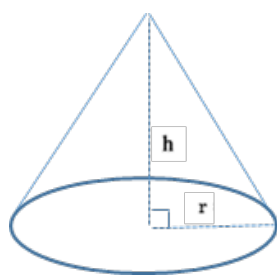


$$V = \frac{1}{3} \pi r^2 h$$
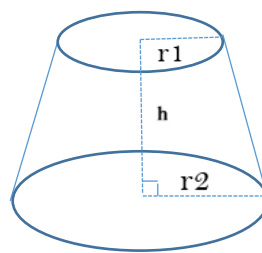
$$V = \frac{1}{3} \pi h_2 (r_2{}^2 + r_1{}^2 + r_1 r_2)$$

Where: r = lower radius of the cone; $h_1$ = height of cone; $h_2$ = height for the truncated cone; $r_2$ = lower radius of the truncated cone; $r_1$ = upper radius of the truncated cone

3

**Calculations:**

1. Volume for the cone:    h = 5 cm and r = 12.5 cm

$V = \frac{1}{3} \pi r^2 h_1$

$V = \frac{1}{3} \pi 12.5^2 x 5$

| $V = 818$ cm³ |

2. Volume for the truncated cone:  h = 16 cm; $r_1$ = 12.5 cm; $r_2$ = 9 cm

$V = \frac{1}{3} \pi h (r_2{}^2 + r_1{}^2 + r_1 r_2)$

$V = \frac{1}{3} \pi 16 (9^2 + 12.5 + 12.5 \text{ x } 9)$

| $V = 5860$ cm³ |

3. Total volume for desiccator

$$V_T = V_{cone} + V_{truncated\ cone}$$

Where:  $V_T$ = total volume; $V_{cone}$ = volume of the cone; $V_{truncated\ cone}$ = volume of the truncated cone

$V_T = 818.12 + 5860.11$

| $V_T = 6678$ cm3 |

### 3.2 Amount of CO2 within the desiccator

To calculate the amount of carbon dioxide available for carbonation within the desiccator, it is taken as a reference the global average amount of $CO_2$ at earth's atmosphere, as it is shown on the table 1.

Table 1. Air composition by mass.

| $N_2$ | $O_2$ | Ar | $CO_2$ |
|-------|-------|-----|--------|
| 78.09% | 20.95% | 0.93% | **0.039%** |

The amount of $CO_2$ within the desiccator is calculated based on the percentage of CO2 in 100 ml of air and the volume of the desiccator($V_T$).

Total amount of $CO_2$ in desiccator $= \frac{VT \ x \ mL \ CO2 \ in \ 100 \ ml}{100 \ ml}$

Total amount of $CO_2$ in desiccator $= \frac{6678.11 \ mL \ x \ 0.039 \ mL}{100}$         | **2.603 mL** of CO2 |

Finally the carbon dioxide moles are calculated using the following density and mole number formulas:

$$\delta = \frac{m}{v} \qquad n = \frac{m}{mw}$$

Where:  density of $CO_2$ = 1.98 g/L (0.00198 g/mL) and MW of $CO_2$ (molecular weight) = 44.01 g/mol

**Calculations:**

m = 0.00198 g/mL x 2.6 mL    m = 0.0051 grams of $CO_2$ in desiccator

$n = \frac{0.0051\ g}{44.01\ g/mol}$    n = 0.00011 moles    $\boxed{\textbf{0.11 mM} \text{ of } CO_2 \text{ in desiccator}}$

### 3.3 Amount of Ca(OH)$_2$ in the samples

The amount of $Ca(OH)_2$ introduced in the weathered marble samples was calculated taking in consideration the number of applications and the concentration of the product. Each sample absorbed a total of 15 brush applications and we estimate that each brush application corresponds approximately to 1mL of the nanolime product, giving a total of 15 mL of absorbed product. The nanolime has concentration of 25 g/L, so the approximate grams introduced on weathered samples is calculated by multiplying:

Grams of $Ca(OH)_2$ introduced on samples $= \frac{Total\ product\ absorbed\ \ x\ 25\ grams}{1000\ mL}$

Grams of $Ca(OH)_2$ introduced on samples $= \frac{15\ mL\ \ x\ 25\ g}{1000\ mL}$    $\boxed{\textbf{0.375 g} \text{ of } Ca(OH)_2 \text{ per marble sample}}$

From this value, the number of calcium hydroxide moles are calculated:

$$n = \frac{m}{mw} \qquad \text{MW of } Ca(OH)_2\ = 74\ g/mol$$

$n = \frac{0.375\ g}{74\ g/mol}$    n = 0.0050 moles of $Ca(OH)_2$ per marble sample    $\boxed{n = \textbf{5.06 mM} \text{ of } Ca(OH)_2 \text{ per marble sample}}$

Since there were two samples, this would correspond roughly to 10 mM of $Ca(OH)_2$ that to carbonate totally would require 10 mM of $CO_2$, i.e., it would require a closed environment 100 times larger than the desiccator used in this experiment.

# Report on the SEM-EDS examination/analysis of an extremely weathered marble specimen

Jorge Otero (MCI Intern), A. Elena Charola (Research Scientist), Thomas F. Lam (Physical Scientist), Carol Grissom (Senior Objects Conservator)

June 16, 2016

## Introduction

The specimen examined in this report is a severely weathered piece of white marble obtained from a pile of architectural marble blocks at the Garber facility. The marble is being studied as part of a research project, for which cubes of the marble have been consolidated with nano-lime solutions by the first author. The purpose of the current study is to identify components in the marble sample and the source of red discolorations; that is, whether the latter are from biocolonization or soiling.

## Description

The specimen of white marble had degraded to the point where it was delicate to handle and showed extreme surface disaggregation (Figure 1). It is roughly triangular in shape with the longest edge measuring around 7.5 cm and the other two edges approximately 5.5 cm in length; thickness ranges between 2 and 2.5 cm. The surface has a grayish tint, probably from soiling and/or biocolonization, and a reddish coloration below, thought to be from biocolonization.
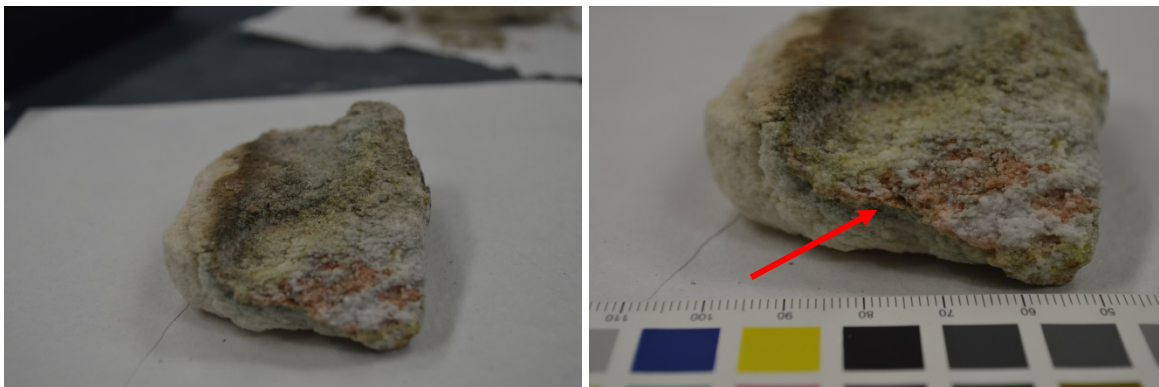


Figure 1. The deteriorated marble sample showing reddish coloration along a subsurface plane parallel to the exterior grayish surface. Arrow point to the area from which the specimen used for SEM was taken.

On May 5, 2016, the sample was examined microscopically to visualize fungal hyphae from biocolonization in reddish areas using MCI's Hirox optical microscope and Hitachi 3700-N SEM operated by Lam. Hyphae or other biocolonizing species failed to be seen using the Hirox at 160x

magnification, and a specimen of the sample (see Figure 1 for location) was then placed in the variable pressure Hitachi scanning electron microscopy (VP-SEM) at an acceleration voltage of 10 kV. EDS analyses were performed using the Bruker XFlash Detector 4010 energy dispersive spectrometer with Esprit software. A probe current of approximately between 2 and 8 nA was used in acquisition of the EDS data.

Figure 2, a low magnification BSE (backscattered electron mode) image of the severely weathered marble, shows extensive cracking between calcite crystals of the marble. Figure 3 shows a higher magnification of these grains. Figure 3 shows a higher magnification of these grains. An observable lower atomic number contrast film (darker feature in backscattered electron mode (BSE) was present. The lower atomic number contrast and the fiber-like nature of the film is consistent with the reported morphology of a hyphae biofilm (Koestler et al., 1985). Figure 4 shows examples of fiber like hyphae bridging over the cracks of the calcite crystal.
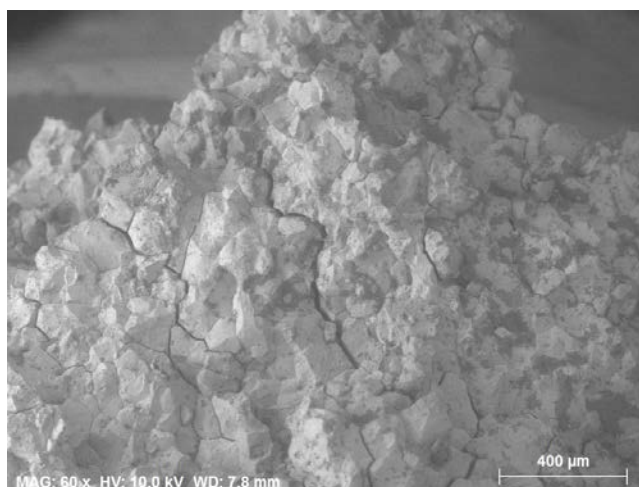


Figure 2. BSE SEM micrograph showing extensive cracking between calcite crystals of the marble at 60x magnification.

Figure 3. Higher magnification BSE SEM micrograph of the calcite grains covered by a biofilm with hyphae visible. Area marked by the circle is shownin detail in the following figure.
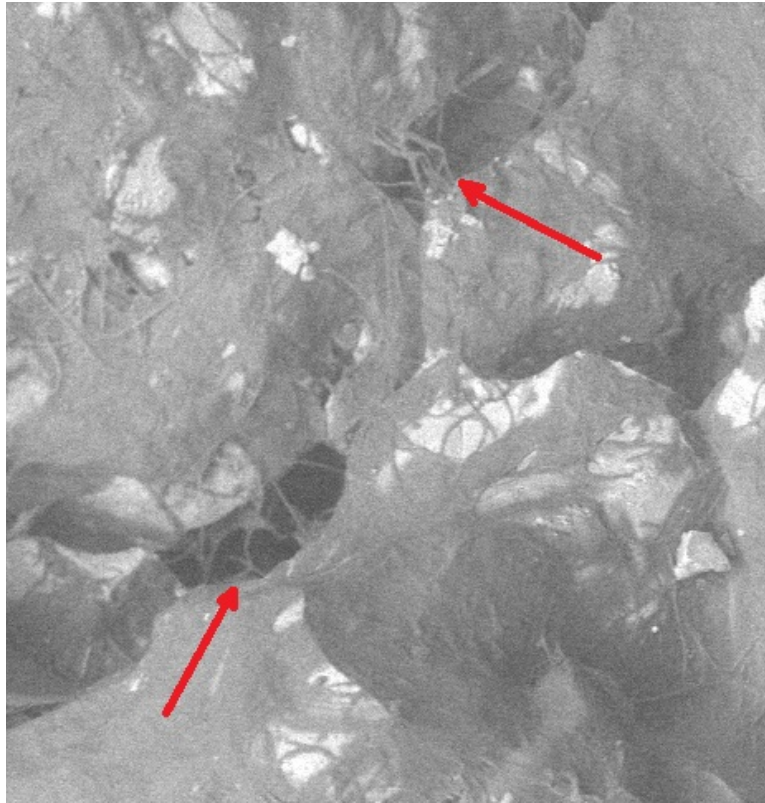


Figure 4. Detail of the previous figure; arrows indicate hyphae covering and bridging calcite grains.

Figure 5 shows a region of interest where six areas were selected for elemental analyses via energy dispersive spectroscopy (EDS); elemental analyses for the areas are reported in Table 1. Particles 1 and 2 appear to be either a mica or alkali feldspars, based on their appearance and the relatively high content of silicon and aluminum, as well as calcium, sodium, potassium, and magnesium. Areas 4, 5 and 7 have a similar composition, while areas 3 and 6 are similar to each other. Interestingly, point 5 shows the presence of fluorine and the highest value for phosphorous; no nitrogen was detected.
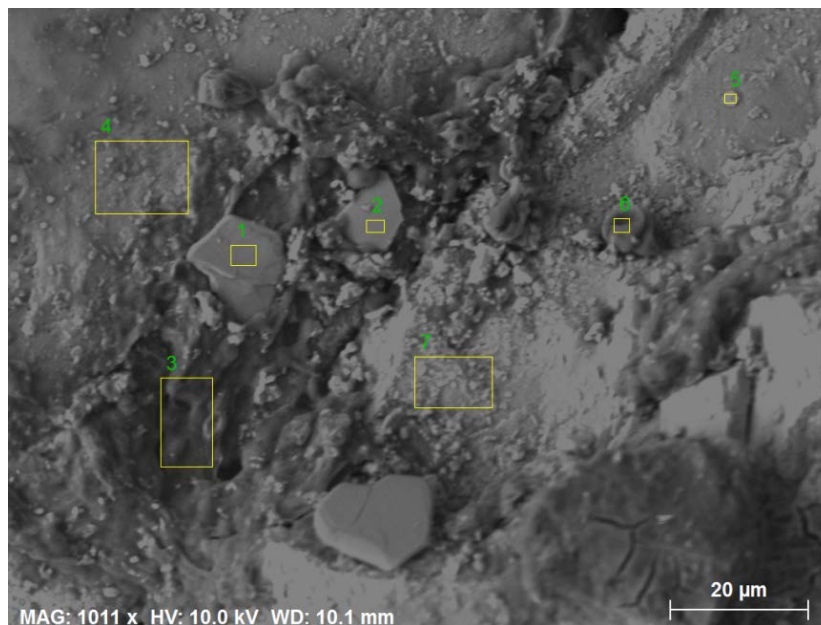
Figure 5.  BSE SEM micrograph of the surface. Elemental analysis via EDS was carried out on the
points marked and data is shown in Table 1.

Table 1. Atomic % composition of the seven points marked on the above SEM photomicrograph.

| Spectrum | C | N | O | F | Na | Mg | Al | Si | P | S | Cl | K | Ca |
|---|---|---|---|---|---|---|---|---|---|---|---|---|---|
| 1 | 25.07 | 1.97 | 53.04 | | 1.68 | 0.17 | 6.05 | 5.93 | 0.03 | 0.03 | | 0.33 | 5.69 |
| 2 | 23.06 | 1.65 | 56.06 | | 0.28 | 0.23 | 5.18 | 6.17 | 0.05 | 0.07 | | 1.41 | 5.84 |
| 3 | 47.17 | 5.00 | 38.31 | | 0.15 | 0.11 | 0.82 | 0.13 | 0.20 | 0.56 | 0.08 | 0.20 | 7.26 |
| 4 | 27.66 | 2.22 | 55.14 | | 0.07 | 0.06 | 0.94 | 0.12 | 0.09 | 0.08 | | | 13.62 |
| 5 | 24.74 | | 58.45 | 0.59 | 0.10 | 0.06 | 0.82 | 0.07 | 1.11 | 0.09 | 0.03 | | 13.93 |
| 6 | 47.86 | 4.32 | 39.42 | | 0.11 | 0.11 | 0.61 | 0.07 | 0.07 | 0.12 | 0.02 | 0.16 | 7.14 |
| 7 | 27.00 | 2.74 | 56.03 | | 0.03 | 0.05 | 0.69 | 0.07 | 0.24 | 0.06 | 0.05 | | 13.06 |

Table 2.  Mass % composition of the seven points marked on Figure 5.

| Spectrum | C | N | O | F | Na | Mg | Al | Si | P | S | Cl | K | Ca |
|---|---|---|---|---|---|---|---|---|---|---|---|---|---|
| 1 | 16.79 | 1.54 | 47.33 | | 2.15 | 0.23 | 9.11 | 9.29 | 0.06 | 0.06 | | 0.72 | 12.72 |
| 2 | 15.26 | 1.27 | 49.41 | | 0.35 | 0.31 | 7.70 | 9.55 | 0.09 | 0.13 | | 3.04 | 12.90 |
| 3 | 35.24 | 4.35 | 38.13 | | 0.21 | 0.17 | 1.38 | 0.23 | 0.39 | 1.13 | 0.17 | 0.49 | 18.09 |
| 4 | 18.17 | 1.70 | 48.25 | | 0.09 | 0.09 | 1.39 | 0.18 | 0.15 | 0.14 | | | 29.85 |
| 5 | 15.91 | | 50.05 | 0.60 | 0.12 | 0.07 | 1.19 | 0.11 | 1.85 | 0.15 | 0.06 | | 29.89 |
| 6 | 36.19 | 3.81 | 39.70 | | 0.16 | 0.16 | 1.03 | 0.13 | 0.13 | 0.24 | 0.04 | 0.38 | 18.02 |
| 7 | 17.86 | 2.11 | 49.37 | | 0.04 | 0.06 | 1.02 | 0.11 | 0.41 | 0.10 | 0.09 | | 28.83 |

With the known information that the bulk material of marble consists of calcite, EDS results for regions 4, 5 and 7 can be calculated as having the highest calcite ($CaCO_3$) content, around 70%. Region 3 shows the highest content of sulfur. Assuming the sulfur content is the result of gypsum ($CaSO_4.2H_2O$), the mass % of sulfur present can be calculated to be approximately 5% gypsum, with the remaining content of calcium corresponding to about 40% calcite. Area 6 could be calculated to have nearly 45% calcite. The remaining about 50% is given by the sum of carbon, nitrogen and oxygen, possibly reflecting the biocolonization materials. However, it should be noted these results are only approximations, since data were acquired in variable pressure mode; the exact carbon and oxygen content are likely to be lower than reported here.

An additional set of EDS analyses was carried out on another area of the sample (Figure 6).
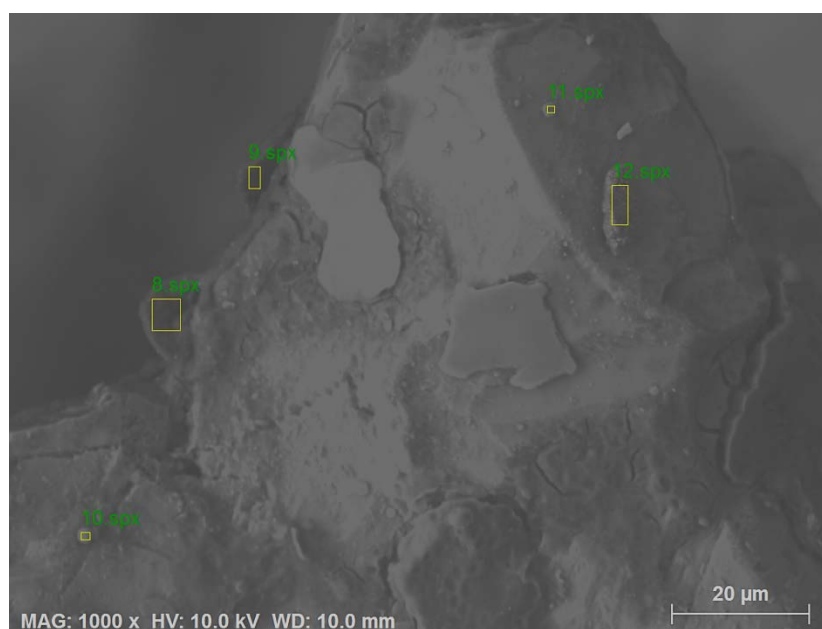


Figure 6. BSE SEM micrograph of another area of the sample, showing some flaking and areas marked where EDS analyses were carried out (see Tables and 4)

Table 3. Atomic % analyses of the 5 areas marked in Figure 6.

| Spectrum | C | N | O | F | Na | Mg | Al | Si | P | S | Cl | K | Ca | Ti | Fe |
|---|---|---|---|---|---|---|---|---|---|---|---|---|---|---|---|
| 8 | 49.77 | 7.39 | 34.76 | | 0.31 | 0.09 | 1.36 | 0.22 | 0.04 | 0.13 | 0.24 | 0.18 | 5.51 | | |
| 9 | 48.24 | | 39.33 | | 0.37 | 0.18 | 2.26 | 0.67 | 0.08 | 0.15 | 0.22 | 0.34 | 7.84 | 0.33 | |
| 10 | 45.50 | | 40.92 | | 0.05 | 0.03 | 1.00 | 7.12 | 0.04 | 0.03 | 0.07 | | 5.25 | | |
| 11 | 25.47 | | 56.31 | 0.85 | 0.13 | 0.04 | 1.29 | 0.07 | 1.72 | 0.08 | 0.08 | 0.16 | 13.79 | | |
| 12 | 50.30 | | 38.42 | | 0.14 | 0.24 | 1.52 | 0.28 | 0.07 | 0.03 | | | 5.27 | | 3.72 |

Table 4.  Mass % analyses of the 5 areas marked in Figure 6.  Both titanium and iron were identified in spot 9 and 12, respectively.

| Spectrum | C | N | O | F | Na | Mg | Al | Si | P | S | Cl | K | Ca | Ti | Fe |
|----------|------|------|-------|------|------|------|------|-------|------|------|------|------|-------|------|-------|
| 8 | 38.53 | 6.67 | 35.84 | | 0.45 | 0.14 | 2.36 | 0.41 | 0.07 | 0.27 | 0.54 | 0.46 | 14.24 | | |
| 9 | 34.91 | | 37.91 | | 0.51 | 0.27 | 3.67 | 1.13 | 0.15 | 0.29 | 0.47 | 0.81 | 18.92 | 0.96 | |
| 10 | 33.23 | | 39.81 | | 0.07 | 0.04 | 1.63 | 12.16 | 0.08 | 0.06 | 0.14 | | 12.79 | | |
| 11 | 16.26 | | 47.88 | 0.86 | 0.16 | 0.05 | 1.85 | 0.10 | 2.84 | 0.14 | 0.14 | 0.34 | 29.37 | | |
| 12 | 35.56 | | 36.17 | | 0.20 | 0.34 | 2.42 | 0.47 | 0.12 | 0.07 | | | 12.43 | | 12.23 |

A third set of analyses was carried out on the area of the sample as shown in Figure 7; results are listed in Tables 5 and 6.
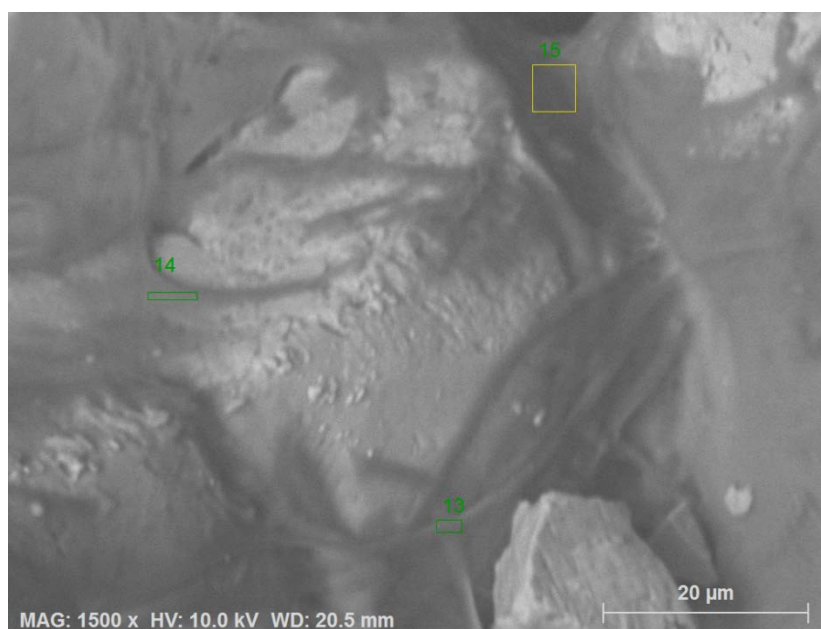


Figure 7. The areas marked show the three spots where EDS analyses were carried out.

Table 5. Atomic % analyses of the three areas marked in Figure 7.  Phosphoros is found in spots 14 ad 15, taken on hyphae, and nitrogen on spot 13, which appears to be covered by a biofilm.

| Spectrum | C | N | O | Na | Mg | Al | Si | P | S | K | Ca |
|----------|-------|------|-------|------|------|------|------|------|------|------|------|
| 13 | 43.12 | 7.20 | 43.42 | 0.03 | 0.08 | 0.16 | 0.46 | 0.00 | 0.03 | 0.18 | 5.31 |
| 14 | 43.29 | | 50.00 | 0.04 | 0.03 | 0.06 | 0.19 | 0.07 | 0.02 | 0.04 | 6.25 |
| 15 | 51.22 | | 44.03 | | | 0.08 | 0.17 | 0.05 | | 0.02 | 4.43 |

Table 6. Mass % analyses of the three areas marked in Figure 7.  Phosphoros was found in spots 14 ad 15, and nitrogen on spot 13, which appears to be covered by a biofilm.

| Spectrum | C | N | O | Na | Mg | Al | Si | P | S | K | Ca |
|---|---|---|---|---|---|---|---|---|---|---|---|
| 13 | 33.33 | 6.49 | 44.70 | 0.04 | 0.13 | 0.28 | 0.83 | 0.01 | 0.07 | 0.44 | 13.68 |
| 14 | 32.83 | | 50.51 | 0.06 | 0.05 | 0.10 | 0.34 | 0.14 | 0.04 | 0.11 | 15.82 |
| 15 | 40.84 | | 46.77 | | | 0.14 | 0.32 | 0.09 | | 0.05 | 11.78 |

**Conclusion**

SEM examination of an extremely deteriorated, discolored marble sample confirmed the presence of biocolonization in the form of hyphae and elemental results. The biocolonization was not visible using a Hirox microscope, which was puzzling.  As expected, the EDS analyses confirmed that the marble consists largely of calcite and the presence of gypsum as an agent of deterioration, indicating that the building, not identified as yet, was exposed to air pollution for some years. EDS analyses on the various areas showed that phosphorous was present in all 15 areas analyzed, while nitrogen only appeared in 8 of them.

**Reference**

Koestler, R.J., Charola, A.E., Wypyski, M., Lee, J.J. 1985. *Microbiologically Induced Deterioration on Dolomitic and Calcitic Stone as viewed by SEM*. 5th Int. Conf. Deterior. Conserv. Stone, ed. G. Félix, pp. 617-626. Lausanne: Presses Polytechniques Romandes.

Smithsonian
Museum Conservation Institute

# Appendix 3

# Report: Identification of carbonated nanolime phases by XRD

MCI#: 6702.1
Date: modern
Materials: carbonated nanolime
Sample: white powder
Requested by: Jorge Otero (Intern, MCI), A. Elena Charola (Research Scientist, MCI)
      Telephone: 301-238-1213
      E-mail: OteroJ@si.edu, CharolaA@si.edu
Unit: MCI
Analyst: Nicole Little, Physical Scientist
Analysis date: 6-6-2016

*XRD Method (X-ray diffraction)*
    Instrument: Rigaku D/Max Rapid Micro X-ray Diffractometer

    Radiation: Copper Kα

    Power: 50 kV; 40 mA; 2.00 kW

    Goniometer:

      a) chi: fixed at 45°

      b) phi: fixed at 0° unless otherwise indicated

    Samples were mounted on a glass fiber

    Experimental Conditions:

| Sample | Collimator | Omega | Phi | Exposure (minutes) |
|---|---|---|---|---|
| Sample A-Isopropanol | 0.8 mm | Fixed, 0° | Spin, 360° | 15 |
| Sample B- $H_2O$ | 0.8 mm | Fixed, 0° | Spin, 360° | 15 |
| Sample C-Urea | 0.8 mm | Fixed, 0° | Spin, 360° | 15 |
| Sample C-Urea from edge | 0.8 mm | Fixed, 0° | Spin, 360° | 15 |
| Sample D-Rice $H_2O$ | 0.8 mm | Fixed, 0° | Spin, 360° | 15 |
| Sample F-Carbonate $H_2O$ | 0.8 mm | Fixed, 0° | Spin, 360° | 15 |

     *Both the requestor and the report author, Nicole Little, must review any manuscripts or presentations reporting results of this request prior to its submission, presentation or publication.*
     *When referring to XRD results from this report, co-authorship must be given to Nicole Little.*

*Purpose of Investigation and Results:*

Samples of carbonated nanolime were taken for analysis by XRD to identify the phases present. X-ray diffractograms for samples A, B, C, D and F are shown in Figures A1 – A6. The XRD results show calcite as the major mineral phase detected in all samples. In addition, vaterite was detected as a minor phase in Sample B, while urea was identified as a component of Sample C. Upon further examination, clear material from the edge of Sample C's petri dish was taken for analysis and identified as urea, with no additional phases detected.

*Both the requestor and the report author, Nicole Little, must review any manuscripts or presentations reporting results of this request prior to its submission, presentation or publication.*
*When referring to XRD results from this report, co-authorship must be given to Nicole Little.*
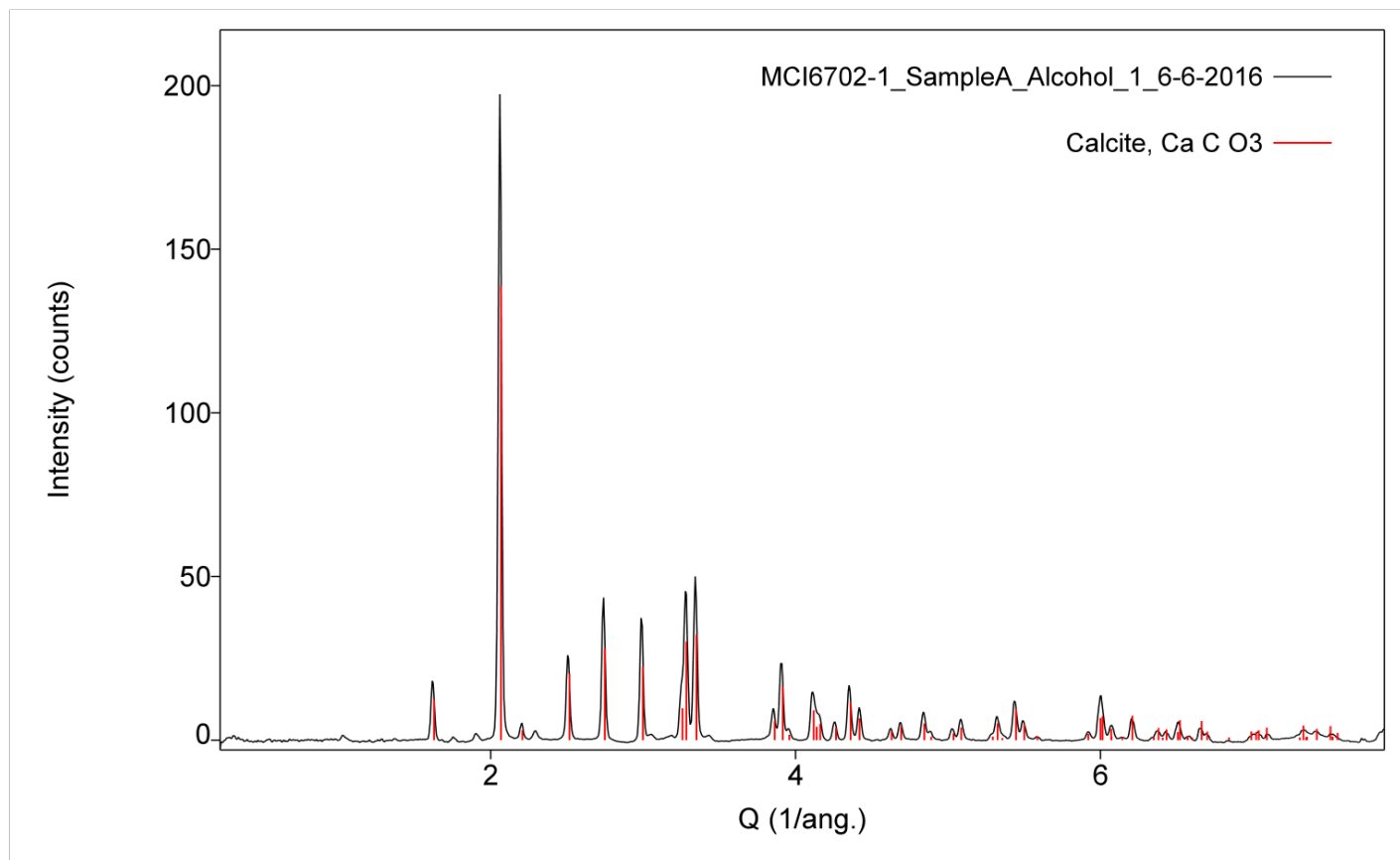
Figure A1
Sample: Sample A in isopropanol alcohol
Major phase: Calcite
Minor phases: n/a

*Both the requestor and the report author, Nicole Little, must review any manuscripts or presentations reporting results of this request prior to its submission, presentation or publication.*
*When referring to XRD results from this report, co-authorship must be given to Nicole Little.*
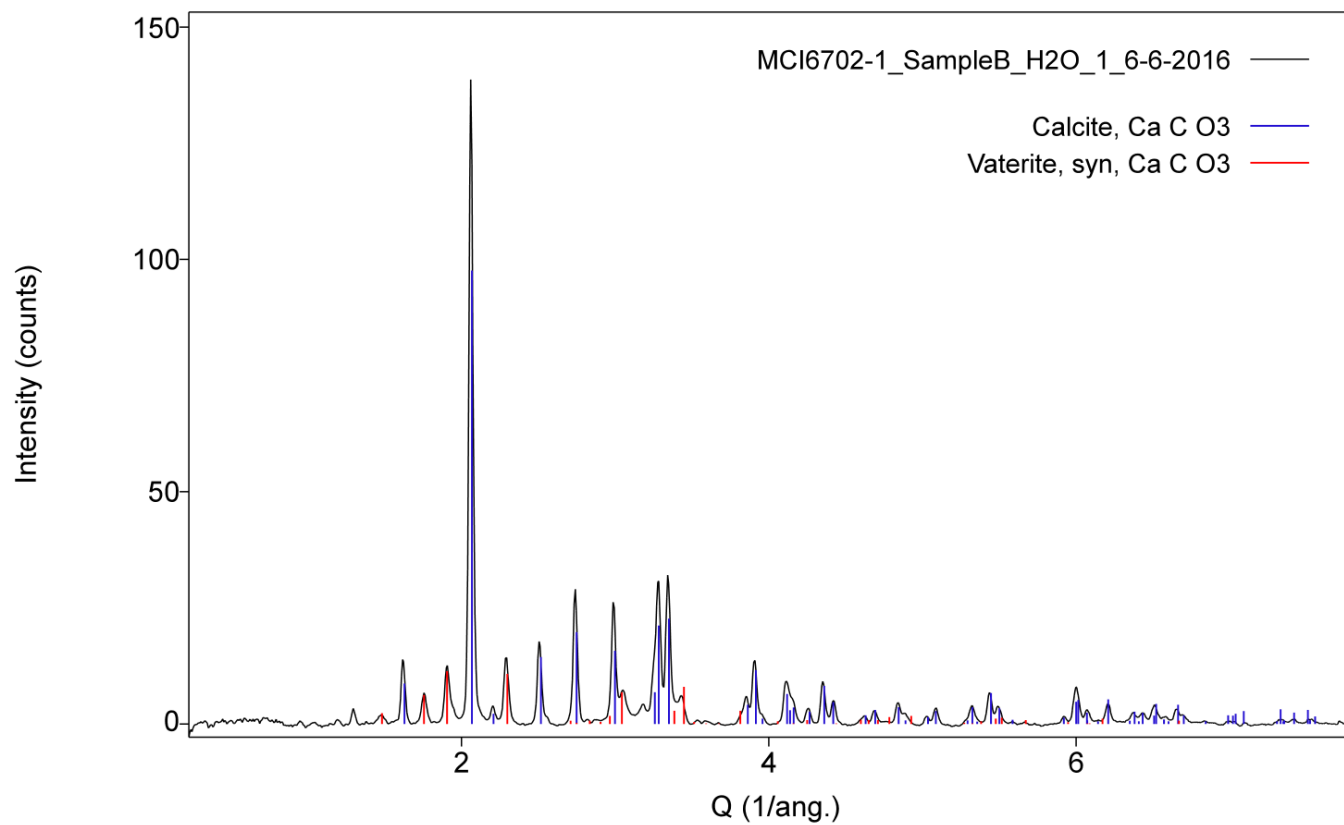
Figure A2
Sample: Sample B in H2O
Major phase: Calcite
Minor phases: Vaterite

*Both the requestor and the report author, Nicole Little, must review any manuscripts or presentations reporting results of this request prior to its submission, presentation or publication.*
*When referring to XRD results from this report, co-authorship must be given to Nicole Little.*
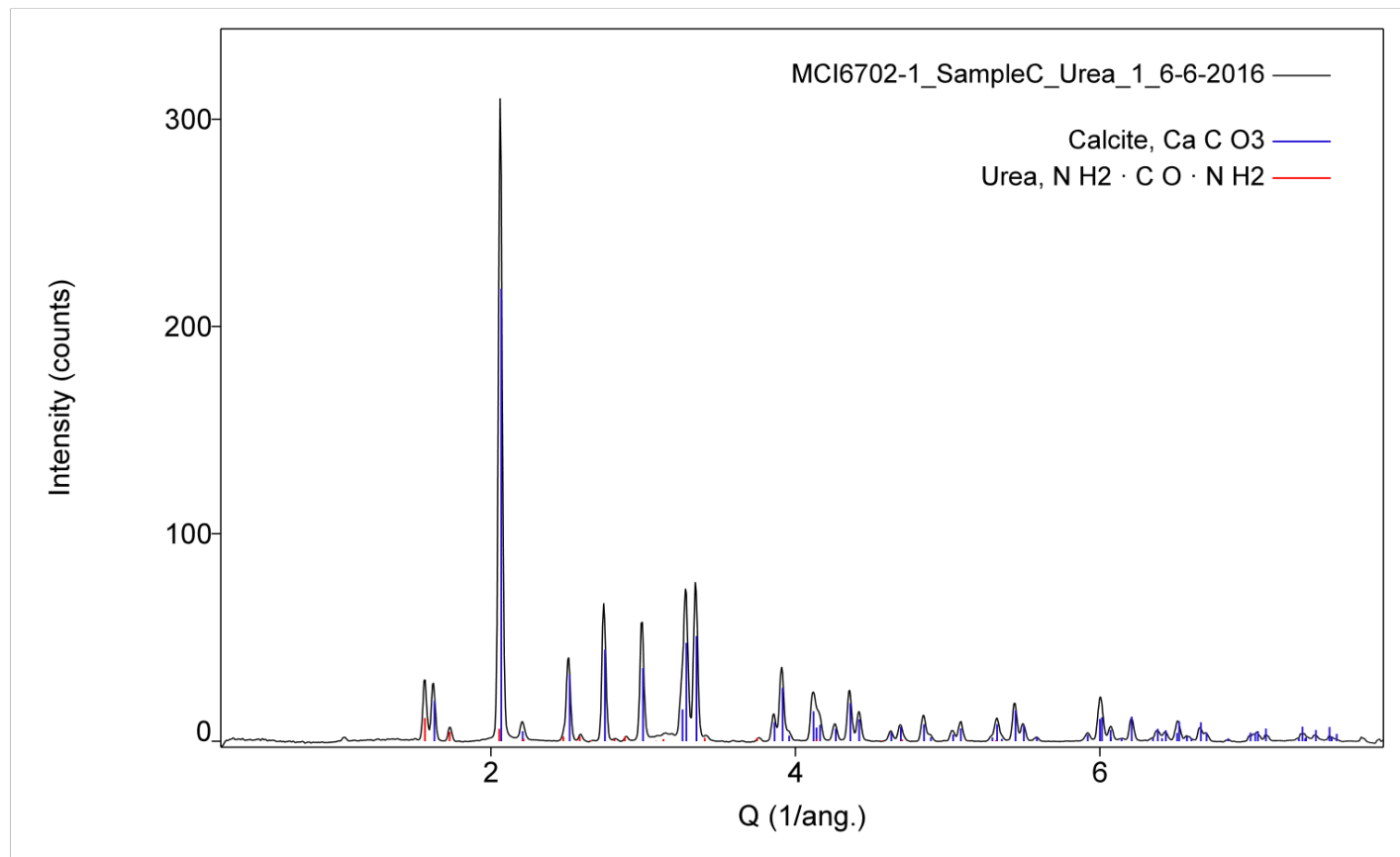
Figure A3
Sample: Sample C in urea
Major phase: Calcite
Minor phases: Urea

*Both the requestor and the report author, Nicole Little, must review any manuscripts or presentations reporting results of this request prior to its submission, presentation or publication.*
*When referring to XRD results from this report, co-authorship must be given to Nicole Little.*
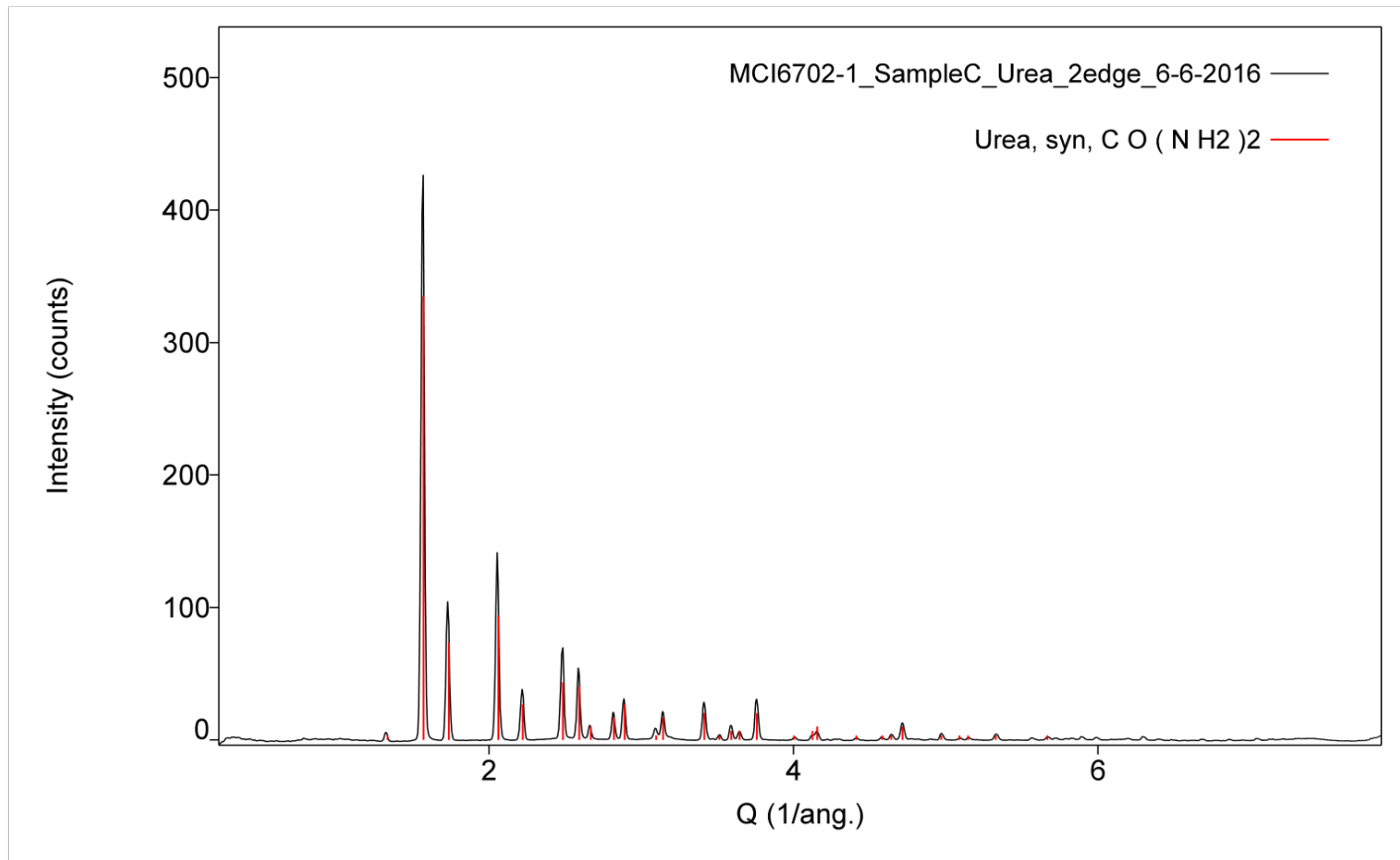
Figure A4
Sample: Sample C in urea-from edge of glass
Major phase: Calcite
Minor phases: Urea
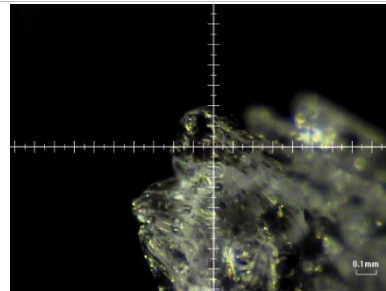
*Both the requestor and the report author, Nicole Little, must review any manuscripts or presentations reporting results of this request prior to its submission, presentation or publication.*
*When referring to XRD results from this report, co-authorship must be given to Nicole Little.*
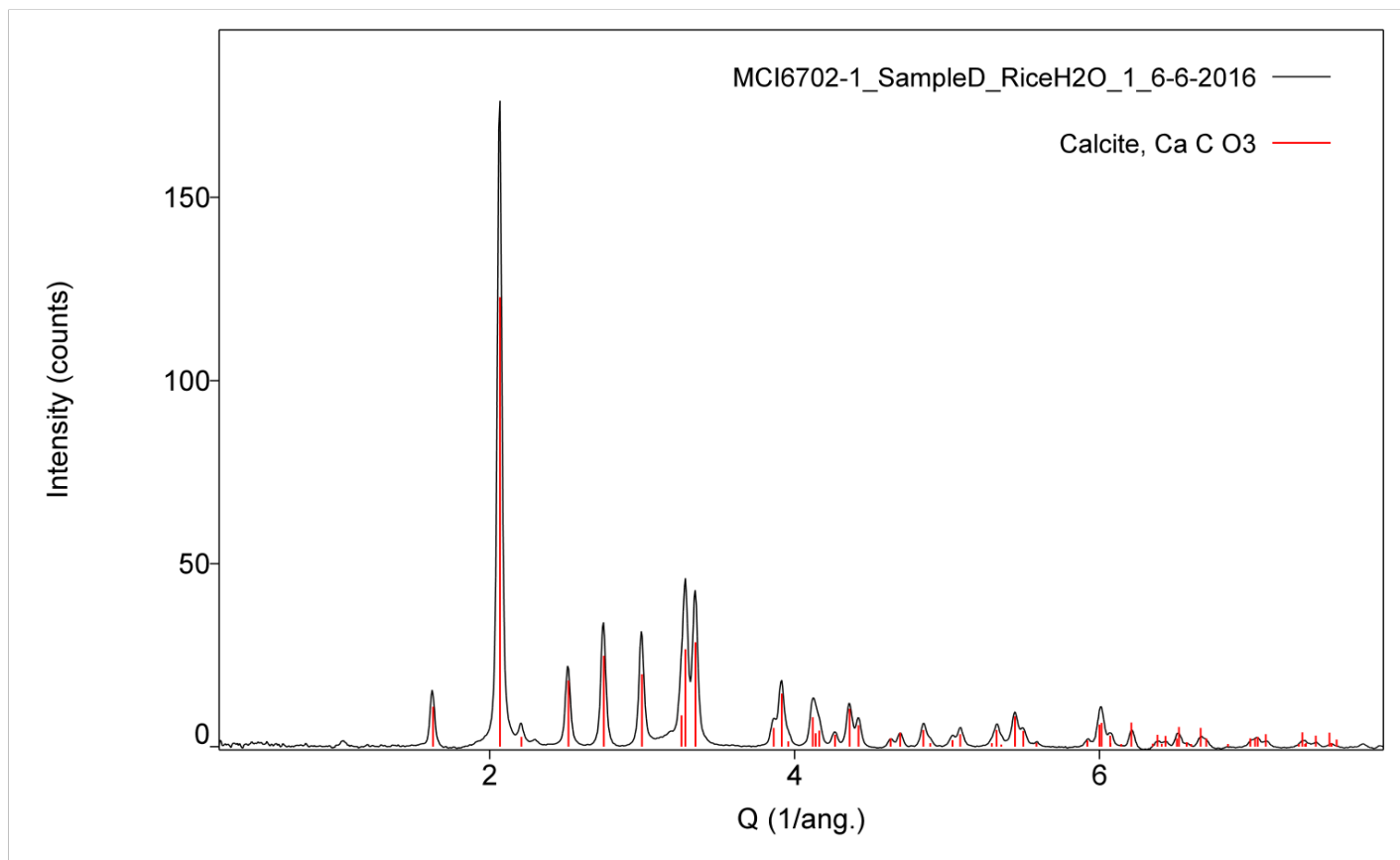
Figure A5
Sample: Sample D in rice H2O
Major phase: Calcite
Minor phases: n/a
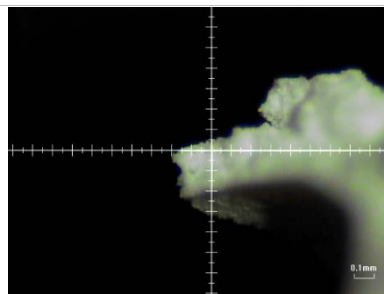
*Both the requestor and the report author, Nicole Little, must review any manuscripts or presentations reporting results of this request prior to its submission, presentation or publication.*
*When referring to XRD results from this report, co-authorship must be given to Nicole Little.*
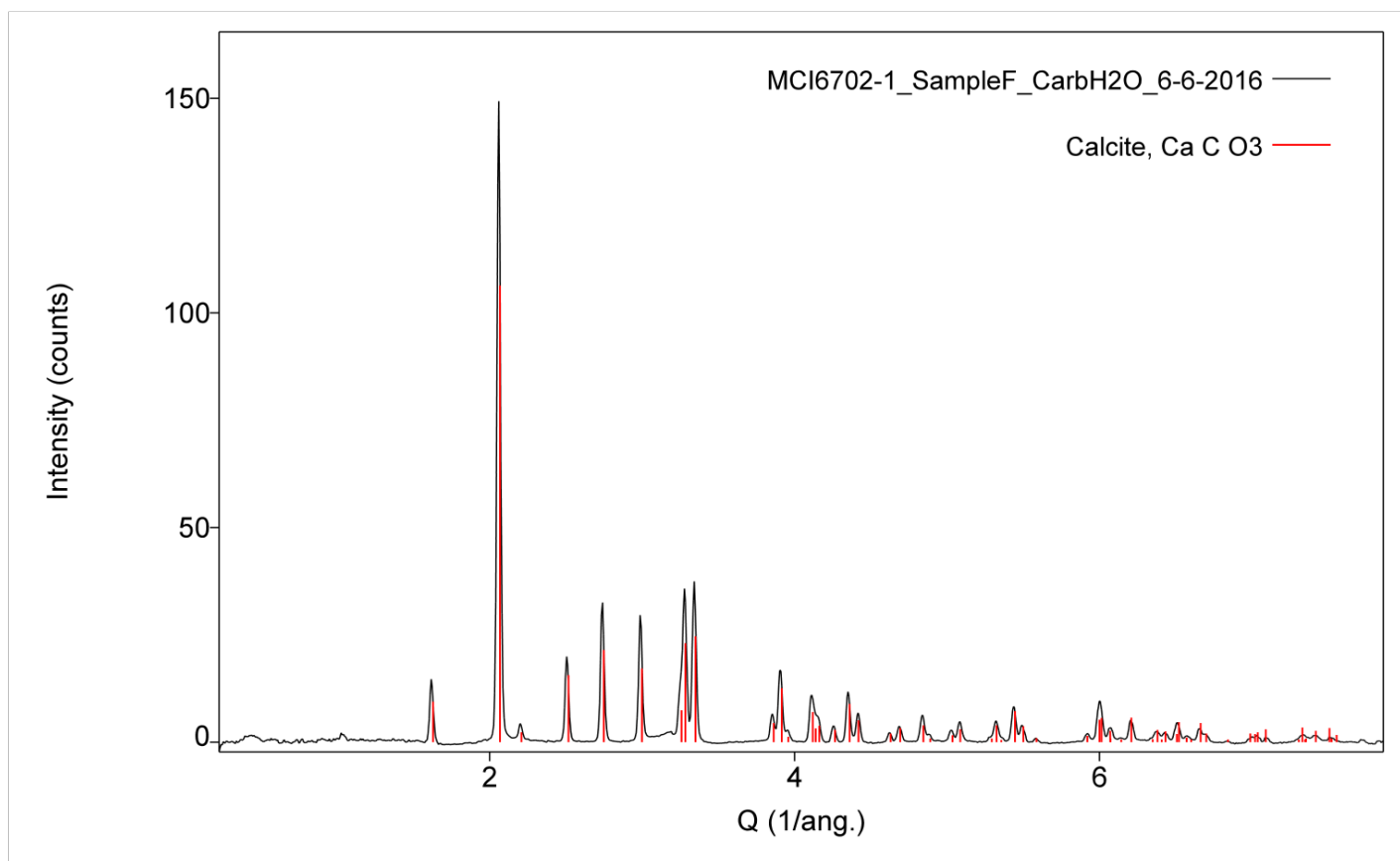
Figure A6
Sample: Sample F in carbonated H2O
Major phase: Calcite
Minor phases: n/a

*Both the requestor and the report author, Nicole Little, must review any manuscripts or presentations reporting results of this request prior to its submission, presentation or publication.*
*When referring to XRD results from this report, co-authorship must be given to Nicole Little.*

# Report on the SEM examination of marble and Indiana limestone samples treated with nanolime

A. Elena Charola (Research Scientist), Jorge Otero (MCI Intern), Thomas F. Lam (Physical Scientist)

June 20, 2016

## Sample description

A marble piece, possibly the cornice of a building, was taken from the pile of marble blocks at the Garber facility and was cut into roughly cubic samples.  Three sides were weathered, one of which appeared to have been attached with a mortar, while the other three were recently cut sides to obtain the various samples. The two similarly weathered sides were treated with a nanolime dispersion in ethanol.  The samples were then left to carbonate under different conditions [in brackets their identification code]: 75% RH [7-x], 55% RH [5-x], room environment [R-x], and at room environment sprayed regularly with carbonated water [R-x-S]. Control samples [C-x] were kept at room environment.

Unweathered Indiana limestone cubes (5 x 5 x 5 cm) were treated on all sides with a nanolime dispersion in isopropanol. All samples, including the control ones [C-x], were kept at room environment [R-x]; and at room environment sprayed regularly with carbonated water [R-x-S].

Small specimens were taken from these samples.  For the marble, the corner of two untreated sawn faces with a weathered one was chipped off using a hammer and chisel.  One of the untreated faces was examined to estimate depth of penetration as the nanolime dispersion would evaporate through it.  The same approach was used for the Indiana limestone cubes, but in this case, the interior fractured surface was examined.

## Specimen preparation

The specimens were gold coated, and were then mounted in an orientation so that a cross-sectional surface could be examined.  The samples were examined using Hitachi S3700-N SEM at an acceleration voltage of 20 kV on June 16.

## Results

The most representative photomicrographs obtained for the various marble specimens examined are shown in the following pages (Figures 1 to 5).
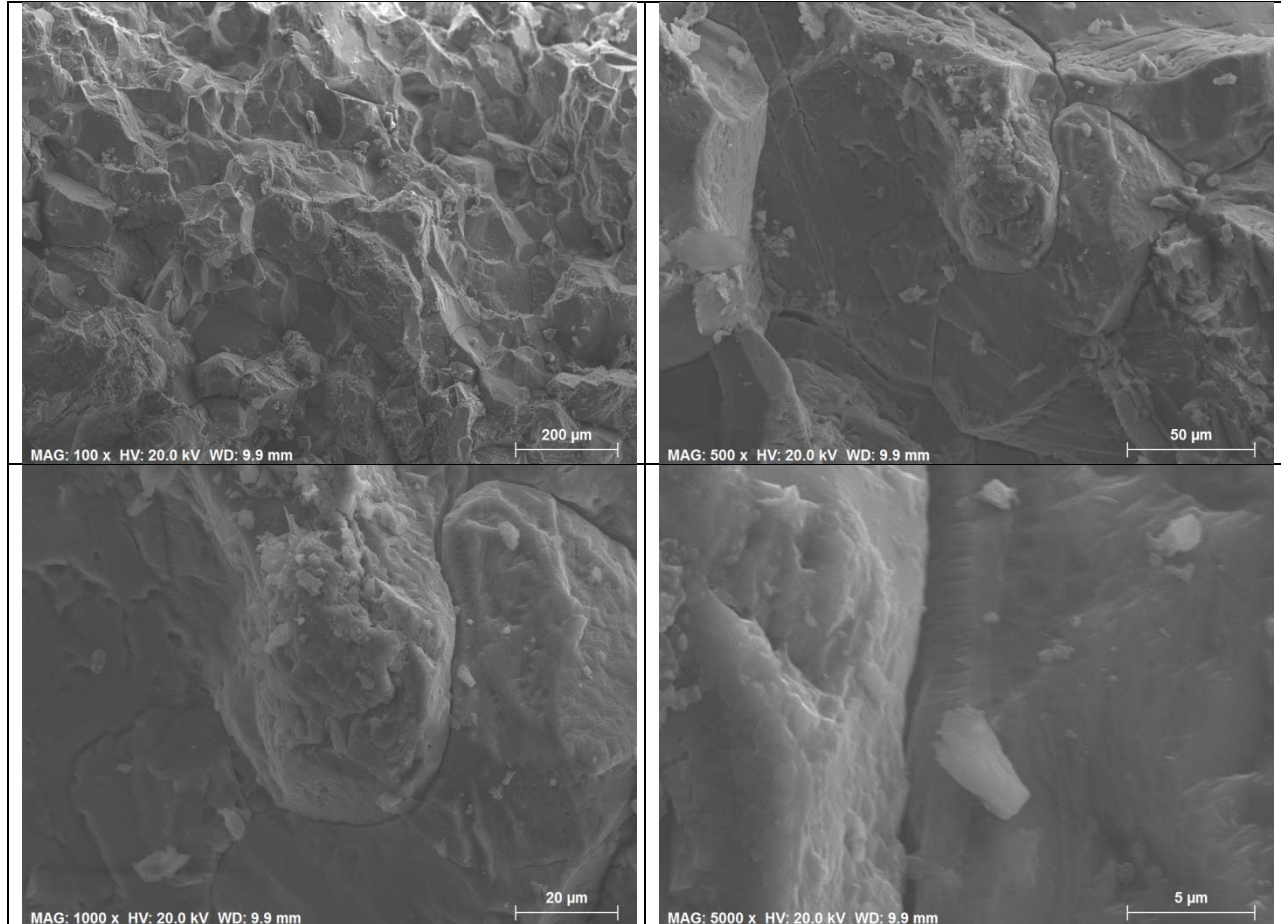


Figure 1. **Marble control specimen [C-1]** at various magnifications, from 100x (top left) to 5000x (bottom right).
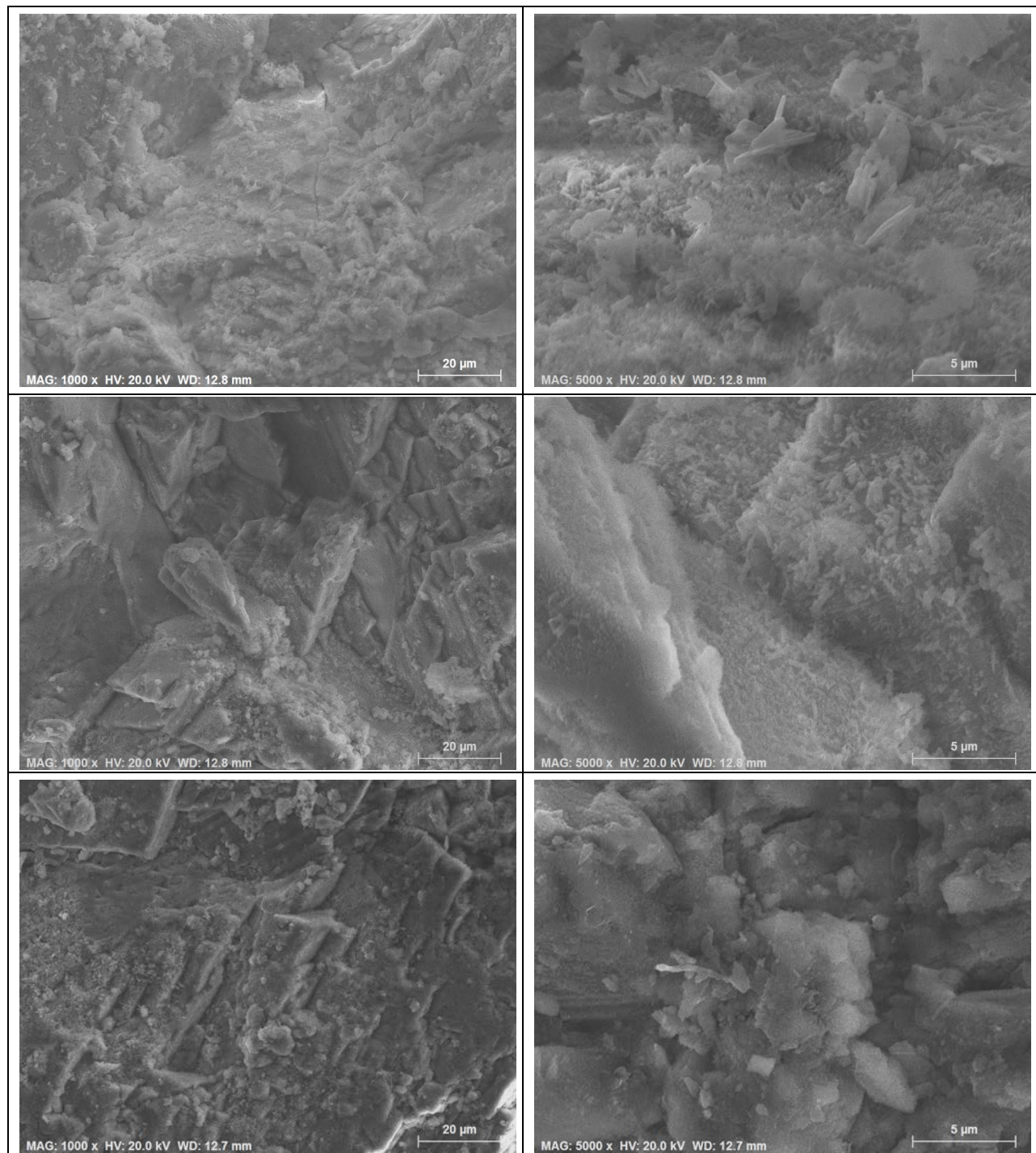
Figure 2. **Treated marble specimen [7-1]** cured at 75% RH in a diseccator at 1kx left, and 5kx, right. Top row, area close to treated surface, the presence of nanolime particles is visible; middle, an area below where carbonated nanolime is apparent; and bottom, area further down from the edge showing differently crystallized particles.
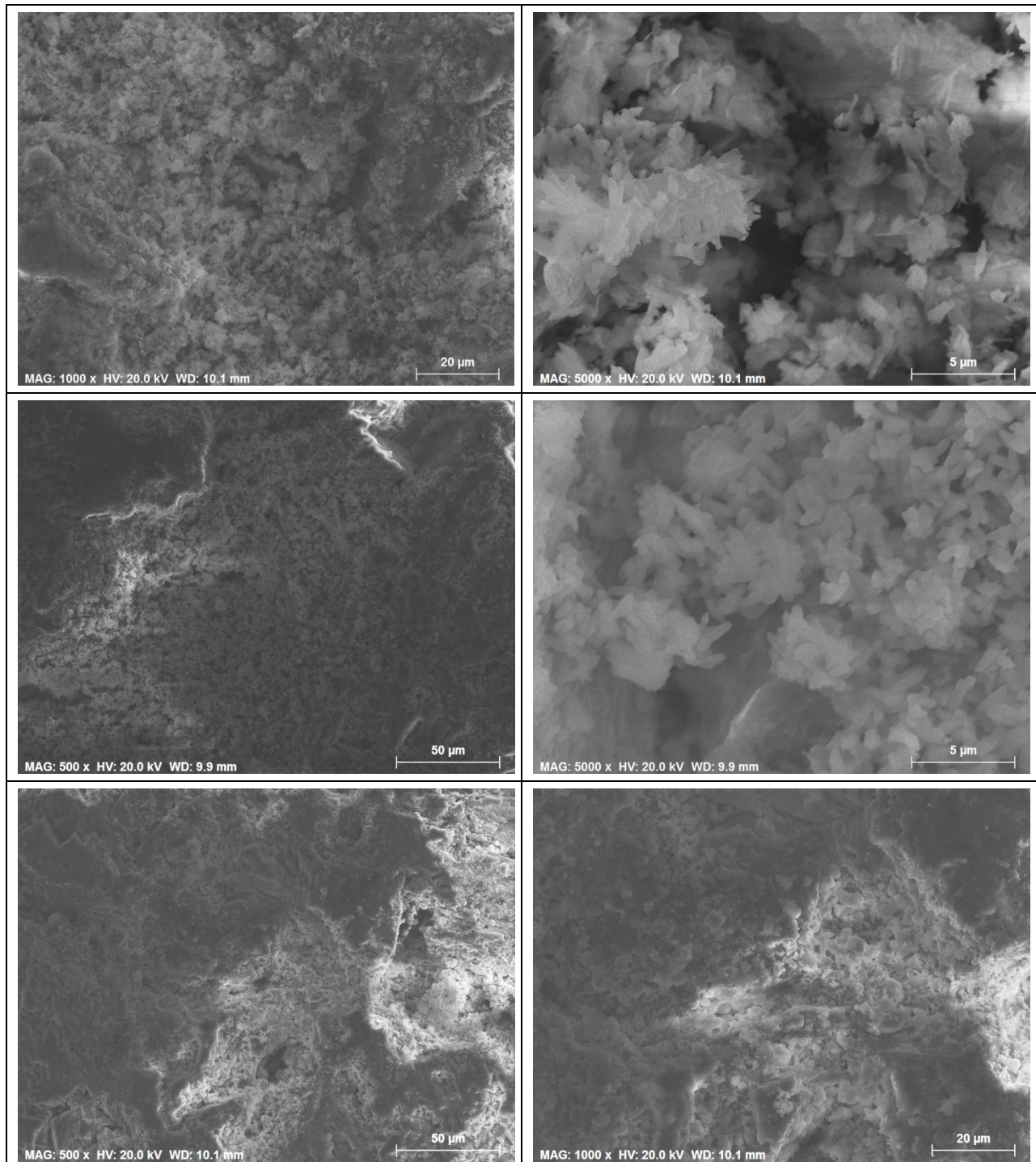
Figure 3. **Treated marble specimen [5-2]** cured at 55% RH in a diseccator at higher magnification. Top row, area close to treated surface, the presence of carbonated nanolime crystals is visible (1kx and 5kx); middle, an area below where carbonated nanolime is apparent (500x and 5kx); and bottom, area further down from the edge showing differently crystallized particles viewed at lower magnification because of charging effects (500x and 1kx).
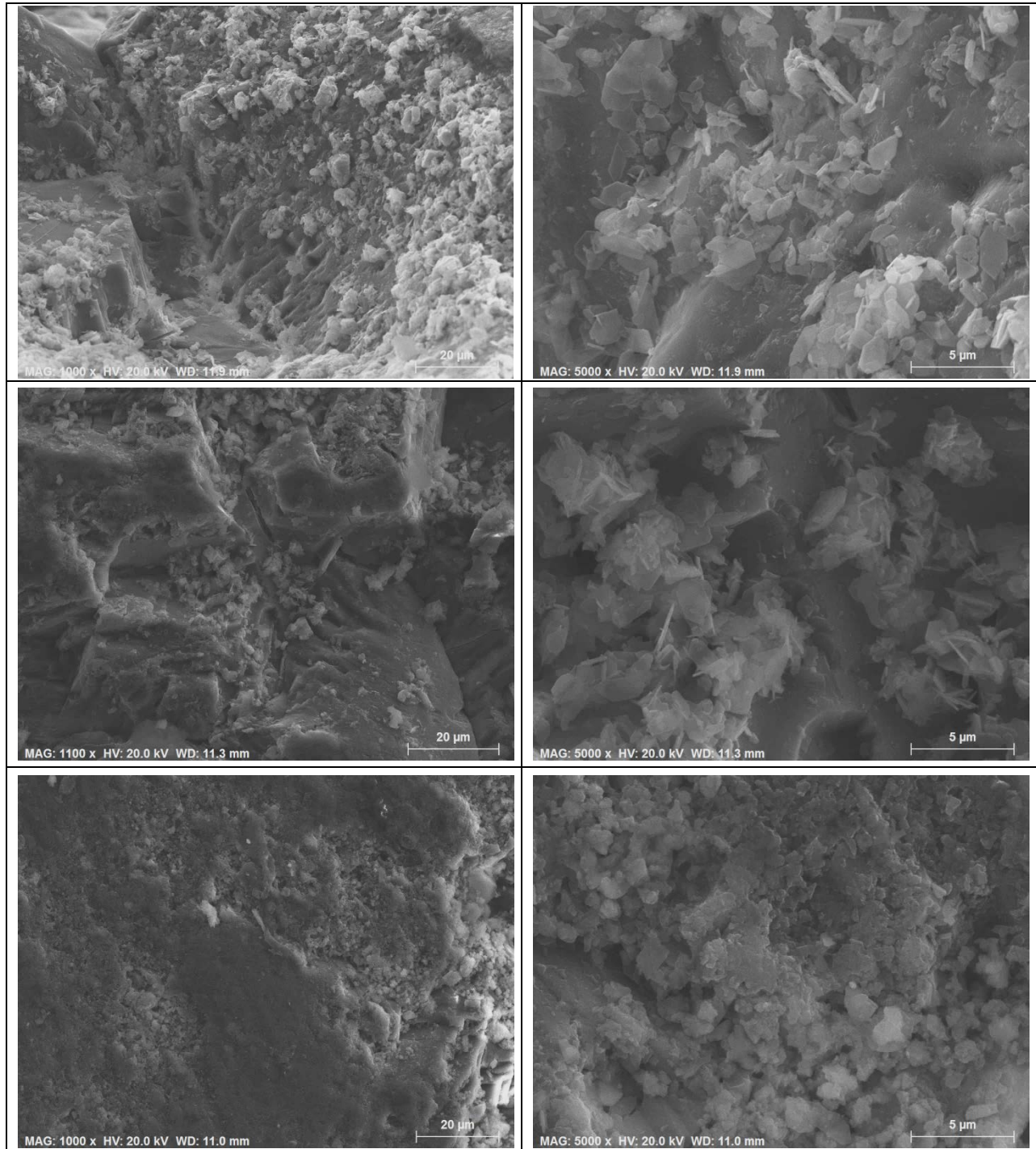
Figure 4. **Treated marble specimen [R-2]** cured at room conditions. Top row, area close to treated surface, the presence of better crystallized nanolime crystals is visible (5kx and 10 kx respectively); middle row, an area below where crystallized nanolime particles is apparentkx and 5kx, respectively; and bottom, area further down from the edge showing differently crystallized particles (1kx and 5 kx, respectively).
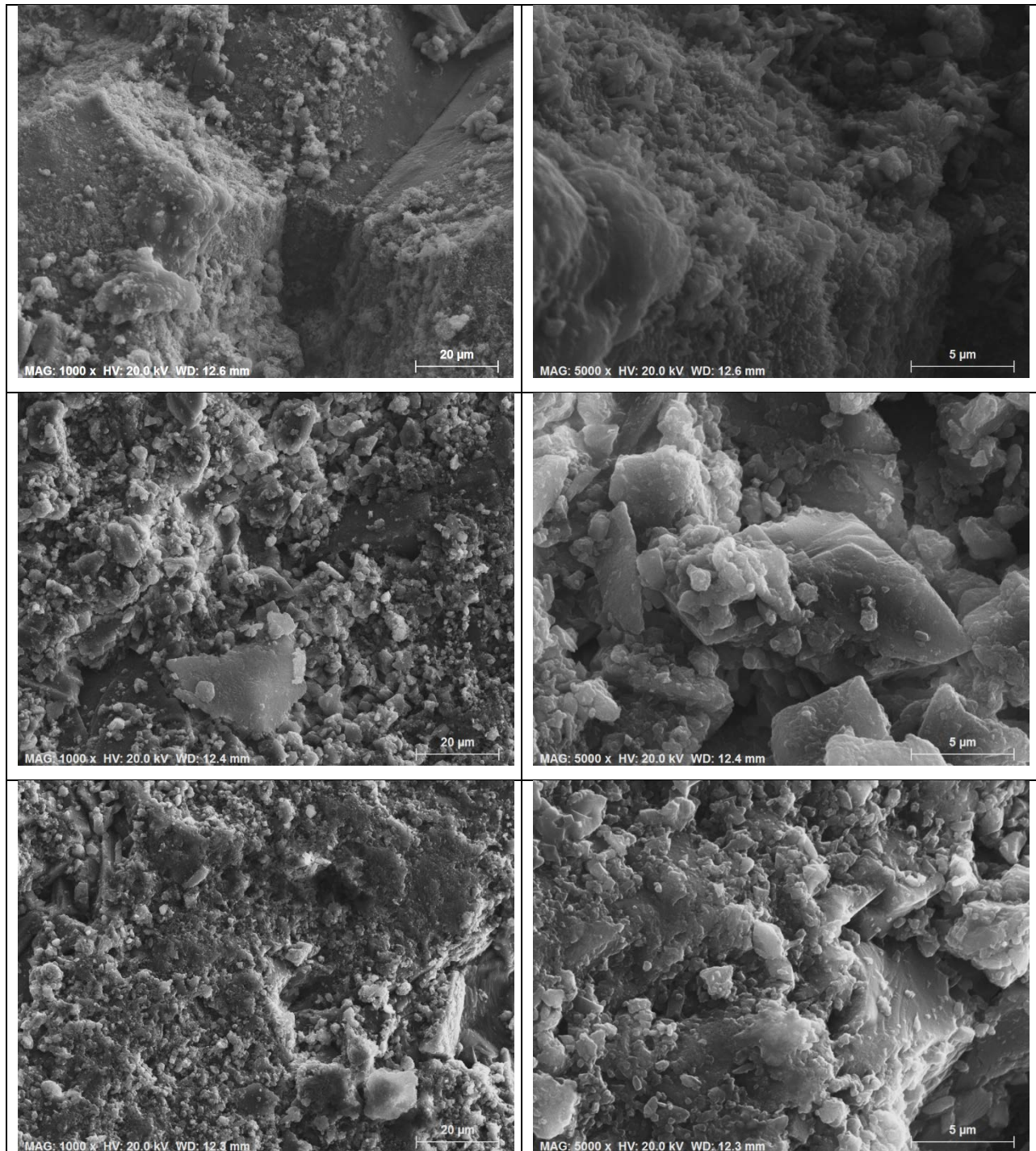
Figure 5. **Treated marble specimen [R-2-S]** cured at room conditions and sprayed with carbonated water at 1kx left, and 5 kx, right. Top row, area close to treated surface, the presence of small crystallized carbonated nanolime crystals; middle row, an area below where fewer particles are visible; and bottom, area further down from the edge which is similar to the previous one.

The photomicrographs obtained for the Indiana limestone are shown in Figures 6 to 8.



Figure 6. **Indiana limestone control [C-1]**. Top row, near the surface; center row, an area below; bottom row, an area further away from the surface,  at 1kx left, and 5 kx right. No significant differences between them.

Figure 7. **Treated Indiana limestone [R-1]**. Top row, near the surface; center row, an area below; bottom row, an area further away from the surface,  at 1kx left, and 5 kx right. No significant differences between them

Figure 8. **Treated Indiana limestone [R-1-S]** sprayed regularly with carbonated water. Top row, near treated surface; center row, an area below it; bottom row, area further away from the treated surface at 1kx left, and 5kx right. No significant differences can be seen with respect to the control [C-1] samples.

**Conclusions**

In the marble samples, the nanoparticles are readily visible by comparison between the treated and the control samples.  This is not the case for the Indiana limestone samples because its heterogeneous texture of larger calcite crystals surrounded by a finer matrix makes it harder to visualize the nanoparticles that may be deposited on or around them.

**Smithsonian**
*Museum Conservation Institute*

# FTIR Analysis Report

**MCI request number:** 6702.1

**Title / Object:** Nanolime preparation

**Accession number:** n.a.

**Manufacturer:** n.d.

**Geographic region:** n.d.

**Date:** n.d.

**Materials:** unknown material suspected to contain rice starch

**Requested by:** Jorge Otero, MCI Intern

> **Telephone:** n.a.
> **E-mail:** OteroJ@si.edu

**Unit:** Museum Conservation Institute (MCI)

**Analyst(s):** Gwénaëlle Kavich, Conservation Scientist (KavichGM@si.edu).

**Analysis date:** 23rd June 2016

## Summary

Jorge Otero, MCI intern, has asked to have analyzed the thin surface layer that developed during the carbonation of nanolime prepared with rice water. The yellowish tint that the nanolime took over time, suggested the presence of rice starch. FTIR analysis confirmed the presence of rice starch in the sample. Calcium carbonate is also present as expected.

## Method: FTIR (Fourier Transform Infrared spectroscopy)

*ATR-FTIR Method (Attenuated Total Reflectance)*

> Instrument: Thermo Nicolet 6700 Fourier transform infrared (FTIR) spectrometer
> Sampling accessory: Golden Gate ATR with diamond crystal, single bounce, 45°
> Detector: DTGS
> Correction: ATR corrected
> Resolution: 4 cm$^{-1}$
> Number of scans: 64

The sample for ATR-FTIR was placed directly on the diamond crystal of the ATR accessory. A piece of aluminum foil was used to back the sapphire anvil to eliminate any sapphire absorption in the IR spectrum. The obtained FTIR spectrum was identified using the IRUG (Infrared and Raman Users Group) libraries, the HR Hummel Polymer and Additives library as well as the ASTER mineral library.

## Results and Discussion

*Sample: unknown material suspected to contain rice starch*

The ATR-FTIR spectrum of the unknown material from the precipitate (reported in Figure 1) shows spectral features that may be attributed to the presence of rice starch (2922, 1149, 1078, 1021, and 932 cm$^{-1}$), thus confirming its presence in the sample. In addition, some calcium carbonate (2507, 1792, 1405, 871, and 711 cm$^{-1}$) is also present. Additional peaks at 3567, 1584, and 859 cm$^{-1}$ could not be identified and may be attributed to other reaction products.
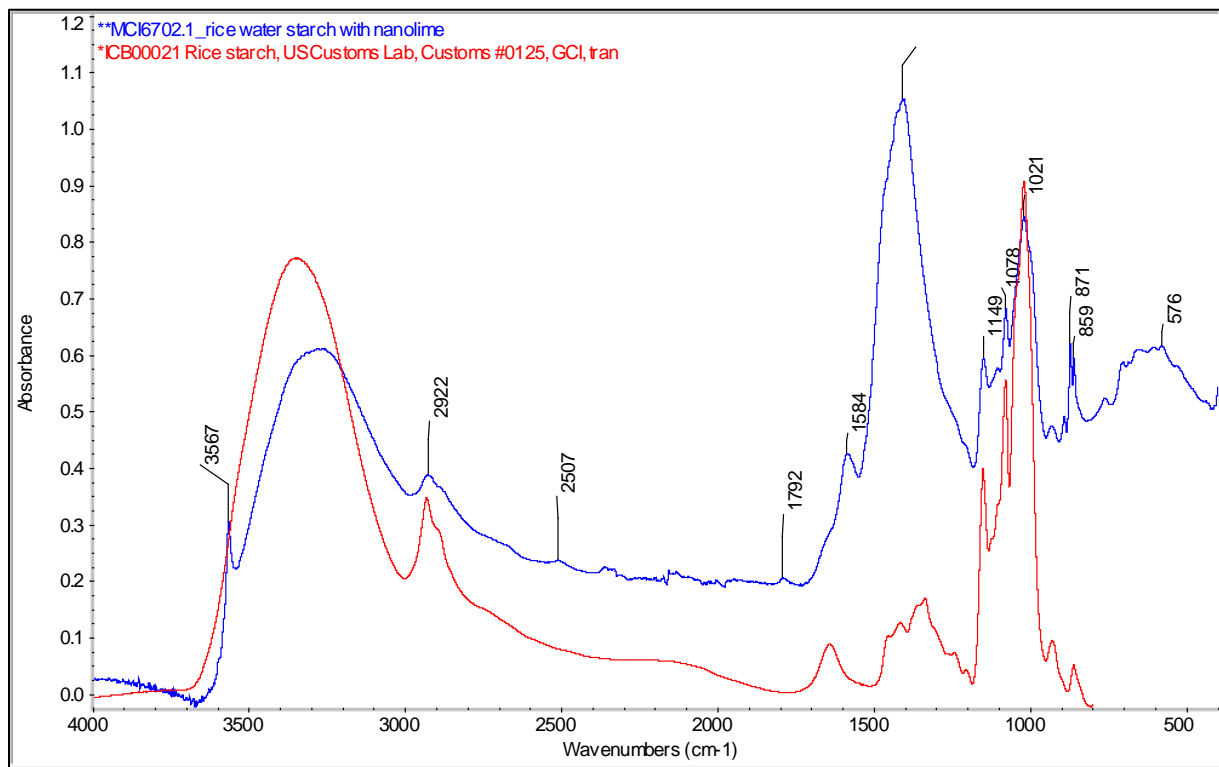


Figure 1: overlay of ATR-FTIR spectrum of the unknown material (blue) with reference spectrum of rice starch.

Appendix 2

Peer Review Journal Articles

Articles:

1. **Otero J**., Starinieri V., Charola A. E., A comparison between nanolime treatments on lime-mortar, Construction and Building Materials (paper submitted).

2. Taglieri G., **Otero J.**, Daniele V., Gioia G., Macera L., Starinieri V., Charola A. E., The biocalcarenite stone of Agrigento (Italy): preliminary investigations of compatible nanolime treatments, Journal of cultural Heritage. https://doi.org/10.1016/j.culher.2017.11.003.

3. **Otero, J**., Charola A. E., Grissom C., Starinieri V., An overview of nanolime as a consolidation method for calcareous substrates. Ge-conservación, vol.1, n.11, p.71-78, 2017. ISSN 1989-8568. http://ge-iic.com/ojs/index.php/revista/article/view/455.

# An overview of nanolime as a consolidation method for calcareous substrates

Jorge Otero, A. Elena Charola, Carol A. Grissom, Vincenzo Starinieri

**Abstract**: Ca(OH)$_2$ particles with submicrometric dimensions (nanolimes) represent one of the most promising consolidants for the conservation of calcareous substrates. The nanolime treatment is similar to the limewater technique, traditionally used for its durability and high compatibility with the calcareous matrix but requiring a large number of applications and not always yielding a highly effective consolidation. Since 2001, alcohol-based dispersions of Ca(OH)$_2$ nanoparticles have been synthesised to overcome the limitations of the limewater treatment. Nanolimes present the same high compatibility and durability of the traditional technique but superior properties in terms of higher consolidation, penetration and reactivity, and fewer side effects. Since their discovery, nanolimes have been investigated by several research groups with the aim of refining their synthesis process, properties and applications. This paper presents an overview of the most relevant literature about nanolime as a consolidant for calcareous substrates.

**Key words:** Nanolime, Calcium hydroxide, Consolidation, Limewater, Conservation, Nanoparticles, Synthesis, Calcareous substrates.

## Una visión general de la nanocal como método de consolidación para sustratos calcáreos

**Resumen**: Partículas de nanocal, Ca(OH)$_2$ con dimensiones sub-micrométricas, es uno de los principales consolidantes emergentes dentro de la conservación de sustratos calcáreos. La nanocal se basa en la técnica de agua de cal, utilizada tradicionalmente por su alta compatibilidad y durabilidad con el substrato calcáreo; pero su aplicación requiere de un gran número de aplicaciones y la consolidación no siempre es muy eficaz. Desde 2001, dispersiones alcohólicas de nanopartículas de Ca(OH)$_2$ se han sintetizado para obviar las limitaciones de los tratamientos tradicionales. La nanocal presenta la misma alta compatibilidad y durabilidad del método tradicional y propiedades superiores en términos de mayor consolidación, penetración, reactividad y menores efectos secundarios. Desde su creación, estas formulaciones han sido estudiadas por varios grupos de investigación con el objetivo de perfeccionar su proceso de síntesis, propiedades y aplicaciones. Esta publicación revisa la bibliografía más relevante para identificar áreas donde un mayor estudio es necesario.

**Palabras clave:** Nanolime, Hidróxido de calcio, Consolidación, Agua de cal, Conservación, Nanopartículas, Síntesis, Sustratos calcáreos.

## Introduction

The recent development of nanoscience and nanotechnology has opened the way to new applications in many scientific fields, including that of the conservation of cultural heritage. One example of a nanomaterial developed over the last decades is the so-called "nanolime", nanoscale particles of Ca(OH)$_2$ with potentially superior consolidation properties compared to traditional lime-based treatments. So far, nanolime has been studied mainly within the built cultural heritage conservation field.

Scientific investigations on nanolime began around the year 2000 at the University of Florence -CSGI, in Italy, with

the first results on its synthesis and application for the conservation of wall paintings published in 2001 (Ambrosi et al. 2001). The researchers in Florence modified the synthesis methodology several times by reactions in diols (Salvadori and Dei 2001), aqueous solutions (Ambrosi et al. 2001) or water-in-oil (w/o) micro-emulsions (Nanni and Dei 2003). In 2003, another research group (Ziegenbalg 2003) prepared nanolime from a heterogeneous-phase reaction, which was patented under the brand name Calosil®. This was the first nanolime product introduced to the market in 2006 (IBZ-Salzchemie GmbH & Co. KG) followed by Nanorestore® (CSGI) in 2008. With these products made available to the scientific community, European researchers began investigating the properties

and consolidation efficacy of nanolime. Three main EU research projects, STONECORE (2008 - 2011), NANOMATCH (2011 - 2014) and NanoforART (2012 - 2015) have made significant contributions to understanding the technologies and preparing the way for a range of applications of nanolime in the conservation field.

Nanolime is used mainly to recuperate the cohesion between particles in calcareous substrates such as wall-paintings, limestone, lime mortar, etc. In the past, organic and inorganic consolidants have been used for the consolidation of these substrates. The use of organic consolidants such as acrylic, epoxy, or vinyl resins were very common in restoration treatments since 1960 (Dei and Salvadori 2006). However, the low compatibility with the substrate and poor aging and durability of these treatments may cause unwanted degradation processes, including cracking and aesthetic changes, and may interfere with future treatments. In contrast, inorganic-based consolidants such as barium hydroxide and limewater have a high physico-chemical compatibility with the substrate and good durability, although their use requires a large number of applications and the consolidation is not always highly effective. The effectiveness of the traditional limewater technique has been controversial. Price (Price et al. 1988) concluded that the limewater technique does not produce a noticeable consolidation as most of the lime is deposited within the outer 2mm and the low amount of particles does not produce consolidating effect. Nevertheless, another research (Brajer and Kalsbeek 1999) demonstrated that a prolonged and uninterrupted application of limewater over 80 days produces a positive consolidation effect. However, this treatment is tedious and has to be repeated up to 40 times due to the low solubility of calcium hydroxide in water (1.7 g/L$^{-1}$ at 20°C). Other limitations are the reduced penetration depth of the lime size-particles and the possible decay processes associated with the use of large amounts of limewater solution (salt movement, etc.). The use of nanolime in alcohol allows incorporation of larger amounts of lime into the treated substrate with far less water, yielding better penetration and faster carbonation (Ambrosi et al. 2001). TThis paper expands the extended abstract (Otero et al. in press) reviewing the considerable literature on this topic.

## Synthesis

Nanoparticles can be produced through either the top-down or bottom-up processes. In the top-down method the nanoparticles are created by "breaking" a bulk micro-scale particle until fragments in the nanometer range are obtained. This normally involves using a source of high energy in processes such as laser ablation, thermal decomposition or mechanical milling. In the bottom-up method, the nanoparticles are built atom by atom through chemical precipitation using several techniques for the deposition and crystal growth

from vapour (Chemical Vapour Condensation (CVC)) hydrogen plasma hydrogen plasma-metal reaction (HPMR) and liquid phases (micro-emulsions, solvo-thermal, etc.). Most calcium hydroxide nanoparticles are synthesized through the bottom-up reaction by chemical precipitation from a liquid phase.

A survey of different synthesis methods from literature is summarized in Table 1. In 1997, colloidal dispersions of calcium hydroxide in organic solvents were obtained (Delfort et al. 1997) and, in 2000, CSGI-group (Giorgi et al. 2000) also obtained stable alcohol dispersions of Ca(OH)$_2$ particles. Both researchers found that dispersions in alcohol are far more stable and able to incorporate larger amounts of lime than limewater. With the aim of preparing stable nanoparticles of Ca(OH)$_2$, the researchers at CSGI carried out a series of studies based on the works of Matijevic group (Pe et al. 1998) in the field of colloid synthesis. They reported that nucleation of nanoscale particles is affected by reaction time, high temperature (above 100°C) and high degree of super saturation, and it can be achieved with slow synthesis and peptization processes. In 2001, CSGI group (Dei and Giorgi 2001) obtained Ca(OH)$_2$ particles (1-2μm) by a hydrolytic method at medium-high temperature (60°C) and super-saturation. In order to reduce the size of particles, they synthesized calcium hydroxide nanoparticles (30-60 nm) from diols, which allowed higher temperatures to be reached during the process (Salvadori and Dei 2001). However, this synthesis method proved to be time consuming and produced a low quantity of nanoparticles. In the same year, they successfully obtained highly reactive and colloidal sub-micrometer Ca(OH)$_2$ particles (±300nm) via an homogeneous phase following the aqueous reaction CaCl$_2$ + 2NaOH $\rightarrow$ Ca(OH)$_2$ + 2NaCl, heated up to 90 °C under supersaturation conditions (Ambrosi et al. 2001). But, this process has drawbacks: 1) slow mixing rates; 2) the necessity of removing the produced NaCl by washing; and 3) low yield of nanoparticles production. Ca(OH)$_2$ nanoparticles (2-10 nm) were also obtained using w/o micro-emulsions (Nanni and Dei 2003), but low yield and high production time make this method less practical. The synthesis method developed by CSGI (Dei and Giorgi 2001; Ambrosi et al. 2001; Dei and Salvadori 2006), which was commonly named "drop by drop method", was also adopted by several research groups with the aim of refining the synthesis process and properties (Sequeira et al. 2006; Daniele and Taglieri 2010; Daniele et al. 2008). In 2012, the Taglieri team (Daniele and Taglieri 2012) managed to reduce the synthesis time while decreasing the particle size (<50 nm) by adding a surfactant (Triton X-100) in the initial aqueous solution. In other synthesis pathways based on CSGI researches, Bhattacharya (Bhattacharya 2010) obtained nanolime by hydrolysing calcium nitrate tetrahydrate [Ca(NO$_3$)$_2$•4H$_2$O] as a precursor in diols at a high temperature (175°C) and Samanta (Samanta et al. 2016) synthesized nanolime using calcium nitrate

**Table 1**.- Brief summary of literature on the synthesis of nanolime.

| Year | Research group | Synthesis route | Inorganic precursor(s) | Synthesis media | Processing | T (°C) | PS (nm) |
|---|---|---|---|---|---|---|---|
| 2001 | CSGI group | CP-HS | $CaCl_2$ and NaOH | aqueous | high T, wash. and pept. | 60 | 1-2 (µm) |
| 2001 | CSGI group | CP-HS | $CaCl_2·2H_2O$ and NaOH | diols | high T, filtration, wash. and pept. | 195 | 30-150 |
| 2001 | CSGI group | CP-HS | $CaCl_2·2H_2O$ and NaOH | aqueous | high T, wash. and pept. | 90 | 300 |
| 2003 | CSGI group | CP-HS | $CaCl2·2H_2O$ and NaOH | w/o microemulsions | wash. and pept. | ≤ 15 | 2-10 |
| 2010 | Bhattacharya et al. | CP-HS | $Ca(NO_3)_2·4H_2O$ and NaOH | diol (1,2-ethanediol) | hot vacuum filtration and pept. | 115 | 35 |
| 2010 | Liu et al. | CP-HPMR | melted Ca ingot and $H_2O$ | H plasma | Ca vapour reacts O, CaO reacts with $H_2O$ | room T | 10-100 |
| 2012 | Taglieri et al. | CP-HS | $CaCl_2$ and NaOH | aqueous & Triton-X100 | wash. and pept. | 90 | <100 |
| 2015 | Taglieri et al. | CP-HS | $CaCl_2·2H_2O$ and AER (OH) | aqueous | pept. | room T | <100 |
| 2016 | Samanta et al. | CP-HS | $Ca(NO_3)_2·2H_2O$ and NaOH | aqueous | pept. | room T | 350 |
| 2016 | CSGI group | CP-HPS | calcium metal | alcohol and H2O (high P & T) | high P reactor (High P & T) | 65-130 | 200 |

CP (chemical precipitation), HS (homogeneous synthesis), HPS (heterogeneous phase synthesis), HPMR (hydrogen plasma metal reaction), H (hydrogen), Ca (calcium), $CaCl_2$ (calcium chloride), NaOH (sodium hydroxide), w/o (water in oil), $Ca(NO_3)_2 ·4H_2O$ (calcium nitrate tetrahydrate), CaO (calcium oxide), w/o (water in oil), P (pressure), T (temperature), PS (particle size), AER (anion exchange resin), wash (washing with deionized water), pept (peptization process)

dihydrate $[(NO_3)_2·2H_2O]$ as a precursor in an aqueous medium at room temperature without requiring purification, obtaining nanoparticles of about 250 nm.

Other approaches for obtaining nanosized $Ca(OH)_2$ use calcium alkoxides as precursors (Ziegenbalg 2003; Poggi et al. 2016; Rodriguez-Navarro et al. 2013). Nanolime also has been developed from a hydrogen plasma-metal reaction method (HPMR), obtaining low cost, high purity and crystalline particles (10-100nm) (Liu et al. 2010), and recently the Taglieri team (Taglieri et al. 2015) synthesised nanolime by means of an anion-exchange process using an anion-exchange resin (OH⁻ group), obtaining nanoparticles with better features in terms of size, morphology and reactivity, and reducing the synthesis time by eliminating purification processes.

**Applications**

During the last two decades nanolimes have been tested as conservation treatments for various substrates. Most of these studies focused on the pre-consolidation of wall paintings, limestone, lime mortars, renders and plasters; and on the de-acidification of cellulose-based materials such as paper, canvas and wood (Poggi et al. 2016).

The use of lime dispersions in alcohol was first reported by Giorgi et al. (Giorgi et al. 2000), who obtained higher consolidation effect than with aqueous solutions and less superficial white glazing. Later, Ambrosi and co-workers, (Ambrosi et al. 2001, Dei and Giorgi 2001) successfully tested the first synthesized $Ca(OH)_2$ nanoparticles in lime mortar, limestone and wall paintings, achieving good results and good re-adhesion of detached pigment flakes without side effects. The nanolime developed by CSGI was further tested on several Italian frescoes (Baglioni et al. 2003, Baglioni and Giorgi 2006), limestone (Dei 2006) and a wall painting in the archaeological site of Calakmul (Baglioni et al. 2006) in Mexico, achieving a good degree of consolidation. All work undertaken by CSGI between 2001 and 2006 achieved better superficial re-cohesion and quicker carbonation with fewer applications

than limewater and without any aesthetic changes; thus demonstrating that nanolime is so far the best treatment for the consolidation of wall paintings.

Calosil® and Nanorestore® were tested by several authors in Europe since 2008. Using Calosil®, Drdácký (Drdácký et al. 2009) documented significant strength increase in lime mortars with far fewer applications than with limewater. Other authors (Daniele et al. 2008; Campbell et al. 2011; Daniele and Taglieri 2011) studied the consolidation and penetration of nanolime on limestone(s) and lime mortars and found high superficial strengthening, although nanolime penetration only occurred within 200 µm-1 mm from the surface, depending on the porosity and degree of deterioration of the treated limestone (Ruffolo et al. 2014). These results highlight the importance of the material's pore structure in the effectiveness and penetration of the product. Other authors (Borsoi et al. 2012; Costa et al. 2012) observed insufficient nanolime penetration, no consolidation and nanolime migration back to the surface of the substrate in highly porous limestone, renders and mortars. Afterwards, it was verified that this phenomenon occurs during evaporation of the solvent (Borsoi et al. 2015). The strength and penetrability of Calosil® products in plasters, lime mortars and wall paintings was also studied (Daehne and Herm 2013). It was found that the strength of lime mortar can be increased up to seven times when Calosil® E-25 is applied with cellulose ether gels (hydroxypropylcellulose gel) and that the addition of a low amount of Calosil®-Micro (contains 1-3 µm calcium hydroxide particles) enhances penetration and reduces back-migration.

Treatments combining nanolime and other products were also studied. The CSGI team (Baglioni et al. 2003; Baglioni et al. 2006) used a combined treatment of barium hydroxide and nanolime for the treatment (desulphation and consolidation) of wall paintings. This combined application was improved later in 2010 (Giorgi et al. 2010) with nanoparticles of both barium and calcium hydroxides. The combination of nanolime dispersions (CaLoSiL®) with silicic acid esters (SAE) can be used to enhance the affinity of SAE to a calcareous

matrix (Piaszczynski and Wolf 2011). Photo-catalytic nanolime (Nuño et al. 2015) has been successfully used for self-cleaning coatings and environmental pollution control.

## Factors influencing nanolime performance

There are several factors influencing the effectiveness of nanolime as a consolidant: nanolime characteristics (concentration and type of solvent, particle size, morphology and specific surface area), physical and mechanical characteristics of the substrate, extrinsic factors (RH, temperature, exposure time, $CO_2$ available) and application method. Some of the published literature explains its effectiveness as a consolidant.

It has been shown that nanolimes have superior consolidation properties to limewater, including both higher and faster carbonation with greater penetration (Ambrosi et al. 2001; Dei and Giorgi 2001; Dei and Salvadori 2006). A short-chain alcohol dispersion provides the following benefits: 1) greater colloidal stability (Dei and Giorgi 2001); 2) solvent evaporation so that higher concentrations of $Ca(OH)_2$ are attained (Giorgi et al. 2000); 3) higher amounts of lime (up to 30 times higher), resulting in an increased lime incorporation into the treated substrate and lower number of applications (Dei and Salvadori 2006); 4) enhancement of carbonation kinetics and $CaCO_3$ polymorph nucleation (Rodriguez-Navarro et al. 2013); 5) significant reduction of the amount of water introduced into the treated material. Nanoparticles in an alcohol dispersion penetrate better in porous structures and carbonate faster due to their higher specific surface area (Sequeira et al. 2006).

The role of the solvent for in-depth consolidation was studied recently (Borsoi et al. 2016). It was found that solvents with high boiling points improve the depth of nanolime deposition in stones with large pores (35–40 µm), while solvents with lower boiling points perform better in materials with finer pores (0.5-2 µm), which reduces nanolime migration back to the surface during the solvent drying. Comparison of different concentrations (5 and 25 g/L in isopropanol) of different products (Calosil®, Nanorestore® and Merck®) for the consolidation of lime mortars found that lower concentrations (Calosil® 5 g/L) yield the most significant improvement in the degree of carbonation in the pores (Arizzi et al. 2015). A percentage of residual water content in the alcohol medium (1:10 w/a ratio) clearly enhanced the carbonation process (Dei and Salvadori 2006; Daniele and Taglieri 2010). The colloidal behaviour of $Ca(OH)_2$ nanoparticles in alcohol was studied (Rodriguez-Navarro et al. 2013; Rodriguez-Navarro et al. 2016) and showed that, upon contact with alcohol, $Ca(OH)_2$ nanoparticles partially transform into Ca-alkoxides via the reaction $Ca(OH)_2 + 2ROH \rightleftarrows Ca(OR)_2 + 2H_2O$. The Ca-alkoxide conversion is time-dependent; therefore a long period of storage will produce higher conversion. The rate of carbonation of $Ca(OH)_2$ particles is reduced by this conversion, so that a freshly prepared alcohol dispersion should be preferred. The influence of repeated applications (1 to 6) of Calosil® with different concentrations on high porosity stone showed that the appropriate amount of consolidant has to be chosen in relation to the stone porosity; the optimal treatment for stones with large pores (±48 µm) seems to be 2 applications of Calosil® at 25 g/L concentration (Slizkova et al. 2012).

Relative humidity, temperature, and exposure time strongly influence the carbonation kinetics and the precipitation of $CaCO_3$ polymorphs (López-Arce et al. 2010). It was shown that the nucleation of polymorphs varies as a function of RH and time, and the optimum carbonation rate is achieved at high RH (75-90% RH). The full carbonation may be achieved in 9-10 days at room temperature, ambient $CO_2$ concentration and high RH values (75%) (Baglioni et al. 2014). An important factor in the consolidation of porous substrates using nanolime is the availability of sufficient $CO_2$ in the pores of the treated material for the calcium hydroxide to fully carbonate. Some research groups investigated the possibility of increasing the amount of $CO_2$ in the pores of treated substrates. For example, the Taglieri team (Daniele et al. 2008) achieved full and faster carbonation by adding sodium bicarbonate ($NaHCO_3$) to the alcohol solution. However, the addition of $NaHCO_3$ may induce the formation of salt efflorescence. Other researchers (Lopez-Arce and Zornoza-Indart 2015) obtained good results and a full conversion in 21 days by creating a $CO_2$-rich atmosphere in a yeast-sugar environment.

## Conclusions

The paper gives an overview of the available literature about nanolime as a consolidant for calcareous substrates. There is no question that nanolime represents one of the most promising materials for the conservation of calcareous substrates because of its compatibility and minimal side effects. However, it is clear that more technical and practical knowledge needs to be acquired. The main conclusion is that whilst nanolime appears to be an effective consolidation treatment for superficial consolidation, when an in-depth consolidation is needed, as in the case of large portions of weathered porous substrates, the results vary significantly between materials. In-depth consolidation is influenced by several factors such as substrates' porous structure and nature, nanolime concentration, nature of solvent, RH, time, $CO_2$ exposure, additives, storage and application method. The interaction between all of these factors requires further study. Furthermore, the literature lacks data on the long-term performance of nanolime treated materials. The popularity of nanolime is growing and future investigations will hopefully contribute to addressing its current limitations.

## Bibliography

AMBROSI M., DEI L., GIORGI R., et al., (2001). "Colloidal particles of $Ca(OH)_2$: Properties and applications to restoration of frescoes", Langmuir, 17(14), pp.4251–4255.

ARIZZI A., GOMEZ-VILLALBA L.S., LOPEZ-ARCE P., et al., (2015), "Lime mortar consolidation with nanostructured calcium hydroxide dispersions: the efficacy of different consolidating products for heritage conservation". European Journal of Mineralogy, 27(3), pp.311–323.

BAGLIONI, P., CARRETTI, E., DEI, L., et al., (2003). "Nanotechnology in wall painting conservation". Self-Assembly, ed. B.H. Robinson, (IOS-Press), pp.32–41.

BAGLIONI P., CHELAZZI D., GIORGI R., et al., (2014). "Commercial $Ca(OH)_2$ nanoparticles for the consolidation of immovable works of art". Applied physics. A, Materials science & Processing, 114(3), pp.723–732.

BAGLIONI P., CARRASCO-VARGAS R., CHELAZZI D., et al., (2006). "The Maya site of Calakmul: In situ preservation of wall paintings and limestone using nanotechnology". IIC Congress, the object in context: Crossing conservation boundaries: Contributions to the Munich, Munich, pp.162–169.

BAGLIONI, P., GIORGI, R., (2006). "Soft and hard nanomaterials for restoration and conservation of cultural heritage". Soft Matter Journal, Royal Society of Chemistry, pp.293–303.

BORSOI G., LUBELLI B., VAN HEES R., et al., (2016). "Effect of solvent on nanolime transport within limestone: How to improve in-depth deposition". Colloids and Surfaces A: Physicochemical and Engineering Aspects, 497, pp.171–181.

BORSOI G., TAVARES M., VEIGA R., et al., (2012). "Microstructural characterization of consolidant products for historical renders: an innovative nanostructured lime dispersion and a more traditional ethyl silicate limewater solution". Journal of Microscopy Society of America, 18(5), pp.1181–9.

BORSOI G., LUBELLI B., VAN HEES R., et al., (2015). "Understanding the transport of nanolime consolidants within Maastricht limestone". Journal of Cultural Heritage, pp.1–8.

BRAJER, I., KALSBEEK, N. (1999), "Limewater absorption and calcite crystal formation on a limewater-impregnated secco wall-painting". IIC Studies in Conservation 44(3), pp.145–156.

CAMPBELL A., HAMILTON A., STRATFORD T., et al., (2011). "Calcium hydroxide nanoparticles for limestone conservation: Imbibition and adhesion". Proceedings of symposium, adhesives and consolidants for conservation, Ottawa, pp.1–16.

COSTA, D., RODRIGUEZ DELGADO, J., (2012). "Consolidation of a porous limestone with nanolime". Proceedings of the 12th International Congress on the Deterioration and Conservation of Stone, New York.

DAEHNE A., HERM C., (2013). "Calcium hydroxide nanosols for the consolidation of porous building materials". Heritage Science, 1(1), p.1-9.

DANIELE, V., TAGLIERI, G., (2011). "$Ca(OH)_2$ nanoparticle characterization: microscopic investigation of their application on natural stones". Materials Characterisation, 72, pp.55–66.

DANIELE, V., TAGLIERI, G., (2010). "Nanolime suspensions applied on natural lithotypes: The influence of concentration and residual water content on carbonatation process and on treatment effectiveness". Journal of Cultural Heritage, 11(1), pp.102–106.

DANIELE, V., TAGLIERI, G., (2012). "Synthesis of $Ca(OH)_2$ nanoparticles with the addition of Triton X-100. Protective treatments on natural stones: Preliminary results". Journal of Cultural Heritage, 13(1), pp.40–46.

DANIELE, V., TAGLIERI, G., et al., (2008). "The nanolimes in cultural heritage conservation: Characterisation and analysis of the carbonatation process". Journal of Cultural Heritage, 9(3), pp.294–301.

DEI, L., SALVADORI, B., (2006). "Nanotechnology in cultural heritage conservation: nanometric slaked lime saves architectonic and artistic surfaces from decay". Journal of Cultural Heritage, 7(2), pp.110–115.

DEI, L., GIORGI, R., (2001). "Stable dispersions of $Ca(OH)_2$ in aliphatic alcohols: properties and application in cultural heritage conservation". Progress in Colloid and Polymer Science, 118, pp.68–72.

DELFROT B., BORN M., CHIVÉ A., (1997). "Colloidal calcium hydroxide in organic medium: Synthesis and analysis".J Colloid Interface Science, 157(189), pp.151–157.

DRDÁCKY M., SLÍZKOVÁ Z., ZIEGENBALG G., (2009). "A Nano approach to consolidation of degraded historic lime mortars". Journal of Nano Research, 8, pp. 13-22.

GIORGI R., AMBROSI M., TOCCAFONDI N., et al., (2010). "Nanoparticles for cultural heritage conservation: Calcium and barium hydroxide nanoparticles for wall painting consolidation". Chemistry - A European Journal, 16(31), pp.9374–9382.

GIORGI, R., DEI, L., BAGLIONI, P., (2000), "A new method for consolidating wall paintings based on dispersions of lime in alcohol". Studies in Conservation, 45(3), pp.154–161.

LIU T., ZHU Y., ZHANG X., et al., (2010). "Synthesis and characterization of calcium hydroxide nanoparticles by hydrogen plasma-metal reaction method". Materials Letters, 64(23), pp.2575–2577.

LÓPEZ-ARCE P., GÓMEZ-VILLALBA L.S., PINHO L., et al., (2010). "Influence of porosity and relative humidity on consolidation of dolostone with calcium hydroxide nanoparticles: Effectiveness assessment with non-destructive techniques". Materials Characterization, 61(2), pp.168–184.

Jorge Otero, A. Elena Charola, Carol A. Grissom, Vincenzo Starinieri
**An overview of nanolime as a consolidation method for calcareous substrates**

pp. 71-78

LOPEZ-ARCE, P., Zornoza-Indart, A., (2015). "Carbonation acceleration of calcium hydroxide nanoparticles: induced by yeast fermentation". Applied Physics A, 120(4), pp.1475–1495.

NANNI, A., DEI, L., (2003). "Ca(OH)$_2$ nanoparticles from W/O microemulsions". Langmuir, 19(13), pp.933–938.

NUÑO M., PESCE G. L., BOWEN C. R., et al., (2015). "Environmental performance of nano-structured Ca(OH)$_2$/TiO$_2$ photocatalytic coatings for buildings". Building and Environment, 92, pp.734–742.

OTERO, J., CHAROLA, A. E., GRISSOM, C., STARINIERI, V., "An overview of nanolime as a consolidant for calcareous substrates". Proceedings of the 5th International Conference Youth in Conservation of Cultural Heritage YOCOCU 2016, MNCARS (in press).

PE, L.A., WANG, L., MATIJEVIC, E., et al., (1998). "Nanosize indium hydroxide by peptization of colloidal precipitates". Langmuir, 7463(8), pp.4397–4401.

POGGI G., TOCCAFONDI N., CHELAZZI D., et al., (2016). "Calcium hydroxide nanoparticles from solvothermal reaction for the deacidification of degraded waterlogged wood". Journal of Colloid and Interface Science, 473, pp.1–8.

PIASZCZYNSKI, E., WOLF, V. (2011). "The combination of nano-lime and silicic acid ester for stone conservation". Proceedings of the European Workshop on Cultural Heritage Preservation, Berlin 2011, Fraunhofer IRB:Verlag, 254.

PRICE C. A., ROSS K., (1988). "A further appraisal of the 'lime technique' for limestone consolidation, using a radioactive tracer. Studies in Conservation, 33(4), pp.178–186.

RODRIGUEZ-NAVARRO C., SUZUKI A., RUIZ-AGUDO E., (2013). "Alcohol dispersions of calcium hydroxide nanoparticles for stone conservation". Langmuir, 29(36), pp.11457–11470.

RODRIGUEZ-NAVARRO C., VETTORI I., RUIZ-AGUDO E., (2016). "Kinetics and mechanism of calcium hydroxide conversion into calcium alkoxides: Implications in heritage conservation using nanolimes". Langmuir, 32(20), pp. 5183-5194.

ROY, A., BHATTACHARYA, J., (2010). "Synthesis of Ca(OH)$_2$ nanoparticles by wet chemical method". Micro & Nano letters, (3), pp.131–134.

RUFFOLO S. A., LA RUSSA M.F., ALOISE P., et al., (2014), "Efficacy of nanolime in restoration procedures of salt weathered limestone rock". Applied Physics A: Materials Science and Processing, 114, pp.753–758.

SALVADORI, B., DEI, L., (2001). "Synthesis of Ca(OH)$_2$ nanoparticles from diols". Langmuir, 17(8), pp.2371–2374.

SAMANTA A., CHANDA D. K., SEKHAR-DAS P., et al., (2016). "Synthesis of nano calcium hydroxide in aqueous medium". Journal American Ceramic Society, 795(37004), pp.787–795.

SEQUEIRA S., CASANOVA C., CABRITA E.J., (2006). "Deacidification of paper using dispersions of Ca(OH)$_2$ nanoparticles in isopropanol". Journal of Cultural Heritage, 7, pp.264–272.

SLIZKOVA, Z., FRANKEOVA, D., (2012). "Consolidation of a porous limestone with nanolime". Proceedings of the 12th International Congress on the Deterioration and Conservation of Stone, New York.

TAGLIERI G., DANIELE V., DEL RE G., et al., (2015). "A new and original method to produce Ca(OH)$_2$ nanoparticles by using an anion exchange resin". Advances in Nanoparticles, 4, pp.17–24.

ZIEGENBALG, G., (2003). Verfahren zur verfestigenden Behandlung von mineralischen anorganischen Baustoffen, Patent number: DE:10327514

**Jorge Otero**
jorge.otero@student.shu.ac.uk

Jorge Otero is a Vice Chancellor's PhD student at the Materials and Engineering Research Institute at Sheffield Hallam University, UK. He received his Master's degree in technologies for the conservation of unmovable heritage from the University of Vigo (2011), Spain. He was Icon Intern in Preventive Conservation at the National Trust for Scotland, UK (2014-15) and MCI intern at the Museum Conservation Institute of the Smithsonian Institution, USA (2016).

**Dr. A. Elena Charola**
CharolaA@si.edu

Dr. A. Elena Charola obtained her doctorate in Chemistry from the Universidad Nacional de La Plata, Argentina. After having served at the Metropolitan Museum of Art, New York City (1981-85) and at ICCROM, Rome (1986-87), she has been in private practice, working mainly for World Monuments Fund and its Portuguese affiliate WMF-Portugal as Scientific Advisor and Program Coordinator (2005-08). For over 15 years, she was Lecturer at the Graduate Program of Historic Preservation at the University of Pennsylvania and a Guest Lecturer at the Katholieke Universiteit Leuven in Belgium. At the Museum Conservation Institute of the Smithsonian Institution in Washington, DC, she was a Visiting Scientist (2008-2010) and is currently a Research Scientist since 2011. She has published extensively in the field of stone conservation.

Jorge Otero, A. Elena Charola, Carol A. Grissom, Vincenzo Starinieri
**An overview of nanolime as a consolidation method for calcareous substrates**

pp. 71-78

**Carol Grissom**
GrissomC@si.edu

Carol Grissom has been Senior Objects Conservator at the Smithsonian's Museum Conservation Institute since 1984. She obtained a master's degree in art conservation from Oberlin College and gained further training at the national conservation institutes of Belgium and Italy. Her special interests include stone and metals conservation, notably of nineteenth-century zinc sculpture.

**Dr. Vincenzo Starinieri**
v.starinieri@shu.ac.uk

Dr. Vincenzo Starinieri is a Research Fellow in the Materials and Engineering Research Institute at Sheffield Hallam University. He holds a PhD in Science for Conservation of Cultural Heritage from the University of Bologna and a Master's Degree in Geology from the University of Chieti - Pescara. He specialises in the characterisation of masonry materials, the investigation of their degradation phenomena and the development of materials and technologies for their conservation and repair.

Original article

# The biocalcarenite stone of Agrigento (Italy): Preliminary investigations of compatible nanolime treatments

Giuliana Taglieri [a], Jorge Otero [b], Valeria Daniele [a],*, Gianluca Gioia [a], Ludovico Macera [a], Vincenzo Starinieri [b], Asuncion Elena Charola [c]

[a] Department of Industrial and Information Engineering and Economics, University of L'Aquila, via G. Gronchi 18, 67100 L'Aquila, Italy
[b] Materials and Engineering Research Institute, Sheffield Hallam University, S1 1WB Sheffield, UK
[c] Museum Conservation Institute, Smithsonian Institution, Washington, DC, USA

## ARTICLE INFO

## ABSTRACT

Nanolime is a promising consolidant for the conservation of most historic structures thanks to its high compatibility with carbonate-based substrates. Nanolime can recover the superficial cohesion of deteriorated surfaces thanks to its potential to complete the carbonation process, recreating a thin network of new cementing calcium carbonate. In this paper, the nanolime was produced by an innovative, time and energy-saving and scalable method, and its efficacy was tested preliminary on biocalcarenite stones from Agrigento. The stones characterization as well as the treatment effectiveness, in terms of protection against water and superficial consolidation, was investigated by several techniques such as X-ray fluorescence, X-ray diffraction, scotch tape test, water absorption by capillarity, mercury intrusion porosimetry, drilling resistance measurement system and colorimeter. Investigations showed that nanolime could guarantee a complete transformation in pure calcite together with a superficial consolidation and a reduction in water absorption.

© 2017 Elsevier Masson SAS. All rights reserved.

## 1. Introduction

Calcareous materials have been one of the main construction materials throughout the ages and proved to be very durable over the centuries. However, they may suffer several degradation processes (e.g. flaking of the surface, powdering and formation of small blisters) that can be recovered through the application of consolidants. Over the last century, several consolidants have been used: silicate-based products or organic consolidants, such as alkoxysilanes, acrylic, epoxy or vinyl resins, have been commonly used in restoration treatments, mainly due to their immediate strength enhancement and ease of application. However, the low physico-chemical compatibility, the lack of bonding between the mineral calcareous matrix and the consolidant material and even the deterioration of the organic consolidant itself, discourages their use and in some cases may compromise the conservation of the monument [1–3]. Inorganic consolidants and, among others, lime-based consolidants present the great advantage of their total chemical compatibility with the calcitic substrate, thanks to their aptitude to react with atmospheric carbonic dioxide to produce calcium carbonate (carbonation process). However, traditional lime-based treatments were considered to have some limitations, such as the reduced impregnation depth and the very slow rate of carbonation [4–6]. In order to reduce such limitations, in 2001 Ca(OH)$_2$ nanoparticles, dispersed in an alcoholic or hydro-alcoholic medium, (nanolimes) were synthesised. So far, nanolimes have been tested on mural paintings, stuccoes and natural stones, and on all the carbonatic-based substrate where a restoration treatment was required [5,7–20]. The efficacy of nanolime dispersions can be affected by several factors, such as the dispersion concentration, solvent type, porosity of the substrates to be treated and relative humidity (RH) conditions. It is commonly agreed that lower concentration of the suspensions (i.e. 5 g/L) help reduce the accumulation of the consolidating product near the surface and significantly improve the yield of carbonation in the pores [16,17]. Furthermore, it has been proved that the concentration and the number of treatments cycles have a significant influence on the strengthening effect, in relation to the stone porosity as well [16,18]. A percentage of residual water content in the dispersing medium (> 10% in volume) clearly enhanced the carbonation process [19]. Recent investigations suggests that nanolime penetrates well in porous materials, but it can be transported back to the surface as the solvent evaporates [20]. Moreover, the type of alcoholic solvent and the RH conditions seem to have an influence

* Corresponding author.
  E-mail address: valeria.daniele@univaq.it (V. Daniele).

on the rate of the carbonation reaction, and the formation of different polymorphs of calcium carbonate [21,22]. Currently, nanolimes have been synthetized according to several routes, [10,23–26], where $Ca(OH)_2$ was rarely the only reaction product. Washings and purification steps were frequently needed to eliminate the by-products and/or organic compounds, leading to low yield and prolonged synthesis time. The development of a versatile, cost effective and up-scalable method can be essential to the success of introducing nanolime for widespread usage on carbonatic substrates. Recently, an innovative and patented method, based on the ion exchange process, was proposed [27]. This method worked at room temperature and ambient pressure, and it allowed producing, in few minutes and without intermediate steps, pure and crystalline $Ca(OH)_2$ nanoparticles in aqueous suspension. The resulting portlandite nanocrystals, less than 100 nm in size, are very reactive, with a complete carbonation process, forming pure calcite in few hours or up to 7 days, depending on solvent, concentration and RH of the environment [28–31]. In addition, the produced nanolime can be dispersed, at different solid concentrations, in mixed water/alcohol (W/A) mixtures in order to improve both the colloidal stability and/or the amounts of consolidant. Specifically, nanolime dispersions in a mixture of 50% water and 50% isopropanol in volume, (W/A = 50%), demonstrated to be particularly suitable in optimizing the carbonation process [14,29].

The aim of the present work is to test the effectiveness of this nanolime as a compatible treatment on biocalcarenite stones. Specifically, these stones constitute the building material used for most of the buildings of the "Valley of the Temples" in Agrigento – Sicily, Italy, characterized by a documented advanced decay [32–34]. The paper has been divided into three parts:

- synthesis and characterization of the nanolime;
- characterization of the biocalcarenite stone from a physicochemical and mechanical point of view;
- testing, in a preliminary way, of different nanolime formulations by varying the solvents and the nanolime concentration. The evaluation of the treatment effectiveness in terms of protection against water and superficial consolidation was properly investigated.

## 2. Research aim

Colloidal $Ca(OH)_2$ nanoparticles (also called nanolime) are emerging as effective conservation material for all carbonatic-based substrate. Nanolime can recover the superficial cohesion of deteriorated surfaces, thanks to its potential to complete the carbonation process, recreating a thin network of new cementing calcium carbonate.

In the present paper we report, for the first time, results about the effectiveness of the treatments by a not commercial nanolime on biocalcarenite stones from "Valle dei Templi" – Agrigento. In particular, the nanolime is synthesized in laboratory by our original, eco-friendly, one-step and scalable method that provides pure and crystalline nanoparticles in a reproducible way. Moreover, the simplicity and rapidity of this novel procedure provides an ideal opportunity to scale up the nanoparticles production in order to extend their uses in all the application fields where large amounts of such compatible consolidant should be requested. The effectiveness of the nanolime treatments, in terms of reduction of porosity, protection against water absorbed by capillarity and superficial consolidation, is investigated by means of several techniques. The physico-chemical and mechanical characterization of the untreated stones is reported too.

## 3. Material and methods

### 3.1. Synthesis and characterization of nanolime

$Ca(OH)_2$ nanoparticles were synthesized by an anionic exchanges process, at room temperature and ambient pressure, by mixing under moderate stirring an anion exchange resin with an aqueous calcium chloride solution [27]. The supernatant water of the produced nanolime suspension ($N_W$) was partially extracted and substituted with isopropanol or with 1-buthanol. Three nanolime dispersions were prepared: two of them, named $N_{50\%}$ and $N^*_{50\%}$, were characterized by a water/isopropanol mixture, (W/A = 50%), and a solid concentration of 5 g/L and 10 g/L, respectively; and the third dispersion, named $N_B$, was characterized by a water/1-butanol mixture (W/A = 5%) and a solid concentration of 5 g/L. In particular, $N_B$ was considered to assess its influence on nanolime performance due to its slow evaporation rate. The size, shape and degree of agglomeration of the nanoparticles were determined by transmission electron microscopy (TEM, Philips CM200) and the crystalline phase was analyzed by XRD (PANalytical XPertPRO). Both TEM and XRD samples were prepared diluting the suspension in ethanol under nitrogen atmosphere to avoid the carbonatation process. In addition, by means of XRD, we analyzed the carbonation reaction of each dispersion, taking 0.12 mL of nanolime sample, left to dry in air in room conditions (T = 20 ± 2°C, R.H. = 5 0 ± 5%), until complete solvent evaporation (about 20 minutes). XRD patterns were recorded in step size of 0.026°2θ, in the angular range 10–70°2θ. HighscorePlus software by PANalytical and ICSD and ICDD reference databases were used for the mineralogical identification and to perform the quantitative analysis (Rietveld refinement).

Kinetic stability of the produced suspensions was determined by turbidity measurements, analysing their absorbance at λ = 600 nm by using UV/VIS Spectrophotometer (Lambda 2 Perkin-Elmer). Before the test, nanolimes were sonicated for 20 minutes (Ultrasonic bath by Ultra Sonik 300) to reduce the nanoparticle agglomeration. Measurements were taken for up to 2 hours. The KS % was measured in function of time and was calculated using the following formula:

KS % = 1 − [(A0−At)/A0] × 100

where $A_0$ is the starting absorbance and At the absorbance at time t, both evaluated at wavelength 600 nm [35]. The relative kinetic stability (KS %) decreases as result of the nanoparticle settling; values range from 0 (unstable dispersion) to 100 (not settling of the nanoparticles).

### 3.2. The Agrigento's biocalcarenite

The stones used in this work, which were obtained from the local quarry of Villaseta, have similar characteristics to the ones used for the construction of the Temples [36]. Chemical, mineralogical and physical features of the stones were studied using different techniques. A general examination was performed using a stereomicroscope (SM, Leica Stereozoom S8APO). The chemical and mineralogical composition was determined by X-Ray Fluorescence (XRF, Philips PW2440), X-Ray Diffraction (XRD, PANalytical XPert PRO) and Attenuated Total Reflectance – Fourier Transform Infrared, (ATR-FTIR, Thermo Nicolet Nexus instrument). In particular, XRF samples were prepared as FP pellets. For XRD measurements, stone samples were milled and sieved through a 50 μm mesh and placed over a XRD zero-background sample holder; the patterns analysis was performed as reported above. FTIR spectra were collected by 64 scans in the range 400–4000 cm$^{-1}$ at a spectral resolution of 4 cm$^{-1}$. The obtained FTIR spectrum was identified using the Infrared and Raman users Group (IRUG) libraries, the HR Hummel Polymer and Additives library as well as the ASTER

mineral library. The pore structure of the stone was determined, on three samples (named $B_1$, $B_2$ and $B_3$ respectively), by Mercury Intrusion Porosimetry, (MIP, PASCAL 140/240). A contact angle of 141° was assumed between mercury and the stone. An equilibration time of 30 s was used between each pressure increase step and the measurement of the intruded volume. Prior to MIP analysis, samples were dried in a fan-assisted oven at 80°C to constant weight. The water absorption by capillarity (WAC) of the stones was measured on three cubic samples ($30 \times 30 \times 30$ mm) following the standard procedure [10]. A Drilling Resistance Measurement System (DRMS) from SINT-Technology was used to measure changes in strength along the drilling path into the stone. The DRMS measures the force required to drill a hole at constant rotation (rpm) and lateral feed rate (mm/min). The force is known to correlate with the compressive strength of the material. Values were calculated as mean of 3 tests. The test was carried out using drill bits of 5 mm diameter, rotation speed of 200 rpm, a rate of penetration of 15 mm/min and penetration depth of 10 mm.

## 3.3. Nanolime treatments applied on the Agrigento stones

In order to investigate, in a preliminary way, the nanolime effectiveness in reducing capillary water absorption and yielding superficial consolidation, three stones samples with irregular shape, S1, S2 and S3 (Fig. 1a), were treated with $N_{50\%}$, $N^*_{50\%}$ and $N_B$ respectively. The use of irregularly shaped stone samples was considered to reproduce the real in situ application on irregular surfaces. Nanolimes were applied by brushing until stone saturation was achieved, by using about 100 mg of calcium hydroxide for each stone surface. Brushing treatment was applied to the side with largest and mostly flat surface (approx. 10 cm² each). Straight after treatment, samples were wiped with a wet cloth to remove the excess of consolidant and to mitigate surface whitening. Stones were stored for 2 days at RH = $(75 \pm 5)$%. Then, the samples were oven-dried at 60°C until constant mass was reached, and then stored in a desiccator. Finally, we considered additional three samples (Fig. 1b): two for WAC (S4, S5 samples) and one (S6 sample) for the STT and DRMS resistance measures (carried out on 6 different points, in order to reduce the influence caused by the inhomogeneity of the stone). These were treated with nanolime applications repeated three times, following the same procedure reported above. In particular, for S4, S5 and S6 samples, we used the $N^*_{50\%}$ nanolime suspension that provided, as shown in the results section, the best compromise in terms of treatment efficacy and costs.

The effectiveness of the treatments, in terms of protection against water and superficial consolidation, was evaluated by
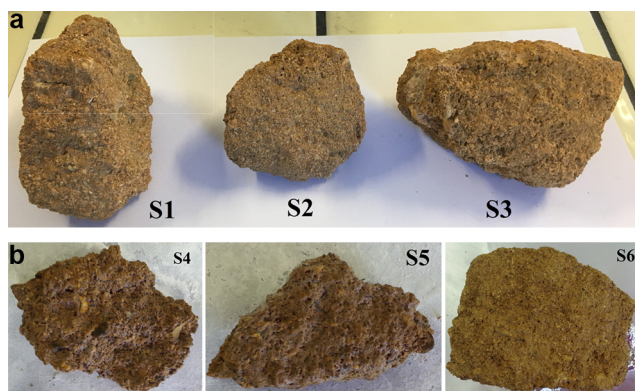


**Fig. 1.** Irregular biocalcarenite samples used for the nanolime treatments: a: S1 (approx. 17 cm²), S2 (approx. 14 cm²) and S3 (approx. 17 cm²); b: S4 (approx. 13 cm²), S5 (approx. 5 cm²) and S6 (approx. 22 cm²).

means of several tests. WAC was carried out, before and after treatment, following the method proposed by LNEC [37]. For each sample, we measured the values of the coefficient of average absorption in 30 minutes (CA), the amount of absorbed water at the end of the test (Qf) and the variation of CA values referred to untreated and treated stones (ΔCA). The effective protective efficacy (Ep), defined as the percentage variation of Qf before and after treatment, was evaluated too. Surface cohesion was estimated by the "Scotch Tape Test" (STT), according to ASTM D3359 [38]. Results were taken as the mean of three tests for each sample. In order to better assess the improvement of the consolidation efficacy of the treatment, we evaluated the difference of the superficial resistance (untreated and treated) using DRMS, generally considered the most suitable methodology for quantifying consolidation effectiveness and penetration depth of the consolidant, particularly in soft stones [39].

Pores size distribution and open porosity was measured by MIP; the tests were carried out on samples measuring approximately $8 \times 8 \times 8$ mm taken from both treated and untreated stones.

Finally, the color changes, before and after treatment, were evaluated on samples S1, S2 and S3 by using a spectrophotometer (Minolta CM508D Colorimeter) in CIE-Lab system colorimeter [40], considering 10 evaluations per stone in different areas of the treated face. Total color variation (ΔE) was calculated by the formula:

$$\Delta E = \sqrt{\Delta L^{*2} + \Delta a^{*2} + \Delta b^{*2}}$$

where $\Delta L^*$ was the change in luminosity (white-black parameter), $\Delta a^*$ (red-green parameters) and $\Delta b^*$ (blue-yellow parameters) were the chromaticity coordinates. Analyses were focused on total color variations and changes in the luminosity (white-black parameters).

## 4. Results and discussion

TEM micrograph on the nanolime sample $N_W$ (Fig. 2a) showed nanoparticles with dimensions < 20 nm, with a tendency to agglomerate forming hexagonally shaped clusters.

XRD results revealed that only pure $Ca(OH)_2$ was formed after synthesis (Fig. 2b). From the analysis of the carbonation process, we observed that whilst $N_{50\%}$ and $N^*_{50\%}$ showed a completed carbonation process, i.e., pure calcite ($CaCO_3$), only a partial conversion into calcite was observed for $N_B$ (Fig. 3a). In addition, an intermediate and metastable form, namely calcium carbonate hydroxide hydrate (CCH), was observed as in previous work [29]. As concerns the kinetic stability (Fig. 3b), $N_{50\%}$ and $N_B$ samples were consistently stable in the first 2 h (gradual settling process < 10%), showing a good kinetic stability for practical purposes. $N^*_{50\%}$ presented a rapid settling in the first 5 minutes but the KS parameters remained then stable, similarly to the other samples.

From the stereomicroscope investigations, the studied stones are rocks of clastic sedimentary origin composed mainly of bioclasts and whole skeletal fossil remains of marine aquatic organisms.

The observed bioclasts and whole skeletal fossil remains belonged to marine bivalves, gastropods, rhodoliths, echinoderms and bryozoans. Carbonate lithoclasts were also observed together with few quartz grains. All grains were bound together by a fine-grained calcite (micrite). Based on these results, the stone samples can be classified as calcarenite, biomicrite or grainstone [41–43], commonly defined as biocalcarenite and belonging to the limestone rock deposits described as "Formazione di Agrigento" [44].

The chemical analysis of the considered stone was reported in Table 1.

From XRD results (Fig. 4a), the main mineralogical phases were 88.8% of magnesium calcite ($Mg_{0.03}Ca_{0.97}(CO_3)$, ICSD# 980086161),
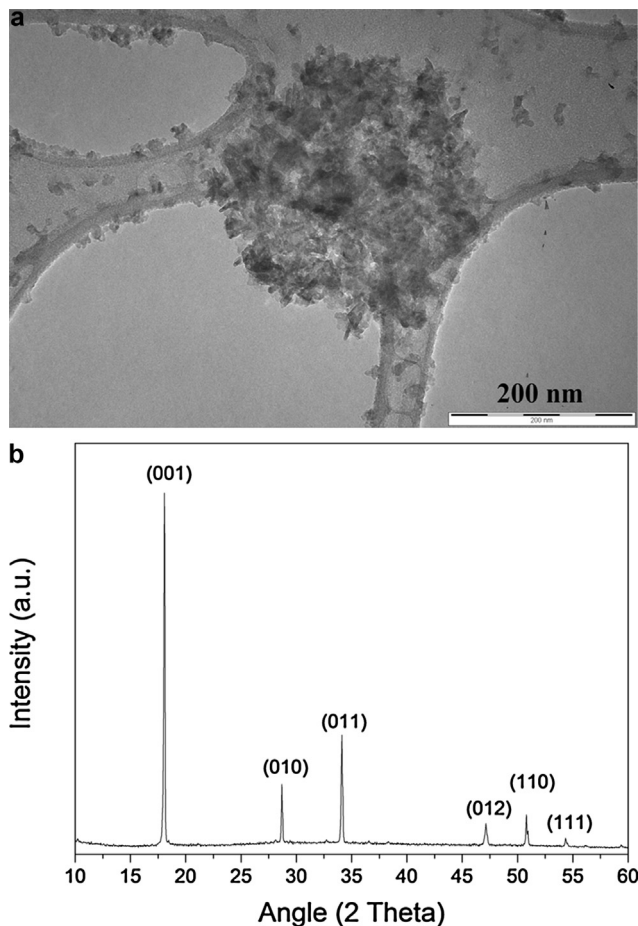
**Fig. 2.** a: TEM micrograph of the nanolime sample $N_w$; b: XRD pattern of dried particles from $N_w$ sample. Bragg peaks of $Ca(OH)_2$ pattern (ICSD#96-100-8782) were indexed.

**Fig. 3.** Analysis of the $N_B$, $N_{50\%}$ and $N^*_{50\%}$ suspensions, used for the treatments: a: the carbonatation process in ambient air ($Ca(OH)_2$, ICSD #96-100-8782; Calcite, ICSD # 98-015-8258; CCH: calcium carbonate hydroxide hydrate, ICDD # 00-023-0107); b: kinetic stability (KS) versus time, (at $\lambda = 600$ nm).

9.9% of quartz ($SiO_2$, ICSD# 980083849), 1.3% of lipscombite ($Fe_{2.95}(PO_4)_2(OH)_2$, ICSD# 980202937). XRD results were confirmed by FTIR investigation (Fig. 4b). The absorbance bands at 712, 876, 1429 $cm^{-1}$, assigned to the calcite, was readily detectable. For quartz, the absorbance bands at 798 and 1079 $cm^{-1}$ can be attributed to absorbance of the SiO group. The peaks for goethite at 796, 912 and 1044 $cm^{-1}$ cannot be easily distinguished due to the low concentration and the shifting with Si-O and carbonate groups.

In agreement with literature results, which assessed porosity in the range 20–30% for the biocalcarenite of Agrigento's Temples [36], from MIP we obtained an average porosity of 26.1% and a density of 1.8807 $g/cm^3$. In Fig. 4c the pore size distribution from MIP, referred to the three samples, is reported. Even if the samples presented some differences between them, the pore diameters were found to be mainly distributed in the 10–100 μm range (i.e., within the larger capillary pores range that has high capillary suction), without relevant contributions under 1 μm [45,46]. This explains the fast absorption observed below (WAC analyses) for the untreated samples as compared to the treated ones, where the larger pores have been reduced significantly. As concerns standard WAC measurements on the cubic samples, mean values of CA = 12.7 $mgcm^{-2}s^{-1/2}$ and $Q_f$ = 509 $mgcm^{-2}$ were evaluated. Finally, results coming from DRMS showed values of resistance that reach 6 N within the first 3 mm, reaching a maximum value of about 10 N between 3 and 10 mm, similar to what observed from literature [47].

MIP measurements of the S1, S2 and S3 treated samples, compared to the untreated ones, are reported in Fig. 5.

**Table 1**
XRF of the biocalcarenite sample (wt %).

| Ca | Si | Fe | Mg | Al | K | P |
|---|---|---|---|---|---|---|
| 23.30 | 7.20 | 1.67 | 0.40 | 0.34 | 0.14 | 0.11 |

As concerns S1 sample (Fig. 5a), the treatment yielded an increase in the population of pores with diameters between 13 and 50 μm, and a decrease in the population of pores with diameters between 2–3 and 13 μm; moreover, we observed a disappearing of the smallest pores ($\leq$ 0,1 μm). In the S2 and S2 samples (Fig. 5 b–c), the treatment worked mainly to reduce the number of pores with diameters between 30–100 μm.

Table 2 showed the results from the nanolime treatment on the irregular samples (WAC measurements), while in Fig. 6, we reported the WAC curves obtained for S4 and S5 before and after the nanolime treatment.

It can be observed that, already after one treatment, all the samples showed a clear reduction both in the kinetics of capillary absorption ($\Delta$CA) and in the protective efficacy $E_p$. In particular, we observed that the S1 sample showed the highest ability to absorb water both kinetically and in the saturation values, probably due to the higher porosity mainly related to the pores in the 10–100 μm
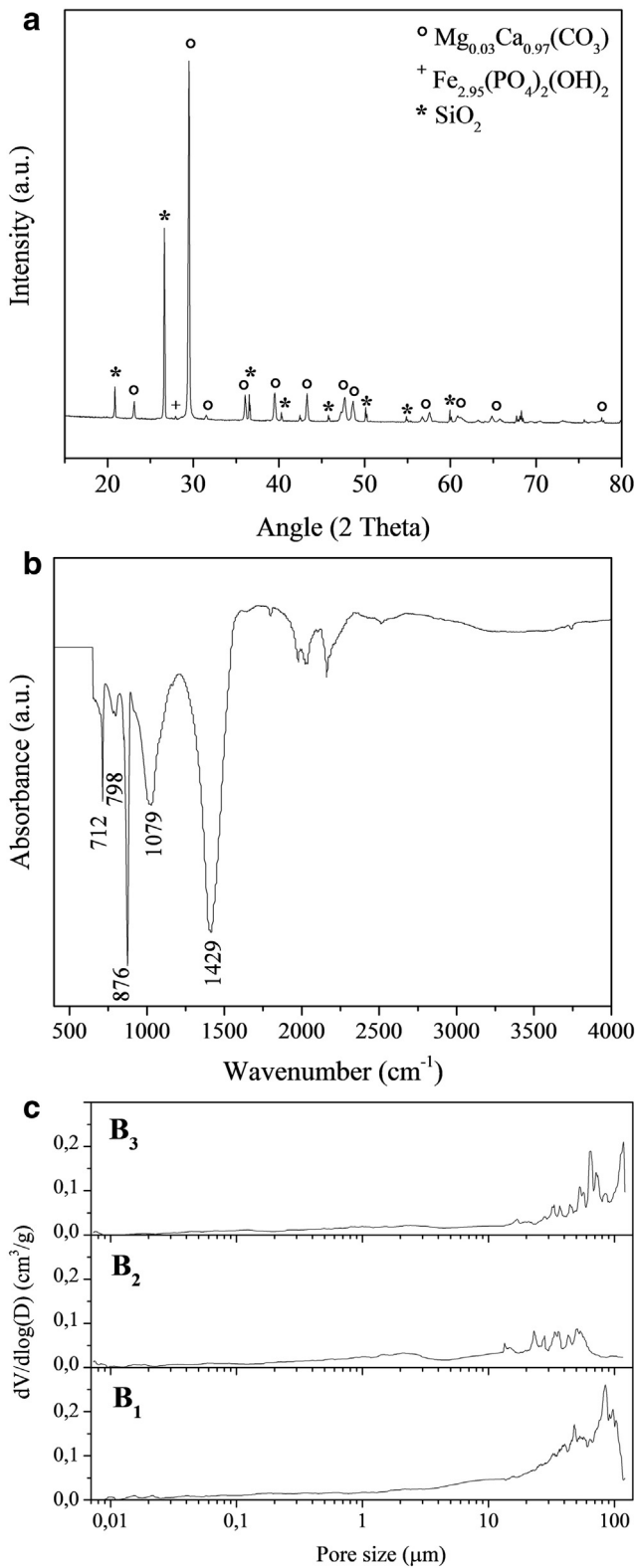
**Fig. 4.** a–b: XRD and FTIR spectra of the biocalcarenite sample; c: pore size distribution (MIP) obtained from three samples, $8 \times 8 \times 8$ mm each.



**Fig. 5.** Differential volume of intruded mercury versus pore diameter of treated (dot lines) and untreated (continuous lines) stone samples: S1 (a), S2 (b), S3 (c).

range (Fig. 5a). In this case, the nanolime treatment seemed to have a greater influence on $\Delta CA$ than on $E_p$, and this could be due to the nanolime ability to reduce pore sizes by partially filling them, but without occluding them. In parallel, the samples treated by using $N^*_{50\%}$ and $N_B$ reached the highest efficacy (about 50%) in the
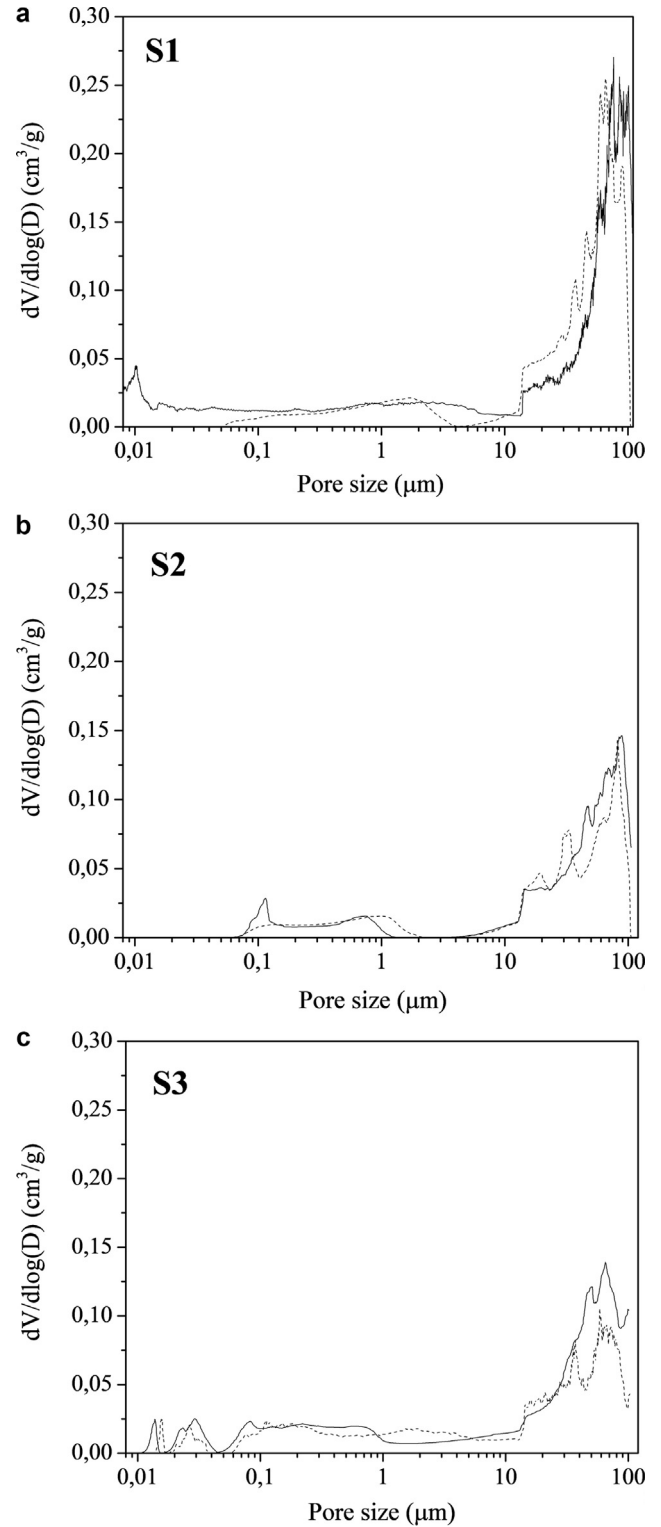
protection towards water. Then, when the $N^*_{50\%}$ treatment was repeated three times, the WAC results tended to improve respect to what obtained after only one treatment (Fig. 6).

This improvement was confirmed by MIP measurements, revealing a clear reduction in the population of pores with diameters between 40 and 100 $\mu$m, together with a decrease in the average porosity of about 60% (Fig. 6c).

**Table 2**
WAC results performed on irregular stones, before and after one nanolime treatment.

| | Untreated (UT) | Treated (T) | | |
| --- | --- | --- | --- | --- |
| | $Q_f$ (mg cm$^{-2}$) | $Q_f$ (mg cm$^{-2}$) | $\Delta CA$ (%) | $E_p$ (%) |
| S1 | 1013 | 720 | 44 | 28 |
| S2 | 646 | 355 | 21 | 45 |
| S3 | 625 | 324 | 30 | 48 |

S1, S2 and S3 were treated with $N_{50\%}$, $N^*_{50\%}$ and $N_B$ respectively.

In Table 3, the STT results indicated that the nanolime treatments determined an increase of the superficial cohesion of the treated stones, with a reduction in the percentage quantity of removed material ($\Delta M$) after one treatment of 10%, 14% and 30% for S1, S2 and S3 samples respectively. By repeating the treatment three times (S6) a clear $\Delta M$ improvement was obtained, reaching a mean value $\Delta M \approx 60\%$.

The drilling resistance profiles, performed before and after the nanolime treatment, showed that a significant increase can be observed only when the treatment was repeated for three times (S6 sample). The results, reported in Fig. 7, showed that before the treatment the S6 sample presented a value of resistance of $4 \pm 1$ N, slightly decreasing inside the stone. After treatment, in addition to a small improvement at the surface, we observed an increase of the resistance up to 10 mm from the surface with a medium value of $8 \pm 3$ N.

The colorimetry results were reported in Table 4, showed that the nanolime treatments do not cause major aesthetic changes ($\Delta E^*$ 5–9) and do not cause a significant increase in luminosity ($\Delta L^*$1–5). In particular no significant white glazing was observed after the treatment for S1, S2 and S3 ($\Delta L^*$ 3, 5 and 1 respectively).

S2 seemed to show the lowest chromatic alteration of the surface ($\Delta E^*$ 5) but the highest difference of luminosity ($\Delta L^*$ 5). S3 shows higher value with $\Delta E > 9$ due to a significant alteration with $b^* > 8$ (blue-yellow axis). S2 increases the $L^*$ parameter, probably due to the effect of higher concentration (10 g/L). The negligible chromatic changes for S1 and S2 (and $\Delta E^*$ 5–6) and the absence of a significant white glazing ($\Delta L^*$3–5) [40,48–50], make such nanolimes dispersions suitable for practical conservation interventions.

## 5. Conclusions

The present paper presented preliminary investigations to test the efficacy of a compatible conservative treatment for the biocalcarenite stones of the Valle dei Templi (Agrigento, Italy). The treated stone is a biocalcarenite mails composed by calcite, with less amount of quartz, lipsocombite, and shells; the measured average porosity is about 26%, mainly distributed in the range 10–100 μm, which can be responsible for the quick water ingress by capillarity. The conservative treatments were carried out by using a nanolime, ad hoc synthesized by means of an innovative method that can guarantee high yields and a high reactivity of the final product. The characterization analyses confirmed the high reactivity of the $Ca(OH)_2$ nanoparticles, reflecting a full carbonation process occurring, in ambient condition, in only the first 30 minutes. Moreover, the process led to the formation of calcite, as pure and unique phase, and this result is fundamental to guarantee a perfect compatibility with the treated surface, from a chemico-physical and mechanical point of view. As concerned the treatment efficacy, the best results were obtained by using the hydro-alcoholic nanolime suspension (50% water and 50% alcohol) at a concentration of 10 g/L, and by repeating the application for three times. This nanolime worked well as a superficial consolidant, increasing the superficial cohesion, with a reduction of material removed from the surface up to 60%, and a good increase of the mechanical resistance particularly
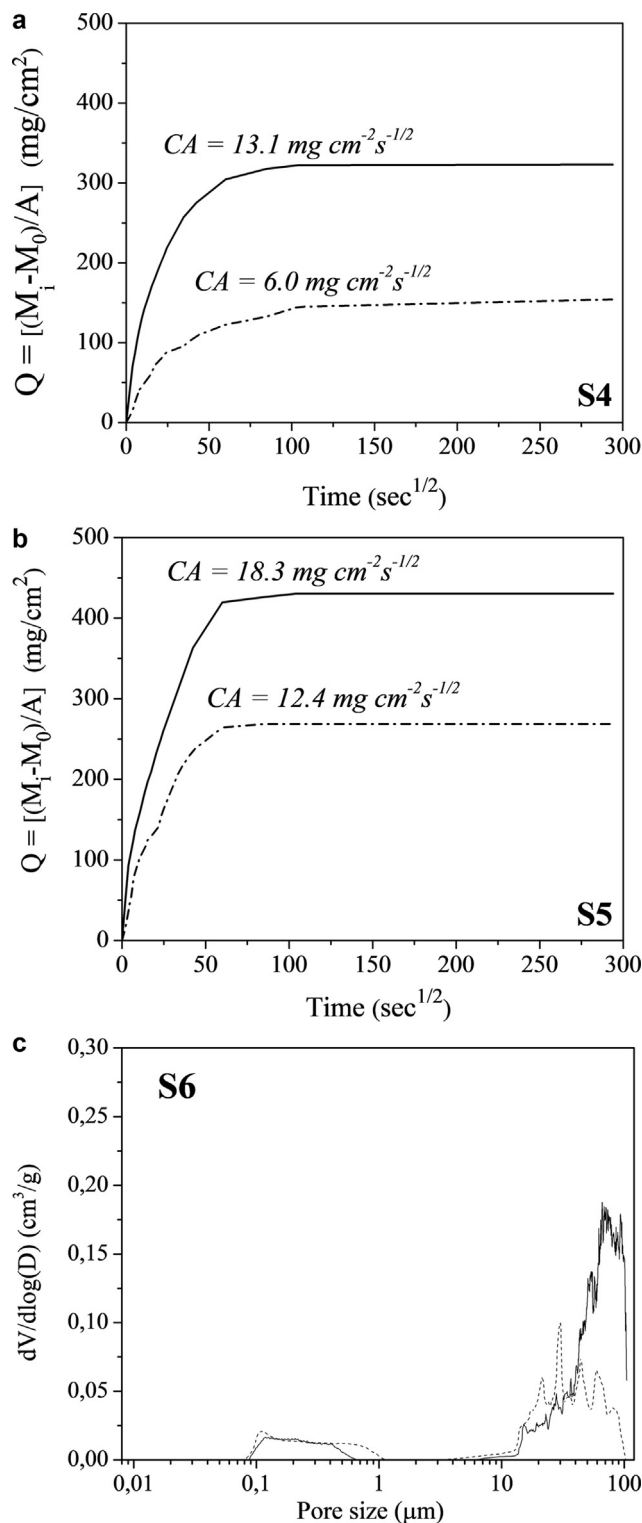
**Fig. 6.** WAC curves and MIP measurements before (continuous lines) and after (dot lines) the $N^*_{50\%}$ treatment, repeated 3 times. CA values were reported too.

in the first 10 mm beneath the surface. A decrease of the water adsorption by capillarity up to 50% was observed too, confirmed by a reduced porosity and a clear reduction in the population of pores with diameters between 40 and 100 μm. Nevertheless, the nanolime treatment caused some superficial whitening that needs to be removed by proper actions or examined in depth in a next study.

**Table 3**
Results of the STT performed on untreated and treated stones.

| | UT (mg cm$^{-2}$) | T (mg cm$^{-2}$) | $\Delta M$ (%) |
|---|---|---|---|
| S1 | 1.92 | 1.69 | 9.5 |
| S2 | 3.15 | 2.65 | 14.3 |
| S3 | 1.17 | 0.57 | 29.6 |
| S6 | 10.25 | 4.05 | 60.5 |

Scotch area: 12.72 cm$^2$ (S1, S2 and S3) and 9.5 cm$^2$ (S6).
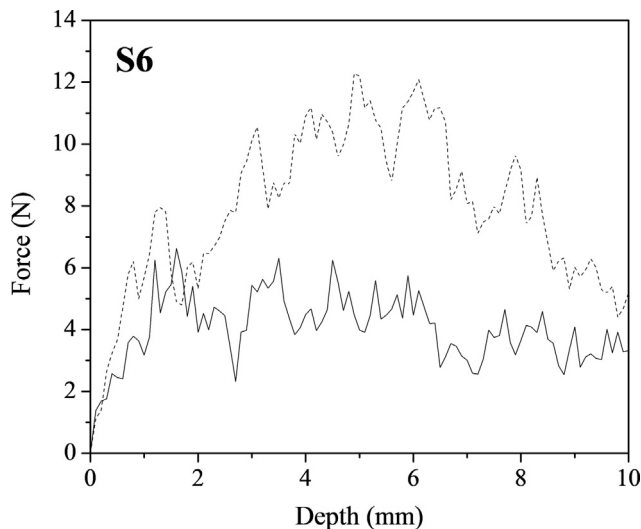


**Fig. 7.** Drilling resistance profiles of untreated (continuous line) and treated (dot line) biocalcarenite (S6 sample).

**Table 4**
Results of the colorimetric analysis performed on the treated stones.

| | $\Delta L$ | $\Delta a$ | $\Delta b$ | $\Delta E$ |
|---|---|---|---|---|
| S1 | 3.041 | −0.526 | −5.170 | 6.024 |
| S2 | 5.050 | 0.397 | −0.003 | 5.065 |
| S3 | 1.641 | 4.017 | 8.752 | 9.769 |

## Acknowledgements

## References

[1] E. Doehne, C.A. Price, Stone conservation: an overview of current research, Second ed., The Getty conservation institute, Getty publications, Los Angeles, 2011, pp. 35–37 (Research in conservation).

[2] F. Jroundi, et al., Bioconservation of deteriorated monumental calcarenite stone and identification of bacteria with carbonatogenic activity, Microb. Ecol. 60 (2010) 39–54.

[3] M. Tortora, et al., Non-destructive and micro-invasive testing techniques for characterizing materials, structures and restoration problems of mural paintings, Appl. Surf. Sci. 387 (2016) 971–985.

[4] D. Costa, J. Delgado Rodrigues, Consolidation of a porous stone with nanolime, 12th Int. Congress on Deterioration and Conservation of Stone, New York (USA), 2012.

[5] P. Baglioni, et al., Commercial Ca(OH)$_2$ nanoparticles for the consolidation of immovable works of art, Appl. Phys. A 114 (2014) 723–732.

[6] M.C. Mascolo, et al., An approach for a rapid determination of the aging time of lime putty, Thermochimica Acta 648 (2017) 75–78.

[7] A. Zornoza-Indart, et al., Consolidation of a Tunisian bioclastic calcarenite: from conventional ethyl silicate products to nanostructured and nanoparticle based consolidants, Construct. Build. Mater. 116 (2016) 188–202.

[8] I. Brajer, N. Kalsbeek, Limewater absorption and calcite crystal formation on a limewater-impregnated secco wall-painting, Stud. Conserv. 44 (3) (1999) 145–156.

[9] A. Daehne, C. Herm, Calcium hydroxide nanosols for the consolidation of porous building materials, EU-STONECORE, Herit. Sci. 1 (2013) 11.

[10] V. Daniele, et al., Synthesis of Ca(OH)$_2$ nanoparticles with the addition of Triton X-100. Protective treatments on natural stones: preliminary results, J. Cult. Herit. 13 (2012) 40–46.

[11] C. Rodriguez-Navarro, et al., Alcohol dispersions of calcium hydroxide nanoparticles for stone conservation, Langmuir 29 (2013) 11457–11470.

[12] J. Otero, et al., An overview of nanolime as a consolation method for calcareous substrates, Ge-Conservación 1 (11) (2017) 71–78.

[13] I. Natalia, et al., Consolidation and protection by nanolime: recent advances for the conservation of the graffiti, Carceri dello Steri Palermo and of the 18th century lunettes, SS. Giuda e Simone Cloister, Corniola (Empoli), J. Cult. Herit. 15 (2014) 151–158.

[14] G. Taglieri, et al., Eco-compatible protective treatments on an Italian historic mortar (XIV century), J. Cult. Herit. 25 (2017) 135–141.

[15] V. Daniele, G. Taglieri, Ca(OH)$_2$ nanoparticle characterization: microscopic investigation of their application on natural stones, WIT Trans. Eng. Sci. 72 (2011) 55–66.

[16] Z. Slizkova, et al., Consolidation of a porous limestone with nanolime, proceedings of the 12th international congress on the deterioration and conservation of stone, New York, 2012.

[17] A. Arizzi, et al., Lime mortar consolidation with nanostructured calcium hydroxide dispersions: the efficacy of different consolidating products for heritage conservation, Eur. J. Miner. 27 (3) (2013) 311–323.

[18] M. Drdácký, et al., A Nano approach to consolidation of degraded historic lime mortars, J. Nano Res. 8 (2009) 13–22.

[19] V. Daniele, G. Taglieri, Nanolime suspensions applied on natural lithotypes: the influence of concentration and residual water content on carbonatation process and on treatment effectiveness, J. Cult. Herit. 11 (2010) 102–106.

[20] G. Borsoi, et al., Understanding the transport of nanolime consolidants within Maastricht limestone, J. Cult. Herit. 18 (2016) 242–249.

[21] P. Lopez-Arce, et al., Influence of relative humidity on the carbonation of calcium hydroxide nanoparticles and the formation of calcium carbonate polymorphs, Powder Technol 205 (2011) 263–269.

[22] C. Rodriguez-Navarro, et al., Kinetics and mechanism of calcium hydroxide conversion into calcium alkoxides: implications in heritage conservation using nanolimes, Langmuir 32 (20) (2016) 5183–5194.

[23] B. Salvadori, L. Dei, Synthesis of Ca(OH)$_2$ Nanoparticles from Diol, Langmuir 17 (2001) 2371–2374.

[24] A. Samanta, et al., Synthesis of calcium hydroxide in aqueous medium, J. Am. Ceram. Soc. 99 (3) (2016) 787–795.

[25] G. Poggi, et al., Calcium hydroxide nanoparticles from solvothermal reaction for the deacidification of degraded waterlogged wood, J. Colloid Interface Sci. 473 (2016) 1–8.

[26] T. Liu, et al., Synthesis and characterization of calcium hydroxide nanoparticles by hydrogen plasma-metal reaction method, Mater. Lett. 64 (2010) 2575–2577.

[27] R. Volpe, et al., A process for the synthesis of Ca(OH)$_2$ nanoparticles by means of ionic exchange resin, 2016 (European patent EP2880101).

[28] G. Taglieri, et al., Analysis of the carbonatation process of nanosized Ca(OH)$_2$ particles synthesized by exchange ion process, proceedings of the institution of mechanical engineers, Part N, J. Nanoengineering Nanosystems 230 (1) (2016) 25–31.

[29] G. Taglieri, et al., Nano Ca(OH)$_2$ synthesis using a cost-effective and innovative method: reactivity study, J. Am. Ceram. Soc. 100 (2017) 5766–5778.

[30] J. Otero, V. Starinieri, Development of a high performance nanolime for the consolidation of heritage, materials and engineering research institute doctoral research RF2 assessment, Sheffield Hallam University, 2016.

[31] G. Taglieri, et al., Mg(OH)$_2$ nanoparticles produced at room temperature by an innovative, facile and scalable synthesis route, J. Nanoparticles Res. 17 (2015) 411–424.

[32] R. Rossi-Manaresi, A. Tucci, Pore structure and the disruptive or cementing effect of salt crystallization in various types of stone, Stud Conserv 36 (1) (1991) 53–58.

[33] R. Rossi-Manaresi, Scientific investigation in relation to the conservation of stone, science and technology in the service of conservation, IIC, London, 1982, pp. 39–45.

[34] A.E. Charola, Salts in the deterioration of porous materials: an overview, J. Am. Inst. Conserv 39 (3) (2000) 327–343.

[35] R. Giorgi, et al., A new method for consolidating wall paintings based on dispersions of lime in alcohol, Stud. Conserv. 45 (2000) 154–161.

[36] C. Bennardo, et al., Comparative study of different methods for gap filling applications and use of adhesive on the biocalcarenite surfaces of the "Tempio della Concordia" in Agrigento, 9th Intern. Congress on deterioration and conservation of stone, Elsevier, 2000.

[37] M. Rosario Veiga, et al., Capillary test on historic mortar samples extracted from site. Methodology and compared results, in: 13th International Brick and Block Masonry Conference, Amsterdam, July 4-7, 2004.

[38] ASTM D3359-02: "Standard test methods for measuring adhesion by tape test", ASTM International, 10 August, 2002.

[39] F. Fratini, et al., A new portable system for determining the state of conservation of monumental stones, Mater. Struc. 39 (286) (2006) 125–132.

[40] C.M. Grossi, et al., Colour changes in architectural limestones from polution and cleaning, Color Res. Appl. 32 (2007) 320–331.

[41] A.W. Grabau, On the classification of sedimentary rocks, Am. Geologist 33 (1904) 228–247.

[42] R.L. Folk, Practical petrographic classification of limestone, Am. Assoc. Pet. Geol. Bull. 43 (1) (1959) 1–38.

[43] R.J. Dunham, Classification of carbonate rocks according to depositional texture. In Ham, W.E. classification of carbonate rocks, Am. Assoc. Petroleum Geologists Mem. 1 (1962) 108–121.

[44] Istituto Superiore per la Protezione e la Ricerca Ambientale, Servizio Geologico d'Italia. Note Illustrative della Carta Geologica d'Italia alla scala 1:50.000, Foglio 636 Agrigento.

[45] S. Siegesmund, H. Dürrast, Physical and mechanical properties of rocks, in: S. Siegesmund, R. Snethlage (Eds.), Stone in architecture, Springer, Berlin, Heidelberg, 2014.

[46] A.E. Charola, E. Wendler, An overview of the water-porous building materials interactions, Restorat. Build. Monum. 21 (2–3) (2015) 55–65.

[47] C. Mirabelli, et al., in: Rogerio-Candelera, Lazzari, Cano (Eds.), Effectiveness of a new nanostructured consolidant on the biocalcarenite from agrigento temples valley, international congress on science and technology for the conservation of cultural heritage, science and technology for the conservation of cultural heritage, Taylor & Francis Group, London, 2013.

[48] C. Rodriguez-Navarro, et al., alcohol dispersions of calcium hydroxide nanoparticles for stone conservation, Langmuir 29 (2013) 11457–11470.

[49] C.M. Grossi, et al., Color changes in architectural limestones from pollution and cleaning, Color Res. Appl. 32 (2007) 320–331.

[50] NORMAL 20/85: "Interventi conservativi: progettazione esecuzione e valutazione preventiva", Roma, Italy, 1985.

1    **Nanolime for the consolidation of lime mortars: a comparison of three available products**

2    J. Otero[a*], V. Starinieri[a], A. E. Charola[b]

3    [a] *Materials and Engineering Research Institute, Sheffield Hallam University, Sheffield, S1 1WB, UK*

4    [b] *Museum Conservation Institute, Smithsonian Institution, Washington DC, USA*

5

6    * corresponding author: Tel: +44 1142253500; Fax: +44 114 225 3501; b5039083@my.shu.ac.uk.

7

10

11    **Abstract.** Nanolime products are one of the most promising consolidation methods for historic calcareous

12    substrates. Whilst the popularity of nanolime has been growing, its consolidation mechanism still needs to be fully

13    understood when applied to highly porous substrates. The aim of this paper is to compare the three available

14    nanolime products in terms of consolidation efficacy on lime mortar specimens. It is shown that repeated

15    applications of a low concentrated nanolime can increase the superficial cohesion and the mechanical strength of

16    the mortar within 1cm from the surface, while also reducing porosity, number of micro-pores and capillary water

17    absorption coefficient. Nanorestore Plus® yielded the highest short-term consolidation effect. However, L'Aquila

18    nanolime showed a higher durability which was attributed a better developed crystalline structure.

19

20    **1. Introduction**

21    The consolidation of degraded calcareous materials is one of the main challenges in the conservation of historic

22    structures. Calcareous substrates degrade by weathering processes such as crystallisation of salts, biological activity,

23    freeze-thaw action and chemical attack by acid atmospheric pollutants [1-3]. Consolidants can help in recovering

24    the strength of degraded materials as well as decreasing the deterioration rate of the substrate. In general, suitable

25    consolidants must meet the following criteria: i) be physically, mechanically and chemically compatible with the

26    substrate; ii) have a good adhesion to the substrate; iii) increase the substrate's mechanical properties; iv) not

27    induce colour or aesthetic changes to the substrate; v) reduce porosity but not hamper moisture transport through

28    the substrate. The effectiveness of the consolidation depends on the interaction of a number of factors such as the

29  characteristics of the substrate, the properties of the consolidant and its compatibility with the substrate, and the

30  application methods and conditions [4].

31

32  Limewater, which is a saturated solution of calcium hydroxide with a maximum of concentration of 1.5g/L with

33  lime particles in a colloidal suspension [5], has been used over centuries to consolidate deteriorated limestone or

34  plaster. It has the advantage of being durable and compatible with the substrate as it is based on the precipitation of

35  calcium carbonate into the pores of the treated material by reaction of the calcium hydroxide with the atmospheric

36  carbon dioxide ($CO_2$). The main constraint of the limewater technique is a low consolidation depth due to limited

37  penetration of carbon dioxide into the substrate [6]. Furthermore, the application of limewater can cause whitening

38  of the treated surface. The effectiveness of limewater has been greatly discussed in literature. According to Price et

39  al. [7] when using limewater most particles are deposited within 2 mm from the surface yielding an ineffective

40  consolidation. Price's research has led some stone conservators to be skeptical of this treatment. Nonetheless,

41  Brajer [8] demonstrated that a prolonged uninterrupted application produces a noticeable consolidation effect and

42  some authors brought up new perspectives to its practical work such as the use of lime poultices and of an

43  increased number of limewater applications [3, 9, 10].

44

45  During the last century, organic consolidants (i.e. synthetic polymers, such as Paraloid B-72, Mowilith 30 and

46  Primal AC33) were extensively used in restoration treatments for calcareous materials due to their immediate

47  strength enhancement, ease of application and the limitations shown by limewater [11]. These consolidants proved

48  to be effective in the short and medium term for some calcareous substrates. However, the low compatibility with

49  the mineral substrate and their short durability caused more substrate degradation in the long term, particularly in

50  environments where temperatures increase above 40ºC [3, 9, 11]. Specifically, physical and mechanical

51  incompatibility between organic consolidants and calcareous substrates can cause crack development, aesthetic

52  changes and interference with future treatments [12, 13], sometimes with severe consequences [14, 15].

53

54  Nanolimes were developed to overcome the limitations of the traditional limewater treatment. Their consolidating

55  effect takes place by the same mechanism as for the limewater technique but the smaller size of the lime particles

56  (nanoscale) improves their performance. The advantages of nanolime compared to limewater are: i) nanolimes

57  contain higher amounts of calcium hydroxide particles; ii) lime nanoparticles are more reactive due to their higher

58    specific surface thus increasing the carbonation rate; iii) nanolimes penetrate deeper into the substrate because of

59    their smaller particle size; iv) nanolimes have better colloidal stability due to their smaller particle size and the

60    electrostatic repulsion forces between them; and, v) reduced whitening of the treated surface when nanolimes are

61    used. An overview of nanolime synthetisation methods and use as a consolidant for calcareous substrates can be

62    found elsewhere [16].

63

64    The first nanolime to become available on the market was Calosil® (IBZ-Salzchemie GmbH & Co.KR, Germany)

65    in 2006, followed by Nanorestore® (CSGI - University of Florence, Italy) in 2008. Recently, the University of

66    L'Aquila has patented a new method to synthesise nanolime where nanoparticles are produced by an anion

67    exchange process at ambient room conditions in aqueous suspensions [17-19]. Nanolime produced through this

68    method is currently in the process of being commercialised.

69

70    Both Calosil and Nanorestore have been extensively used for the conservation of wall paintings and stuccoes,

71    achieving good re-adhesion of detached particles or pigment flakes [5, 16, 20] and consolidating powdering

72    surfaces [15, 20]. However, the effectiveness of the nanolimes decreases when mass consolidation of a porous

73    substrate such as deteriorated stone or mortar is required [21-23]. The effectiveness of nanolime as a consolidant

74    appears to be influenced by several factors: i) multiple applications of low  nanolime concentration suspensions (i.e.

75    5 g/L) reduce the accumulation of consolidating product near the surface and improves the yield of carbonation

76    within the pores [24, 25]; ii) the type of alcohol used can influence the nanolime deposition in the pores [26, 27] as

77    well as the carbonation process [28], iii) external factors such as relative humidity (RH) and exposure time appear

78    to influence the carbonation rate and precipitation of polymorphs [29, 30]; iv) age and storing temperature of the

79    nanolime affects the conversion of $Ca(OH)_2$ particles into Ca-alkoxides which can decrease its effectiveness [31].

80

81    The aim of this work is to compare the consolidation effectiveness of the three available nanolime products on lime

82    mortars and investigate their long term performance. The influence of the nanolime treatments on mortar

83    superficial cohesion, water absorption by capillarity, drying rate, drilling resistance, pore structure and aesthetic

84    properties have been investigated.

85

**2. Materials and methods**

87 *2.1 Lime and sand*

88 Singleton Birch Ultralime CL90 ($\geq$ 98% $Ca(OH)_2$, measured by XRD and XRF) and silica sand from Pentney

89 (UK) were used throughout this work for the mortar mixes. The sand grading is shown in Figure 1. The

90 mineralogical composition of the sand, which was determined by XRD (*PANalytical XPert PRO*) using Rietveld

91 refinements, is 96.3% Quartz ($SiO_2$, ICSD #00-046-1045) and 3.7% Potassium Feldspar ($KAlSi_3O_8$, ICSD #01-076-

92 0831).



93
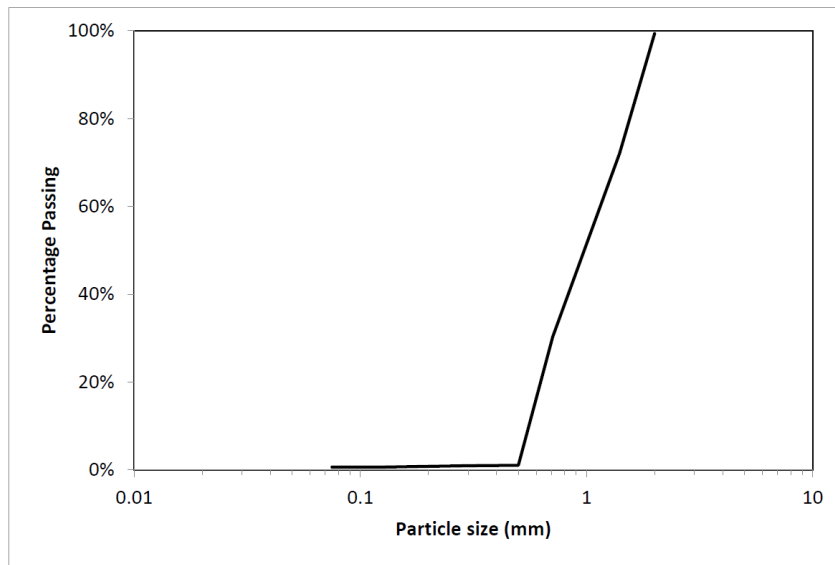
94 **Figure 1**. Sand grading curve

95

96 *2.2 Nanolime*

97 Three nanolime dispersions were used throughout this work:

98 – **Nanorestore Plus Propanol 5®** (CSGI Consortium - University of Florence, Italy): 5 g/L calcium

99 hydroxide in 2-propanol. Particle size 100-300 nm. This dispersion is referred to as NAN.

100

101 – **Calosil IP5®** (by IBZ Salzchemie GmbH & Co.KG, Germany): 5 g/L calcium hydroxide in 2-propanol.

102 Particle size 50-150 nm. This dispersion is referred to as CAL.

103

104      –   **Nanolime synthesised through the method developed by Taglieri et al [17] at the University of**

105           **L'Aquila**: 5 g/L calcium hydroxide in 50-50% water - 2-propanol. Particle size 20-80 nm. This dispersion

106           is referred to as LAQ.

107

108   LAQ was synthesized through an anionic exchange process carried out at room temperature and ambient pressure

109   by mixing under moderate stirring an anion exchange resin (Dowex Monosphere 550A OH from Dow Chemical)

110   with an aqueous calcium chloride solution following a methodology described by Taglieri et. al. [17, 18] and Volpe

111   et. al. [19]. When these two components are mixed together, the substitution of OH groups in the resin with

112   chloride ions ($Cl^-$) in solution leads, in conditions of supersaturation, to the formation of pure $Ca(OH)_2$

113   nanoparticles, following the reaction:

114

115                    $$CaCl_2 + 2(R\text{-}OH) \rightarrow Ca(OH)_2 \downarrow\ + 2(R\text{-}Cl)$$
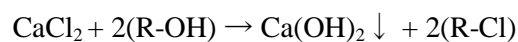
116

117   The concentration of chloride was monitored during the process (Vernier Chloride Ion-Selective Electrode CL-

118   BTA) and when this reached a constant value below 30 mg/L, the stirring was stopped and the aqueous suspension

119   was separated from the resin by means of a sieve (80μm). The supernatant water was then extracted through a

120   pipette and replaced with 2-propanol in order to maintain a concentration of 5 g/L in a 50-50% vol. water-2-

121   propanol solvent. This is considered the optimal formulation for this nanolime in terms of carbonation and kinetic

122   stability [18, 32].

123

124   The decrease rate of chloride content during the synthesis was very rapid, with about 97% of the reduction

125   occurring within the first minute of the process. The synthesis was stopped after 15 minutes when the ion exchange

126   process was completed (zero kinetic exchange), with a total reduction of chloride content of 99.82% and a residual

127   chloride content of 0.18% (29.4 mg/L). Similar results have been reported by Taglieri et. al. [17-19, 32].

128

129   *2.3 Mortar preparation and testing*

130   Mortars were produced with a volumetric binder:sand ratio of 1:2.5 to a constant flow of 16 cm measured

131   according to BS EN 1015-3:1999 [33]. Although mix proportions are expressed by volume, mortars were batched

132   by weight after accounting for component densities, which were measured in accordance with BS EN 459-2:2010

133   [34]. The water:binder ratio was 1.56 to obtain the desired flow. Mortars were produced by mixing the dry

134   ingredients with water in a Hobart mixer. The mix protocol was as follows: 1) dry mix sand and lime for 2 minutes

135   at 62 rpm; 2) add water while continuing mixing at 62 rpm for 30 s; 3) stop the mixer for 30 s and scrape the mixer

136   bowl; 4) mix for 5 min at 125 rpm. Samples were cast in $40\times40\times160$ mm steel moulds in two layers and vibration-

137   compacted. Immediately upon floating off the fresh mortar, the moulds were transferred to a temperature and

138   humidity controlled room maintained at 20 ºC and 65% RH.  Mortar beams were de-moulded after 5 days and

139   stored in the same room for the following 23 days. On the 28th day of curing, each prism was cut into 4 cubes

140   measuring approximately 40x40x40 mm prior to curing for further 28 days in the same conditions.

141

142   The mineralogical composition of the mortar was determined by X-Ray Diffraction. Samples obtained from the

143   core of the cube were ground and sieved through an 80 μm sieve mesh and placed over an XRD zero-background

144   sample holder; the XRD patterns were recorded with a step size of 0.026˚2θ, in the angular range 5-70°2θ.

145   Quantitative analyses were carried out by means of Rietveld refinement [35, 36]. X-ray data were fitted using the

146   pseudo-Voigt profile function. Specimen displacement, polynomial coefficients for the background function, lattice

147   parameters, profile parameters, and Gaussian and Lorentzian profile coefficients were refined. Quantitative analysis

148   by Rietveld refinement shows the mineralogical composition of the mortar is 82.3% Quartz ($SiO_2$, ICSD #00-046-

149   1045) and 17.7% Calcite ($CaCO_3$, ICSD #00-005-0586).

150

151   *2.4 Nanolime characterisation*

152   The size, shape and degree of agglomeration of the calcium hydroxide particles in the three nanolime products were

153   determined by TEM (Philips CM200), while the crystalline phase was analysed by XRD. TEM samples were

154   prepared by dispersing 0.2 ml of nanolime suspension in 20 ml of ethanol and placing a few drops of the resulting

155   liquid on a carbon-coated copper grid. XRD samples were prepared by using the zero-background silica sample

156   holder. Both TEM and XRD samples were prepared in nitrogen atmosphere, to prevent carbonation of the lime.

157

158   The kinetic stability (KS) of the three products was determined by turbidity measurements, analysing their

159   absorbance at $\lambda$ = 600 nm by means of a UV/VIS Spectrophotometer (UV-VIS Spectrophotometer Varian

160   50SCAN). Before the test, nanolimes were agitated, instead of sonicated. Sonicating has been the normal practice

161     in previous studies [18, 20, 26, 28], however, agitation was preferred in this work to simulate in-situ conditions

162     where conservators normally have no access to an Ultrasonic Bath. Measurements were taken over a period of up

163     to 2 hours. The relative kinetic stability (KS %) was calculated using the following formula:

164

165                           $KS \% = 1 - [(A_0 - A_t)/A_0] \times 100$

166

167     Where $A_0$ is the starting absorbance and $A_t$ the absorbance at time t, both at a wavelength of 600 nm [5, 28]. KS %

168     decreases as a result of the nanoparticles settling; values range from 0 (unstable dispersion) to 100 (no deposition of

169     nanoparticles).

170

171     *2.5 Nanolime carbonation process characterisation*

172     The carbonation process was investigated by means of TEM, SEM (SEM, NOVA 200 NanoSEM 450) and XRD.

173     For TEM observations, samples were prepared as described in section 2.4 and exposed to air for 1 minute prior to

174     carrying out the observations. For SEM investigations, 0.10 ml of each suspension were placed on a copper SEM

175     sample holder and exposed to outdoor conditions in a sheltered area (T ≈ 5–15°C, RH ≈ 60-80%) for 7 days prior to

176     carrying out the observations. SEM micrographs were taken with an ETD detector, a working distance of

177     approximately 3 mm, an optimum accelerating voltage of 15 kV and a spot size of about 30 nm. Specimens were

178     coated with a 20 nm thick layer of gold using a Quorum Q150T coater unit to prevent surface charging.

179

180     Samples for XRD were prepared by exposing 0.12 ml of each suspension (NAN, CAL and LAQ) to outdoor

181     conditions in the same sheltered area mentioned previously for 1 hour and 7 days prior to analysing by the

182     diffractometer. XRD patterns were recorded in step size of 0.026˚2θ. Each experimental diffraction pattern was

183     elaborated by means of a Profile Fit Software (HighScorePlus, PANalytical), and each crystalline phase was

184     identified using the ICSD and ICDD reference databases. Quantitative analyses were carried out by means of

185     Rietveld refinements.

186

187     *2.6 Nanolime treatment application*

188    Each of the three nanolimes was agitated and applied by brush on the top face (as cast) of three 40x40x40 mm

189    mortar cubes, allowing the nanolime to be fully absorbed by the mortar between two consecutive brushstrokes.

190    Nanolimes were also agitated between each brushstroke. The treatment was continued until no further absorption

191    was observed for a period of at least one minute after a brushstroke. At this time, the application was interrupted

192    and was repeated 24 hours later when the specimen was dry. Samples were weighed before and after each

193    application (after full evaporation of the solvent) to determine the total amount of nanolime absorbed by the mortar.

194    The treatment was considered complete when each mortar cube absorbed 500mg of calcium hydroxide

195    (approximately 100ml of nanolime). This required about 20 consecutive days of application for each nanolime.

196    Upon treatment completion, the samples were stored outdoor in the sheltered area for a period of 28 days (T ≈ 5–

197    15°C, RH ≈ 60-80%). A set of untreated control samples was also stored in the same conditions.

198

199    *2.7 Evaluation of treatment effectiveness*

200    Following 28-day outdoor exposure, the mortar cubes were dried to constant mass at 60 ℃ in a fan assisted oven

201    and subsequently stored in a desiccator until testing. The effectiveness of the nanolime was evaluated by means of

202    the tests described below.

203

204    The influence of the treatments on pore size distribution and porosity of the mortars was investigated by Mercury

205    Intrusion Porosimetry (MIP) using a PASCAL 140/240 instrument. Each test was carried out on one fragment

206    measuring approximately 5x5x10 mm collected within 5 mm from the top surface (as cast) of both treated and

207    control samples. The samples were dried in a fan-assisted oven at 60 ℃ until constant weight prior to testing. The

208    mercury contact angle was taken to be 140°.

209

210    The water absorption coefficient by capillarity (WAC) of both treated and control samples was measured according

211    to EN 13755 [39]; three samples being tested for each mortar. Upon completion of this test, once asymptotic water

212    absorption was reached, samples were immersed in water for 24 hours and their apparent porosity was calculated

213    following ASTM C 97-96 (American Society for Testing and Materials, 1996) [40], although the actual immersion

214    time was half of that recommended in this standard. Their drying behaviour was sequentially calculated according

215    to CEN EN 16322 [41]. This sequence simulates a real situation in an outdoor condition (cycles of dry-wet-dry).

216

217    The influence of the nanolime treatments on the surface cohesion of the mortar was evaluated by means of the

218    'Scotch Tape Test' (STT) carried out in accordance with ASTM D3359 [42]. The test was performed on both

219    treated and control samples and results taken as the average of 9 measurements per sample.

220

221    The consolidation effectiveness of the three nanolimes was also assessed by means of a Drilling Resistance

222    Measurement System (DRMS) from SINT-Technology. The DRMS measures the force required to drill a hole at

223    constant rotation (rpm) and lateral feed rate (mm/min). It is generally considered the most suitable methodology for

224    quantifying consolidation effectiveness and depth of penetration of consolidants, particularly in soft stones [43, 44].

225    Tests were performed on both treated and control mortar cubes using drill bits of 5 mm diameter, a rotation speed

226    of 200 rpm, a rate of penetration of 15 mm/min and a drilling depth of 20 mm. Drilling resistance values per each

227    treatment were calculated as the mean of 6 tests carried out on 2 cubes per each of the nanolimes.

228

229    The surfaces of both treated and control samples were observed under a Scanning Electron Microscope in order to

230    evaluate the morphology and distribution within the pores of the calcite crystals originated from the carbonation of

231    nanolime.

232

233    Any surface colour variations induced by the nanolime treatments were evaluated with a spectrophotometer

234    (Minolta CM508D Colorimeter) with the CIELab system [45]. 30 measurements were taken in different areas of

235    the surface of each of the treated and control mortar cubes. Total colour variation (ΔE) was calculated by the

236    formula:

$$\Delta E^* = \sqrt{\Delta L^{*2} + \Delta a^{*2} + \Delta b^{*2}}$$

237    where ΔL*, Δa* and Δb* are the change in luminosity for white-black, red-green and blue-yellow parameters,

238    respectively.

239

240    The durability of the treatments was evaluated using a QUV/SE Accelerated Weathering Tester from Q-Lab

241    Europe Ltd. Both treated and control mortar cubes were exposed to alternating cycles of UV light and moisture

242    condensation at controlled temperatures in accordance to ASTM G154 CYCLE 4 [46] for a period of 340 hours.

243    Each UV cycle has duration of 8 hours and uses an irradiance of 1.55 W/m$^2$ at a temperature of 70 ºC. The moisture

244     condensation cycles are carried out at 50 ºC with no UV irradiation. The influence of the accelerated weathering on

245     the mortars surface colour and drilling resistance were assessed by colorimetry and DRMS as described above.

246

## 3. Results and Discussion

*3.1 Characterisation of the nanolime suspensions*

249     Figure 2 shows TEM photomicrographs of the three nanolime products. Hexagonal $Ca(OH)_2$ nanoparticles with

250     identical morphology can be observed in all three of the nanolimes. The crystals tend to agglomerate due to the

251     nanoparticle phenomenon caused by their high surface energy [26, 28, 31] (Figures 2a and 2b). The size of the

252     observed nanoparticles is 250 - 100 nm for NAN (Figure 2a), 150 - 80 nm for CAL (Figure 2b) and 80 - 20 nm for

253     LAQ (Figure 2c). These results are in line with those reported by the developers of the three products [5, 17-20, 47,

254     48].
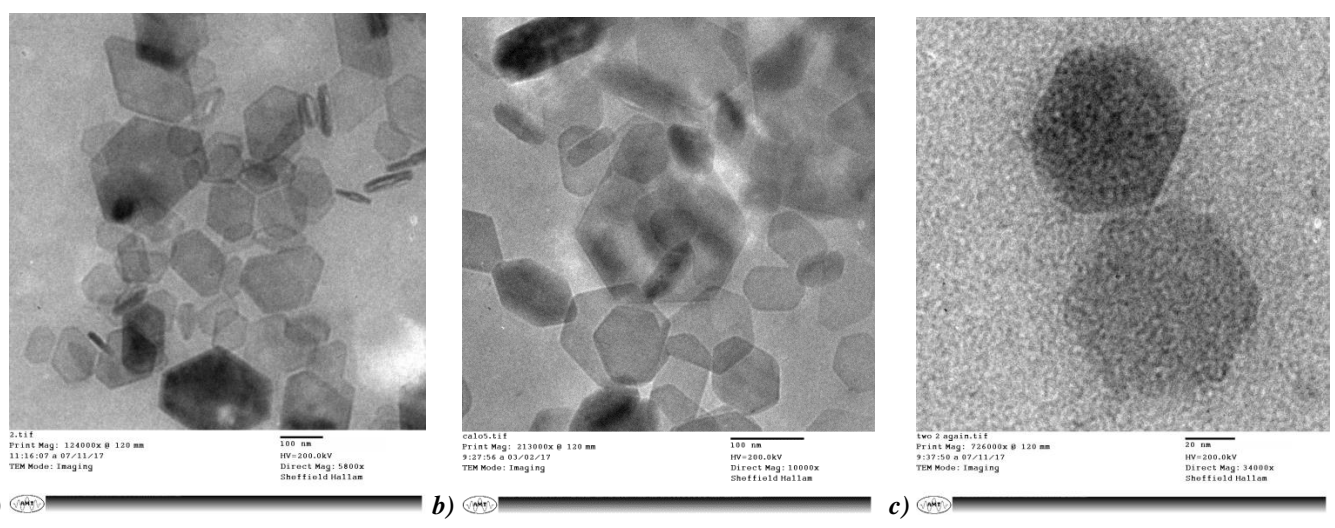


**Figure 2.** TEM images of: a) NAN; b) CAL; c) LAQ. Please note that the magnification bar is 100 nm for NAN and CAL, and only 20 nm for LAQ.

259     The XRD analysis in nitrogen atmosphere (Fig. 3) shows that the only crystalline phase of the three nanolimes is

260     Portlandite ($Ca(OH)_2$, ICSD #01-087-0674), confirming the results of the observations by TEM. For the three

261     samples the strongest peak corresponds to the {001} basal plane. However, XRD Rietveld refinements showed that

262     LAQ $Ca(OH)_2$ particles have a preferred orientation to the side plane {010}. NAN and CAL did not show any

263     significant preferred orientation. The Rietveld refinement factors are included in Table 1.

264

**Table 1**. Rietveld refinement factors of samples dried in Nitrogen atmosphere and exposed to air in outdoor conditions (60-80%RH) for 1h and 7 days.

| | Nitrogen | | | 1 hour in air | | | 7 days in air | | |
|---|---|---|---|---|---|---|---|---|---|
| | NAN | CAL | LAQ | NAN | CAL | LAQ | NAN | CAL | LAQ |
| R-expected | 10.1 | 9.35 | 13.89 | 20.24 | 20.24 | 20.03 | 19.53 | 15.67 | 20.03 |
| R-profile | 11.69 | 7.98 | 11.77 | 16.13 | 16.13 | 15.64 | 18.52 | 16.31 | 15.64 |
| Weighed R profile | 14.66 | 10.38 | 16.11 | 20.67 | 20.67 | 20.17 | 24.1 | 20.81 | 20.17 |
| Goodness of fit | 3.49 | 1.23 | 4.34 | 2.04 | 2.04 | 3.01 | 1.52 | 1.76 | 4.31 |
| Phase proportions | 100% P | 100% P | 100% P | 90.3% C 9.7% P | 100% P | 100% C | 100% C | 75.8%C 24.2% V | 100% C |
| Direction of preferred orientations | NPO | NPO | 10 | NPO | NPO | NPO | NPO | NPO | 104 |

NPO (No preferred orientation), P (Portlandite); C (Calcite); V (Vaterite)

265



266    a)                                                                                  b)



267                              c)
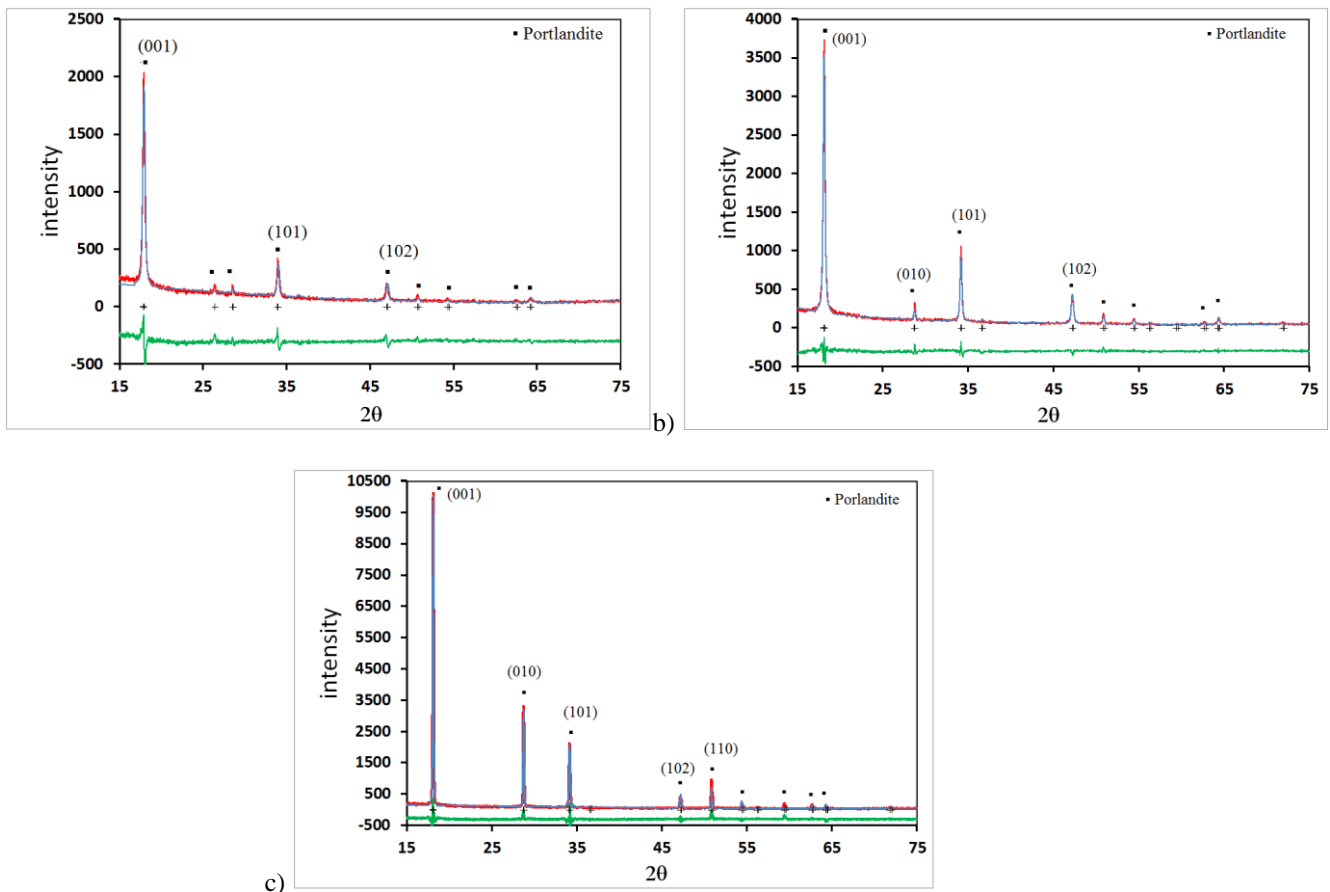
268    **Figure 3.** XRD patterns for NAN (a), CAL (b) and LAQ (c) samples dried in nitrogen atmosphere. Red line corresponds to

269    Intensity observed, blue line to Intensity calculated and green line to the Intensity observed - Intensity calculated difference

270    curve. The crystal phases are shown in brackets and the "+" symbol corresponds to the main peaks.

271

272    Figure 4 shows the absorbance (at 600nm) of NAN, CAL and LAQ dispersions over a period of 2 hours following

273    a moderate agitation. A high colloidal stability was observed for NAN and CAL $Ca(OH)_2$ nanoparticles. Previous

274 studies have shown that NAN and CAL nanolimes can keep the colloidal state for more than one week [49]. In

275 contrast, LAQ $Ca(OH)_2$ nanoparticles start to settle about 2 min after agitation (sedimentation rate ≈ 6% per h) and

276 that 12% of the particles settle after 2 hours of the testing period. This sedimentation process is considerably slower

277 than that occurring in limewater, where more than 90% of the particles settle in 2 hours [50]. The colloidal stability

278 of LAQ dispersion during the first 2 minutes after agitation can be considered acceptable for practical purposes as

279 most of the particles remain in colloidal state for the whole length of each application [28]. High colloidal stability

280 is critical to prevent the formation of undesired surface whitening as colloidal particles penetrate better into the

281 pores reducing accumulation on the surface [50].
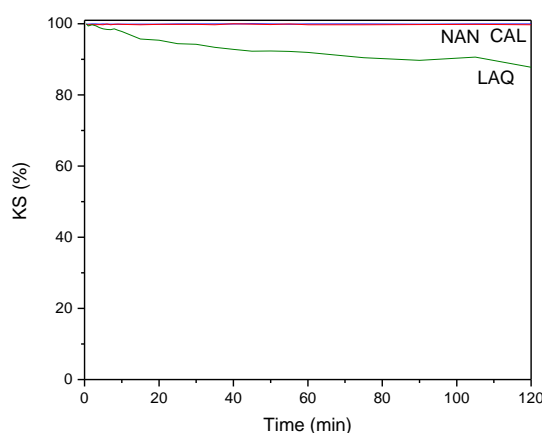


282

283 **Figure 4.** Kinetic stability KS (%) of NAN, CAL and LAQ dispersions

284

285 *3.2 Nanolime carbonation process*

286 The XRD patterns of nanolimes exposed to air for 1 hour (Fig. 5) show the LAQ nanoparticles to be the most

287 reactive, with calcite (ICSD # 01-085-1108) being the only detected crystalline phase (Fig. 5c). NAN nanoparticles

288 (Fig. 5a) also showed good reactivity within the 1 hour of air exposure time, with 90.3% of the sample being

289 composed of calcite (ICSD # 01-072-1652) and 9.7% of portlandite (ICSD # 01-087-0674). The only crystalline

290 phase detected for CAL was portlandite (ICSD # 01-072-0156), indicating a slower carbonation process (Fig. 5b).

291 The relatively high background combined with broad and weak Bragg peaks recorded for these samples suggest the

292 presence of poorly crystalline phase(s) (Fig. 5).

293

294 a)

295 c)
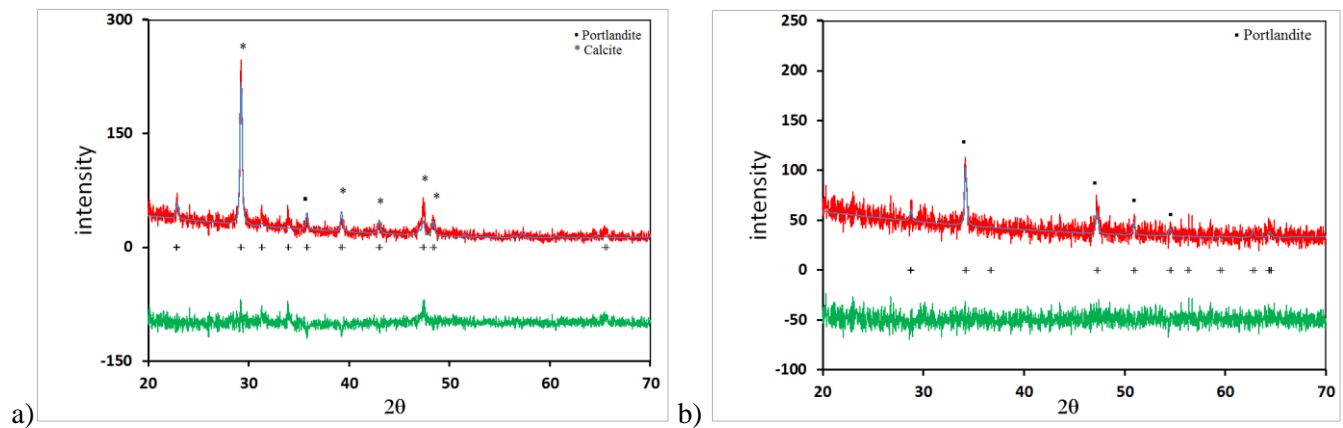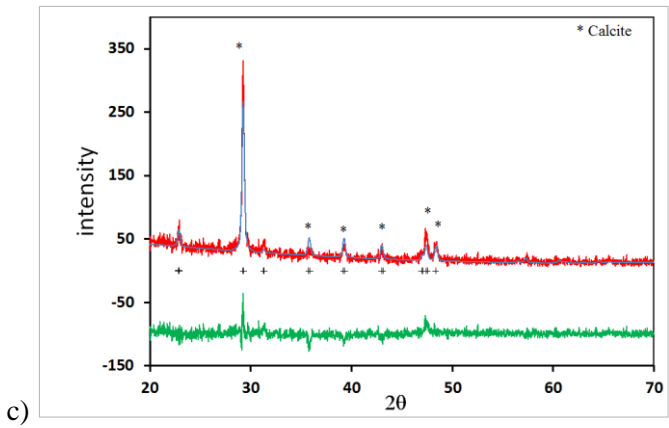
**Figure 5.** XRD patterns of NAN (a), CAL (b) and LAQ (c) samples exposed to air in outdoor conditions for 1 hour (60-80%RH). Red line corresponds to Intensity observed, blue line to Intensity calculated and green line to the Intensity observed - Intensity calculated difference curve. The crystal phases are shown in brackets and the "+" symbol corresponds to the main peaks.

XRD analysis after 7 days of air exposure shows a better defined crystalline structure for all three samples (Fig. 6) resulting from the completion of the carbonation process. Both NAN and LAQ samples consist entirely of calcite ($CaCO_3$, ICSD# 01-086-2334 and ICSD #01-083-0578 respectively) while CAL is composed of 75.8% of calcite ($CaCO_3$, ICSD# 01-081-2027) and 24.2% of vaterite (ICSD# 01-072-0506). Vaterite is the least stable polymorph of calcium carbonate, calcite being the most stable one [29, 30]. In previous studies [24], Calosil was found to precipitate as calcite and aragonite. XRD-Rietveld shows the calcite crystals in LAQ (Fig. 6c) are fully oriented to {104} while the crystals in NAN and CAL have no preferred orientation. The Rietveld refinement factors are included in Table 1.

310 a)

311 c)
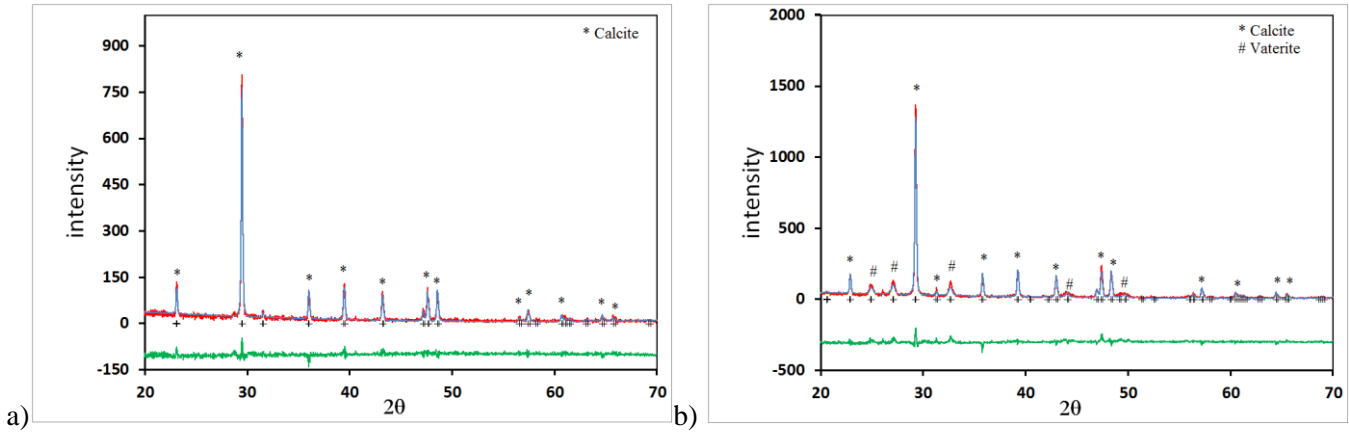
**Figure 6.** XRD patterns of NAN (a), CAL (b) and LAQ (c) samples exposed to air in outdoor conditions for 7 days (60-80%RH). Red line corresponds to Intensity observed, blue line to Intensity calculated and green line to the Intensity observed - Intensity calculated difference curve. The crystal phases are shown in brackets and the "+" symbol corresponds to the main peaks.

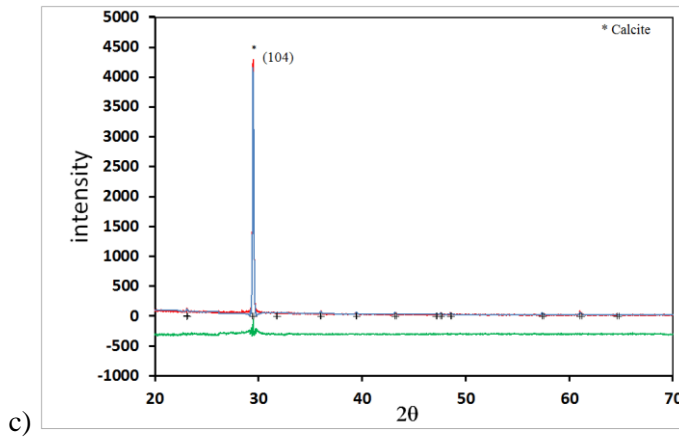TEM images taken after 1 minute of air exposure show that during the carbonation process NAN and CAL tend to grow mainly as hexagonal plates (Fig. 7a, b) while LAQ nanoparticles can be seen to grow preferentially through the {010} side plane (Fig. 7c). SEM images taken after 7 days exposure to outdoor conditions show NAN and CAL being characterised by calcium carbonate crystals of irregular shape (Fig. 7d - 7e), while LAQ shows calcite in well-formed hexagonal prisms and parallelepiped shapes (Fig. 7f), presenting larger size (10µm) than NAN and CAL ones, despite the smaller original nanoparticle size. Prismatic calcite crystals with similar shape to that observed for LAQ have been described by Ukrainczyk *et al* [51] when examining the influence of additives on the growth of calcite crystals.
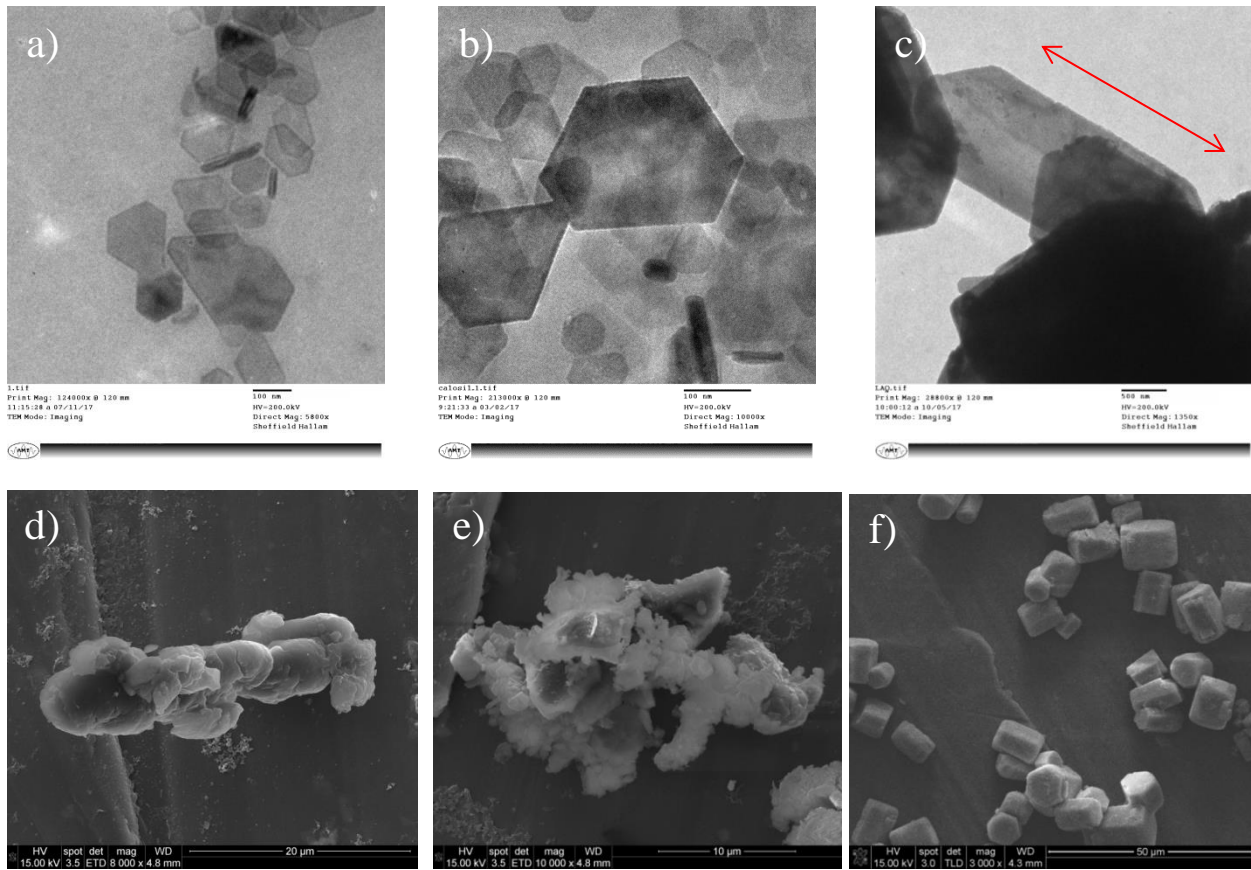
**Figure 7.** a) TEM image of NAN after 1 minute of air exposure at 124,000x; b) TEM image of CAL after 1 minute of air exposure at 213,000x; c) TEM image of LAQ after 1 minute of air exposure at 28,800x; d) SEM image of NAN after 7 days at 8,000x; e) SEM image of CAL after 7 days at 10,000 x; f) SEM image of LAQ after 7 days at 3,000x.

*3.3 Effectiveness of the nanolime treatments*

The pore structure properties of treated and control mortars are summarised in Table 2. It is evident that all three treatments affect the pore structure of the mortar by reducing the modal pore diameter and the porosity while increasing the total pore surface area. The highest porosity decrease was observed for the mortar treated with NAN (26% decrease), followed by those treated with LAQ (21%) and CAL (16%). The pore size distributions of control and treated mortars are shown in Fig. 8. It can be seen that the control sample has a tri-modal pore size distribution, coarser pores with diameters between 25 μm and 100 μm, intermediate pores with diameters between 3 μm and 25 μm and finer pores with diameters between 0.06 μm and 0.7 μm. Following the treatments, a complete removal of the coarsest mode and enhancement of the intermediate mode can be observed (Fig 8). Such enhancement is more prominent for the mortar treated with CAL (Fig. 8), which is in line with the lower decrease in porosity observed for this mortar.

**Table 2.** Pore structure properties of treated and control mortar samples measured by MIP

| Sample | Porosity (%) | Modal pore diameter (μm) | Total pore surface area (m²/g) |
|--------|--------------|--------------------------|--------------------------------|
| Control | 22.63 | 18.09 | 0.45 |
| NAN | 16.75 | 15.23 | 0.575 |
| CAL | 18.92 | 13.55 | 0.585 |
| LAQ | 17.87 | 14.15 | 0.781 |

346
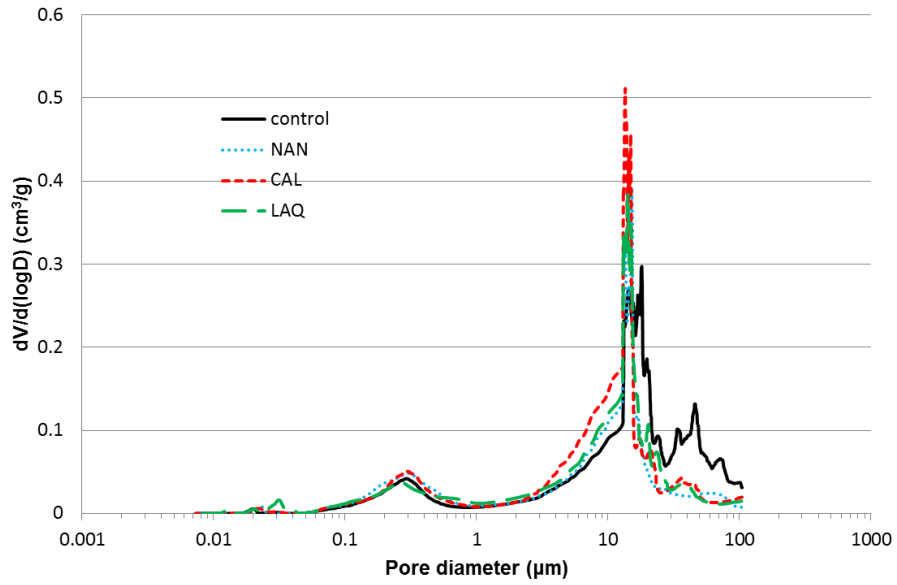


347

**Figure 8**. Differential volume of intruded mercury versus pore diameter of treated and control mortar samples

349

The water absorption and drying curves are reported in Fig 9. Apparent porosity by immersion, water absorption

and drying characteristics are reported in Table 3.

352



a)                                                            b)
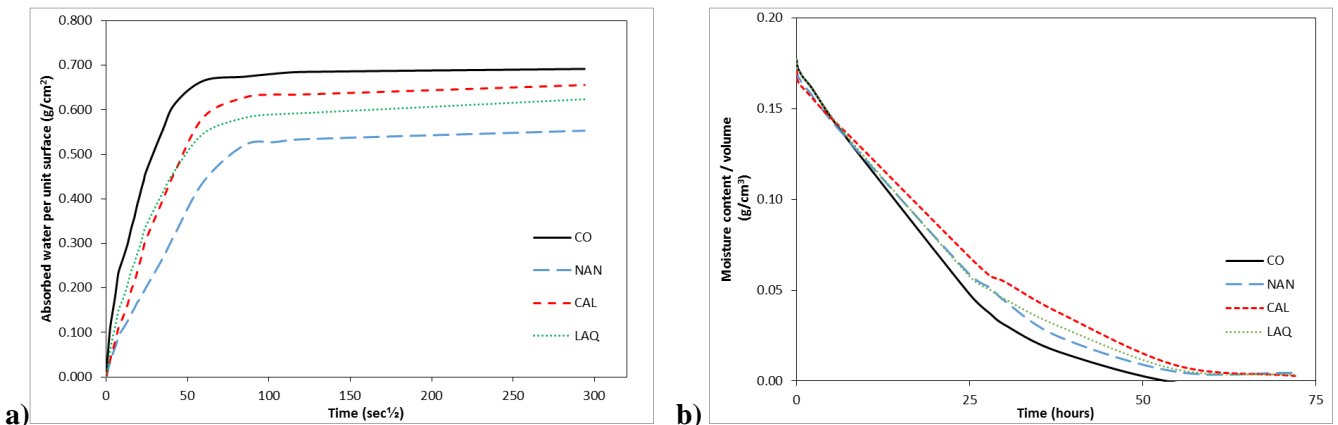
354 **Figure** 9. Capillary absorption (a) and drying curves (b) for control and NAN, CAL and LAQ treated mortars

355

**Table 3.** Apparent porosity by immersion, capillary water absorption and drying characteristics

| Parameter | CO | NAN | CAL | LAQ |
|---|---|---|---|---|
| Apparent porosity (%) | 11.84 (± 0.20) | 10.49 (± 1.63) | 11.60 (± 0.40) | 11.17 (± 0.65) |
| Water absorption coefficient ($10^{-3}$g/cm$^2$ s$^{0.5}$) | 9.5 (± 0.78) | 5.5 (± 1.7) | 8.2 (± 2.5) | 9.1 (± 0.5) |
| Water absorbed at asymptotic value (g) | 11.00 (±0.06) | 8.95 (±1.05) | 10.60 (±0.52) | 10.32 (±0.68) |
| Water absorbed after 24-hour immersion (g) | 11.57 (± 0.16) | 10.34 (± 1.61) | 11.49 (± 0.38) | 11.07 (± 0.50) |
| Initial drying rate ($10^{-3}$g/ cm$^3$ h) | 4.9 (± 0.1) | 3.9 (± 0.3) | 4.4 (± 0.5) | 4.4 (± 0.3) |
| Final drying rate ($10^{-3}$g/cm$^3$ h) | 1.0 (± 0.3) | 1.0 (± 1.0) | 1.2 (±0.6) | 1.2 (± 0.5) |
| Moisture content after 72 hours (g/cm$^3$) | 0.01 (±0.01) | 1.81 (±0.01) | 1.94 (±0.02) | 2.02 (±0.02) |
| Time for total drying (h) | ±50 | > 72 | > 72 | > 72 |

Values in parentheses are standard deviation of the three cubic samples.
356

357 Capillary rise in a porous material is strongly influenced by pore size distribution. The pore diameter range

358 affecting water capillary rise and transport could theoretically be considered to range between 1 mm and 1 μm

359 diameter [52]. It is shown that all three treatments yield a decrease of the capillary water absorption coefficient of

360 the mortar. This decrease can be attributed to the reduction in the number of pores with diameters between 17 μm

361 and 100 μm, which results from the applied treatments and was also recorded by the MIP measurements. Figure 9a

362 and Table 3 show that the NAN treatment yielded the biggest decrease in WAC (42%), followed by CAL (14%)

363 and LAQ (4%). Control samples required about 7 hours of contact with water to reach asymptotic values while

364 treated samples took nearly 9 hours (Fig. 9a). The latter absorbed less water by both capillarity and 24-hour

365 immersion, with the NAN treated sample showing the greatest decreases.

366

367 The treatments also reduced the apparent porosity of the mortar, with the NAN treated samples showing the highest

368 reduction (11.4%) followed by LAQ (5.7%) and CAL (2.1%). These results are fully compatible with the results of

369 the porosity measurements by MIP reported above. The average apparent porosity of the treated samples show a

370 relatively high standard deviation reflecting the inhomogeneity of the applied treatment, with the CAL (±0.40)

371 being only twice the value of the control, while LAQ (±0.65) is thrice higher than the control and NAN (±1.63)

372 being significantly higher (Table 3).

373

The drying curves (Fig. 9b) and the measured initial and final drying rates (Table 3) show that treated mortar samples take far more time to dry than the control ones. This is an undesirable behaviour as it increases the risk of spalling when the mortar is exposed to freeze-thaw cycles (limited to the external 1 cm plus where the nanolime precipitates) and / or biological attack [53]. The drying rate reduction is attributed to the finer pore structure of the mortar near the surface of the sample which results from the nanolime treatment. The smaller pores in the denser mortar layer reduce the liquid water transport towards the surface hence slowing down the drying kinetics [53]. The lowest initial drying rate was observed for the mortar treated with CAL while NAN and LAQ yielded similar rates. Whilst control samples were completely dry after 50 hours, treated samples still contained some residual moisture after 72h (Table 3).

Table 4 shows the results of the Scotch Tape Test (STT). A significant decrease of removed material ($\Delta V \approx 90\%$) was observed for all treated mortars with no significant differences in the performance of the three nanolimes. The standard deviation of the $\Delta V$ (%) (SD) shown in the table confirms a good reliability for this test in the measuring of surface cohesion.

**Table 4.** Scotch tape test results. Values determined on 9 measurements.

| Treatment | Removed material (mg/cm$^2$) | | $\Delta V$ (%) | SD |
| --- | --- | --- | --- | --- |
| | Before treatment | After treatment | | |
| NAN | 26.85 ($\pm$1.24) | 2.54 ($\pm$3.96) | 90.54 | 5.1 |
| CAL | 26.71 ($\pm$1.56) | 1.71 ($\pm$0.73) | 93.60 | 2.3 |
| LAQ | 26.76 ($\pm$1.04) | 3.16 ($\pm$2.57) | 88.19 | 3.6 |

Scotch area: 3 x 1.5 cm; Values in parentheses are standard deviation for the nine measurements taken on each of the three cub samples

Drilling resistance results are shown in Figure 10. It can be seen that whilst the control sample shows a steady drilling resistance throughout the drilling depth (average force $\approx$ 0.07N), the treated samples show increased resistance within the first 10 mm from the surface. The highest average drilling resistance was observed for the mortar treated with NAN (average force $\approx$ 0.57), followed by those treated with CAL (average force $\approx$ 0.32) and LAQ (average force $\approx$ 0.27). This is fully compatible with the porosity results which showed a more marked decrease of porosity for NAN treated samples than for CAL and LAQ treated samples. The average drilling resistance in the outer 5 mm is 0.09 N for Control, 1.12 N for NAN, 0.68 N for CAL and 0.64 N for LAQ, which is also in line with the results of the MIP measurements. This trend was not observed in the results of the Scotch Tape

Test, possibly due to a lower sensitivity of this technique compared to that of the DRMS. The DRMS profiles in Figure 10a-c show that the drilling resistance of the treated samples decreases with depth until it reaches the resistance of the control sample at about 10 mm for NAN and CAL and about 6 mm for LAQ. This data seems to indicate for the NAN and CAL treatments a deeper penetration into the mortar compared to the LAQ treatment.

The drilling resistance tests were repeated after exposing the samples to alternating cycles of UV light and moisture (Fig. 10d-f) and the results show for the NAN and CAL treated samples a reduction of the depth at which the drilling resistance reaches that of the control samples. This could indicate that a certain amount of material got partially dissolved from the surface of these samples as a result of the exposure to the alternating cycles of UV light and moisture condensation at elevated temperatures in the tester. The presence of deposits of white powder material in the water pan just below the sample holder panel seems to support this interpretation. The DRMS profile of the LAQ treated sample is similar to that recorded before the accelerated weathering test (Fig. 10f), which seems to indicate that less or no material loss occurred on the surface of this sample. The apparent higher resistance to weathering of the LAQ treated sample compared to that of the NAN and CAL treated ones could be attributed to a better developed crystalline structure and larger crystals. As described in section 3.2, LAQ produces perfectly shaped prismatic and parallelepiped calcite crystals of a larger size compared to NAN and CAL, which present poorly crystallized ones. The "well-shaped" calcite crystals are more resistant to dissolution than irregular shaped crystals as is well known [54]. In the case of the CAL treated sample, a reduction of the drilling resistance was observed within the first millimeter of depth (Fig. 10e), which could be due to the solubility of metastable amorphous carbonate phases such as vaterite (see section 3.2).



a)　　　　　　　　　　　　　b)　　　　　　　　　　　　　c)
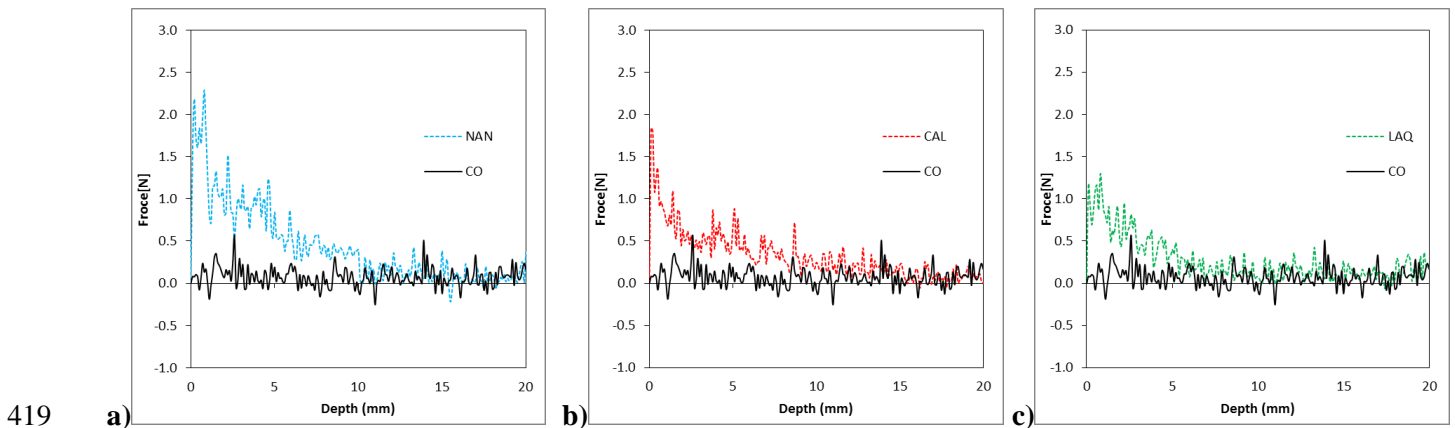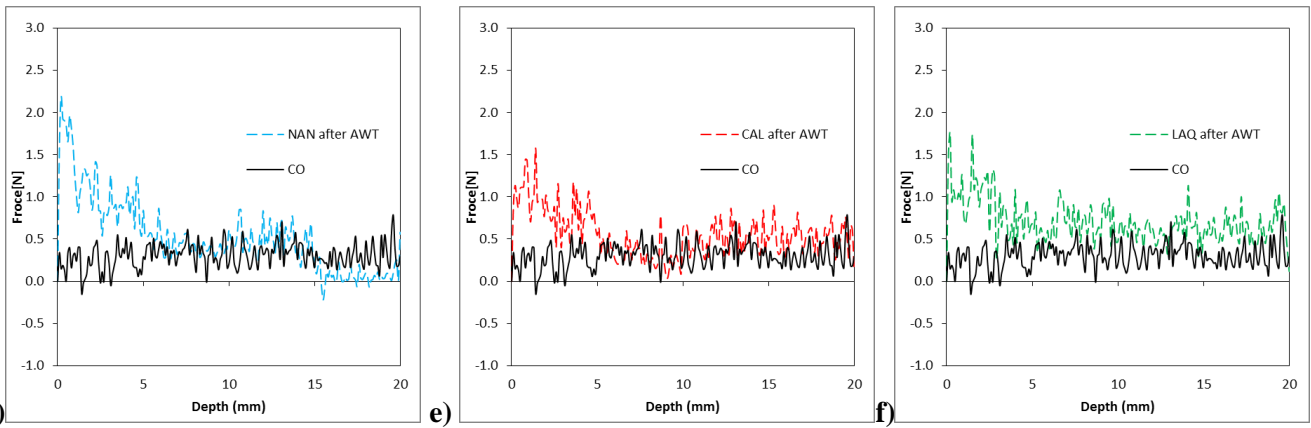
421    **Figure 10**. Drilling resistance of: a) NAN; b) CAL; c) LAQ; d) NAN after AWT; e) CAL after AWT and f) LAQ after AWT.

422

423    Both treated and untreated mortar surfaces were observed by SEM in order to study the distribution of the nanolime

424    in the pores and the morphology of the calcite crystals. SEM micrographs showed for the control samples a great

425    number of large pores (pore diameter >100 μm), which are outside of the measurement range of the used MIP

426    technique (Fig.11a). Following the treatments, the reduction of porosity and pore size due to the deposition of

427    calcite inside the pores is clearly visible (Fig. 11b-d).
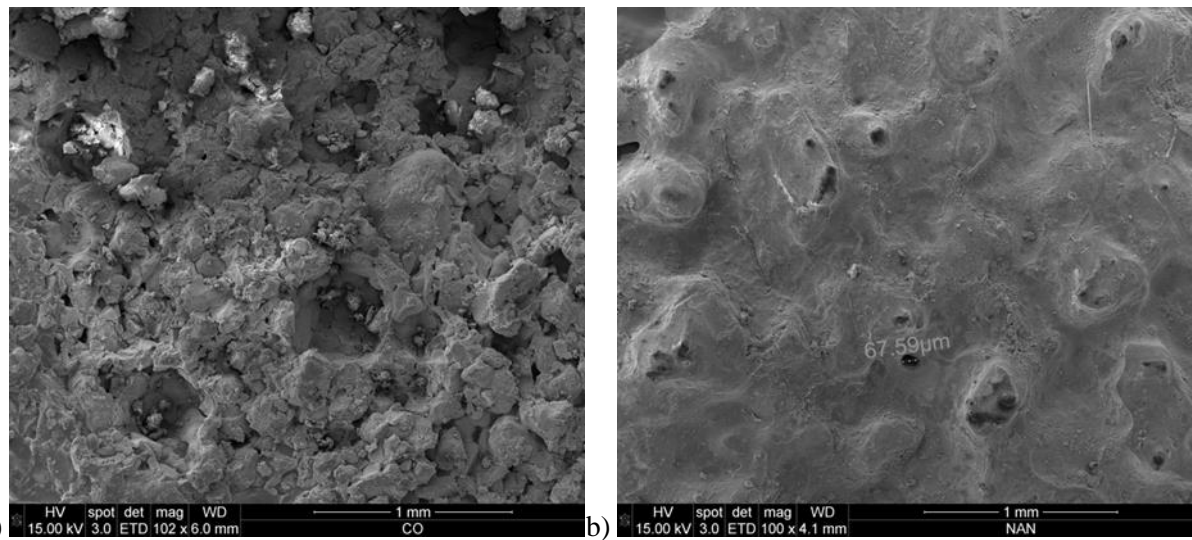


428    a)                                                                                                b)
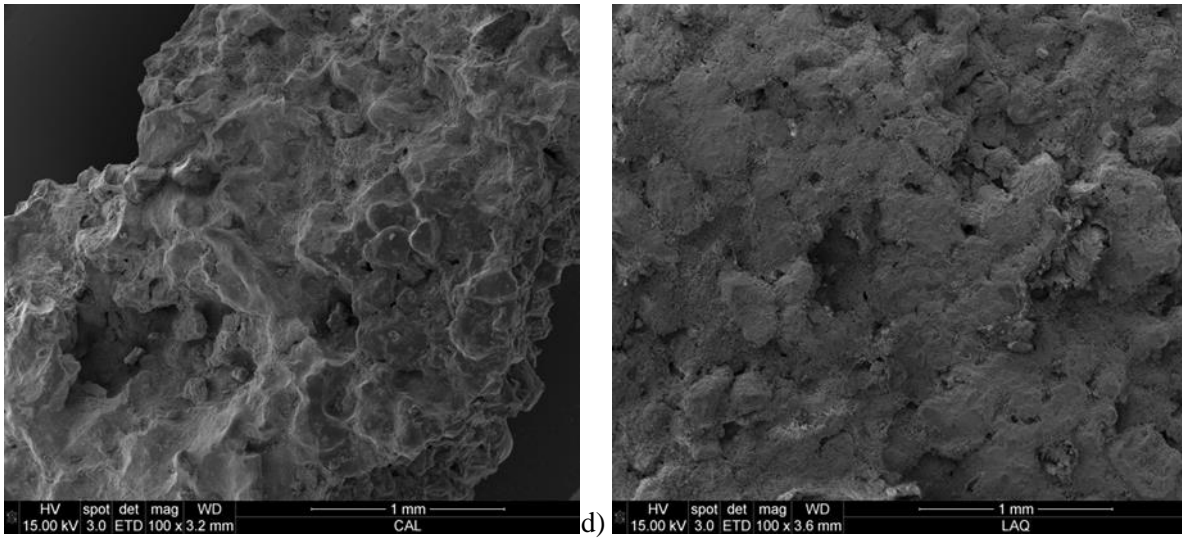
429  c)

**Figure 11**. SEM micrographs of mortar samples (100 X): a) control sample; b) surface treated with NAN; c) surface treated with CAL; d) surface treated with LAQ.

In Figures 11 b-d it can be seen that the nanolime is distributed homogeneously in the pores of the mortar and seems to adhere well to the substrate to the point that it is not easy to distinguish between the mortar and the newly precipitated calcite which fills the pores reducing their size. Fig. 12a shows that the calcitic material resulting from the carbonation of NAN within the mortar presents a different variety of shapes (mostly rhombohedral with scalenohedral terminations), which were observed also in previous studies for the same nanolime [24]. CAL precipitated in the form of calcite rhombohedra and some vaterite (Fig. 12b). Fig 12c shows typical calcite prisms on the LAQ sample. These are larger than those formed by NAN and CAL hence resulting in a smaller specific surface which is associated with higher resistance to weathering [54]. This morphology is similar to that visible on the SEM images (section 3.2).

443 a) 

b) 

444 c) 
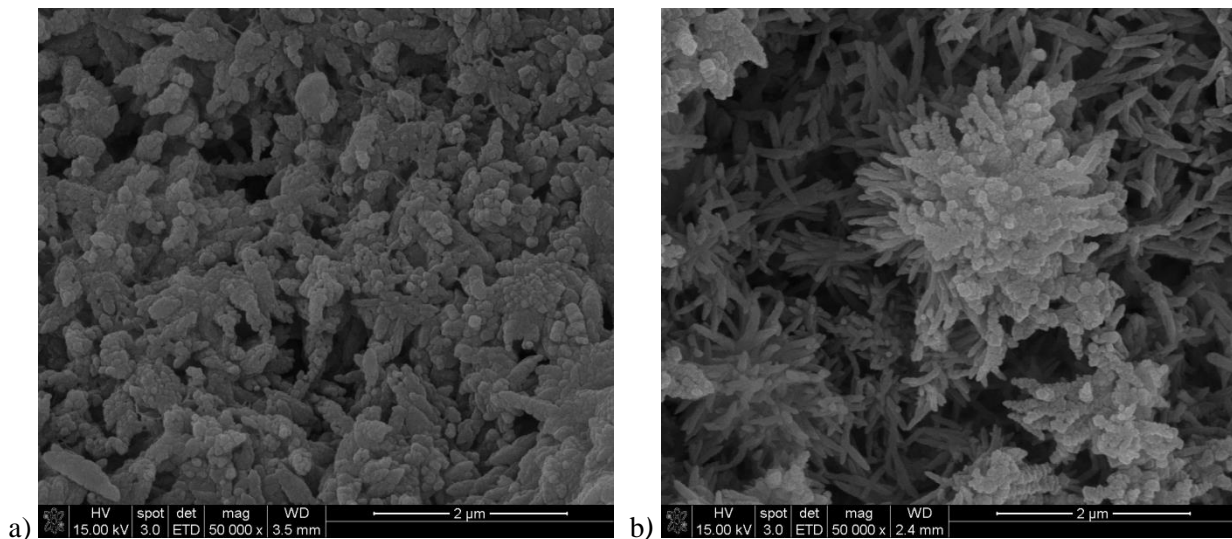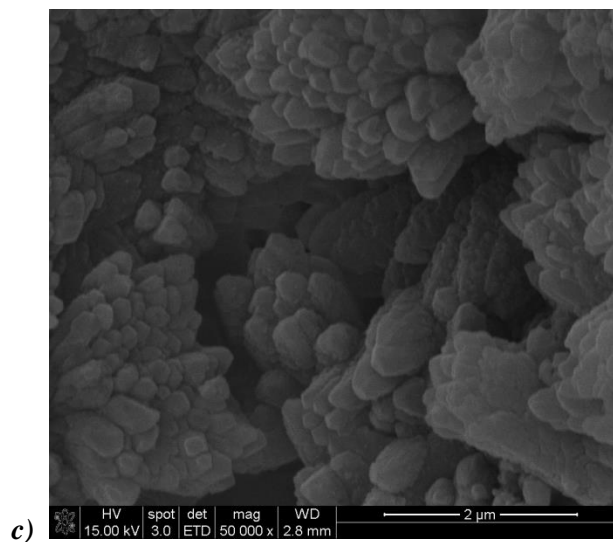
445 **Figure 12.** SEM detail micrographs of carbonated nanolime : a) NAN 50,000x; b) CAL 50,000x; c) LAQ 50,000x.

446

447 Ideally consolidation treatments should improve the physical-mechanical properties of the treated material without

448 affecting its aesthetic appearance. However, a common side effect of the use of nanolime is a whitening of the

449 surface following treatment. In order to investigate the occurrence of this phenomenon in association with the use

450 of the tested nanolimes, spectrophotometric analyses were carried out to measure changes in $L^*$ (white-black

451 parameter) and $\Delta E^*$ (total colour variations) following treatment. $\Delta E^*$ values $< 5$ are considered suitable for

452 practical conservation interventions and visually imperceptible [28]. The results (Table 5) show that all of the three

453 treatments cause whitening of the surface with both $\Delta E^*$ and $\Delta L^*$ values above 5. NAN yielded the lowest

454 whitening effect ($\Delta L^* \approx$ 6 and total colour alteration $\Delta E^* \approx$ 6). CAL and LAQ caused a more significant

455 whitening effect with $\Delta L^* \approx 7.5$ and $\Delta L^* \approx 11.94$, respectively, and total colour change with $\Delta E^* \approx 9$ and $\Delta E^* \approx 14$,

Page **22** of **30**

456 respectively. In previous studies, NAN and CAL yielded chromatic alterations of about $\Delta E^* \approx 6$ and $\Delta E^* \approx 4$,

457 respectively [24]. The lower colloidal stability of LAQ is considered responsible for the more significant formation

458 of undesired surface whitening. Nonetheless, the observed whitening and total chromatic alterations are still lower

459 than those caused by the lime-water technique, which normally vary between $\Delta L^* \approx 50$ to $70$ [9, 25].

460

461 The whitening effect and total colour changes associated with the application of nanolime decreased after the

462 samples were exposed to UV light and moisture cycles in the accelerated weathering test, with both $\Delta E^*$ and $\Delta L^*$

463 decreasing below 5. This could indicate that the induced weathering dissolved a certain amount of material from

464 the surface of the samples, as also detected by the DRMS for the NAN and CAL samples. It is apparent that in the

465 case of the LAQ samples the amount of material that got dissolved from their surface during the accelerated

466 weathering test was sufficient to reduce the whitening but too small to be detected by the DRMS.

467

468

**Table 5.** Chromatic alterations of treated samples before and after the Accelerated Weathering Test.

| | $\Delta L^*$ | | $\Delta a^*$ | | $\Delta b^*$ | | $\Delta E^*$ | |
|---|---|---|---|---|---|---|---|---|
| | Treated | AWT | Treated | AWT | Treated | AWT | Treated | AWT |
| NAN | 6.33 (±0.20) | 3.18 (±0.43) | -1.48 (±0.16) | -0.48 (±0.20) | -0.43 (±0.91) | -1.96 (±0.55) | 6.51 | 3.76 |
| CAL | 7.50 (±0.51) | 2.53 (±0.90) | -0.75 (±0.13) | -0.37 (±0.16) | -4.64 (±0.69) | -0.88 (±1.15) | 8.85 | 2.7 |
| LAQ | 11.94 (±0.96) | 4.04 (±0.63) | -1.25 (±0.15) | -0.55 (±0.0.26) | -6.96 (±1.07) | -1.17 (±1.45) | 13.87 | 4.24 |

Values determined on 30 measurements; AWT (Accelerated Weathering Test)

469

470

471 **Conclusions**

472 This study has shown that NAN, CAL and LAQ can be used effectively for the consolidation of highly porous

473 calcareous materials such as lime mortars and represent a viable alternative to organic consolidants for their

474 consolidation. It has been proven that repeated applications of low concentration dispersions of these nanolimes can

475 restore the substrate superficial cohesion, improve its mechanical properties, reduce its porosity, number of

476 micropores (10 - 100 µm) and water absorption coefficient.

477

478 It has been shown that:

479    •   The $Ca(OH)_2$ nanoparticles of the three nanolimes consist of crystalline hexagonal plates with similar

480         shapes. However, there is a difference in size: LAQ nanoparticles are smaller than both NAN and CAL.

481         XRD-Rietveld refinements showed that LAQ $Ca(OH)_2$ particles tend to align in a preferential direction

482         along the side plane {010} whereas NAN and CAL did not show any significant preferred orientation.

483         Nanorestore Plus® and Calosil® are stable colloidal dispersions while LAQ nanoparticles start to settle

484         about 2 min after agitation (sedimentation rate ≈ 6% per h) and the 12% of the particles has settled after 2

485         hours. This sedimentation rate is considered acceptable for practical purposes as most of the particles

486         remain in colloidal state during the time of the application. However, a moderate agitation is highly

487         recommended before the application of this nanolime. Moreover, the application should ideally be

488         completed within the first 2 first minutes after the agitation, before the particles start to settle.

489    •   Nanolime particles created by anion exchange synthesis (LAQ) are the most reactive with calcite being the

490         only detected crystalline phase after 1 hour of air exposure. NAN particles also showed a good reactivity

491         with 90% of the sample being composed of calcite following the same exposure time. CAL particles

492         showed slower carbonation and no calcite had formed after 1 hour exposure. After 7 days both LAQ and

493         NAN consisted entirely of calcite, while CAL was composed approximately of 75% of calcite and 25% of

494         vaterite, which is a metastable phase of calcium carbonate, less stable than calcite.

495    •   During the carbonation process, NAN and CAL tend to grow mainly as hexagonal plates while LAQ

496         nanoparticles seem to grow preferentially through the {010} side plane. After 7 days of carbonation, LAQ

497         shows well-formed hexagonal calcite prismatic crystals with larger size than NAN and CAL, which

498         consist of calcite crystals of irregular shape. XRD-Rietveld shows the calcite crystals in LAQ are fully

499         oriented to {104} while the crystals in NAN and CAL have no preferred orientation.

500    •   All treatments affect the pore structure by reducing the porosity of the superficial portion of the mortar.

501         The reduction in porosity is attributed mainly to a reduction of the number of pores with diameter between

502         17µm and 100µm, which also decreases the capillary water absorption coefficient. Nanorestore Plus®

503         presented the highest reduction of the porosity and water absorption by capillarity rate.

504    •   All three nanolimes increase the drilling resistance of the mortar surface. The penetration depth of

505         nanolime appears to be approximately 1 cm for NAN and CAL and 0.6 cm for LAQ. NAN treated mortars

506         showed the highest increase in drilling resistance, which is in line with their highest reduction in porosity;

507 followed by those treated with CAL and LAQ. Following an accelerated weathering test, the DRMS
508 detected the loss of a certain amount of material from the surface of mortars treated with NAN and CAL.
509 This was not observed for LAQ treated samples, possibly due to LAQ better developed crystalline
510 structure providing higher resistance to dissolution processes during the accelerated weathering test. The
511 detected loss is slightly more pronounced in Calosil® samples, possibly as a consequence of the
512 dissolution of metastable vaterite. A study of the calcite morphology and structural features of LAQ
513 nanolime must be addressed in future studies to better understand the performance of this nanolime.

514 • Following treatment, the samples take far more time to dry due to a finer pore structure of the mortar near
515 the surface. This is an undesirable behaviour which may lead to deterioration processes. Specifically,
516 spalling can occur where moisture is present and the mortar is exposed to freeze-thaw cycles. Furthermore,
517 longer drying times can favour biological growth and the dissolution of poorly crystallised calcite and
518 vaterite. A full study of the durability of mortars treated with the three nanolimes will be carried out in
519 future research.

520 • All treatments produced an undesired whitening of the surface after application. LAQ treatment induced
521 the highest whitening effect which can be attributed to the lower colloidal stability of this nanolime. The
522 whitening effect associated with all treatments decreases to values which are imperceptible to the naked
523 eye after exposing the samples to the Accelerated Weathering Test. This could indicate that a superficial
524 layer of the consolidated mortar was partially dissolved during the accelerated weathering test, as also
525 observed by DRMS.  In the case of LAQ treated mortars the dissolution decreased the whitening without
526 causing significant thickness reduction.

527

528 One final conclusion of this study is that substrates treated with the studied nanolimes will require regular
529 maintenance (i.e. periodic application of nanolime) in order to achieve long term performance in terms of
530 mechanical and physical properties.  Further work carried out by the authors has focused on the influence of the use
531 of different types of solvents on the performance of LAQ nanolime and a report will be submitted for publication in
532 due course.

533

534 **Declaration of conflicting interests**

535 The authors declare that there is no conflict of interest and take a neutral position to offer an objective evaluation of

536 the consolidation process.

537

541

542 **References**

543 [1] Doehne E., Price C. A., (2011), Stone Conservation: An Overview of current research, 2nd edition', Research in

544 Conservation, The Getty Conservation Institute, Getty Publications, Los Angeles, pp. 35-37.

545 [2] Charola A. E., Ware. R., (2002), Acid deposition and the deterioration of stone: a brief review of a broad topic.

546 Siegesmund GS, Vollbrecht A, Weiss T., (eds) Natural stone, weathering phenomena, conservation strategies and

547 case studies, Special Pu (London), pp. 393–406. Available at: doi:10.1144/GSL.SP.2002.205.01.28 .

548 [3] Hansen E., Doehne E., Fidler J., et. al. (2013), A review of selected inorganic consolidants and protective

549 treatments for porous calcareous materials", Reviews in Conservation, vol. 4, pp. 3630.

550 [4] Young, M. E., Murray M., and Cordiner P., (1999), Stone consolidants and chemical treatments in Scotland.

551 Report to Historic Scotland.

552 [5] Ambrosi, M., Dei L., Giorgi R., et. al., (2001), Colloidal particles of $Ca(OH)_2$: properties and applications to

553 restoration of frescoes, Langmuir, vol. 17 (14), pp. 4251–4255. Available at:

554 ttp://pubs.acs.org/doi/abs/10.1021/la010269b.

555 [6] Henriques, F., Charola, A. E., (1996), A comparative study of standard test procedures for mortars, Proceddings

556 of the 8th International Congress on Deterioration and Conservation of Stone, pp. 1521-1528.

557 [7] Price, C., Ross, K., White, G., (1988), A further appraisal of the 'Lime Technique' for limestone consolidation ,

558 using a radioactive tracer. IIC journal.Studies in Conservation, vol. 33 (4), pp.178–186.

559 [8] Brajer I., Kalsbeek N., (1999), Limewater absorption and calcite crystal formation on a limewater-impregnated

560 secco wall-painting, Studies in Conservation vol. 44 (3), pp. 145–156.

561 [9] Slizkova, Z., Dracky M., Viani A., (2015), Consolidation of weak mortars by means of saturated solution of

562 calcium hydroxide or barium hydroxide, Journal of Cultural Heritage, vol. 16, No. 4, pp. 420-460..

563    [10] Bracci, S., Sacchi, B., Pinto, A. F., et. al., (2008), Inorganic consolidants on stone artifacts: optimization of

564    application procedures for marble and limestones". International Symposium "Stone consolidation in cultural

565    heritage: research and practice", Lisbon 6-7 May, 2008. Proceedings, J. Delgado Rodrigues & João Manuel

566    Mimoso (Eds.), pp. 81-90.

567    [11] Wheeler, G., (2005), Alkoxysilanes and consolidation of stone, The Getty Conservation Institute, Getty

568    Publications, Research in Conservation, Los Angeles,, pp. 31 - 48.

569    [12] Charola A. E., Tucci A., (1986), On the reversibility of treatments with acrilic/silicone resin mistures. Journal

570    of the American Institute for Conservation, Vol. 25, pp. 83–92.

571    [13] Charola A. E., (1995), Water-repellent treatments for building stones : A practical Overview. Association for

572    Preservation Technology International (APT), vol. 26 (2), pp.10–17. Available at:

573    http://www.jstor.org/stable/1504480.

574    [14] Jroundi F., Fernández-Vivas A., Rodriguez-Navarro C., et. al., (2010), Bioconservation of deteriorated

575    monumental calcarenite stone and  identification of bacteria with carbonatogenic activity, Microbial Ecology vol.

576    60, pp. 39–54.

577    [15] Baglioni P., Carrasco-Vargas R., Chelazzi D., et. al., (2006), The maya site of Calakmul: In situ preservation

578    of wall painting and limestone using nanotechnology, Sudies in Conservation, 51:2, 162-169, DOI:

579    10.1179/sic.2006.51.Supplement-2.162

580    [16] Otero J., Charola A. E., Grissom C., et al., (2017), "An overview of nanolime as a consolidation method for

581    calcareous substrates". Ge-Conservación Journal, vol. 11 (1), pp. 71-78. DOI:10.17265/2162-5298.

582    [17] Taglieri G., Daniele V., Macera L., et al., (2017), Nano $Ca(OH)_2$ synthesis using a cost-effective and

583    innovative method: Reactivity study, J.Am Ceram Soc. 2017;100:5766–5778.

584    [18] Taglieri G., Felice B., Daniele V., et al., (2016), Analysis of the carbonatation process of nanosized $Ca(OH)_2$

585    particles synthesized by exchange ion process, Proceedings of the Institution of Mechanical Engineers, Part N:

586    Journal of Nanoengineering and Nanosystems vol. 230 (1), pp. 25-31.

587    [19] Volpe R., Taglieri G., Daniele V., et. al., (2016), A process for the synthesis of $Ca(OH)_2$ nanoparticles by

588    means of ionic exchange resin, European patent EP2880101.

589    [20] Baglioni P., Chelazzi D., Giorgi R., et. al., (2014), Commercial $Ca(OH)_2$ nanoparticles for the consolidation of

590    immovable works of art, Applied Physics A vol. 114, pp. 723–732.

591 [21] Costa D., Delgado Rodrigues J., (2012), Consolidation of a porous limestone with nanolime, in: Proceeding of

592 12th International Congress on Deterioration and Conservation of Stone, Columbia University, New York, October

593 22–26.

594 [22] Campbell A., Hamilton A., Stratford T., et. al., (2011), Calcium hydroxide nanoparticles for limestone

595 conservation: imbibition and adhesion, Proceedings of Symposium Adhesive and Consolidants for Conservation:

596 Research and Applications, ICC, Ottawa, October 17–21.

597 [23] Ghaffari E., Koberle T., Weber J., (2012), Methods of polarising microscopy and SEM to assess the

598 performance of nanolime consolidants in porous solids, Proceeding of 12th International Congress on Deterioration

599 and Conservation of Stone, Columbia University, New York, October 22–26.

600 [24] Arizzi A., Gomez-Villalba L. S., Lopez-Arce P., et. al., (2013), Lime mortar consolidation with nanostructured

601 calcium hydroxide dispersions: the efficacy of different consolidating products for heritage conservation, European

602 Journal of Mineralogy, vol. 27 (3), pp. 311–323.

603 [25] Slizkova Z., Frankeová D., (2012), Consolidation of a porous limestone with nanolime, Proceedings of the

604 12th International Congress on the Deterioration and Conservation of Stone, New York.

605 [26] Borsoi G., Lubelli B., Van Hees R., et. al., (2016), Understanding the transport of  nanolime consolidants

606 within Maastricht limestone, Journal of Cultural Heritage vol. 18, pp. 242-24.

607 [27] Ruffolo S. A., La Russa M. F., Aloise P., et. al., (2014), Efficacy of nanolime in restoration procedures of salt

608 weathered limestone rock, Applied Physics A Materials Science & Processing vol. 114, pp. 753-758.

609 [28] Rodriguez-Navarro C., Suzuki A., Ruiz-Agudo E., (2013), Alcohol dispersions of calcium hydroxide

610 nanoparticles for stone conservation, Langmuir vol. 29, pp. 11457−11470.

611 [29] López-Arce, P., Gomez-Villalba, L. S., Pinho, L., et. al., (2010), Influence of porosity and relative humidity on

612 consolidation of dolostone with calcium hydroxide nanoparticles: effectiveness assessment with non-destructive

613 techniques, Materials Characterization Journal, vol. 61, pp. 168-184.

614 http://dx.doi.org/10.1016/j.matchar.2009.11.007.

615 [30] Lopez-Arce, P., Gomez-Villalba, L. S., Martinez-Ramirez, et. al.,  (2011), Influence of relative humidity on

616 the carbonation of calcium hydroxide nanoparticles and the formation of calcium carbonate polymorphs. Powder

617 Technology, vol. 205, pp. 263-269.  http://dx.doi.org/10.1016/j.powtec.2010.09.026.

618 [31] Rodriguez-Navarro C., Vettori I., Ruiz-Agudo E., (2016), Kinetics and mechanism of calcium hydroxide

619 conversion into calcium alkoxides: Implications in heritage conservation using nanolimes, Lagmuir,  DOI:

620    10.1021/acs.langmuir.6b01065.

621    [32] Taglieri G., Otero J., Daniele V., et. al., (2017), The biocalcarenite stone of Agrigento (Italy): Preliminary

622    investigations    of    compatible    nanolime    treatments,    Journal    of    Cultural    Heritage,

623    https://doi.org/10.1016/j.culher.2017.11.003.

624    [33] The European Standard EN 1015-3:1990, (1990), Methods of test for mortar for masonry. Determination of

625    consistence of fresh mortar (by flow table).

626    [34] The European Standard EN 1015-2:1998, (1998), Methods of test for mortar for masonry. Bulk sampling of

627    mortars and preparation of test mortars.

628    [35] Rietveld H.M., A profile refinement method for nuclear and magnetic structures. Journal Applied

629    Crystallography, 10, 65, 1969.

630    [36] Bish D. L., Post J. E., (1989), Modern powder diffraction. Mineralogical Society of America, Washington.

631    [37] Grabau A.W., (1904), On the classification of sedimentary rocks, Am. Geologist vol. 33, pp. 228–247.

632    [38] BRE Digest 405, (1995), HMSO and the building research establishment.

633    [39] The English Standard EN 13755 for Natural stone test methods (2008). Determination of water absorption at

634    atmospheric pressure.

635    [40] ASTM C97-96 Standard Test Methods for Absorption and Bulk Specific Gravity of Dimension Stone,  (2000),

636    ASTM International, West Conshohocken, PA,https://doi.org/10.1520/C0097-96E01.

637    [41] The European Standard CEN - EN 16322 (2013), Conservation of Cultural Heritage - Test methods -

638    determination of drying properties.

639    [42] ASTM D3359-02: Standard Test Methods for Measuring Adhesion by Tape Test, (2002), ASTM International,

640    10 August.

641    [43] Tiano P., Delgado Rodrigues J., De Witte E., et. al., (2000), The conservation of monuments: a new method to

642    evaluate consolidating treatments, International Journal for Restoration of Build- ings and Monuments vol. 6 (2),

643    pp. 133-150.

644    [44] Pinto A. P., Delgado-Rodrigues J., (2008), Stone consolidation: the role of treatment procedures, Journal of

645    Cultural Heritage, vol. 9, pp. 38-53.

646    [45] Grossi, C. M., Blimblecombe, P., Esbert, R. M., et. al., (2007) Color changes in architectural limestones from

647    pollution and cleaning. Color Res. Appl. vol. 32, pp. 320−331.

648    [46] ASTM 6154 -4. Standard Test Method for the Accelerated Weathering test Method for QUV QUV/BASIC

649    Weathering Tester.

650    [47] Taglieri, G., Felice, B., Daniele, V., et. al, (2014), Analysis of the carbonation process of nanosized $Ca(OH)_2$

651    particles synthetized by exchange ion process, Proceedings of the Institution of Mechanical Engineers, Part N:

652    Journal of Nanoengineering and Nanosystems DOI: 10.1177/1740349914537616.

653    [48] Ziegenbald, G., (2008), Colloidal calcium hydroxide – a new material for consolidation and conservation of

654    carbonate stone. Proceedings of 11th International congress on deterioration and conservation of stone III,

655    Lukaszewicz E&Niemcewicz P., eds., Torun, pp. 1109–1115.

656    [49] Borsoi, G., Lubelli, B., van Hees, R., et. al., (2015). Deposition of modified nanolimes within calcareous

657    substrates. 1-2. Abstract from Green Conservation of Cultural Heritage, 27-28 October 2015, Rome, Italy.

658    [50] Giorgi R., Dei L., Baglioni P., (2000), A new method for consolidating wall paintings based on dispersions of

659    lime in alcohol, Studies in conservation, vol. 45, vol. 3, pp. 154 - 161.

660    [51] Ukrainczyk, M., Greiner M., Elts E., et. al., (2015), Simulating preferential sorption of tartrate on prismatic

661    calcite surfaces, CrystEngComm Journal, vol. 17, 149-159. DOI: 10.1039/c4ce01447b.

662    [52] Charola A. E., Wendler E., (2015), An overview of the water-Porous building materials interactions,

663    Restoration of building and monuments Journal, vol. 21(2-3), pp. 55-63.

664    [53] Charola A. E., Vicenzi E. P., Grissom C. A., et. al., (2017), Composition and characteristics of Kasorta

665    limestons on the exterior of the National Museum of the American Indian Building. pp.17-26. J.Sledge, A. E.

666    Charola, P. T. DePriest and R. Koestler, eds. Conservation of the Exterior of the National Museum of the American

667    Indian Building, Smithsonian Contributions to Museum Conservation, $N^o$. 6. ISSN 1949-2359.

668    [54] Charola, A. E., (1988), Chemical-physical factors in stone deterioration. Durability of Building Materials vol.

669    5, pp. 309-316.

670

671

672